

BLDSC no:- DX179796

LOUGHBOROUGH  
UNIVERSITY OF TECHNOLOGY  
LIBRARY

AUTHOR/FILING TITLE

CHANDLER, R.S.

ACCESSION/COPY NO.

040090930

VOL. NO.

CLASS MARK

30 JUN 1995

Loan copy

13 DEC 1996

MAR 1997

0400909308



BADMINTON PRESS  
18 THE HALFCROFT  
SYSTEM  
LEICESTER. LE7 8LD



**MICROWAVE ANTENNA SYSTEM FOR PASSIVE  
DISCRIMINATION**

by

**R. Sathish Chandran, BTech, MSc, AMIEE.**

*A Doctoral Thesis Submitted in Partial Fulfilment of the  
Requirements for the Award of Doctor of Philosophy of the  
Loughborough University of Technology*

October 1993

Supervisors : Dr. Peter R. Smith  
Dr. John C. Vardaxoglou

Department of Electronic and Electrical Engineering

© by R. Sathish Chandran, 1993.

Loughborough University  
of Technology Library

Date May 94

Class

Acc. No. 040090930

V891 2350

---

Dedicated To

My

Family.

---

---

---

TABLE OF CONTENTS.

Abstract		v
Acknowledgement		vi
CHAPTER 1 INTRODUCTION.		
1.1	Driving Force for the Research	1
1.2	Outline of the Thesis	4
	References	7
CHAPTER 2 PASSIVE ANTENNA CONCEPTS.		
2.1	Introduction to Passive Antennas	9
2.2	Concept of Intelligent Antennas	10
2.3	The Filter Dome	11
2.4	The Detector Array	12
2.5	Intelligent Antennas vs. Sperry Dome Antennas	13
2.6	Reflection Losses and Polarisation Effects	14
2.7	Remarks	15
	References	17
CHAPTER 3 DIELECTRIC MULTILAYERS (DML).		
3.1	Introduction to Multilayers	19
3.2	Material Characteristics	22
3.3	Theory	22
3.3.1	Waves in a Dielectric Layer	24
3.3.2	Governing Electromagnetic Equations	25
3.3.3	Vector Wave Equation	26
3.4	Formulation of the Field	27
3.4.1	TE Component	27
3.4.2	TM Component	29
3.5	Boundary Value Problem Formulation	32
3.6	Numerical Results	36
3.7	Attenuation Properties of a Multilayer	40

---

3.8	Optimisation Technique to Improve the Losses	41
3.8.1	Basic Concepts of Optimisation Algorithm	41
3.8.1.1	One Dimensional Optimisation	42
3.8.1.2	Numerical Results	45
3.9	Summary	45
	References	47

CHAPTER 4            FREQUENCY SELECTIVE SURFACES (FSS).

4.1	Introduction to FSS	49
4.2	Theory	51
4.2.1	Floquet's Theorem	52
4.3	The Method of Moments	55
4.4	Formulation of the Integral Equation for Induced Current	56
4.5	Effects of Periodicity Variation on the Performance of FSS	58
4.6	Effects of the Substrate Thickness on FSS Performance	62
4.7	Frequency Scanning	63
4.7.1	Use of Periodic Gratings	63
4.7.2	Basic Principle	64
4.7.3	Analysis	65
4.8	Numerical Results	66
4.9	Summary	70
	References	71

CHAPTER 5            RESULTS OF PASSIVE ANTENNA COMPONENTS.

5.1	Introduction	74
5.2	Experimental Setup	75
5.2.1	Anechoic Chamber	75
5.2.1.1	Microwave Sweep Oscillator	76
5.2.1.2	Scalar Network Analyser	77
5.3	Objectives of the Measurements	77
5.4	Measurement Procedures	80
5.4.1	Angular Filtering	80

5.4.2	Plane Wave Measurements	81
5.4.3	Radiation Pattern Measurements	81
5.4.4	Near Field Measurements	81
5.5	Preparation of Filters	82
5.6	Inspiration for Curved Measurements	85
5.7	Results	86
5.7.1	Angular Filtering Characteristics	86
5.7.1.1	Dielectric Multilayers	86
5.7.1.2	Frequency Selective Surfaces	92
5.7.2	Plane Wave Measurements	103
5.7.2.1	Dielectric Multilayers	103
5.7.2.2	Frequency Selective Surfaces	104
5.7.3	Radiation Pattern Measurements	106
5.7.3.1	Dielectric Multilayers	106
5.7.3.2	Frequency Selective Surfaces	109
5.7.4	Near-field Measurements	112
5.8	Summary	116
	References	118

Chapter 6            BEAM MODULATION DUE TO VARYING STRUCTURE  
PARAMETERS

6.1	Introduction	121
6.2	Beamsteering	123
6.2.1	Dielectric Multilayers	123
6.2.2	Frequency Selective Surfaces	129
6.2.2.1.	Steering by Frequency Scanning	129
6.2.2.1.1	Numerical Results	132
6.2.2.2	Steering by Rotating the FSS	136
6.3	Dielectric Multilayer as an Electromagnetic Window	139
6.3.1	Experimental Results	140
6.4	Beamforming using Dielectric Multilayer	143
6.5	Concepts of Electromagnetic Lenses	144
6.5.1	Focusing Action of FSS	144
6.6	Beam Directing Array	146
6.6.1	A First Order Approximation of Beamdirecting	147

---

6.6.2	Symmetrically Tapered Array	153
6.7	Summary	158
	References	160
CHAPTER 7          CONCLUSIONS		
7.1	Conclusions	162
7.2	Suggestions for Future Work	167
APPENDIX	Published Papers	169

---

## Abstract

A novel passive antenna system, capable of discriminating specific electromagnetic signals is addressed. This antenna system will be able to detect signals of certain bandwidths, amplitudes and propagation directions. The philosophy behind this design was to maximise the signal discrimination at a stage prior to reception. The development of such systems could relieve the work involved in post detection discrimination, which may be time consuming and expensive. A major motivation of these studies lies in the difficulties inherent in signal detection for mobile radio communication systems operating at microwave frequencies. Such an antenna system consists of two components. They are the filter section and the detector array. The filter is designed in such a way that only the near normal signal to the locally flat area will be admitted and the rest reflected. The detector array will be at an appropriate position below the filter.

Two types of filter structures have been studied for this angular filtering property. They are the Dielectric Multilayers (DML) and periodic arrays of slots as Frequency Selective Surfaces (FSS).

DML are constructed by stacking layers of dielectric material whose permittivities vary in a near sinusoidal manner. Such a structure is known to have the ability to admit certain frequency bands of signals. The conventional transmission/reflection matrix method is used for its analysis. Also an optimisation procedure is carried out to minimise the loss of the signal in the DML. The characteristics of the DML as a beamdirector and beamshaper have also been investigated.

FSS exhibit the characteristics of band pass and band stop filters, depending upon the nature of the surface (periodic arrays of elements or slots). Here the band pass nature is utilised by using arrays of slotted elements. These surfaces are tuned to admit narrow band signals. The well known modal analysis method has been employed to study the FSS characteristics. The FSS have been studied in the context of frequency scanning, beam shaping, beam directing as well as angular scanning.

A prototype has been constructed to simulate a multi signal environment in which the above structures have been experimentally assessed.

---

## ACKNOWLEDGEMENTS

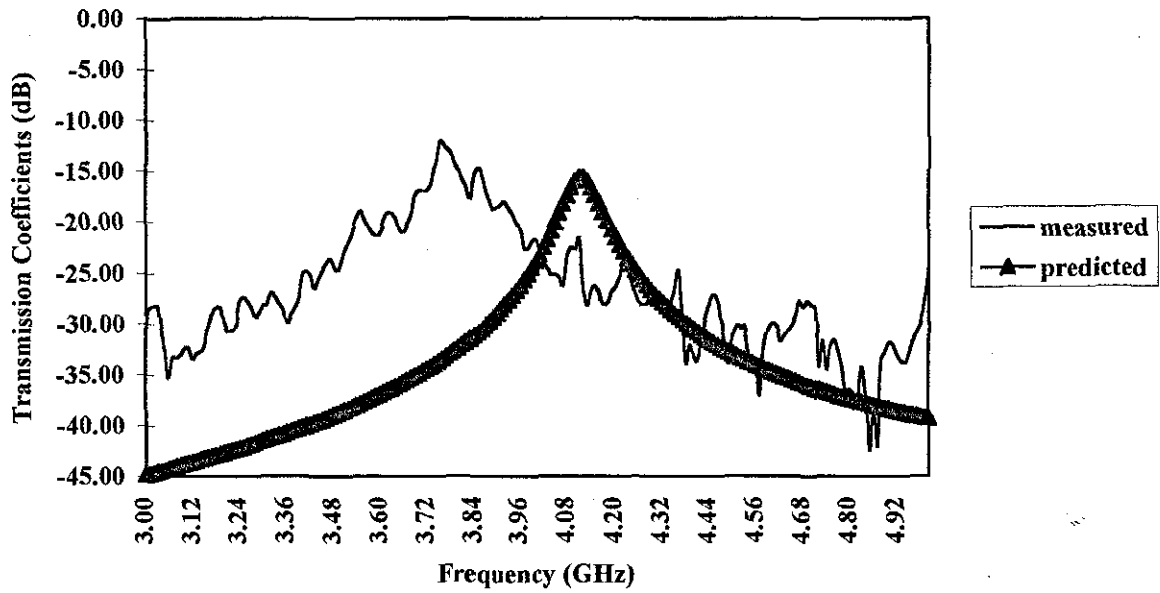
The author would like to express heartfelt gratitude to his supervisors, Dr. P.R. Smith and Dr. J.C. Vardaxoglou for their continuous guidance and constant encouragement throughout this project. He would also like to thank the SERC, UK. for providing financial support for this project.

Thanks are due to Dr. Chris Callender for proof reading this thesis. The author is so grateful to all the colleagues who have helped in various ways to ease his task. The author wishes to thank all the members in the antennas and microwave group, Rohan, Mahadevan, Shanti, Robert, Hayri, Alan, Abi, Masoud, Paul, Steve, Salim etc (if I miss anyone, I am sorry) for their encouragement and support.

The author would like to acknowledge his mates in Paget Arms for providing social chats.

Finally I would like to thank my family for providing me moral support, when I needed it most.

Final Design 1 of Aperture Dipole



3.22	-30.63	-42.44							
3.23	-30.12	-42.32							
3.24	-27.80	-42.20							
3.25	-27.40	-42.08							
3.26	-27.75	-41.96							
3.27	-28.45	-41.84							
3.28	-29.33	-41.72							
3.29	-28.95	-41.59							
3.30	-28.25	-41.47							
3.31	-28.20	-41.34							
3.32	-26.95	-41.22							
3.33	-27.35	-41.09							
3.34	-27.95	-40.96							
3.35	-28.65	-40.82							
3.36	-29.98	-40.69							
3.37	-29.12	-40.56							
3.38	-28.43	-40.42							
3.39	-27.77	-40.28							
3.40	-25.15	-40.14							
3.41	-24.88	-40.00							
3.42	-25.25	-39.86							
3.43	-26.50	-39.71							
3.44	-25.73	-39.57							
3.45	-24.78	-39.42							
3.46	-24.05	-39.27							
3.47	-23.60	-39.12							
3.48	-24.40	-38.96							
3.49	-24.77	-38.81							
3.50	-23.77	-38.65							
3.51	-22.68	-38.49							
3.52	-21.73	-38.33							
3.53	-20.77	-38.16							

# 1 Introduction

## 1.1 Background.

## 1.2 Theory

### 1.2.1 Fundamentals of Periodic Structure

### 1.2.2 Reconfigurable Frequency Selective Surface (RFSS)

## ~~1.3 Mathematical Analysis for RFSS~~

## 2. Objective and Scope.

## 3. Mathematical Analysis for RFSS.

## 4. Survey and Design

### 4.1 Determination the type of surface (RSS/RFSS) and geometry use.

### 4.2 Convergence Check

### 4.3 Stability study on the different incidence angle with TE and TM modes.

### 4.4 Effect due to the RFSS element dimensions

### 4.5 Effect ~~the~~ of the RFSS upon shifting.

### 4.6 Effect of the substrate thickness on RFSS performance.

### 4.7 Effect of the type of substrate used.

### 4.8 Final Design of RFSS.

## 5 Fabrication and Construction

## 6 Methods of Testing and Measurement's.

### 6.1 Methods of Testing

#### 6.1.1 Reflection Coefficient Measurements.

#### 6.1.2 Transmission Coefficient Measurements.

### 6.2 Results from the Representative Arrays.

#### 6.2.1 Aperture Dipole Array

#### 6.2.2 Aperture Square Loop Array

#### 6.3 Waveguide Filter.

## Chapter 1

**INTRODUCTION****1.1 Driving Force for the Research**

Detecting electromagnetic signals in an environment containing superfluous or unwanted signals is an important problem in communications[1], direction finding[2], radio astronomy[3] and radar[4]. There can be several parameters governing the meaning of 'unwanted' in this context, which are best appreciated by considering the properties of the set of signals which one would like to detect. The effectiveness of a microwave communication or radar transceiver system depends critically on its ability to distinguish between the signals in terms of their amplitude, frequency and beam properties. The increasing use of the same spatial channel and spectral band for multiple signal propagation further complicates the electromagnetic environment and motivates the need for antenna systems which provide signal discrimination within a narrow spectral band. It is safe to assume that in the events of signal replicas existing at the receiver, it would be desirable to isolate and if necessary track the strongest. The first property of interest is therefore signal strength. Since the signals may arrive at the receiver from almost any direction it is necessary to determine the source location in order to direct the receiver. The second signal property is therefore propagation direction. The final property addressed is signal bandwidth and this clearly can be a convenient eliminating or indeed discriminating factor.

The above three criteria can be used to distinguish signals at a particular point in time but it is recognised that the parameters may change in time. If a receiver is required to detect a signal defined by these criteria but the parameters of which are unknown, it must either be insensitive to the criteria or it must be able to adapt to changes. A further complication arises when the receiver itself is not a fixed entity as for example in mobile communication[5,6] and airborne radar[7]. Solutions to these problems have been proved by utilising the properties of mechanically or electrically steerable antennas. Perhaps the most elegant design employed in beam steering is the antenna array[8] and many types of elements have been devised. Signal discrimination is achieved under two main classes of approach. The first is purely computational method wherein the signals from each array element is digitally processed to determine the direction of the incoming signal and subsequently the antenna can be directed appropriately. Algorithms have been developed to optimise this process which has been termed adaptive and hence adaptive arrays[9,10]. The same array can be steered by phasing the elements and thereby tracking the main beam. The second approach requires somewhat less computational effort since the antenna itself is mechanically scanned through sectors of interest, storing received signals as it moves. At the end of the scan the signals can be compared and the relevant information obtained.

Current interest in steerable<sup>✓</sup> and direction finding antennas[11] is partly motivated by the projected requirements of microwave communication systems. Carrier frequencies measured in tens of GHz are anticipated with concurrent miniaturisation of transduction. Mobile systems present special difficulties, wherein increasing effort is needed to discriminate a given signal[12], especially in urban environments[6]. Development of particular antenna geometries and loading is an approach

---

to pre-detection discrimination which is entirely passive. For convenience such designs are referred to as intelligent antennas (IA). Realisation of such IAs can reduce the receiver workload considerably and the overall system diversity.

Although other existing techniques provide the required information, there are drawbacks for some areas of application. These stem from the large computational effort required which slows the response of the instrument and may have undesirable influences on design criteria such as size, weight, power and cost. The proposed detector is designed to measure the individual amplitudes of a set of signals occupying a particular frequency band and simultaneously determine the propagation direction of each signal. In some practical circumstances the set of signals of interest will dominate the ambient radiation, in terms of their strength. However this set may change in time and within the set a range of amplitudes may be present. Ideally, the function of the detector is to select the strongest signal in the given bandwidth and determine its source direction. It is envisaged that the detector could operate in conjunction with a steerable antenna which would respond to directives from the detector itself. A particular application may require the antenna to track a signal (or set of signals) or to steer into a direction of minimum signal strength. If the detector and antenna were positioned in the same inertial frame of reference, real time control could be maintained even when the receiver was mobile. The detector may also be used as a selective receiver of signals and the law of reciprocity implies that certain transmissions could also be made.

In this thesis a novel design is proposed which is capable of discriminating signals of particular bandwidths, amplitudes and propagation directions. The design criteria of the proposed antenna system and the

results obtained by using spatial filters will form the body of this thesis. Also few general properties of these filters, particularly frequency scanning, beam forming, beam directing, windowing etc are investigated.

## 1.2 Outline of the thesis

The logical sequence followed in this thesis is shown in Figure 1.1. Chapter 2 is seen as a pre-requisite for all the chapters that follow. It contains all the information about the proposed antenna model and the requirements. The following two chapters review the mathematics involved in the design of the filters and the next two chapters are dedicated to the results.

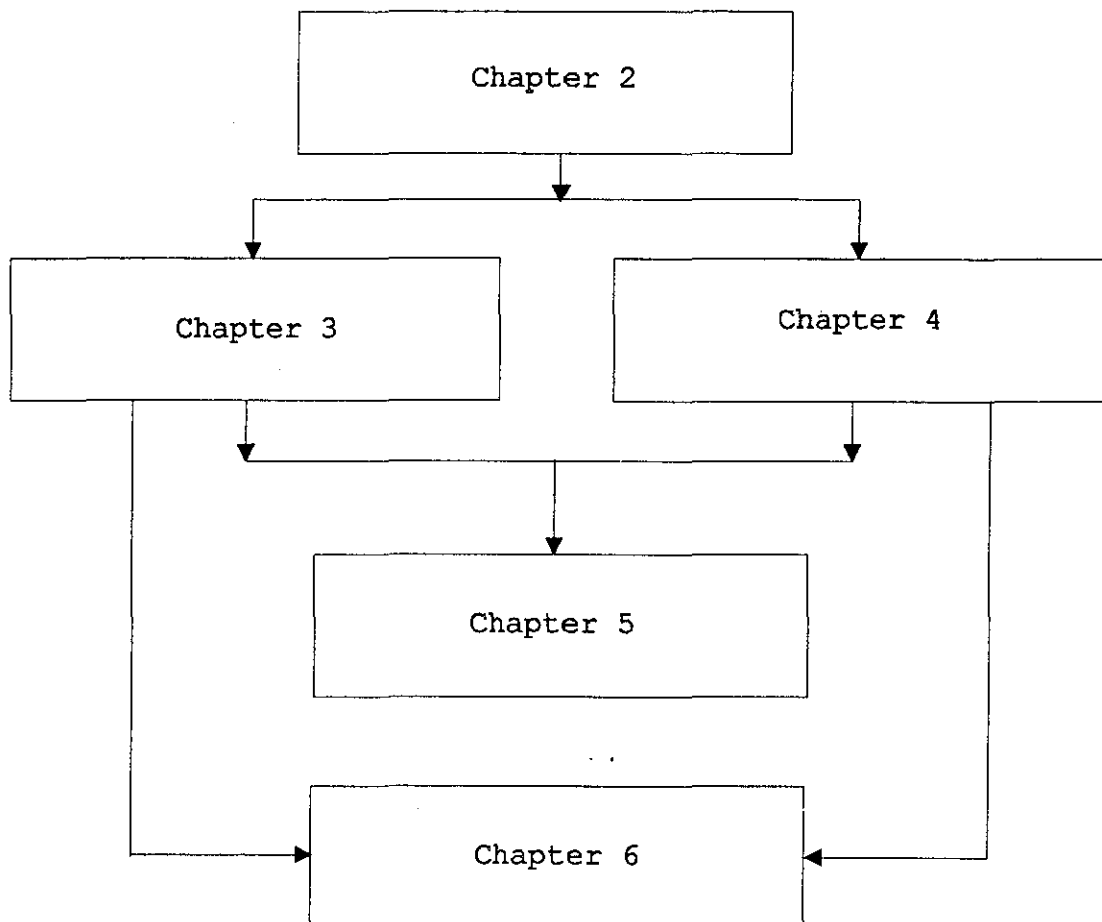


Figure 1.1 Logical sequence of main chapters.

In Chapter 2, the concept of the passive antenna system is described. A schematic model of the proposed antenna system is established. The filter structures and the detector system are presented in real terms. This antenna structure is compared with the Sperry dome structure and the reflection and polarisation effects are discussed.

In Chapter 3, the dielectric multilayer (DML) is discussed. The mathematics involved in the transmission and reflection characteristics is reviewed for completeness. Gradient optimisation methods (one and two dimensional) are introduced and discussed, to reduce the transmission losses through the DML. Results are presented to substantiate these effects.

Chapter 4 gives a review of the modal analysis method used for the development of Frequency selective surfaces (FSS). Parametric studies are carried out to evaluate the performance of FSS as angular filters. Also the general principle of frequency scanning is presented together with the first order numerical results generated.

Chapter 5 presents the results of the passive antenna structure which will be discussed in Chapter 2, which comprises of DML and FSS. Different types of experiments are presented. They are angular filtering, plane wave measurements, radiation pattern measurements and near field measurements. Single and multiple horn combinations are used as the signal source. Both DML and FSS are used for the realisation of the passive antenna structure. Two different geometries of array designs are used for the fabrication of FSS. Both planar and curved structures are subjected to the experiments mentioned above. The theoretical as well as the measured results are compared. For some experiments, theoretical models are not readily available and therefore a practical study is carried out.

In Chapter 6, the beam steering and beam forming actions using DML are verified. The DML is presented as a electromagnetic window and as an apodiser. The effects of the radiated beam due to the variation of the surface parameters of the FSS as well as to the variation of the signal parameters are discussed. The lengths of the slots are varied to provide focusing, beam directing and beam forming. A first order approximate theoretical model for beam directing is derived and the numerical results are presented. A numerical model is also developed to analyse the frequency scanning property of FSS.

Chapter 7 gives the conclusions of the study and suggestions for future work.

---

**References**

1. Compton R.T., Pointing accuracy and dynamic range in a steered beam adaptive array, IEEE Trans. AES-16, 1980, pp.280-287.
2. Gething P.J.D., Radio direction finding and the resolution of multicomponent wave-fields, 1978, Peter Peregrinus Ltd, UK.
3. Kraus J.D., Radio Astronomy, 1982, Cygnus-Quasar Books, Ohio.
4. Johnson R.C. and Jasik H., Antenna Applications Reference Guide, 1987, McGraw-Hill Inc, New York.
5. Lee W.C.Y., Mobile Communications Engineering, 1982, McGraw-Hill Inc, New York.
6. Vaughan R. G., Signals in mobile radio communications: A Review, IEEE Trans VT-35, 1986, pp.133-145.
7. Allen P.W. and Ryan C.E., Aircraft Antennas, in: Antenna Applications Reference Guide, eds. Johnson and Jasik, 1987, McGraw-Hill Inc, New York.
8. Hansen W.W and Woodyard J.R., A new principle in directional antenna design, Proc. IRE-26, 1938, pp.333-345.
9. Brynn F., Optimal signal processing of three dimensional arrays operating on Gaussian signals and noise, J. Acoustical Soc.Am-34, 1962, pp.289-297.
10. Hudson J.E., Adaptive Array Principles, 1981, Peter Peregrinus Ltd, UK.

11. Hudson J. E., Fast signal acquisition by an adaptive antenna moving in a multipath field, Proc. IEE Pt. H 134, 1987, pp.178-180.

12. Clark A. P., Digital modems for land mobile radio, Proc. IEE Pt. F 132, 1985, pp.348-362.

## CHAPTER 2

**PASSIVE ANTENNA CONCEPTS****2.1 INTRODUCTION TO PASSIVE ANTENNAS**

Passive antennas will play an increasingly important role in communications and surveillance. Such antennas offer the flexibility to handle the demand for beam steering as well as beam forming used in airborne and space based applications. Passive antennas are finding many applications in areas of communications. Dielectric based antennas use a monolithic planar technology for a flat low profile design. These radiators can also be frequency scanned, eliminating the need for elaborate gimbals, and mechanically or electronically scanned feeds[1]. Ease of integration and fabrication are key features of passive antennas. Fabricating the antenna as an integral part of the system can significantly reduce cost, along with size and weight.

This chapter describes one such passive antenna concept which is relevant to mobile satellite radio communications systems. It also describes particular designs for one of the critical components. Here the characteristics of DML and FSS are exploited as angular filters which will behave as a spectral and spatial filter. This allows the signals in the desired bandwidth to propagate through the filter structure, thereby providing signal discrimination. Details of the behaviour

of these filters will be discussed here.

## 2.2 CONCEPTS OF INTELLIGENT ANTENNA

The proposed detector has two components corresponding to the signal parameters, the frequency band and the direction/amplitude. These components are the filter and the detector array respectively. The complete structure is azimuthally symmetric and Figure 2.1 shows a vertical slice through the design in schematic form.

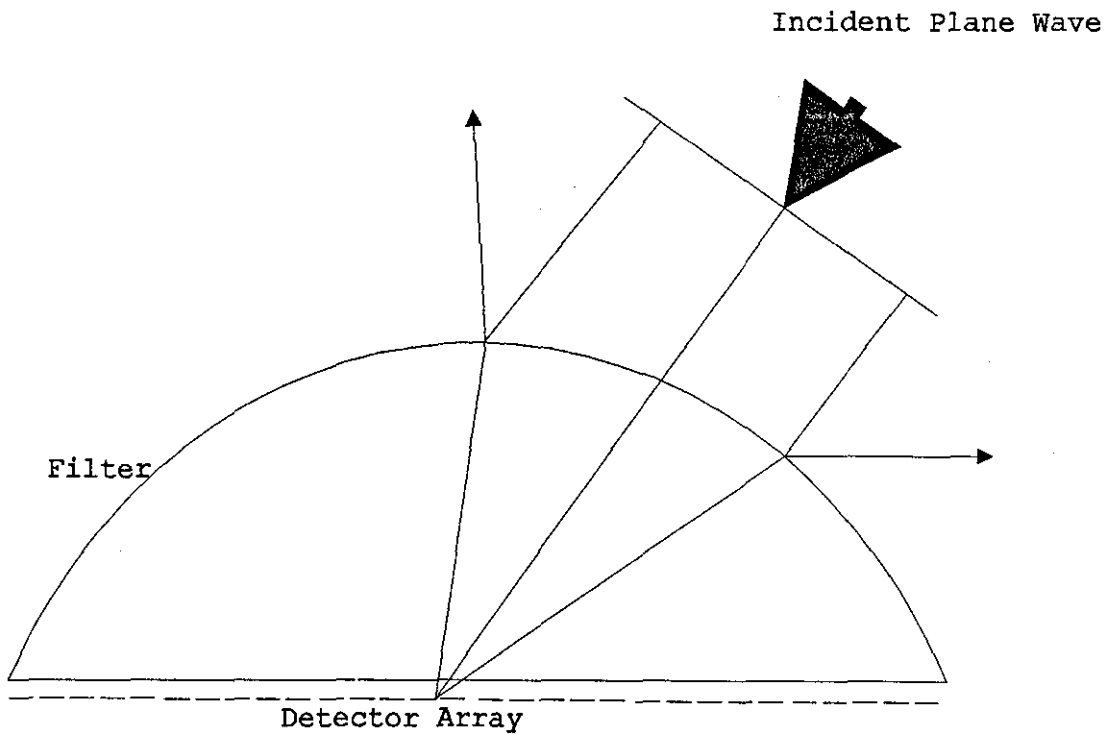


Figure 2.1 Schematic diagram of the passive antenna setup

The detector array lies in the horizontal plane and is surmounted by a dome shaped filter with spherical symmetry. It is assumed that the detector lies in the far field of a given EM source so that phase fronts arriving at the outer surface are plane. The filter is designed to admit radiation at or near its local normal so that a given source will penetrate the outer dome at a

particular angle with respect to the origin of spherical symmetry. The filter can also be tuned to admit radiation of a specific frequency band.

Finally a detector array is added in a plane parallel to the horizontal at some optimal vertical position. Although the array may be similar to a conventional phased array its task is somewhat different. It must make individual measurements of signal amplitude at each element rather than many measurements of the same signal. The resolving power of a conventional array is therefore lost but is replaced by the action of the filter. Information contained in the outputs of the detector elements can be used to effect real time control of a steerable antenna mounted in the same inertial frame as the detector. Some adjustments may be necessary for non-linearities in the operation of the detector and parallax errors between detector and antenna, but these can be determined and preset without the need for changes. Because of the shape and physical property of the complete system it seems appropriate to use the acronym **redome** to indicate "refracting dome" detector. What follows is a more detailed description and analysis of each detector component.

### 2.3 The Filter Dome

It is recalled that the filter will be designed to admit a specific frequency range at or near normal incidence. The external dimension of the dome is chosen so that the surface is locally flat with respect to wavelengths of interest. The dome will therefore typically exceed twenty wavelengths in diameter. The scattering properties of multilayer systems can also be achieved using a single inhomogeneous dielectric layer, which can be analysed and therefore designed in a simple way [2]. A review of some of these techniques can be found in [3].

A supplement or alternative to these techniques can be provided by a tuned frequency selective surface (FSS) on the outer layer of the dome. Frequency selective surfaces (dichroic surfaces) are doubly periodic arrays of conducting elements usually printed on a dielectric substrate[4,5]. FSS are transparent to incident electromagnetic waves of certain frequencies whilst being efficient reflectors of other spectral components. Specific transmission frequency responses of the surface can be achieved by judicious choice of parameters including element and lattice geometry, dielectric permittivity and thickness. The transmission response will also be a function of the angle of incidence and it is possible to design an FSS which will reflect radiation incident at angles other than normal[6].

#### 2.4 The Detector Array

The detector array will be placed at the focal plane of the dielectric lens in order to detect the radiation resulting from incoming convergent rays. Individual element excitations will be recorded and compared so that the direction of signals of interest (weak, strong or both) can be determined. There will not be active phasing or beam steering involved, thereby reducing the complexity of the hardware and processing which can be a limiting factor in conventional phased array applications. A number of array geometries could be used, depending on the specific requirements of the overall **redome** design. Arrays made up of elements such as waveguide feeds [7], microstrip patches[8] and simple linear dipoles are all possible configurations and have been exploited in many communications applications. The operating frequency band, polarisation, size and weight are prime factors influencing design. The element spacing will be chosen so that adequate information about the excited elements is retrieved without deterioration of the spatial resolution. The element spacing will not

necessarily be regular although azimuthal symmetry will probably be required.

### 2.5 Intelligent antennas vs. Sperry Dome antennas

There have been conflicting opinions regarding the similarity in the concept of the passive antenna, mentioned above and the Sperry dome antenna.[11]

Any dome structures perform electronic scanning with a active planar antenna array that is capable of providing hemispheric angle coverage. It uses a passive conformal lens to extend the scan range of a conventional array. But this conformal dome structure is studded with fixed, passive phase shifters. When selected portions of the interior of the dome are illuminated by a transmitted beam, the collective phase shift of the illuminated elements changes the direction of propagation of the energy from the feed array, acting as an RF analog to an optical prism. Thus, the planar feed array need not scan to as large an angle as is ultimately required.

Therefore a planar array, which is normally limited in its scan range to  $\pm 60^\circ$  or less can be improved by changing the beamsteering function by adding the dome which in turn increases the scanning abilities of such arrays.

In the case of an intelligent antenna system, the dome structure serves as a simple "strainer" of electromagnetic signals. Its preliminary intention is not to perform electronic scanning, though the chances cannot be ruled out completely. The dome's average dielectric constant is theoretically the same. This structure is technically much less complicated than the Sperry dome and is economically cheap to construct.

The position of the planar array in the intelligent antenna has to be optimised to avoid signal bunching on the array or the inability of the signals to reach the detector. The Sperry dome antenna system injects the signals into the planar array from any direction, as the dome surface acts as a prism. In other words the intelligent antenna is designed to admit signals which are normal to the locally planar area region of the filter dome and the rest are reflected. These filter domes could be used as a focusing object by altering certain parameters of the surfaces, as discussed in Chapter 6.

## **2.6 Reflection Losses and Polarisation Effects**

Losses at the filter dome will be large in the sense that only radiation incident near local normal will be transmitted. One can think of the filter as a collimator of incident plane waves with the axis of collimation being the direction of local normal. The collimated beam will not have a uniform amplitude distribution, however near the centre of the beam the Poynting flux should be only slightly less than that of the unfiltered incident radiation. Although the power loss can be reduced by applying matched layers of appropriate width and material permittivity, it is useful to consider the worst scenario where no matching is used. As a first approximation the losses can be estimated using geometrical optics, wherein the reflections are functions of the material

permittivity and loss factor of the DML and the angle of incidence. In the case of FSS, the reflections depend upon the periodicity between the elements or slots.

As the angle of incidence increases from  $0^\circ$  at normal incidence the amplitude reflection coefficient initially increases for Transverse Electric (TE) polarised waves and decreases for Transverse Magnetic (TM) polarised waves. For angles greater than the Brewster angle both polarisations have increasing amplitude reflectivity up to total reflection at grazing incidence. Most of the rays are incident between  $0^\circ$  and  $45^\circ$ . Since the Brewster angle is  $\tan^{-1}(\sqrt{\epsilon})$  at the entry surface and  $\tan^{-1}(1/\sqrt{\epsilon})$  at the exit surface, the majority of rays will refract at angles less than the Brewster angle as long as  $\epsilon \leq 3$ . In that case the reflection will only depend weakly on the angle of incidence for both TE and TM modes and will not exceed 10% of the initial intensity.

## 2.7 REMARKS

This chapter has presented an alternative solution to signal discrimination based on a novel detector. The system may enable signals to be classified according to the criteria: frequency band and propagation direction/amplitude. The two design elements corresponding to these criteria are the filter and the detector array. Since the external shape of the detector has a semi-spherical symmetry and EM radiation is refracted through the filter dome, the system has been termed a refracting dome or "redome" detector.

Applications of **redomes** would include signal tracking, when used in conjunction with a steerable antenna. In mobile radio communication systems for example, it is important to simplify the hardware and software demands made on the mobile to reduce weight, size, power

requirement and cost. A **redome** may have positive contributions to make in this context for several reasons. Firstly, the **redome** should be able to direct a steerable antenna in real time to track the strongest available signal. If a dominant signal is not available, the antenna could at least be directed into the sector of maximum signal strength. Since the **redome** incorporates a spectral filter this process can be selective with respect to a particular communication band. The second major advantage of the **redome** detector is that tracking is achieved without placing computational demands on the mobile itself, which would complicate its operation and slow its response to changes in the received signals and antenna position.

It may be possible to track more than one signal using a **redome** detector, which would enable existing advanced modem techniques such as maximum likelihood detection[12] to be supported. If necessary, multi-**redome** designs could be used to track signals. Another possible property of multi-**redome** systems would be communication channel selection, which could be achieved by tuning each detector filter into a different frequency band. Although the function of the **redome** as a signal discriminator has been stressed, it is likely that it could also be used as a highly selective, multi-signal receiver and therefore one cannot rule out its application to transmission also.

---

**References**

1. Henderson A. and James J.R., A survey of milli-metre wavelength planar antenna arrays for military applications, *The Radio and Electronic Engineer*, Vol. 52, No. 11/12, 1982, pp.543-550.
2. Hopcraft K.I. and Smith P.R., Geometrical solution for phase retrieval and the inverse scattering problem in one dimension, *Phys.Rev.Lett.* 60, 1988, pp.2622-2625.
3. Lekner J., *Theory of reflection of electromagnetic and particle waves*, 1987, Kluwer academic publishers group, UK.
4. Agrawal V.D. and Imbriale W.A., Design of a dichroic cassegrain subreflector, *IEEE Trans. AP-27*, 1979, pp.466-473.
5. Vardaxoglou J.C. and Parker E.A., Performance of two tripole arrays as frequency selective surfaces, *Electronics Letters* 19, 1983, pp.709-710.
6. Parker E.A. and Vardaxoglou J.C., Influence of single and multilayer dielectric substrates on the band spacing available from a concentric ring frequency selective surface, *Int.J.Electron.* 61, 1986, pp.291-297.
7. Amitay N., Galindo V. and Wu C.P., *Theory and analysis of phase array antennas*, 1972, Wiley, New York.
8. James J.R., Hall P.S. and Wood C., *Microstrip antenna theory and design*, 1981, Peter Peregrinus Ltd, UK.
9. Evans S., Clouston E.N. and Reader H.C., Gates and domains, *Proc.IEE Colloquium on advances in the direct measurement of antenna radiation characteristics in indoor environments*, 1989, pp.211-213.

10. Macrae R. and Hji pieris G., Use of scalar data to locate faults in the time domain, *Microwaves and RF* 28, No.1, 1989, pp.105-110.

11. Schwartzman L. and Stankel J., The dome antenna, *Microwave Journal*, Oct 1975, pp.31-34.

12. Clark A.P., Digital modems for land mobile radio, *Proc. IEE Pt. F*, 132, 1985, pp.348-362.

## CHAPTER 3

## DIELECTRIC MULTILAYERS

## 3.1 Introduction to Multilayers

Dielectric multilayers have received increased attention in the avenue of optical research, owing to their unique characteristics in impedance matching, polarisation control and reduction in the operational bandwidth. In science and technology a need exists for multilayer filters with an ever increasing complexity of performance. Periodic dielectric multilayer stacks of two different refractive indices in each period have been widely studied for their use in narrow band filters, broadband reflectors, edge filters etc.[1,2,3], in the optical regime. The concept of filtering optical signals by placing a dielectric material with thin film coatings is well established[3].

Frequently, research workers in optics are confronted with the problem of obtaining an optical filter which has a specific spectral transmission function. In most of the cases they use filters which depend upon the selective absorption of individual layers. These multilayers are normally made up of stacks of materials of different permittivities at different thicknesses. The thicknesses of the layers are normally fractional multiples of the wavelength of the signal, in that particular material. The analogy of microwave multilayer filters with optical filters as band-pass frequency devices is well known[4]. The optical filter is also an analogue of the waveguide filter[5].

In the optical sense, since  $\lambda$  is very small (of the order of  $\mu\text{m}$ ), the fractional multiples (say  $\lambda/4$  or  $\lambda/2$ ) are also very small. But in the microwave region, as the frequency reduces from the optical region,  $\lambda$  increases, which in turn increases the thickness of the layers compared with that of the optical filters.

An optical multilayer is usually modelled by assuming that the individual layers of the system are thin, plane parallel, isotropic, homogeneous, scatterless, lossless and have abrupt interfaces. Given such a model, it is a relatively straight forward matter, using matrix methods, to analyse the performance of a multilayer and to calculate any or all of the related quantities of interest. But in the case of a microwave multilayer filter, the thicknesses of the individual layers are larger compared to their optical counterparts, due to higher wavelengths. As a consequence, the dielectric loss associated with each layer contributes significantly to the overall performance of the multilayer filter.

A dielectric multilayer can be theoretically designed to give any desired transmission over a specified bandwidth, but the realisation of the material in practice imposes a severe constraint at microwave frequencies. Ideally the designer wants to have control over the material permittivity, permeability and loss tangent. But the fundamental problem concerns the dearth of material having a relative permittivity  $\epsilon_r$  significantly greater than unity at frequencies in the microwave band, so that the thickness of the material can be realised practically.

Figure 3.1 shows a standard DML bandpass filter having five homogeneous layers, with the thickness of the high permittivity layer at the centre being  $\lambda/2$  and the rest of the high permittivity layers  $\lambda/4$ . The thickness of the low permittivity layers is  $\lambda/2$ .

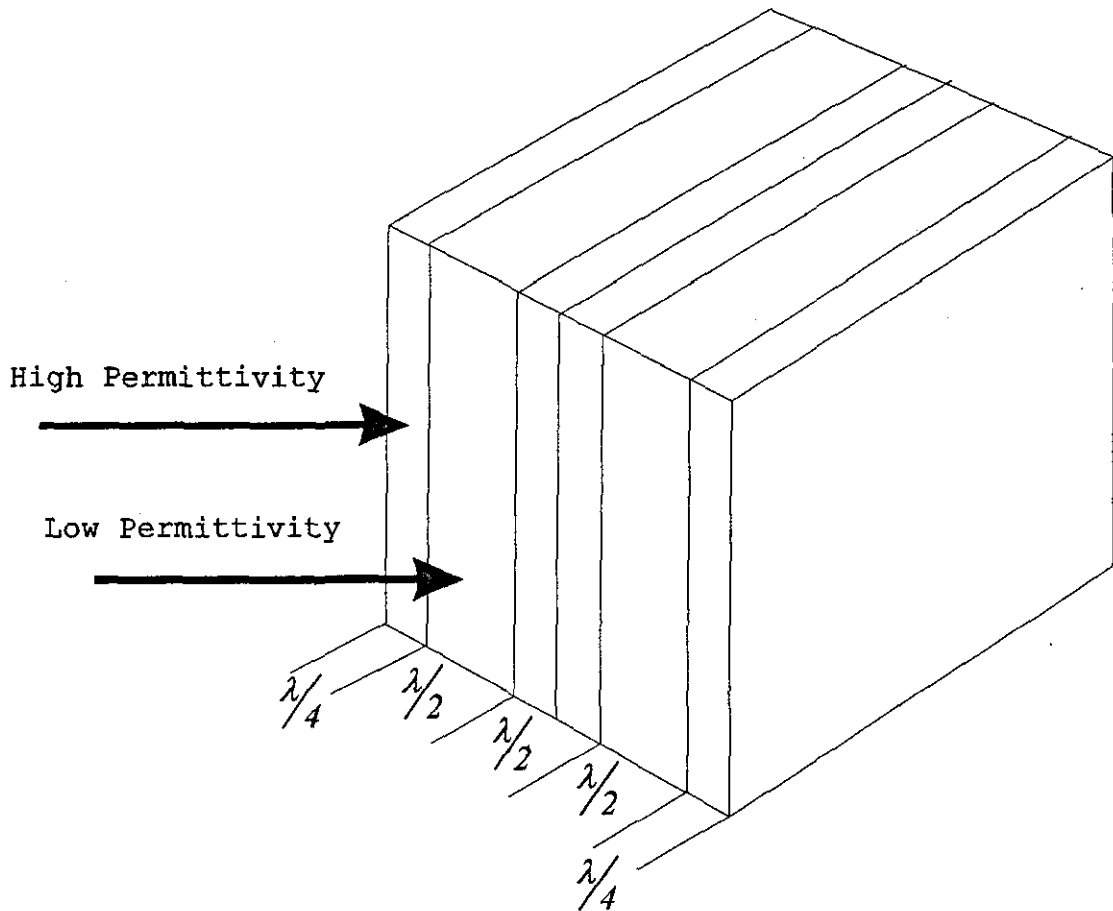


Fig 3.1 Dielectric Multilayer Filter

The applications of these multilayer filters in the microwave region is practically less popular, though there is some renewed interest in the area of microstrip antennas. Jackson[6] used a multilayer stack to cover a microstrip antenna which resulted in the reduction the radar cross section of the antenna. Bonvin et al[7] used a single layer of thick slab to obtain the same effect. Or in other words, in a rather broad sense these structures are employed to serve as radomes. Radomes[8] are electromagnetic windows, consisting of different dielectric layers as well as metal meshes. The primary intention of such structures was to protect the antenna systems from damages and from environmental hazards. To

achieve this, radomes are required to be structurally stable and designed to give low attenuation under certain operating conditions.

In this chapter the mathematics of transmission and reflection properties of the dielectric multilayer is reviewed for the sake of completeness. Full details of the derivation can be obtained in the literature[9,10]. Initially a formulation is made for a planar media and then it is viewed in terms of DML. Also, gradient optimisation methods are implemented to reduce the transmission losses of the DML.

### **3.2 Material Characteristics**

For a material to be efficient as a filter, it should not attenuate the signals passing through it. Or, in other words the loss tangent( $\tan \delta$ ) of the material should be as low as possible. The thickness of the material should be uniform throughout. Irregular surfaces, of course alter the resonant frequency of the structure, which, in fact, disturbs the transmission.

Alumina substrates[11] are recommended for this purpose, since they can be machined with tolerances of fractions of millimetres. The electrical characteristics of the low permittivity polystyrene layers, also play an important role in the filter realisation. Throughout this thesis, it is assumed that the permittivity of the polystyrene material is close to that of free space. The overall weight of the laminates should be as low as possible to enable them to compete with other lightweight systems.

### **3.3 Theory**

It has long been appreciated that dielectric multilayer structures can exhibit characteristics of a spectral filter with respect to EM radiation[9]. Accurate filter

designs are feasible since it is straightforward to model the transmission and reflection properties of a series of homogeneous layers. Although the direct problem is thereby solved, it is not trivial to invert the process and provide a multilayer design to effect a particular filter. The so-called inverse problem only has solutions for particular geometries and or materials. Even if the inverse problem is solved, design compromises are inevitably imposed by the availability of the material parameters.

Multilayer thin films have been designed to achieve maximum (minimum) transmission for a given frequency band and for radiation incident at a given angle. If maximum transmission is required at normal incidence, a standard approach is to construct a laminate of two materials arranged in an alternating sequence. The frequency response of such structures depends on the optical depth of the layers, which must be designed to be resonant with respect to the appropriate frequency band. For optimum effect the two materials must be composed of contrasting dielectric permittivity (usually termed high and low). The simple combination high-low-high-high-low-high (Figure 3.1) is investigated. The structure will resonate when the optical depth of the high permittivity layer is a quarter wavelength and the optical depth of the low permittivity layer is a half wavelength. By this arrangement of thicknesses there will not be any phase difference at the output of the filter. These laminar structures exhibit several pass and stop bands which can be controlled by adjusting the composition, dimension and the number of layers used. Here the requirement of angular filtering is more stringent than a pass band spectral filter since the angular degree of freedom must also be constrained. The particular nature of this extra constraint is unusual in the context of thin film technology and has necessitated some novel design work.

### 3.3.1 WAVES IN A DIELECTRIC LAYER

When a plane wave is in free space ( $\epsilon_r=1$ ,  $\tan \delta=0$ ), it travels along at the velocity of light. This is the velocity of a constant phase point on the wave and is called the phase velocity. But when it travels through a homogeneous dielectric material with a relative permittivity greater than 1, the new velocity will be,

$$v = \frac{c}{\sqrt{\epsilon_r}} \quad (3.1)$$

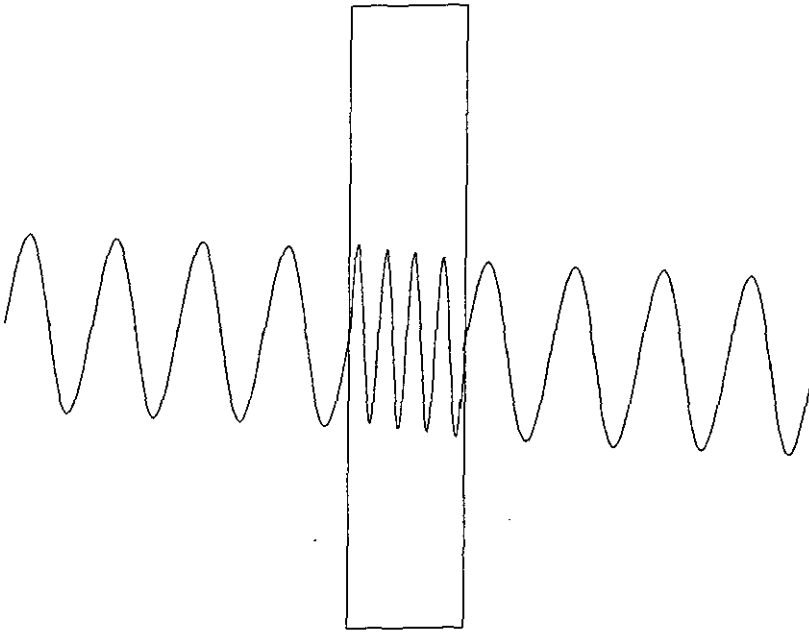


Fig 3.2 Signal travelling through a dielectric slab.

This shows that the wave slows down in comparison with the velocity in free space and the wavelength of the signal in the dielectric will be

$$\lambda' = \frac{\lambda}{\sqrt{\epsilon_r}} \quad (3.2)$$

This is shorter than the free space wavelength. The wave is bunched in the dielectric as it slows down and the wavelength decreases as shown in Figure 3.2.

### 3.3.2 GOVERNING ELECTROMAGNETIC EQUATIONS

This section of the chapter deals with the mathematics involved in the design of a dielectric multilayer filter. Here, the different layers of the DML are assumed to be made of homogeneous, dielectric and lossy material. Since the antenna theory is based on classical electromagnetic theory as described by Maxwell's equations, it would be proper to begin with a brief review of electromagnetic phenomena.

The electric and magnetic fields are vector fields dependent on spatial co-ordinates,  $x$ ,  $y$ ,  $z$  and time  $t$ . Fourier transforms of the Maxwell's equations are taken to translate from the time domain to spectral domain, and in that case all time derivatives may be replaced by  $-j\omega$ .

In a homogenous dielectric medium, the transformed Maxwell's equations are as given below:

$$\underline{\nabla} \times \underline{E} = j\omega \underline{B} \quad (3.3a)$$

$$\underline{\nabla} \times \underline{H} = -j\omega \underline{D} + \underline{J} \quad (3.3b)$$

$$\underline{\nabla} \cdot \underline{B} = 0 \quad (3.3c)$$

$$\underline{\nabla} \cdot \underline{D} = \mathcal{P} \quad (3.3d)$$

Since a dielectric medium is under consideration here, the constitutive relations are assumed to be:

$$\underline{D} = \epsilon_0 \epsilon'_r \left( 1 + j \frac{\epsilon''_r}{\epsilon'_r} \right) \underline{E} \quad (3.4a)$$

$$\underline{B} = \mu_0 \underline{H} \quad (3.4b)$$

where the ratio  $\epsilon''_r/\epsilon'_r$  is usually replaced by the loss tangent  $\tan \delta$ .

### 3.3.3 Vector wave equation

Following substitution of the constitutive relations into Maxwell's equations, the Helmholtz vector wave equation is obtained as[12]

$$\left( \underline{\nabla}^2 + k^2 n^2(x) \right) \Psi = 0 \quad (3.5)$$

where  $n^2(x) = \epsilon'_r(x) \left( 1 + j \frac{\epsilon''_r(x)}{\epsilon'_r(x)} \right)$  in which  $n(x)$  denotes the refractive index,  $\Psi$  is either electric( $\underline{E}$ ) or magnetic( $\underline{H}$ ) vector potential and  $k$  is the free space wave number.

Equation (3.5) is a Helmholtz wave equation for uniform and homogeneous regions. The next section deals with the

formulation of the wave equation for a dielectric sheet for both TE and TM incidence.

### 3.4 Formulation of the Field

In this section the formulation of the field characteristics of a dielectric slab is presented. A dielectric slab possessing a relative dielectric constant  $\epsilon_r$  and with a loss tangent  $\tan \delta$  is situated in a lossless, homogeneous medium, here assumed to be air ( $\epsilon_r = 1.0$ ), is illuminated by a plane wave.

#### 3.4.1 TE Component

For a planar interface (Figure 3.3) lying in the  $yz$  plane and an electromagnetic plane wave propagating in the  $z$  and  $x$  directions, the TE component has  $\underline{E} = (0, E_y, 0)$ .

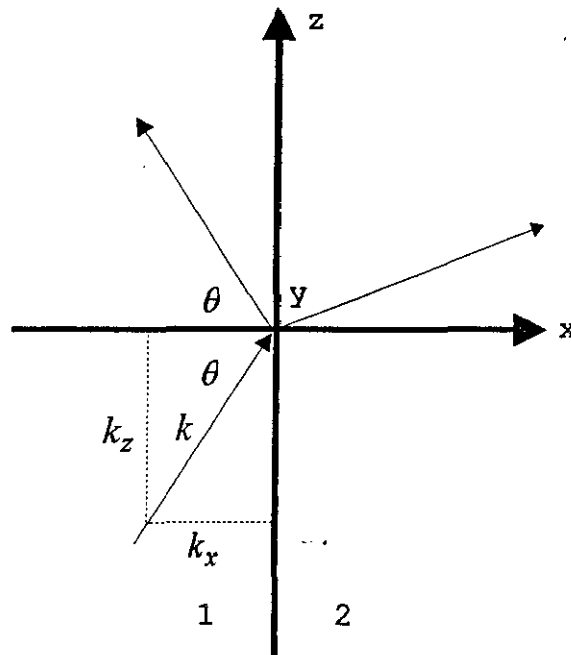


Figure 3.3 A Planar interface

Equation 3.5 can be written in scalar form to represent the x, y and z components.

$$\left(\partial_x^2 + \partial_y^2 + \partial_z^2 + k^2 n^2(x)\right)(E_x, E_y, E_z) = 0 \quad (3.6)$$

But for the TE mode the E vector has only a component in the y direction. Then equation 3.6 can be modified as follows:

$$\left(\partial_x^2 + \partial_z^2 + k^2 n^2(x)\right)(0, E_y, 0) = 0 \quad (3.7)$$

Assuming that the incident medium ( $n_1$ ) is uniform,  $E_y$  has the general solution[10]

$$E_y = E(x)(A \cdot \exp(jkn_1 \sin \theta z) + B \cdot \exp(-jkn_1 \cos \theta z)) \quad (3.8)$$

Now the wave number in the z direction can be derived from Figure 3.3 and it is given as  $k_z = kn_1 \sin \theta$ . For the single interface shown in Figure 3.3 waves propagate in the +z direction only and therefore the second term in (3.8) is omitted. Following a substitution into (3.7), the reduced wave equation is obtained as follows:

$$\left(\partial_x^2 + k^2 n^2(x) - k^2 n_1^2 \sin^2 \theta\right)E(x) = 0. \quad (3.9)$$

Equation (3.9) can be rewritten as

$$\left( \partial_x^2 + k^2 n_1^2 \left[ \frac{n^2(x)}{n_1^2} - \sin^2 \theta \right] \right) E(x) = 0 \quad (3.10)$$

which can be abbreviated as

$$\left( \partial_x^2 + q^2 \right) E(x) = 0 \quad (3.11)$$

where

$$q^2 = k^2 n_1^2 \left( \frac{n^2(x)}{n_1^2} - \sin^2 \theta \right) \quad (3.12)$$

### 3.4.2 TM Component

The vector wave equation  $(\nabla^2 + k^2 n^2(x)) \underline{H} = 0$  can be solved similar to TE, except the fact that the boundary conditions are different. But, because of the simplicity it is approached in the following manner.

$\underline{H}$  is represented as  $(0, H_y, 0)$  for TM modes, so that

$$\nabla \times \underline{H} = (-\partial_z H_y, 0, \partial_x H_y) \quad (3.13)$$

and

$$\underline{\nabla} \times \frac{(\underline{\nabla} \times \underline{H})}{n^2(\mathbf{x})} = \left( 0, \partial_x \left( \frac{1}{n^2(\mathbf{x})} \partial_x H \right) + \partial_z \left( \frac{1}{n^2(\mathbf{x})} \partial_z H \right), 0 \right) \quad (3.14)$$

Thus the wave equation is modified to

$$\partial_x \left( \frac{1}{n^2(\mathbf{x})} \partial_x H \right) + \frac{1}{n^2(\mathbf{x})} \partial_z^2 H + k^2 H = 0 \quad (3.15)$$

Similar to the TE modes the wave number in the  $z$  direction is  $kn_1 \sin \theta$ .

Therefore

$$\partial_x \left( \frac{1}{n^2(\mathbf{x})} \partial_x H \right) + \frac{1}{n^2(\mathbf{x})} (k^2 n^2(\mathbf{x}) - k^2 n_1^2 \sin^2 \theta) H = 0 \quad (3.16)$$

Equation (3.16) can be written as

$$\partial_x \left( \frac{1}{n^2(\mathbf{x})} \partial_x H \right) + \left( \frac{q^2}{n^2(\mathbf{x})} \right) H = 0. \quad (3.17)$$

The variable is changed here because it makes the derivation easier to represent in a Helmholtz equation and can be directly compared with the TE mode. Then changing the variable to  $x'$ ,

$$x' = x \cdot n^2(x) \quad (3.18)$$

$$\partial_x H = n^2(x) \partial_{x'} H \quad (3.19)$$

and

$$n^2(x') \partial_{x'}^2 H + \left[ \frac{q^2}{n^2(x')} \right] H = 0 \quad (3.20)$$

which results in

$$[\partial_{x'}^2 + Q^2] H = 0 \quad (3.21)$$

where

$$Q = \frac{q}{n^2(x')} \quad (3.22)$$

The boundary conditions required to satisfy the requirements are discussed in the next section.

### 3.5 Boundary Value Problem Formulation

The geometry treated here, is that of a multilayer structure (Figure 3.4), which has arbitrary values of widths and other electrical parameters. It is assumed that the multilayer is placed in free space, so that signal propagation takes place from one end of the free space through the multilayer to the other end.

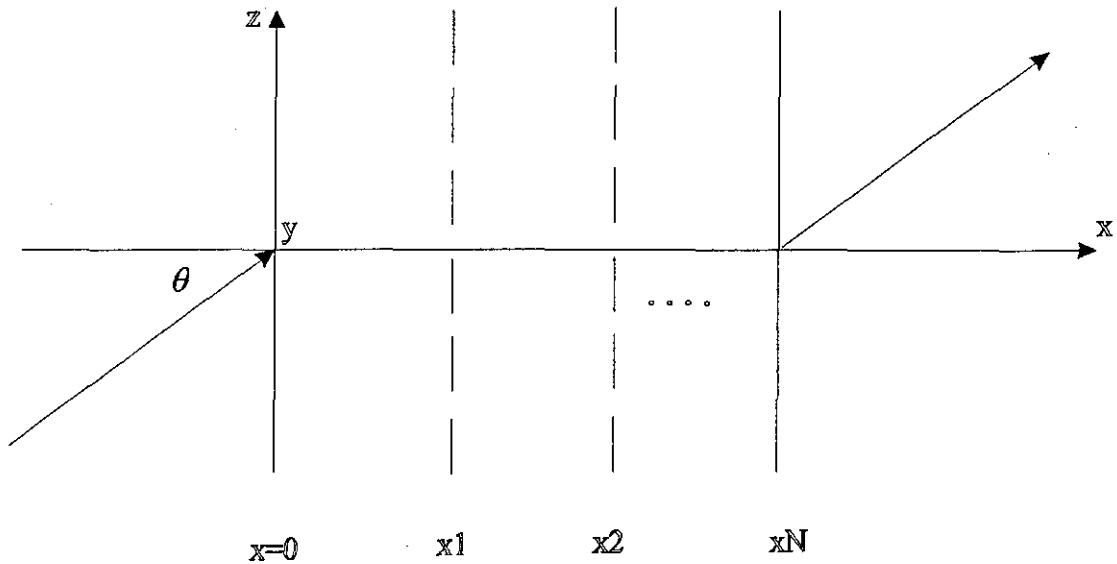


Figure 3.4 A Multilayer Structure with N Slabs

Thus outside the multilayer, 3.12 becomes,

$$q_0^2 = k^2 \cos^2 \theta \quad (3.23)$$

So it is necessary to solve

$$\left( \partial_x^2 + \begin{bmatrix} q_n^2 \\ Q_n^2 \end{bmatrix} \right) \begin{bmatrix} \mathbf{E} \\ \mathbf{H} \end{bmatrix} = 0 \quad (3.24)$$

within the slabs, where

$$q_n^2 = k^2(n_n^2 - \sin^2 \theta) \quad (3.25)$$

Dielectric Multilayer consists of a number of interfaces between various dielectric layers and the signal throughput in the multilayer has to be deduced after formulating the expressions for these scattered fields between these interfaces. In Figure 3.1, a schematic diagram of a DML is shown. It is assumed that the medium is absorption free and that a plane wave is incident on one side of the DML. At the boundaries, the tangential components of  $\underline{\mathbf{E}}$  and  $\underline{\mathbf{H}}$  are continuous across it, since dielectric materials are used as individual layers. The first interface is defined by  $x = 0$ . The tangential components must be continuous for all values of  $y$ ,  $z$  and  $t$ .

The plane wave is split into a reflected wave and a transmitted wave at the interface and the reflection and the transmission coefficients of these signals have to be calculated. It is certain that these signals have an amplitude and a phase term and these waves are represented as follows

For region  $x \leq 0$ , the solution is

$$e^{jq_0x} + R e^{-jq_0x},$$

In layer 1,

$$F_1 e^{jq_1 x} + B_1 e^{-jq_1 x}.$$

Thus, in the  $n^{\text{th}}$  layer, The above equation becomes

$$F_n e^{jq_n x} + B_n e^{-jq_n x}.$$

For the region  $x > x_n$ , there will not be any reflected signal, and the transmitted signal is given by

$$T e^{jq_0 x}.$$

In these equations,  $F$  and  $B$  represent the forward and backward scattered fields and  $R$  and  $T$  represent the backward scattered field from the first interface and the forward scattered field from the  $n^{\text{th}}$  interface.

Now consider the  $n^{\text{th}}$  layer /  $(n+1)^{\text{th}}$  layer interface. The boundary conditions are

1. The continuity of the tangential  $\underline{E}$  and  $\underline{H}$  at every interface.
2. The derivatives of  $\underline{E}$  and  $\underline{H}$  are continuous at every interface.

i.e.,

$$F_n e^{j\alpha_n x_n} + B_n e^{-j\alpha_n x_n} = F_{n+1} e^{j\alpha_{n+1} x_n} + B_{n+1} e^{-j\alpha_{n+1} x_n} \quad (3.26)$$

$$j\alpha_n (F_n e^{j\alpha_n x_n} - B_n e^{-j\alpha_n x_n}) = j\alpha_{n+1} (F_{n+1} e^{j\alpha_{n+1} x_n} - B_{n+1} e^{-j\alpha_{n+1} x_n}) \quad (3.27)$$

which results in

$$F_{n+1} = F_n \frac{1}{2} \left( 1 + \frac{\alpha_n}{\alpha_{n+1}} \right) e^{j(\alpha_n - \alpha_{n+1}) x_n} + B_n \frac{1}{2} \left( 1 - \frac{\alpha_n}{\alpha_{n+1}} \right) e^{-j(\alpha_n + \alpha_{n+1}) x_n} \quad (3.28)$$

Similarly

$$B_{n+1} = F_n \frac{1}{2} \left( 1 - \frac{\alpha_n}{\alpha_{n+1}} \right) e^{j(\alpha_n + \alpha_{n+1}) x_n} + B_n \frac{1}{2} \left( 1 + \frac{\alpha_n}{\alpha_{n+1}} \right) e^{-j(\alpha_n - \alpha_{n+1}) x_n} \quad (3.29)$$

Equations (3.28) and (3.29) can be written in the following matrix form for TE mode.

$$\begin{bmatrix} F_{n+1} \\ B_{n+1} \end{bmatrix} = \begin{bmatrix} \frac{1}{2} \left( 1 + \frac{\alpha_n}{\alpha_{n+1}} \right) e^{j(\alpha_n - \alpha_{n+1}) x_n} & \frac{1}{2} \left( 1 - \frac{\alpha_n}{\alpha_{n+1}} \right) e^{-j(\alpha_n + \alpha_{n+1}) x_n} \\ \frac{1}{2} \left( 1 - \frac{\alpha_n}{\alpha_{n+1}} \right) e^{j(\alpha_n + \alpha_{n+1}) x_n} & \frac{1}{2} \left( 1 + \frac{\alpha_n}{\alpha_{n+1}} \right) e^{-j(\alpha_n - \alpha_{n+1}) x_n} \end{bmatrix} \begin{bmatrix} F_n \\ B_n \end{bmatrix} \quad (3.30)$$

Similarly for TM mode a similar matrix can be derived as

$$\begin{bmatrix} F_{n+1} \\ B_{n+1} \end{bmatrix} = \begin{bmatrix} \frac{1}{2} \left( 1 + \frac{Q_n}{Q_{n+1}} \right) e^{j(Q_n - Q_{n+1})x'_n} & \frac{1}{2} \left( 1 - \frac{Q_n}{Q_{n+1}} \right) e^{-j(Q_n + Q_{n+1})x'_n} \\ \frac{1}{2} \left( 1 - \frac{Q_n}{Q_{n+1}} \right) e^{j(Q_n + Q_{n+1})x'_n} & \frac{1}{2} \left( 1 + \frac{Q_n}{Q_{n+1}} \right) e^{-j(Q_n - Q_{n+1})x'_n} \end{bmatrix} \begin{bmatrix} F_n \\ B_n \end{bmatrix} \quad (3.31)$$

Using these matrices the transmission and reflection coefficients, the scattered fields can be computed for various interfaces. It is necessary to bear in mind that the difference in  $q_n$  and  $Q_n$  is modified by the introduction of the variable  $x'_n$ . Hence during computer manipulations it is not necessary to divide  $q_n$  by  $n^2$  to change from TE to TM.

### 3.6 Numerical Results

Equations 3.30 and 3.31 can be used to simulate the effects of transmission responses with variations in the thicknesses of the individual layers as well as with variations in the permittivity of the dielectric layers.

Figure 3.5.a shows the variation of the frequency responses with variations in the thickness of the low permittivity layer. Here, the thickness of the centre melamine layer is fixed at 1.6 mm ( $\lambda/2$ ) and the rest of the melamine layers at 0.8 mm ( $\lambda/4$ ). The thickness of the low permittivity layer was varied from 0.5 mm to 10 mm. As the thickness increases the resonance becomes visible in the spectrum. The resonance start to move from low frequency region to the high frequency region. Immediately after this narrowband resonance, which can be termed as second order resonance for obvious reasons a broad bandwidth of transmission response is observed

which comprises the zero order and the first order resonances. At 10 mm the transmission response has the zero order resonance set at ~33 GHz. The first order resonances are noted at ~31.5 GHz and ~34.5 GHz. The second order resonances are observed at ~27 GHz and 39 GHz. The narrow bandwidth of the second order resonance is noted, especially for applications in narrowband filters and for frequency dependent beam steering applications.

Similarly from Figure 3.5.b, the variations of the transmission responses with variation in the thickness of the high permittivity region is shown. The thickness of the low permittivity region is maintained at 4.2 mm ( $\lambda/2$ ) and that of the high permittivity layer is varied from 0.5 mm to 10 mm. As the thickness increases the transmission coefficients become more and more wavy in nature. A sharp response in the transmission coefficients is obtained at ~31.5 GHz, when the thickness of the dielectric layer is 0.05 mm. It is apparent that for a given thickness of low permittivity layer, a thin coating of dielectric layer is required to provide a narrow bandwidth signal. In a practical sense, this fact entirely depends on how strong mechanically the low permittivity region is.

A smooth response in the transmission response has resulted as in Figure 3.5.c, when the permittivity of the dielectric layer is varied from 2 to 10. The dielectric layer thicknesses are kept the same as for the results in Figure 3.5.a. The low permittivity layer thickness is 4.2 mm. The frequency response becomes more and more sharp with increasing permittivity. A clear discrimination of frequency is observed around ~28 GHz when the permittivity is 8.0. But this results in a reduction of the transmitted signal amplitude.

**Simulated frequency response of a 5-layer DML.**  
At normal incidence as the thickness of the low permittivity layer varies

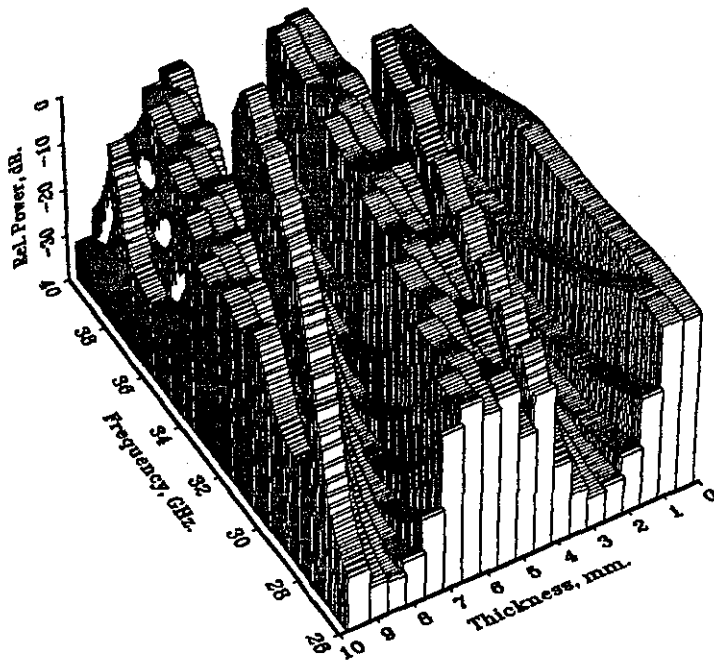


Figure 3.5.a

**Simulated frequency response of a 5-layer DML.**  
At normal incidence as the thickness of the high permittivity layer varies

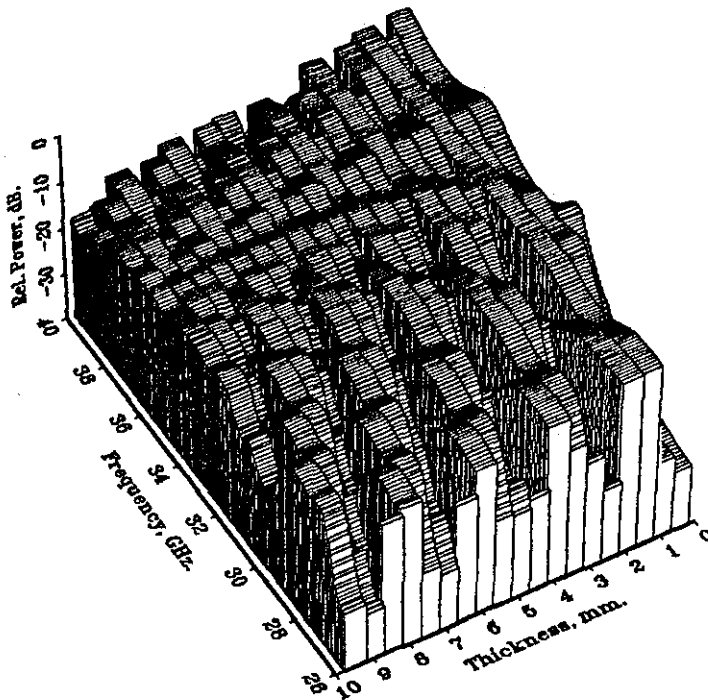


Figure 3.5.b

Simulated frequency response of a 5-layer DML.  
At normal incidence as the permittivity of the dielectric layer varies.

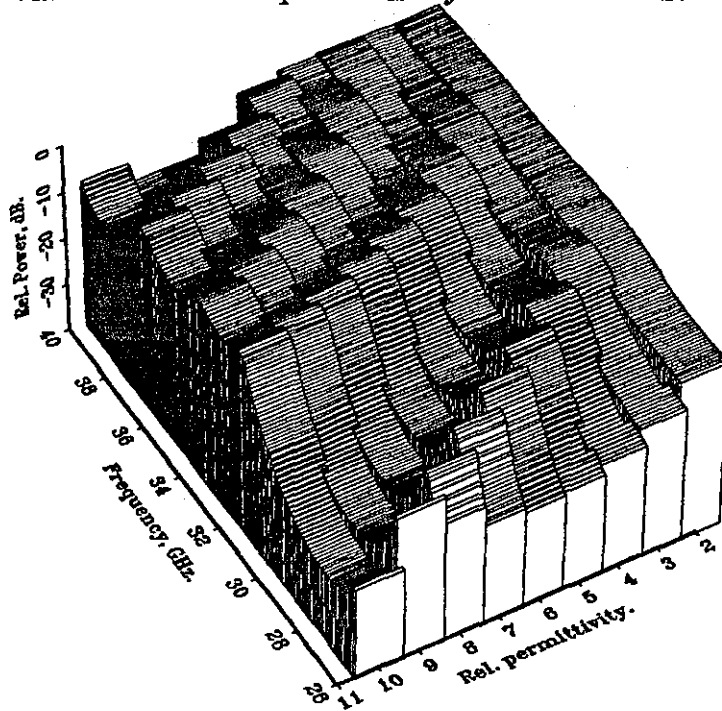


Figure 3.5.c

Simulated frequency response of a 5-layer DML.  
At various incidences as the thickness of the layers remain the same.

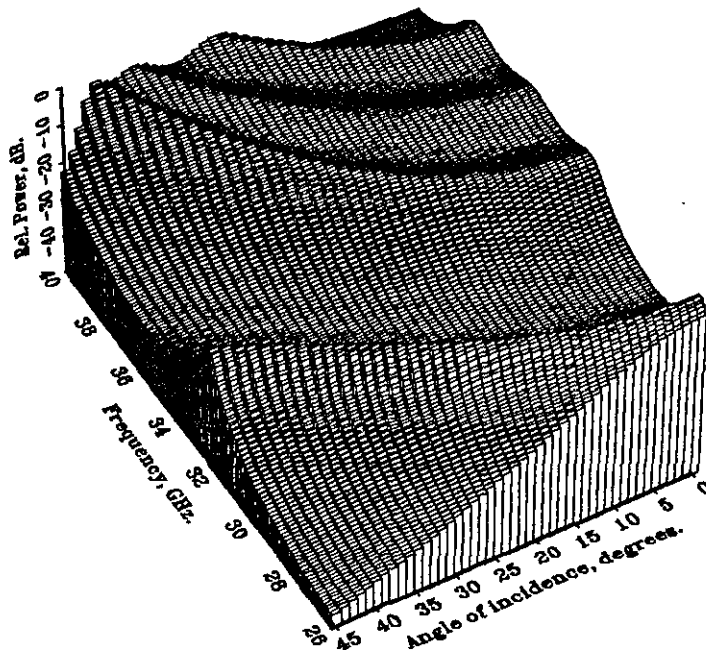


Figure 3.5.d

Figure 3.5.d shows the variation of the transmitted power in terms of angle of incidence and frequency. The thicknesses of the low and high permittivity regions are 4.2 mm and 0.8 mm. The required filtering action in this case is at  $0^\circ$  incidence. Above  $0^\circ$  incidence the signal strength at boresight reduces. At 36 GHz and above at normal incidence the filtering action has more than one peak which denotes the presence of higher order modes. At higher angles of incidences the zero and first order modes move to the high frequency regime leaving in the scene with the second order mode.

### 3.7 Attenuation Properties of a Multilayer

The propagation constant ( $\gamma$ ) of an electromagnetic signal, at a frequency  $f$ , in a medium having permittivity  $\epsilon_0\epsilon_r$  is given by [13]

$$\gamma = \alpha + j\beta = j2\pi f\sqrt{\epsilon_0\epsilon_r} \quad (3.32)$$

where  $\epsilon_r = \epsilon_r' - j\epsilon_r''$ ,  $\alpha$  - the attenuation constant and  $\beta$  - the phase constant. On equating the real parts of equation (3.32):

$$\alpha = 2\pi f\sqrt{\epsilon_0} \sqrt{\frac{\epsilon_r'}{2} \left[ \sqrt{(1 + \tan^2 \delta)} - 1 \right]} \quad (3.33)$$

where

$$\tan \delta = \frac{\epsilon_r''}{\epsilon_r'} \quad (3.34)$$

Here to satisfy the condition of low attenuation and maximum transmission it can be seen from equation (3.34), that  $\tan \delta$  should be as low as possible. That clearly indicates that  $\epsilon_r'$  should be high and  $\epsilon_r''$  should be low.

### 3.8 OPTIMISATION TECHNIQUE TO REDUCE THE LOSSES

Dielectric materials have inherent disadvantages, such as high loss factor, inaccuracy in machining to the required thickness etc. As the thicknesses of these layers increase the loss factor becomes more and more dominant and this results in the reduction of transmitted power through the multilayer. In a practical situation, it is necessary to have more power transmitted, within the dielectric characteristic parameters. The parameters at our disposal for solving the optimisation are numbers of layers, electrical parameters of each layers and the thickness of the layers. In this context the thickness of the high permittivity layer is kept constant as it is difficult to machine to its finest details. The only other way to optimise the performance is by varying the thickness of the air gap. In order to achieve maximum transmission, an optimisation method to vary the gap thickness is proposed and carried out.

#### 3.8.1 Basic concepts of the optimisation algorithm

Optimisation problems surface regularly in many technical and statistical applications and there has been considerable interest in global function optimisation[14]. The optimisation algorithm used here, can be applied to the optimisation of problems where many parameters are involved. The development of the standard method described here, was motivated by the behaviour of

multilayer structures with a large number of degrees of freedom. In this context, large means so large as to preclude any exhaustive analysis of the possible states of the system and admitting only the possibility of a statistical analysis.

Here a simple gradient descent algorithm is used to find the extrema of a cost function (CF) which is chosen to maximise the transmitted power. Starting from an arbitrary initial estimate, this algorithm introduces in each iteration a slightly modified estimate, for which the cost is calculated. The new estimate is then advanced or reversed according to whether the CF has decreased or increased. Moving from one estimate to another, it tries to find the local minimum of the CF. Here a one dimensional optimisation procedure is carried out by optimising the thickness of the low permittivity region at a fixed frequency.

#### 3.8.1.1. One dimensional optimisation

In this technique, the optimisation is carried out for one parameter. i.e., for air gap thickness. At any instance, the frequency is assumed to be constant and the other parameter i.e., the thickness is optimised to get maximum signal transmission.

Consider the design of a multilayer that operates between frequencies  $f_1$  and  $f_2$ . For a fixed thickness the transmittance of the fundamental as well as other modes will be governed by the loss factor of the higher permittivity layer as the low permittivity layer is assumed to be air. Here the main object is to find the thickness at which the signal transmission is maximum by optimisation.

To proceed with such an optimisation one needs to know the definition of a cost function, choice of an initial

estimate of the thickness and an initial increment of thickness. For each estimate it is required to find out the power transmitted and compare it with the next value of thickness. The CF which has to be minimised is defined as the difference in the transmitted power.

The CF which is required to minimise is given as:

$$CF = (1 - T_n) \quad (3.35)$$

where

$T_n$  -transmitted power at the  $n^{\text{th}}$  iteration.

$thilp_n$ -thickness of the air gap at the  $n^{\text{th}}$  iteration.

It may be interesting to include in the above equation, terms expressing a *a priori* information (smoothness, upper and lower bounds) or a regularisation term. Here  $\mu$  is chosen as a seed factor. The value of the seed factor is chosen according to the dynamical range expected for the new thickness. i.e., small enough to satisfy the required precision and yet large enough to enhance convergence speed.

The new value of the thickness after each iteration is given as

$$thilp_{n+1} = thilp_n - \mu \cdot CF \cdot \frac{\partial CF_n}{\partial thilp_n} \quad (3.36)$$

By following this approach, it is expected to reach the most required local maxima. 'Required' is defined in terms of minimal value of the cost function. It is envisaged that such an optimisation can be carried out for events when only one parameter is stable while the other is unstable.

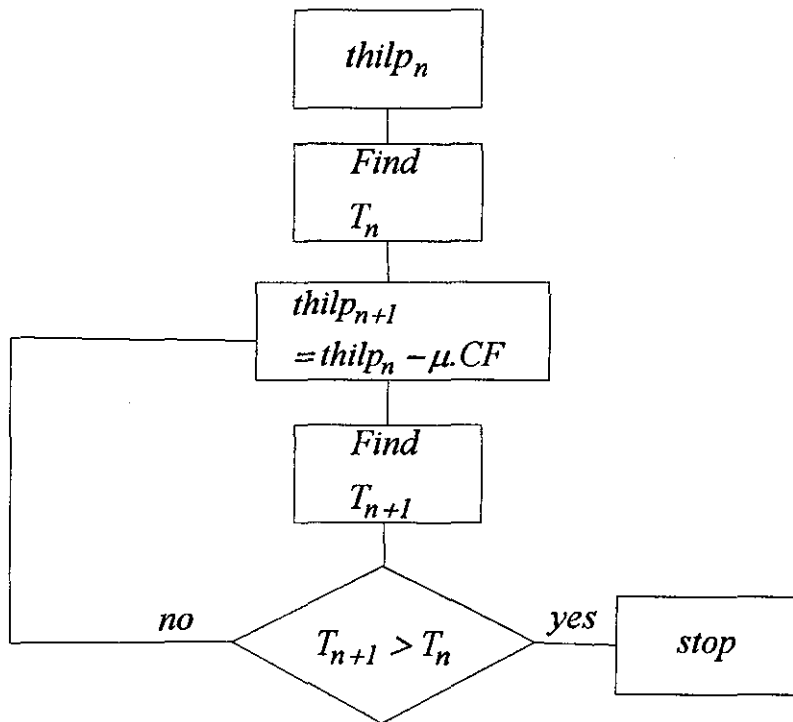


Figure 3.6 One-Dimensional Optimisation

Figure 3.6 illustrates the principle of one dimensional optimisation. The CF causes the variation of the initial estimate. For certain values of CF the modified cost is lower than the previous cost, so the new estimate approaches an optimum value and is accepted. For other values of CF the modified estimate will not be rejected. Thus this procedure ensures to find an optimum solution, given the necessary dielectric properties, which is a maximum in a given range of thicknesses or frequencies.

### 3.8.1.2 Numerical Results

The one dimensional optimisation results are shown in Figure 3.7.a. The thickness optimisation at 26.2 GHz shows a convergence after ~50 iterations. An initial thickness of 4.0 mm is assumed at the start of the iteration. At ~50th iteration, the thickness reaches a value of ~4.38 mm. In the meantime the error decreases from ~0.8 to ~0.36 and stabilises at that point. For the frequency optimisation, the thickness of the airgap is fixed at 4.38 mm.

The frequency response of the DML before and after the one dimensional optimisation is given in Figure 3.7.b. The second order peak shows at least an improvement of ~2 dB, whereas, the shift in frequency is ~1.25 GHz. In the case of the first order peak, this shift is ~2.25 GHz. This suggests that an adjacent channel operation is much more possible in the optimised version than the unoptimised version. This method also suggests that the losses in the DML due to the loss tangents of the individual layers can be minimised and more power can be transmitted through the DML.

### 3.9 SUMMARY

In this chapter, the mathematics of wave propagation through a DML structure was reviewed. The difficulty in constructing a DML accurately at microwave frequencies, due to dielectric losses and inaccuracy in machining the individual layers, was also discussed. To avoid the drawback due to the loss tangent of the high permittivity layer, a gradient descent optimisation method was proposed and analysed. It has been noted that the strength of the signal can be improved by optimising the thickness of the low permittivity to compensate for the loss introduced by the high permittivity layer.

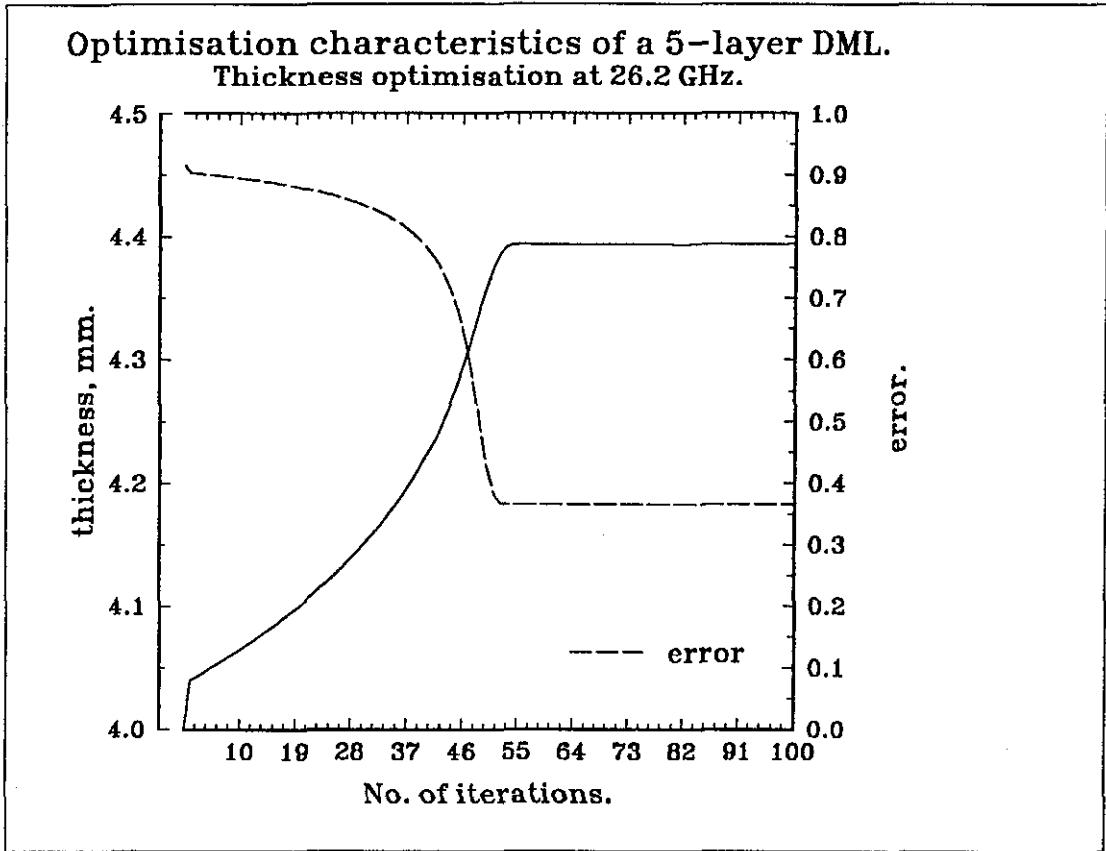


Figure 3.7.a

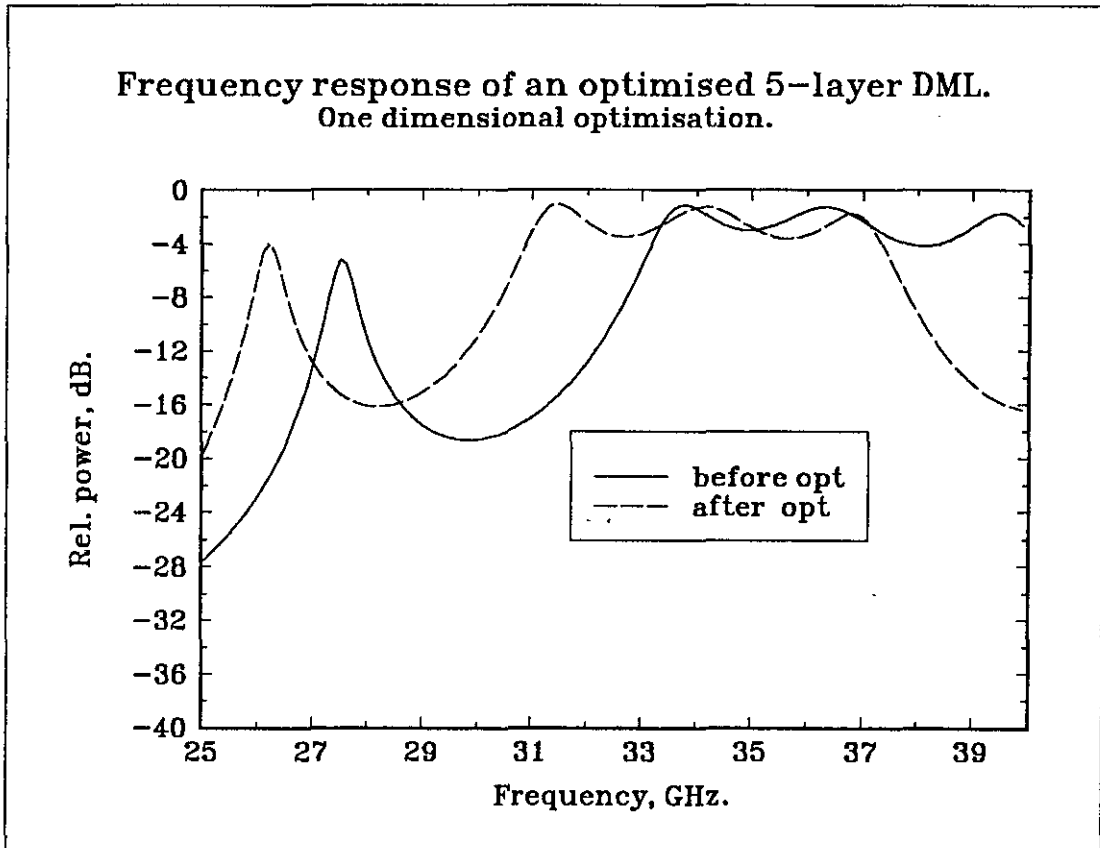


Figure 3.7.b

---

**References**

1. Heavens O. S., Thin film physics, 1970, Methuen.
2. Ritter E., Laser physics handbook, eds. Arechie F.T and Schulz-Dubois E.O., 1972, North Holland.
3. Dragila R., Luther-Davies B. and Vukovic S., High transparency of classically opaque metallic films, Phys. Rev. Lett., 55, 1985, pp.1117-1120.
4. Hecht E and Zajac A, Optics, 1979, Addison-Wesley Publishing Company, New York, Chapter 9.
5. Glen A.B. and Keiser G.E., A perspective of lightwave technology, IEEE Communications, 23, 1985, pp.8-9.
6. Jackson D.R., A multiple-layer radome for reducing the RCS of a microstrip patch, IEEE AP-S Intl. Symp., May 1990, Dallas, Texas. pp.374-377.
7. Bonvin F, Bokhari S.A., Zurcher J.F and Gardiol F.E., Microstrip spatial filters for the H-plane pattern control of microstrip antennas, Microwave and Opt. Tech. Lett., Vol. 5, No. 8, 1992, pp.347-351.
8. Rudge A.W., Milne K., Olver A.D. and Knight P (Eds), Handbook of antenna design, 1986, Peter Peregrinus, UK, Chapter 14.
9. Lekner J., Theory of reflection of electromagnetic and particle waves, 1987, Kluwer academic publishers group, The Netherlands.
10. Hopcraft K.I. and Smith P.R., An Introduction to Electromagnetic Inverse Scattering, 1992, Kluwer Academic Publishers Group, The Netherlands.

11. Von Hippel A.R. (ed), Dielectric materials and applications, 1961, MIT press, Massachusetts.
12. Tsao C., Optical fibre waveguide analysis, 1992, Oxford university press, New York, Chapter 5 and 9.
13. Amin M.B. and James J.R., Techniques for utilisation of hexagonal ferrites in radar absorbers, Journal IERE, 51, 1981, pp.209-218.
14. Bandler J.W. and Chen S.H., Circuit optimisation: the state of the art, IEEE MTT-36, 1988, pp.424-444.

## CHAPTER 4

## FREQUENCY SELECTIVE SURFACES (FSS)

## 4.1 Introduction

FSS are surfaces which exhibit different reflections or transmissions coefficients as a function of frequency. FSS usually consist of arrays of identical elements. For example, it may be an array of elements as given in Figure 4.1. The frequency response of a frequency selective surface is dependent upon the geometry of the array elements.

Periodic arrays of passive metallic elements have many interesting properties and can be used in a large number of applications and they range over much of the electromagnetic spectrum. These can be used as arrays of resonant elements which have frequency filtering properties that allow constructions of surfaces that are reflective at some frequencies, while at other frequency bands the surfaces are almost transparent[1,2]. These FSS are employed as subreflectors in Cassegrain antenna systems in order to obtain two focus feed positions[3,4]. This application may be used to increase the capacity of satellite communication links. FSS are also employed as subreflectors for dual-frequency reflector antennas, and as antenna radomes for radar cross-section (RCS) control[5]. Another example of the exploitation of the frequency selective property of periodic screens in the

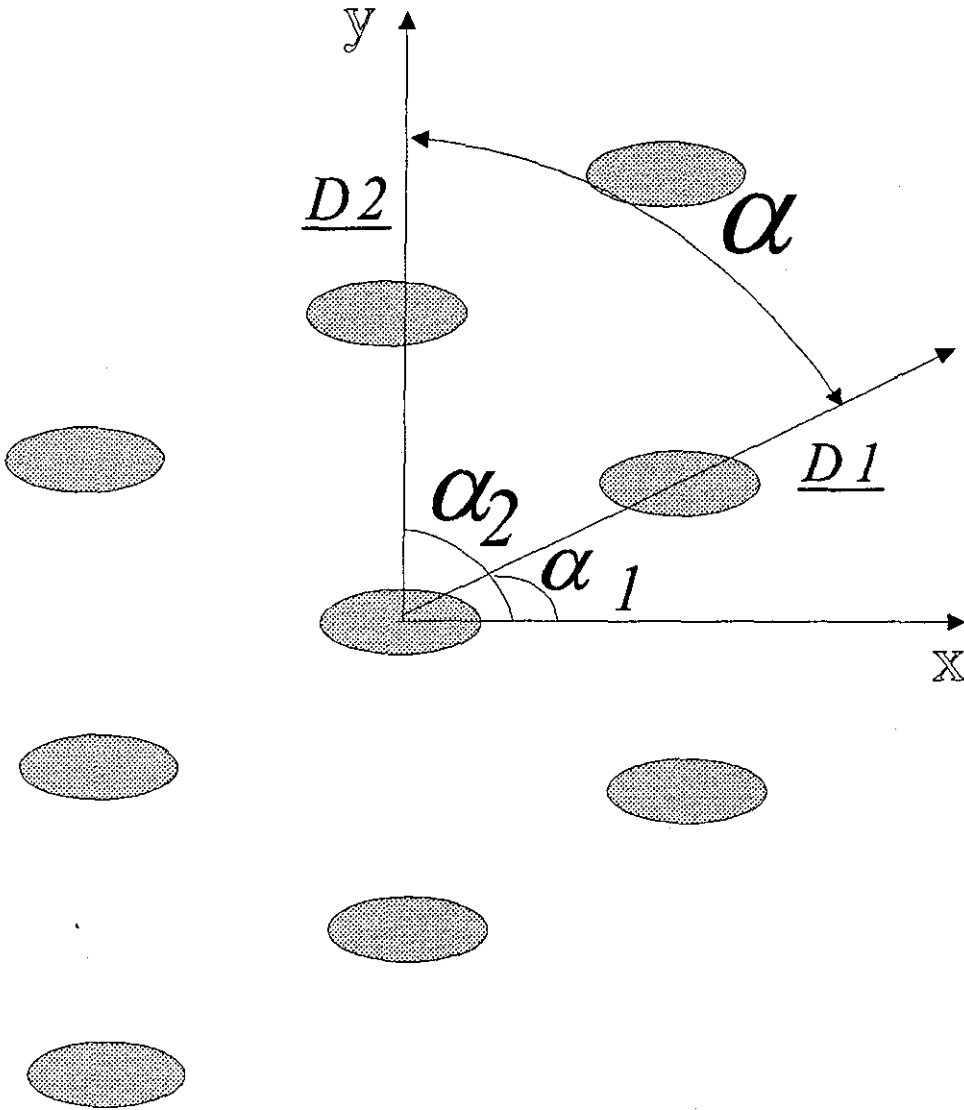


Figure 4.1. Array of periodic elements.

microwave region is the application in the radome design[6]. Periodic arrays of conducting elements can also be used as polarisation sensitive devices and have therefore found applications as different types of polarizers[7].

Another application of the FSS is in infrared sensors where, once again, the frequency selective property of the FSS is used to absorb the desired frequencies in the substrate material backing the screen, while the out-of-band frequencies are rejected. In the near-infrared and

visible portions of the spectrum, periodic screens have been proposed as solar selective surfaces to aid in the collection of solar energy[8]. A screen can be designed such that it is essentially transparent in the frequency band where the solar cells are most efficient and is reflecting frequencies outside this band. Finally, natural occurrences of periodic screens have been discovered in entomological studies[9], e.g., in the corneas of insects-the well-known fly-eye lens.

FSS may be designed in such a way that they give the maximum transmitted power for all possible angles of the incident signal. The application of FSS as a filter which attenuates the signal as the angle of incidence increases, is hardly discussed anywhere in the literature. The periodicity of the elements is altered to get the maximum attenuation as the angle of incidence increases. i.e., at normal incidence the maximum signal at a design frequency should be transmitted. In this thesis, the latter use of the FSS is fully exploited. FSS are used as planar and curved angular filters to discriminate signals coming from various directions in space. These concepts are discussed in Chapters 2 and 5.

## 4.2 THEORY

Several types of formulation are available for the computation of the transmission and reflection coefficients of the array of elements[10,11]. Some of them, however present practical difficulties if one has to take the influence of the dielectric sheet into account. The thickness of the FSS is assumed to be very thin. The method of Floquet modes as described below is used for the analysis of FSS.

### 4.2.1 FLOQUET'S THEOREM

Floquet's theorem[1] provides a means of describing the field in the open region adjacent to the phased array in terms of a complete orthogonal set of modes. The theorem is essentially an extension of the Fourier theorem for periodic functions. It is applicable to phased arrays satisfying the following conditions:

1. The arrays should be periodic and infinite in extent.
2. The arrays are excited with uniform plane wave.

Since the theory is already explained in references[12,13], its description can be abbreviated and only the main aspects are discussed here for the sake of completeness.

Consider the printed array shown in Figure 4.1. The surface is periodic and is assumed infinite in the xy plane.

The lattice vectors  $\underline{D1}$  and  $\underline{D2}$  are the periodicity axes and can be used to represent the relative position of each element on that surface.

From Figure 4.1, the lattice vectors  $\underline{D1}$  and  $\underline{D2}$  can be deduced as follows

$$\underline{D1} = D1(\cos \alpha_1 \hat{x} + \sin \alpha_1 \hat{y}) \quad (4.1)$$

$$\underline{D2} = D2(\cos \alpha_2 \hat{x} + \sin \alpha_2 \hat{y}) \quad (4.2)$$

where

$$\alpha_2 = \alpha_1 + \alpha \text{ and } D1 = |\underline{D1}|, \quad D2 = |\underline{D2}|.$$

The product vector  $A = |\underline{D1} \times \underline{D2}|$  can be defined as the unit cell area.

In an infinite and periodic array, electromagnetic fields can be represented in terms of a complete orthogonal set of scalar Floquet modes. This enables one to formulate the phased array boundary value problem in the form of an integral equation. Each Floquet mode has a propagation constant  $\gamma_{pq}$  along the z-axis. The fields are expressed in terms of conventional waveguide modes  $\underline{\Psi}_{pq}$ , with a characteristic modal admittance  $\eta_{pq}$ .

These Floquet modes are expressed as follows[1]:

$$\underline{\Psi}_{pq} = \sqrt{A} \cdot \exp(-jk_{\underline{t}pq} \cdot \underline{r}_t) \exp(\pm j\gamma z) \hat{k}_{mpq} \quad (4.3)$$

where  $p, q = 0, \pm 1, \pm 2, \dots$   $m=1$  (for TM) and 2 (for TE). Here the time variation  $\exp(-j\omega t)$  has been assumed.

The propagation constants  $k_{\underline{t}pq}$  and  $\gamma_{pq}$  are functions of lattice geometry and given as follows:

$$\underline{k}_{\underline{t}pq} = \underline{k}_{\underline{t}00} + pk_1 + qk_2 = k_x \hat{x} + k_y \hat{y} \quad (4.4)$$

where

$$\underline{k}_{\underline{t}00} = k_{0x} \hat{x} + k_{0y} \hat{y} \quad (4.4a)$$

$$\hat{k}_{1pq} = \frac{k_{tpq}}{|k_{tpq}|} \quad \text{-TM modes} \quad (4.4b)$$

$$\hat{k}_{2pq} = \hat{z} \times \hat{k}_{1pq} \quad \text{-TE Modes} \quad (4.4c)$$

$$\underline{k}_1 = \frac{2\pi}{A} \hat{z} \times \underline{D}_2 \quad (4.4d)$$

$$\underline{k}_2 = \frac{2\pi}{A} \hat{z} \times \underline{D}_1 \quad (4.4e)$$

$$k_x = \underline{k}_{0x} + p\underline{k}_{1x} + q\underline{k}_{2x}, \quad \underline{k}_{0x} = \underline{k}_0 \sin \theta \cos \phi \quad (4.4f)$$

$$k_y = \underline{k}_{0y} + p\underline{k}_{1y} + q\underline{k}_{2y}, \quad \underline{k}_{0y} = \underline{k}_0 \sin \theta \sin \phi \quad (4.4g)$$

$\theta, \phi$  - standard spherical coordinates

$$\underline{r}_t = x\hat{x} + y\hat{y} \quad (4.4h)$$

The z-directed propagation constant is given by

$$\gamma_{pq} = \sqrt{k^2 - (k_x^2 + k_y^2)} \quad (4.5)$$

where

$$k = k_0 \sqrt{\epsilon_r} \quad (4.6)$$

The propagating or evanescent modes are given by the positive or negative imaginary values of  $\gamma_{pq}$ , respectively.

In the next section the method of moments is discussed.

### 4.3 The Method of Moments

The Method of Moments is a general procedure for solving linear equations and owes its name to the process of taking moments by multiplying by appropriate weighing functions and integrating. The use in electromagnetics of moment and related matrix methods has been popular since the references [14,15] showed how powerful and versatile such techniques could be.

When an electromagnetic signal strikes a metal surface, it induces a current flow on the surface. In the case of an FSS, the current flow is restricted within the array of elements.

The induced current ( $\underline{J}_s$ ) can be represented in terms of a set of basis functions  $\underline{h}_n$  defined over the conducting element of a unit cell  $A'$ .

$$\underline{J}_s(\underline{r}_t) = \sum_{n=1}^N c_n \underline{h}_n(\underline{r}_t) \quad (4.7)$$

where  $c_n$  is the undetermined complex coefficients and  $N$  is the number of the functions used to approximate as closely as possible to the actual induced current.

#### 4.4 Formulation of the Integral Equation for the Induced Current

An integral equation can be formulated to find out the induced current density with the aid of the method of moments mentioned in section 4.3.

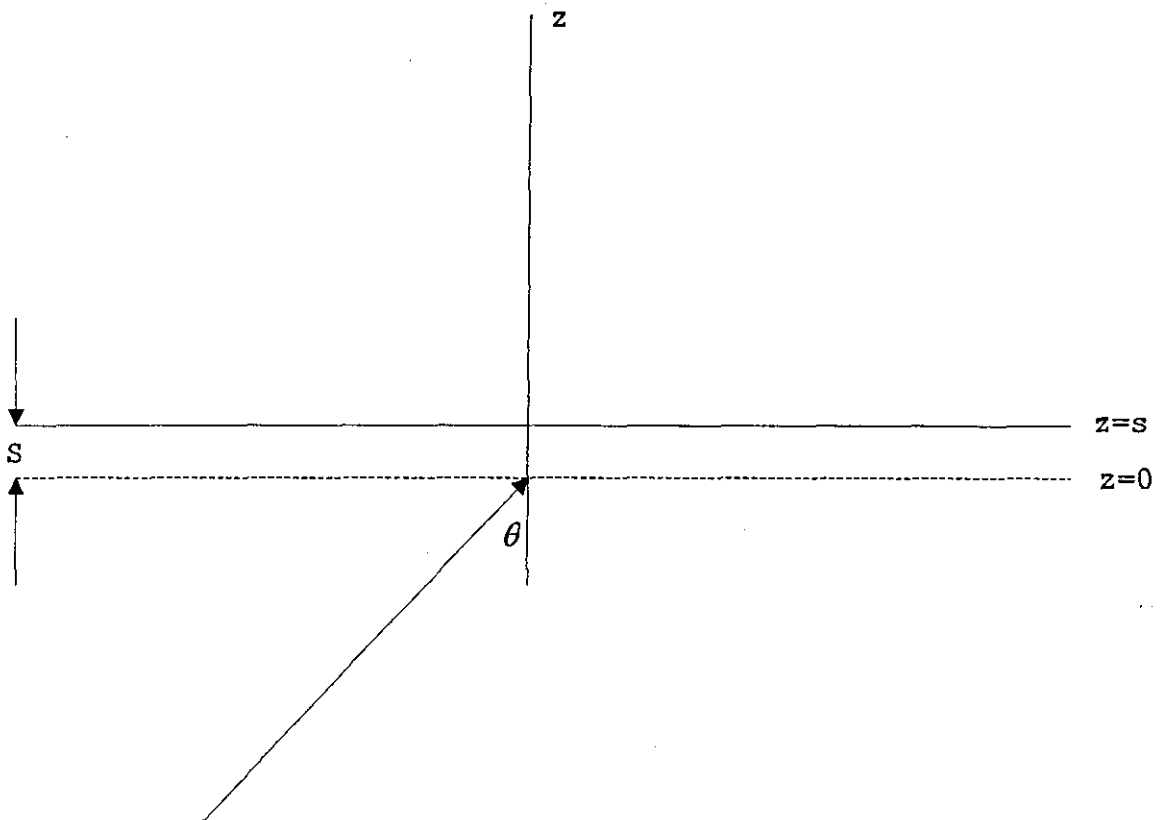


Figure 4.2.

When a periodic array (Figure 4.1), is placed in the signal path as shown in Figure 4.2, the fields can be expanded in three regions, i.e., inside the dielectric sheet and in the air on either side, into Floquet's modes[1,10]. The fields tangential to the interfaces are

expanded in the dielectric layer as a set of Floquet modes  $\psi_{pq}$ . The tangential field component propagating in the +z direction is given as

$$E_t = \sum_{mpq} E_{mpq} \psi_{pq} \exp(-j\gamma_{pq}z) \kappa_{mpq} \quad (4.8)$$

After applying standard electromagnetic boundary conditions on each interface, an integral equation for the unknown current ( $J_s$ ) on the array elements in the plane  $z=0$  is obtained.

Then the method of moments, as given in section 4.3 is applied to reduce the current equation to a set of matrix equations which are to be solved by matrix inversion technique as shown below. Details of these mathematical manipulations can be found in [1,12] and all the symbols bear the same notations as per the references.

$$\begin{bmatrix} L_1 \\ \cdot \\ \cdot \\ \cdot \\ L_n \end{bmatrix} = \begin{bmatrix} G_{11} & \cdot & \cdot & \cdot & G_{1n} \\ \cdot & \cdot & \cdot & \cdot & \cdot \\ \cdot & \cdot & \cdot & \cdot & \cdot \\ \cdot & \cdot & \cdot & \cdot & \cdot \\ G_{n1} & \cdot & \cdot & \cdot & G_{nn} \end{bmatrix} \begin{bmatrix} C_1 \\ \cdot \\ \cdot \\ \cdot \\ C_n \end{bmatrix} \quad (4.9)$$

where

$$L_r = \sum_{m=1}^2 (1 + R_{m00}^{\text{slab}}) b_m^{\text{inc}} \hat{k}_{m00} \cdot g_1^*(\mathbf{k}_{t00}) \quad (4.9a)$$

$$G_{rn} = \sum_m \sum_p \sum_q (\eta_{mpq}^{eq} A)^{-1} \hat{k}_{mpq} \left[ g_1^*(\underline{k}_{tpq}) \hat{k}_{mpq} \right] \cdot \underline{g}_n(\underline{k}_{tpq}) \quad (4.9b)$$

$C_n$  = unknown coefficients of the basis functions.

Equation (4.9) can be solved for the unknown coefficient  $C_n$  to find out the current flowing in the conductor of a unit cell.

The computations of plane wave transmission and reflection coefficients are omitted here, due to repetition in literature[12,13].

#### 4.5 Effects of Periodicity Variation on The Performance of FSS

The periodicity plays an important role on the performance of any grating structure. As shown in Figure 4.2.a, a typical FSS transmission frequency response at normal incidence for a free standing dipole array exhibits a near  $\lambda/2$  resonance. As the ratio  $D/L$  increases the bandwidth decreases. Higher order resonances begin to emerge at  $D/\lambda \sim 1$  and are mainly due to the periodic nature of the surface. As the bandwidth reduces, the surface begins to act like a radiation filter which is sensitive to angle of incidence.

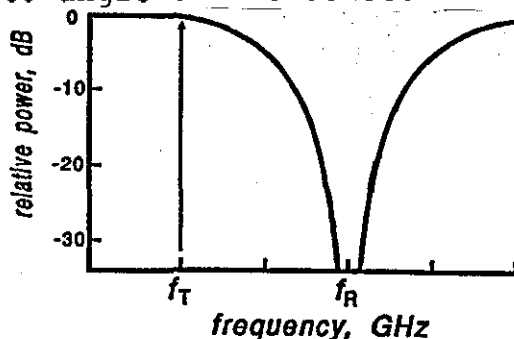


Figure 4.2.a. Typical Freq. Response of an FSS.

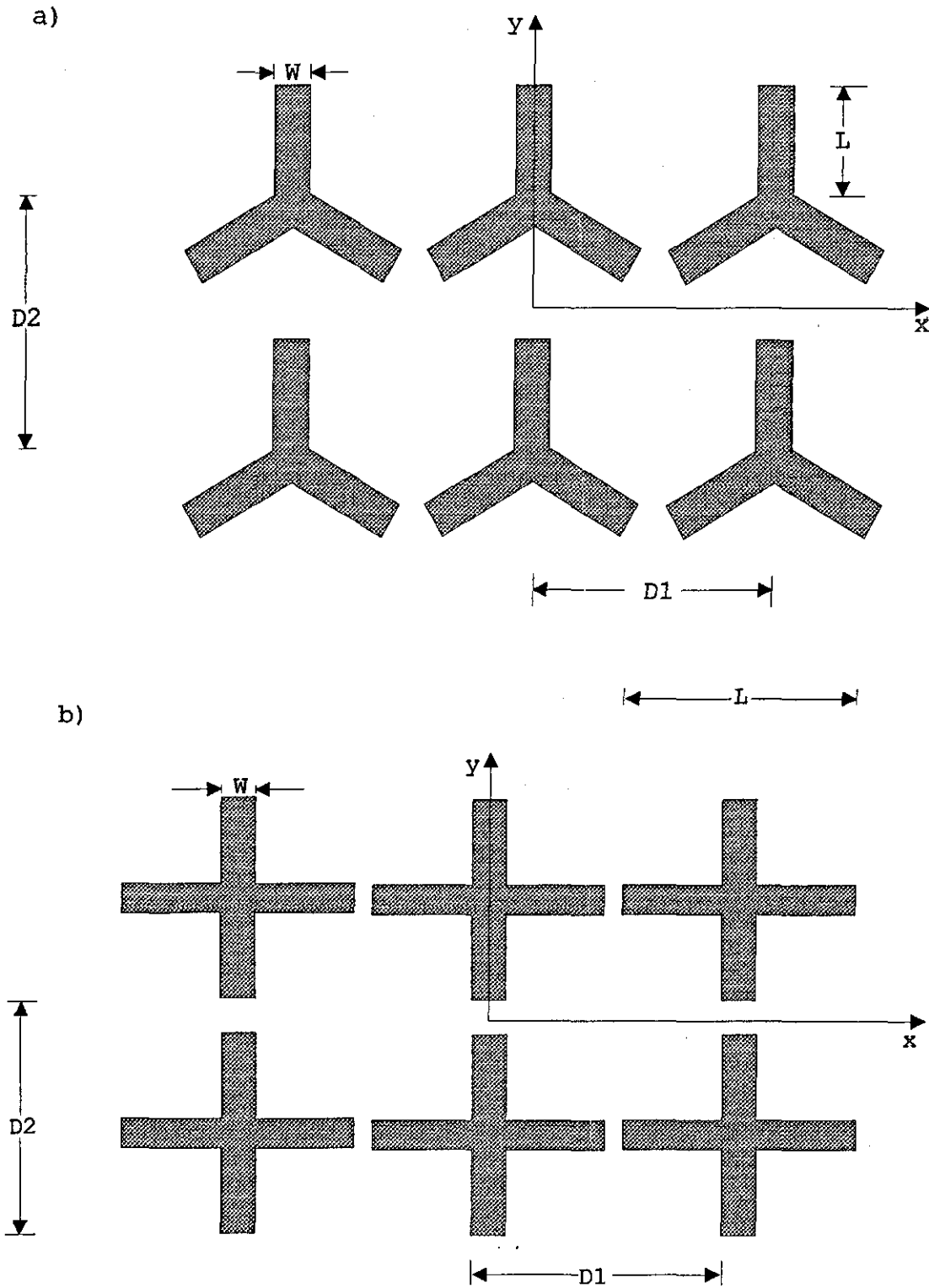


Figure 4.3 Geometry of the two arrays with slotted elements (shaded portions)

a.  $D1 = D2 = 8.9$  mm,  $L = 2.0$  mm,  $W = 0.2$  mm.

b.  $D1 = D2 = 8.6$  mm,  $L = 4.2$  mm,  $W = 0.2$  mm.

As the periodicity increases further, less power will be transmitted at the resonant frequency. Only the TE mode seems to be more dependent on angle of incidence as the TM mode has a relatively higher bandwidth.

The effect of variation of the resonant frequency with periodicity are computed for the geometries given in Figure 4.3 and are shown in Figures 4.4 and 4.5. The resonant frequencies at various periodicities are taken, when the respective transmission coefficients are at their maximum. For crossed dipole FSS, when  $D_1$  is a variable, the resonant frequency tends to decrease sharply as  $D_1$  moves towards a higher value. As the periodicity increases further the transmission coefficient tends to decrease sharply. This is thought to be due to the advent of grating lobes. As  $D_2$  is varied from 7 mm to 15 mm, the resonant frequency reduces by ~5 GHz.

Similar characteristics are observed for tripole FSS. The variation in  $D_2$  shows no apparent change in the resonant frequency.

In Figure 4.3, the direction of the electric field is in the direction of the y axis.

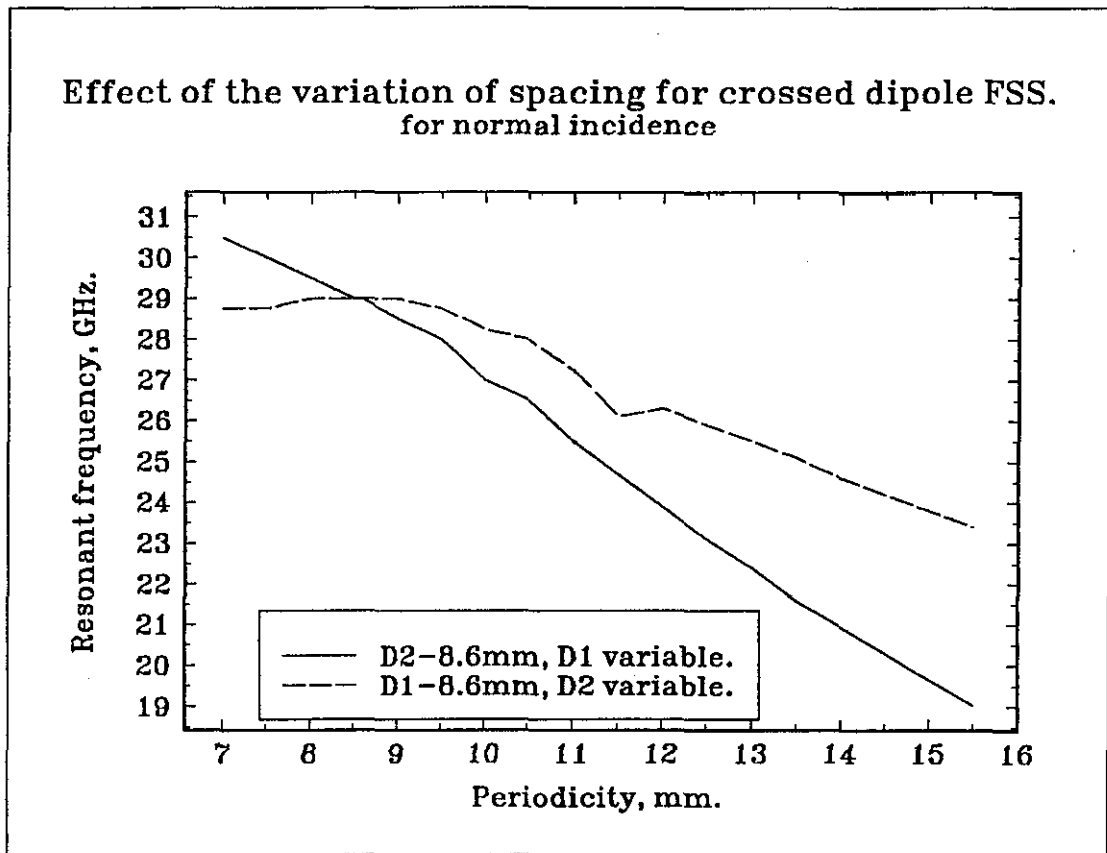


Figure 4.4

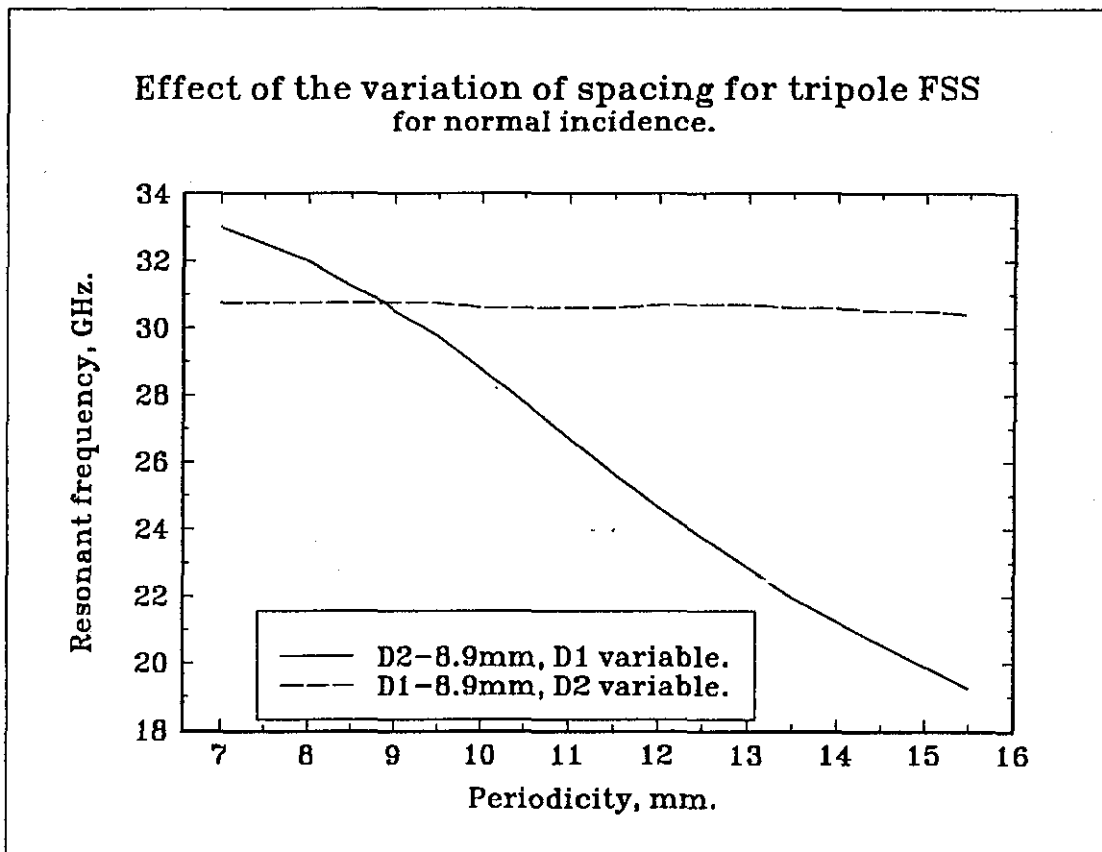


Figure 4.5

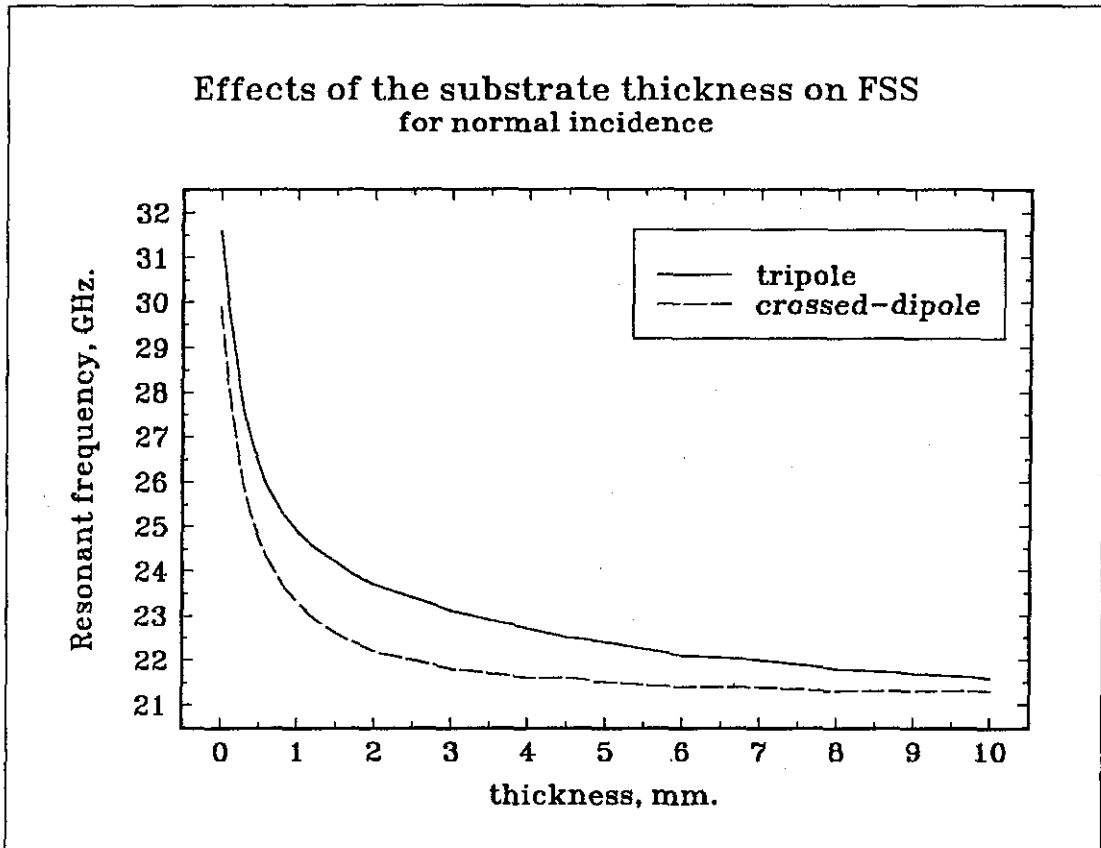


Figure 4.6

#### 4.6 Effects of the substrate thickness on FSS performance

When an FSS is exploited as an angular filter in an antenna system, it should be able to withstand the mounting pressure, atmospheric disturbances etc. As a consequence one has to increase the dielectric thickness to provide mechanical stability. The influence of supporting dielectric layers on the transmission properties of wide band FSS has been reported[16]. Here the same properties of a narrow band FSS are investigated theoretically.

Figure 4.6 shows the effects of increasing the substrate thickness. For both FSS the resonant frequencies reduce with thickness. From 0 to ~2 mm the decline in the resonant frequency is rapid. There after it saturates, which suggests that during the production of thin FSS

layer utmost care should be taken to maintain the dielectric thickness as close as to the design thickness. But in the case of thick dielectric FSS, additional resonances could appear due to the contributions of surface wave trapped in the substrate. Also evident from the graph is that crossed dipole FSS has the lowest resonant frequency compared to tripole FSS.

#### 4.7 Frequency Scanning

The study of frequency scanning forms an independent research to look into the scanning properties of FSS. This investigation is not related to the passive redome concept which was discussed in chapter 2.

##### 4.7.1 Use of Periodic Gratings

In communication applications, it is necessary to move the antenna beam in space to locate the target. The most commonly used method is the conventional rotating antenna in a vertical axis. Linear, planar and conformal arrays can be designed with either a fixed main lobe, or a scanned beam which is rapidly positioned in space by means of electromechanically or electronically actuated devices connected in the feedlines behind the array radiators. These devices change the phase or time-delay between radiators to produce the required phase progression along the array. Scans can be either one-or two-dimensional. Such systems are expensive to construct due to their complex nature of operation. Hybrid antennas[17] are also used to achieve this feat.

It is emphasised here, that periodic grating structures can be utilised to construct antennas with frequency scanning properties. Gratings have found a lot of applications in many areas of physics and engineering. Some important applications include: microwave polarizers, twist reflector antennas, spectrum analysers,

integrated optical devices, holography and acousto-optical devices. Because of their widespread applications, the diffraction properties of gratings have been studied extensively over the last few decades[18]. Periodic grating structures have been proposed to construct antennas with frequency scanning properties[19,20,21].

To reduce the total operational cost of certain complex systems, a method of steering the grating lobes using FSS is introduced, which is considered easy and inexpensive to produce due to the passive nature of the FSS[22,23].

This method of antenna beam steering offers several advantages over that of mechanically steering the beam by using a servo-driven gimbal system, the most obvious being the capability to steer the antenna at higher speeds and without mechanical lags. However, the electronic steering technique also causes some non uniform distortions in the angular spacings among the pattern's lobes, as well as changes in the lobes' amplitude, compared with those of the unsteered pattern.

#### **4.7.2 Basic Principle**

In this section, the characteristics of the first order grating lobe are studied. For this the FSS geometry is selected in such a way that the first order diffracted mode is propagating while the surface is illuminated by an electromagnetic wave. A surface with such a property is known as a blazed grating in optical terminology, which transfers the incident signal power to diffracted power. It is understood that the grating lobes are more sensitive to variation in frequency and can therefore be steered.

The basic principle of the microwave blazed grating is similar to that of its optical counterpart. The

fundamental idea is to select a proper grating structure so that the first higher order diffracted wave is propagating when an electromagnetic signal is incident on the surface. The propagation direction of the diffracted signal will be frequency sensitive and this signal is used to scan as the frequency is varied. In order to increase the signal power of this beam, it is necessary to convert the incident power to the first order beam.

The performance of a frequency scanned grating is dependent on the blazed efficiency of the grating. Here, a numerical algorithm is developed to find out the scanning angle of any higher order diffracted mode.

#### 4.7.3 Analysis

The theoretical analysis of FSS consisting of periodic array of conducting elements, which was reviewed earlier in this chapter is used here for the analysis.

From equation 4.5, it is evident that the propagating modes have the magnitude of the transverse propagation constant  $k_{tpq}$ , less than the propagation constant of the free space  $k_0$ . It is the intention of this section to provide a general equation to find out the scanning angle for any combinations of propagating modes (p,q).

For a plane of incidence (Figure 4.2) in the region  $-90^\circ < \phi < 90^\circ$ , the general expression for the mode index for any higher order diffracted wave is given as per equation 4.4 and substituting for  $pk_1$  and  $qk_2$ , one gets

$$\sin \theta_{p,q} \cos \phi_{p,q} = \sin \theta \cos \phi + \left[ \frac{p\lambda_0}{D1} \right] \left[ \frac{\sin \alpha_2}{\sin(\alpha_2 - \alpha_1)} \right] - \left[ \frac{q\lambda_0}{D2} \right] \left[ \frac{\sin \alpha_1}{\sin(\alpha_2 - \alpha_1)} \right] \quad (4.10)$$

$$\sin \theta_{p,q} \sin \phi_{p,q} = \sin \theta \sin \phi - \left[ \frac{p\lambda_0}{D1} \right] \left[ \frac{\cos \alpha_2}{\sin(\alpha_2 - \alpha_1)} \right] + \left[ \frac{q\lambda_0}{D2} \right] \left[ \frac{\cos \alpha_1}{\sin(\alpha_2 - \alpha_1)} \right] \quad (4.11)$$

where  $(\theta_{p,q}, \phi_{p,q})$  is the diffraction angle of the  $pq^{\text{th}}$  diffracted wave and  $\lambda_0$  is the wavelength of free-space.

Now the mode index of a first order diffracted wave is  $(p,q)=(-1,0)$ , for which equation 4.10 and 4.11 become

$$\sin \theta_{-1,0} \cos \phi_{-1,0} = \sin \theta \cos \phi - \left[ \frac{\lambda_0}{D1} \right] \left[ \frac{\sin \alpha_2}{\sin(\alpha_2 - \alpha_1)} \right] \quad (4.12)$$

$$\sin \theta_{-1,0} \sin \phi_{-1,0} = \sin \theta \sin \phi + \left[ \frac{\lambda_0}{D1} \right] \left[ \frac{\cos \alpha_2}{\sin(\alpha_2 - \alpha_1)} \right] \quad (4.13)$$

Therefore the frequency scanned angle of the surface depends upon the incident angle  $(\theta, \phi)$ , grating periodicity  $D1$ , and the relative position of the elements with respect to the x-axis.

#### 4.8 Numerical Results

Assuming that  $\phi = 0$ ,  $\alpha_2 = 90^\circ$  and  $\alpha_1 = 0^\circ$ , then from equations (4.12 and 4.13), the  $(-1,0)$  mode will be transmitted in the plane of incidence given by

$$\sin \theta_{-1,0} = \left[ \frac{\lambda_0}{D_1} \right] - \sin \theta \quad (4.14)$$

Four incidence angles are chosen to demonstrate the dependency of the diffracted mode in relation to frequency and periodicity. They are 30°, 45°, 60° and 75°.

From Figures 4.7, for TE incidence, it is clear that the periodicity determines the scan angle. As the periodicity increases the scan angle increases. Also the scan angle range increases. For TM incidence, when  $\phi=90^\circ$ ,

$\phi_{-1,0}$  does

not remain at 90° as  $\phi$  does.

For a fixed periodicity, say 13 mm, a frequency scan of ~10° is predicted in the range of 30 to 40 GHz and the scan range also increases. More efficient scanning can be seen at lower periodicities. At 9 mm, ~25° shift of the beam is noted in the range of 23-25 GHz, which suggests that a greater range can be covered with lower periodicities and a lower range of frequency.

These figures are based on the information available from the basic grating equation 4.14. The information given in these graphs is not based on the amplitude of the transmitted power. Results of a rigorous approach based on the modal analysis method in which the effect of the first order component is presented in Chapter 6. This provides information regarding other parameters such as the transmitted powers of various higher order modes.

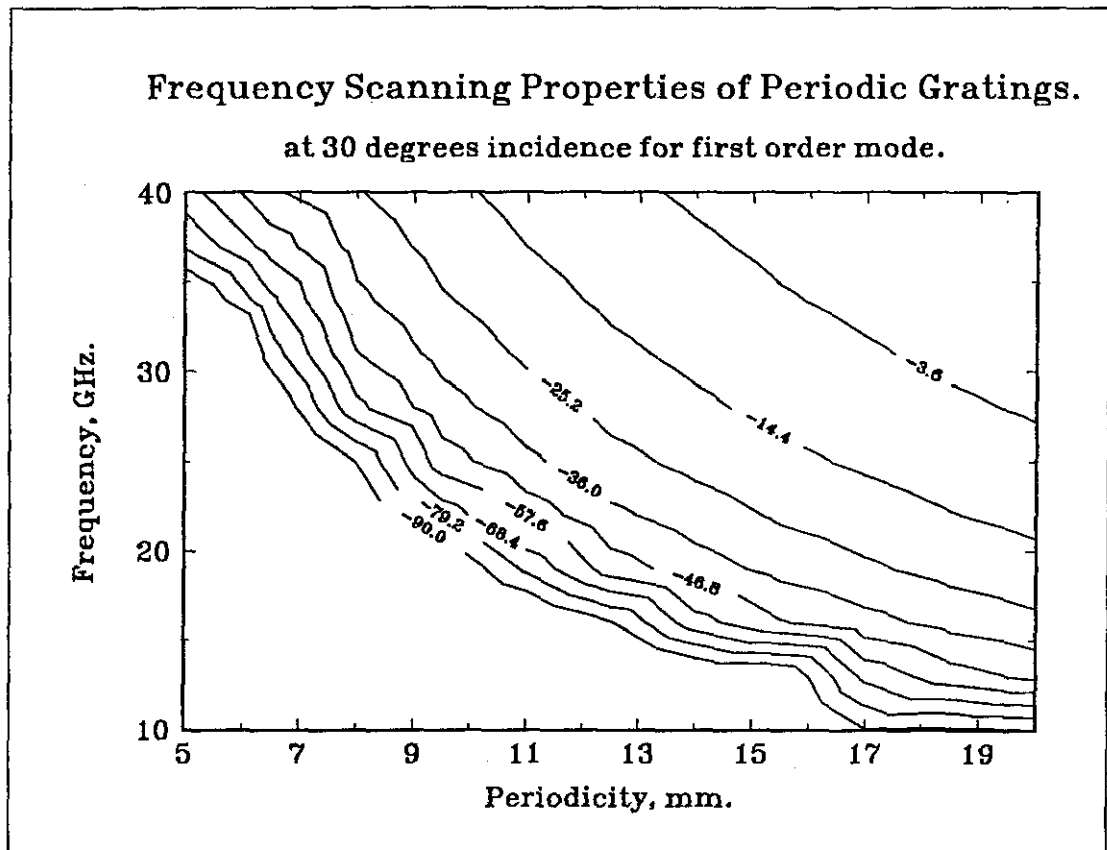


Figure 4.7.a

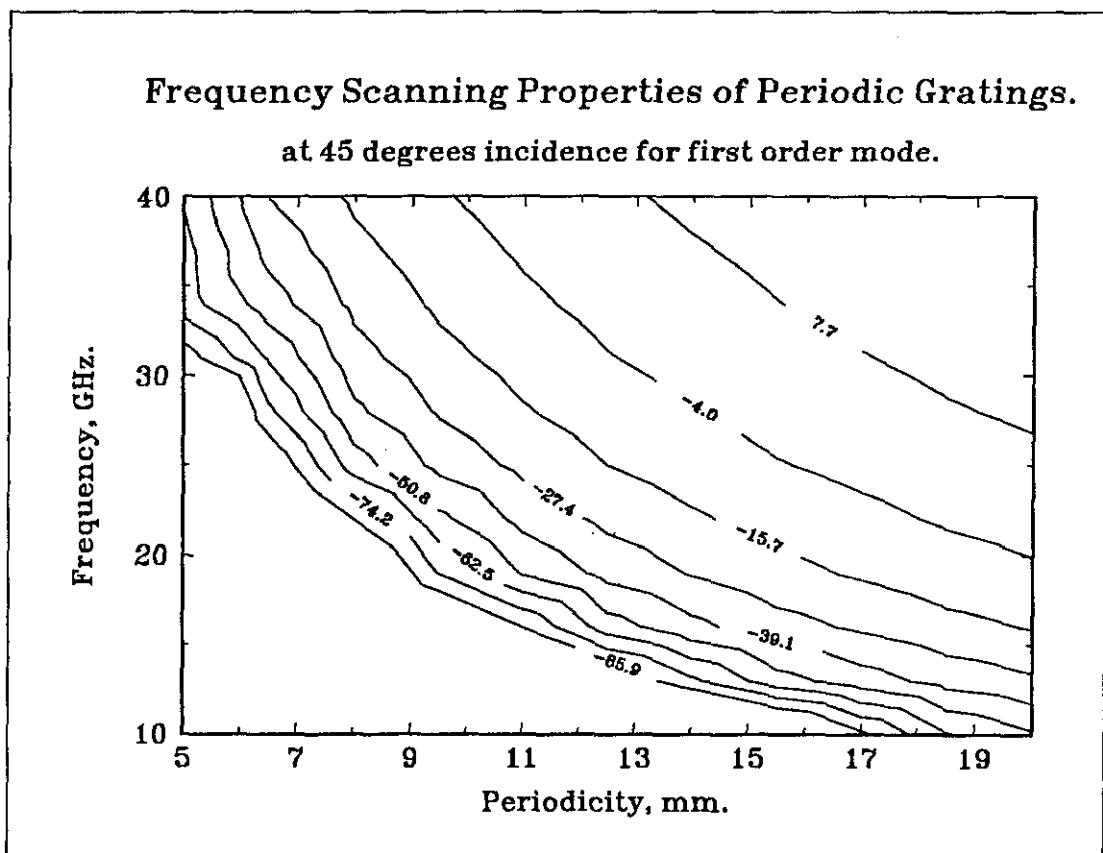


Figure 4.7.b

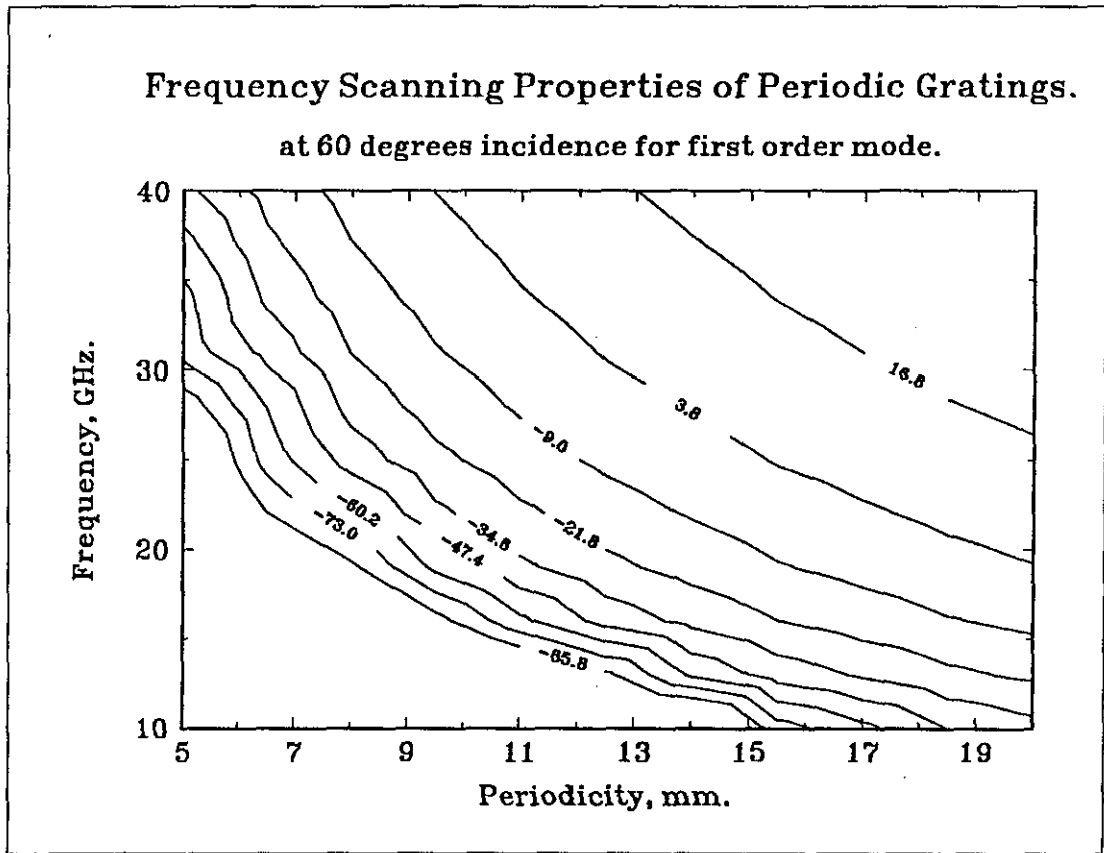


Figure 4.7.c

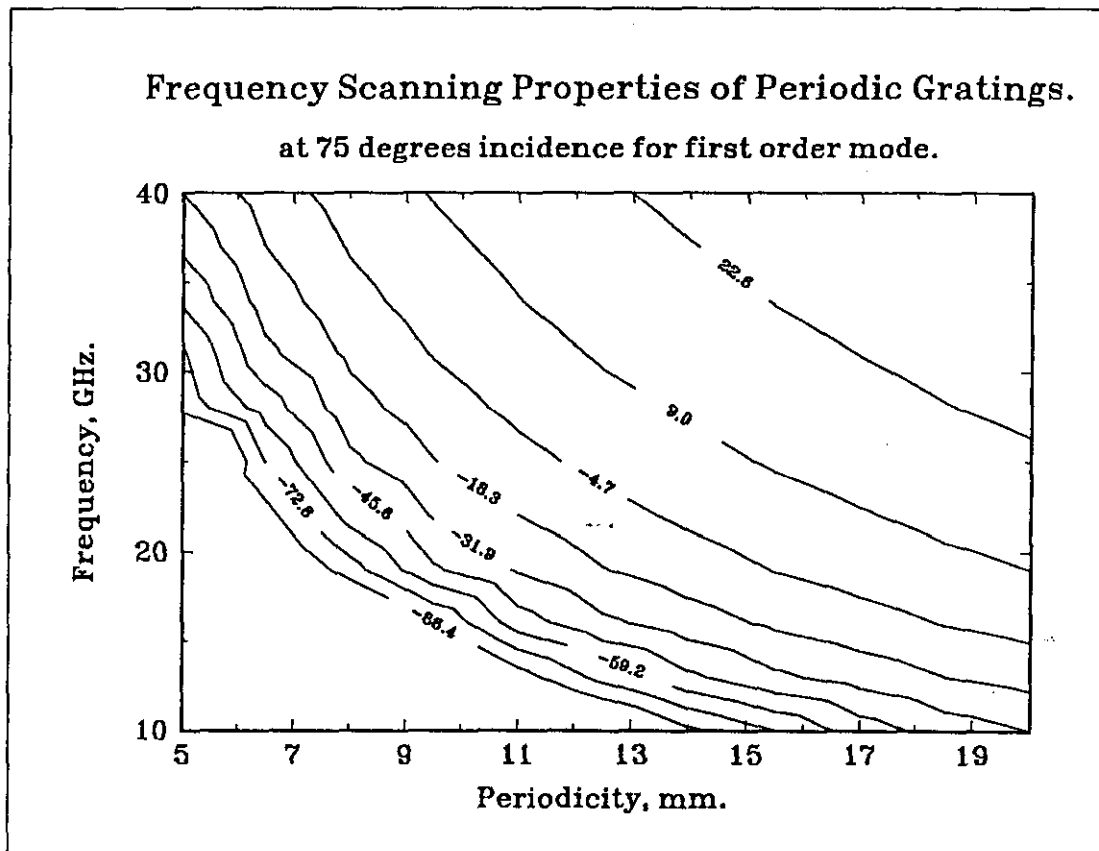


Figure 4.7.d

#### 4.9 Summary

In this chapter the basic properties of FSS were described. The modal analysis method was reviewed, in view of finding the scan angle of the various higher order diffracted modes on a frequency scanned grating structure. The design procedure of an angular filter which is to be used as a redome was also investigated, in terms of element periodicities of the FSS. The effect of dielectric thickness on the resonant frequency was studied. The frequency scanning property has been obtained by selecting a periodicity in such a way that the first higher order diffracted wave propagates and serves as the frequency scanned beam. Numerical examples were provided to substantiate the range of frequency scanning and the results showed that wider scanning angles can be obtained using FSS with higher periodicities.

---

**References**

1. Montgomery, J. P., Scattering by an infinite periodic array of thin conductors on a dielectric sheet, 1975, IEEE Trans., AP-23, pp.70-75.
2. Johansson F. S., Analysis of double layer frequency selective surfaces, 1985, Proc IEE, Pt.H, Vol. 132, pp.319-325.
3. Agrawal V. D. and Imbriale W. A., Design of a dichroic Cassegrain subreflector, 1979, IEEE Trans., AP-27, pp.466-473.
4. Derneryd A. G., Ingvarson P., Johansson F. S., Petterson L. E. and Schuley N. V., 1986, Design of a dichroic subreflector for an offset reflector antenna, International Symposium on antennas, JINA-86, Nice, France, PP.370-374.
5. Mittra R., Chan C. H. and Cwik T., Techniques for analyzing frequency selective surfaces-a review, 1988, Proc.IEEE, Vol.76, No. 12, pp.1593-1614.
6. Lee S. W., Scattering by dielectric loaded screen, 1971, IEEE Trans., AP-19, no.5, pp.656-665.
7. Durschlag M. S. and DeTemple T. A., Far-IR optical properties of free standing and dielectrically backed metal meshes, 1981, Appl.Opt., vol.20, no.7, pp.1245-1253.
8. Horwitz C.M., A new solar selective surface, 1974, Opt. Commun., vol.11, no.2, pp.210-212.
9. Miller W. H., Bernard G. D. and Allen J. L., The optics of insect compound eye, 1968, Science, vol.162, pp.760-767.

10. Chen C. C., Scattering by a two-dimensional periodic array of conducting plates, 1990, IEEE Trans., AP-18, pp.660-665.

11. Lee C.K. and Langley R.J., Design of a single layer FSS, 1987, Int. J. Electronics, Vol.63, No. 3, pp.291-296.

12. Shuley N.V.Z, Analysis of dichroic surfaces, 1985, Ph.D thesis, School of Electrical and Computer Eng., Chalmers University of Technology, Goteberg, Sweden.

13. Amitay, Galindo & Wu, Theory and analysis of phased array antennas, 1972, Wiley, N.Y., pp.310-313.

14. Harrington R.F., Matrix methods of field problems, 1967, Proc IEEE, Vol. 55, pp.136-149.

15. Richmond J.H., A wire-grid modelling for scattering by conducting bodies, 1966, IEEE Trans., AP-14, pp.782-786.

16. Callaghan P., Parker E.A and Langley R.J., Influence of supporting dielectric layers, 1991, Proc IEE, Part.H, Vol. 138, No. 5, pp.448-454.

17. Schwartzman L. and Stankel J., The dome antenna, Oct 1975, Microwave journal, pp.31-34.

18. Gaylord T.K. and Moharam M.G., Analysis and applications of optical diffraction by gratings, 1985, Proc. IEEE, Vol. 73, No. 5, pp.894-937.

19. Mittra R. and Kastner R., A spectral domain approach for computing the radiation characteristics of a leaky wave antenna for millimeter waves, 1981, IEEE Trans., AP-29, No.4, pp.652-654.

20. Shmoy J. and Hessel A., Analysis and design of frequency scanned transmission gratings, 1983, Radio Sci, Vol. 18, No. 4, pp.513-518.

21. Lagerholm R., Study of metallic strip gratings for frequency scanning, 1992, Microwave & Opt. Tech. Lett, Vol. 5, No. 14, pp.713-715.

22. Johansson F.S., Periodic arrays of metallic elements as frequency scanning surfaces, Mar 1987, Proc IEE Ant. & Prop. Conf, York, UK, pp.71-74.

23. Johansson F.S., Frequency scanned gratings consisting of photoetched arrays, 1989, IEEE Trans.,AP-37, No. 8, pp.996-1002.

## CHAPTER 5

**RESULTS OF PASSIVE ANTENNA COMPONENTS****5.1 Introduction**

In this chapter, the realisation of dielectric multilayer (DML) and frequency selective surfaces (FSS) as spatial passive filters are studied towards implementing a novel passive antenna concept. Theoretical models of the DML and FSS are based on the analysis provided in Chapters 3 and 4. Experiments were carried out in an anechoic chamber. Some experiments, however were carried out without any theoretical model, as they are beyond the scope of this thesis.

In many of applications of the DML and FSS mentioned in literature are employed as spectral filters. The structures are usually designed to have a uniform angular response in the pass-band (e.g. for filters, dielectric mirrors and beam splitters) or they function at specific incidence angles (e.g. polarising filters). For certain applications, it is required to produce a filter which has more than one specific spectral pass-band [1,2]. Recently a similar study on fractal [3] and chiral [4] multilayer filters and reflectors has been presented. In this several properties of the diffractals generated by a cantour fractal medium with relatively low number of layers illuminated by a plane wave have been established.

Although the spectral properties of multilayers have been exploited, especially in optics, studies of the angular response of such structures in the context of microwave component technology are less common. In particular the

possibility exists of utilising the angular response to extend the role of dielectric multilayers into that of frequency dependent spatial filters.

Curved structures were subjected to a practical study in this chapter. The inspiration of curving filter surfaces forms a pilot study of the proposed semi-spherical dome structure in Chapter 2. The curved structure admits the signal which incidents normally to the locally flat region on the redome. The rest of the signals will be reflected. This provides discrimination of the signal according to the direction of arrival. Also such designs would provide less aerodynamic drag when installed at certain positions in a moving vehicle.

In this chapter, the experimental setup and the measurement procedures are discussed, together with the results. Four sets of measurements were carried out to establish the passive antenna concepts discussed in Chapter 2. They were angular filtering measurements, plane wave measurements, radiation pattern measurements and near field measurements. These measurements would suggest the operation of the proposed antenna system.

## **5.2 Experimental Set-up**

### **5.2.1 Anechoic Chamber**

A schematic diagram of the measurement system in the anechoic chamber is given in Figure 5.1. The transmit and receive antennas are pyramidal horns. The transmitting horn is connected to a microwave sweep oscillator (HP8350B) and the receiving horn to a scalar network analyser (HP8757A). The transmitting antenna is mounted on a table and the receiving horn is placed on a purpose-built jig.

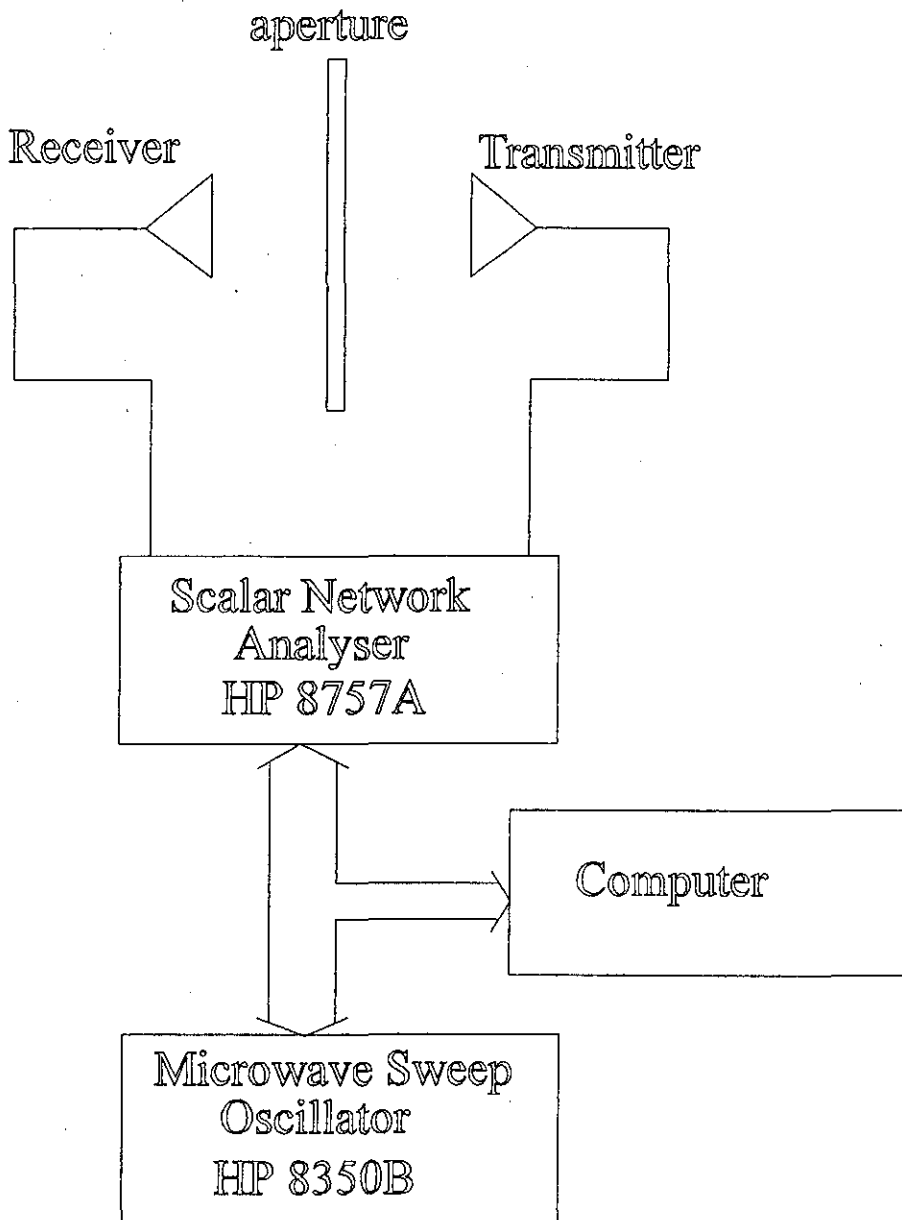


Figure 5.1

#### 5.2.1.1 Microwave Sweep Oscillator (HP 8350B)

In the anechoic chamber a microwave sweep oscillator (HP 8350B), is used to generate microwave signals of the required bands. To have a complete operating unit, this sweep oscillator must be used with an RF plug-in unit which operates in the desired frequency range. This plug-in unit is capable of producing signals from 2.4 GHz to 40.75 GHz with an maximum output power up to 15 dBm. For

the experiments carried out in this thesis, the frequency range 26-40 GHz is utilised.

#### **5.2.1.2 Scalar Network Analyser (HP 8757A)**

The HP 8757A is a microprocessor-based receiver capable of making scalar (magnitude only) reflection and transmission measurements over a frequency range determined by the external detectors used. It has a large screen for display of measurements. It is programmable over the HP-IB (Hewlett-Packard Interface Bus). Whether or not it is being controlled remotely through HP-IB, it can control a specified plotter and/or source through the 8757 Systems Interface. A measurement with the HP 8757A requires the connection of detector(s) and/or directional bridge(s) to the detector inputs on the front panel, and the use of a compatible RF/microwave source.

The equipments mentioned above have remote programming interfaces using the HP-IB, which provides a remote operator with the same control of the instrument available to a local operator. Remote control is maintained by a system controller, a computer, that sends commands to and receives data from the HP8350B using the HP-IB.

### **5.3 Objectives of the Measurements**

The antenna structures proposed in Chapter 2 should be able to detect signals emerging from any direction in space within a certain frequency band and amplitude. The dome structure consists of passive filters such as DML or FSS. It is necessary to study both the planar and curved structures as radomes to compare their performances to determine which structure provides the better radiation performance. The curvature of the surface results in the angle of incidence varying from one edge of the surface to other edge. The expected effects of curving the radome

is demonstrated in Figures 5.2.a and 5.2.b. For flat geometries, as the wave is incident on the surface at an angle, the filtered signal has the same amplitude at the exit plane, which would be fed to the detector. For curved structures, the filtered signal component which has the maximum intensity is the part of the signal which impinges normally to the locally planar area of the surface. The rest of the signal will be attenuated according to its angle of incidence. This provides some information to locate the source of transmission. The redome structure determines the frequency band of the signal transmission.

A set of near field measurements are therefore required to determine the interception point of the signal on the detector. The proposed measurement setup of a multihorn system an assessment is shown in Figure 5.2.c. A Ku-band horn antenna was used to measure the received signal and it was moved in steps of 1 cm to serve as a detector, in the horizontal plane. For the curved structure two types of hyperbolic curves were used. The curve dimensions were obtained by plotting the equation

$$z = h_a \left( 1 - \sqrt{1 + \left( \frac{x}{h_b} \right)^2} \right) \quad (5.1)$$

for various values of  $x$ .

Where  $h_a$  and  $h_b$  for each curvature in Figure 5.2.c are given as

Curve	$h_a$	$h_b$
H0	0	-----
H1	0.217	0.508
H2	0.217	0.281



# A.K.S MOTORS

CLOCK TOWER S/S  
ASHBY ROAD,  
COALVILLE.  
Tel: (0530) 813814

ST. PETERS S/S  
ST. PETERS BRIDGE,  
BURTON-ON-TRENT  
Tel: (0283) 40024

ELMS PARK  
164 LEICESTER ROAD,  
LOUGHBOROUGH,  
Tel: (0509) 211184

PARKVIEW FILLING STATION  
178 EAST PARK ROAD,  
LEICESTER.  
Tel: (0533) 736151

5.00 is

HOME TIME  
TO COME

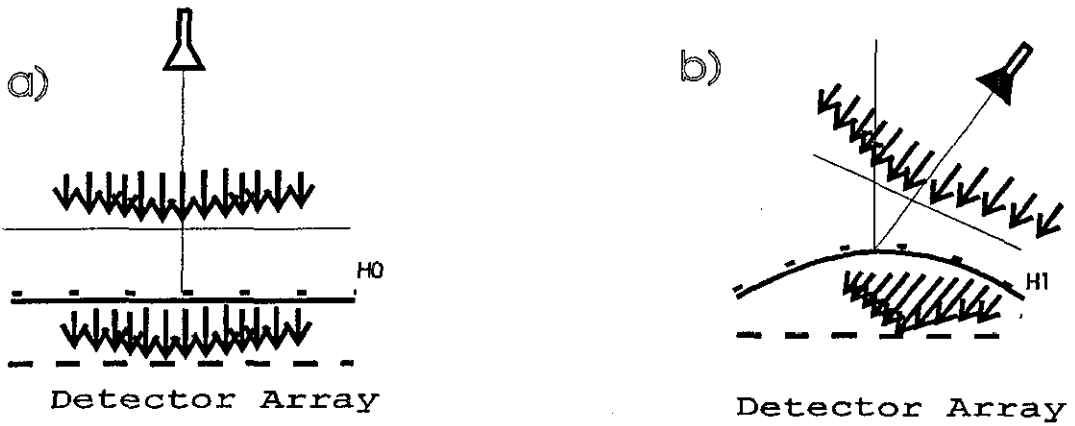
BACK BECAUSE

it is LAYF E  
at niteh

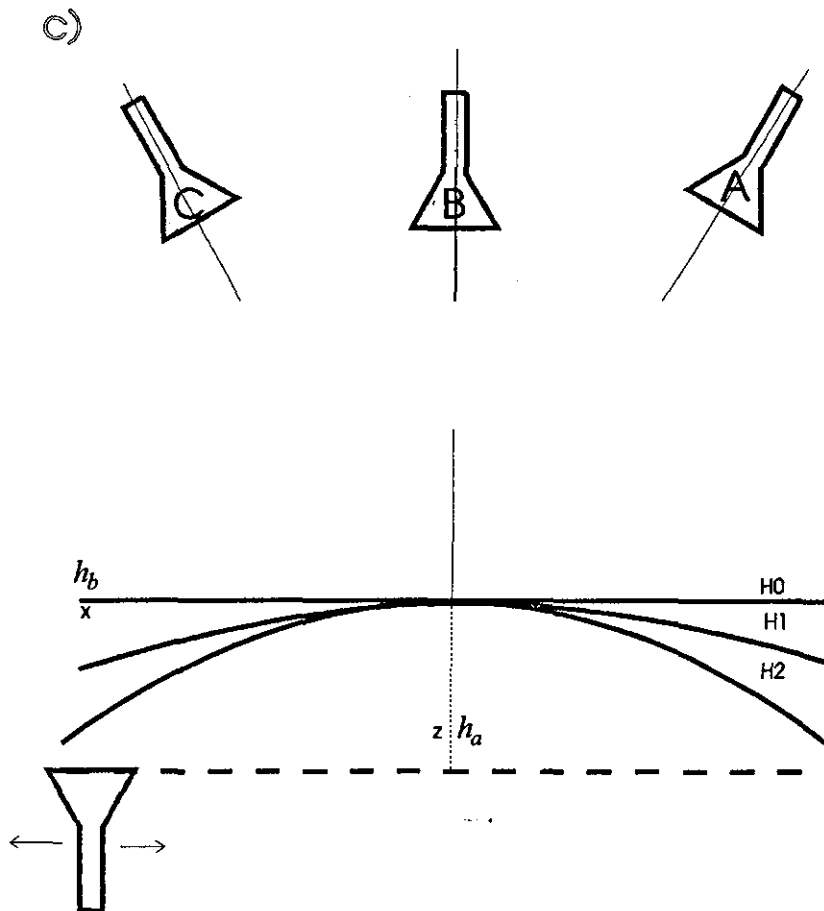
AT 690

COME AND

CITOUIN EVERTI



Principle of angular filtering



Schematic diagram of the lab setup for multiple horn measurements.

Figure 5.2.

The hyperbolic structures were formed by machining polystyrene blocks according to the necessary dimensions. Polystyrene blocks were selected because they show characteristics close to that of air. FSS were then glued to the machined blocks to provide the necessary curvature to the surface. For DML, due to its rigidity, wooden frames were made to provide the necessary curvature.

#### **5.4 Measurement Procedures**

The data acquisition systems were automated to reduce the human effort involved and it was carried out in the chamber as a part of an M. Sc project [20]. Measurements were carried out for both TE and TM polarisations. Four types of practical measurements were performed in the chamber, to study the characteristics of the filters. They are given as follows:

##### **5.4.1. Angular Filtering**

The variation of the received signal with the angle of incidence was obtained as follows:

A rotatable wooden frame with a square aperture in the middle was positioned normal to the angle of incidence, i.e., at  $0^\circ$ . The network analyser was normalised with respect to the maximum power at bore-sight. Then the DML or FSS was placed over the aperture and the received power was recorded. After removing the filter, the aperture was positioned at a new angle and the normalisation procedure was carried out again. This setup enables the incident wave to strike on the surface at an angle, which gives information of the transmitted power as the change of angle of incidence changes. The rest of the region in the wooden frame, apart from the aperture was covered with microwave absorbers. The angle of incidence can be varied in steps of  $2.5^\circ$ .

17 - 0.226

20 - 0.607

21 - 1.6090

22 - 1.63

23 - 2.328

13 - 3.374

14 - 1.57

15 - 0.5674

16 - 0.132

17

18

- 0.035

19

- 0.176

- 0.498

- 0.274

25 - 6.57 - 1.59.

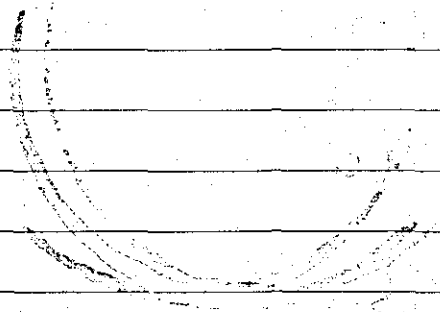
26 - 7.6

27 - 11.84

28 - 18

29 - 22

30 -



17. 4802  
22. 86  
D 35-30  
62  
25

#### 5.4.2 Plane Wave Measurements

The plane wave measurements were conducted in the chamber to establish the variation of received power at various angles of incidence, at a given frequency. The wooden aperture onto which the surfaces are mounted can be rotated about its vertical axis. The centre of the aperture lines up with the transmitter and receiver horns, which are in the line of sight. For the angular response measurements, the aperture is rotated in steps of  $5^\circ$ , while the positions of the transmitter and receiver horns are fixed.

#### 5.4.3. Radiation Pattern Measurements

A conventional method for measuring the field pattern of an antenna consists of varying the angular position between the antenna being tested and a receiving probe located at a fixed distance. This is equivalent to moving the receiving probe over an arc of an imaginary spherical surface centred on the antenna being tested and it is this method which is utilised for the radiation pattern measurements and was carried out in the following manner.

The receiver horn was placed on a rotatable arm in the horizontal plane and was normalised at boresight. The filter was then placed in the aperture area. The receiver horn was used to scan the radiation patterns of the filters.

#### 5.4.4. Near field measurements

In this setup the transmitting antenna was mounted on a table and the filter was once again put onto the aperture. The receiving horn was placed on a separate jig close to the filter. The jig was designed in such a way that the horn antenna can be moved in all possible

directions in space. The receiving horn was moved slowly in the lateral direction in steps of 1 cm, to scan the fields close to the filters.

### 5.5 Preparation of the filters

The main objective of the design of the DML, is to attenuate the incoming wave, as the angle of incidence increases. This provides better signal discrimination and helps to find out the direction of signal source.

The theoretical analysis of plane wave scattering from dielectric multilayer structures is given in Chapter 3. Here the study is based on a structure familiar to spectral filter designers consisting of two materials arranged in an alternating sequence. For optimum effect the two materials must be composed of contrasting dielectric permittivity usually termed 'high' (H) and 'low' (L). In particular the combination 'HLHLHLHLH' will be considered, which exhibits a fundamental resonance (pass-band), with respect to normally incident plane waves, when the thickness of the high(low) permittivity layer is  $\lambda/4$  ( $\lambda/2$ ), where  $\lambda$  is the wavelength in the material.

In the context of microwave radiation the choice of material for the high permittivity layer is governed by the needs to achieve narrow band performance at an appropriate frequency, to minimise the insertion loss and to limit manufacturing costs. For these reasons a high permittivity layer composed of the glass fibre laminate melamine (manufacturer's data: relative permittivity,  $\epsilon_r = 7.5$  and loss tangent,  $\tan\delta = 0.02$  at 1 MHz), being tough and durable was selected. Melamine sheets with thickness  $\sim 0.76$  mm will be considered as these are supplied as standard and the resulting multilayer structures will possess transmission resonances near to the atmospheric attenuation window ( $\sim 25-45$  GHz) between

water and oxygen molecular absorption. Expanded polystyrene is used for the low permittivity ( $\sim 1$ ) layer. Having chosen these materials the fundamental resonance ( $\sim 36$  GHz) is fixed and as a consequence the design thickness of the polystyrene layer is  $\sim 4.2$  mm. The 9-layer DML chosen for the measurements, was  $65 \text{ cm}^2$  and was sandwiched by a square frame to form a multilayer structure.

Periodic metal gratings have been used as angular filters that can be integrated with conventional antennas to improve the radiation characteristics [5,6,7,8,9]. The primary objective for the design of the FSS is to provide a narrow beam performance for an antenna. Here slotted FSS are used to generate a rapid variation of the transmission response with angle of incidence. For the slotted FSS, a magnetic integral equation was formulated for the unknown magnetic current  $M$  [12,13], in the presence of a dielectric slab of thickness  $d$ , as follows:

$$\sum_{m=1}^2 2\eta_{m00} b_m^{\text{inc}} \Psi_{m00} = - \sum_{mpq} \left( \xi_{mpq} \eta_{mpq} + \eta_{mpq}^d \right) \Psi_{mpq} \iint_{\substack{\text{unitcell} \\ \text{aperture}}} M \cdot \Psi_{mpq}^* dr \quad (5.2)$$

where  $b^{\text{inc}}$  is the amplitude of the plane wave exciting the structure and

$$\xi_{mpq} = \frac{1 - \Lambda_{mpq}}{1 + \Lambda_{mpq}} \quad (5.3)$$

$$\Lambda_{mpq} = e^{-2j\gamma_{pq}^d} \frac{\eta_{mpq}^d - \eta_{mpq}}{\eta_{mpq}^d + \eta_{mpq}} \quad (5.4)$$

$\gamma$  and  $\eta$  are the modal propagation constants and admittances respectively, where in the dielectric region they are denoted by the superscript  $d$ .  $(p, q)$  are the Floquet indices for TM ( $m=1$ ) and TE ( $m=2$ ) modes and  $\Psi$  is the vector Floquet mode.

As mentioned in section 4.3, a method-of-moments solution was employed to determine the electric current on the element. The slotted FSS were made by taking the Babinet's complement of the element FSS. Entire domain basis functions were used for this solution, of the form

$$\cos\left(\frac{m'\pi u}{L}\right), \sin\left(\frac{n'\pi u}{L}\right).$$

$L$  is the length of the segment under consideration, which is along an arbitrary direction  $u$ .  $m'$ ,  $n'$  may take integer as well as half integer values. In total, three magnetic current bases were used for the tripole, each corresponding to index  $m' = 1/2$ . Seven basis functions were used:  $m' = 1, 3$  and  $n' = 2, 4, 6, 8, 10$  in each horizontal and vertical arm of the crossed dipole. One hundred and sixty nine Floquet modes were found adequate to represent the tangential field adjacent to the array. The transmission and reflection coefficients were calculated using the zero-order propagating mode.

In the design procedure, the parameters were initially adjusted to obtain a passband near 30 GHz at normal incidence, beyond which the array is highly reflective with increasing incident angles. This was achieved by varying the array periodicity whilst keeping the element length fixed. The radiation pattern of these FSS as spatial filtering arrays, under plane wave illumination at normal incidence will therefore be associated with the

above variation. For practical purposes, such as the size of the array to the wavelength, it was found that an appropriate design for the tripole slots[11] and crossed-dipole slots[10] was a periodicity of 8.9 mm and 8.6 mm, respectively. Figure 4.3 shows the lattice and element geometries and the physical parameters of both the designs. The arrays were backed by a 0.037 mm thick dielectric substrate (polyester) with  $\epsilon_r = 3.0$ , and the copper thickness was about 10  $\mu\text{m}$ . The FSS measured 60  $\text{cm}^2$  and were stretched over a rigid wooden frame.

### 5.6 Inspiration for Curved Measurements

The concept of curving DML and FSS is actually an intermediate stage in the proposed design of a semi-spherical refracting dome. Curved surfaces have been used in practice[14,15], although no attempt was made to analyse the effect of curvature explicitly. Here a practical study to establish the effects of the curved surface is carried out.

The planar filters can be conveniently formulated due to their finite shape and geometry in a three dimensional plane. However, modelling the scattered fields from curved surfaces is a formidable problem. For an arbitrary surface where general integrals of differential equation formulations are necessary, rigorous numerical modelling may not be realistic and it is beyond the scope of this project. However, work has been going on in the area of curved FSS which would form a future study in this region[16,17,18].

Here the planar theory is applied to the curved multilayer and it has been expected that this approach is to be reasonably accurate when the curvature is small compared with the wavelength and with the scale size of the surface variations.

## 5.7 Results

Both the DML and the FSS are measured to determine the angular filtering characteristics. Radiation patterns and the near-field patterns from which the passive nature of the planar redomes can be compared to that of curved redomes.

### 5.7.1 Angular filtering characteristics

An angular filter, transmits or reflects an electromagnetic signal depending upon the angle of incidence, relative to the filter surface. The main intention of such a filter is to provide a narrow beam width radiation characteristics. This filter, if placed in front of a directive antenna can reduce the sidelobes. The main lobe of the antenna corresponds to a wave that is incident in the angular passband of the antenna and is not affected by the filter. Once the angle of incidence is varied, the signal will be attenuated which results in less transmitted power. Here the characteristics of DML and FSS, as angular filters are investigated.

#### 5.7.1.1 Dielectric Multilayer

The simulated and theoretical frequency responses of the melamine multilayer filter for various angles of incidence are plotted in Figure 5.3. The response at normal incidence is nearly symmetric about the fundamental resonant frequency (~36 GHz) and the departure from symmetry is due to material absorption within the melamine. Also clearly noticeable in the figures are higher order resonance features which arise because of the presence of more than one layer. When the angle of incidence changes to  $30^\circ$  the frequency response approximately shifts by a few GHz as shown in Figure 5.3. A notable change is in the behaviour of the second-order response. The TE component shifts its position by

Frequency response of a 5-layer dielectric multilayer (TE).  
at 0, 10, 20 degree incidence.

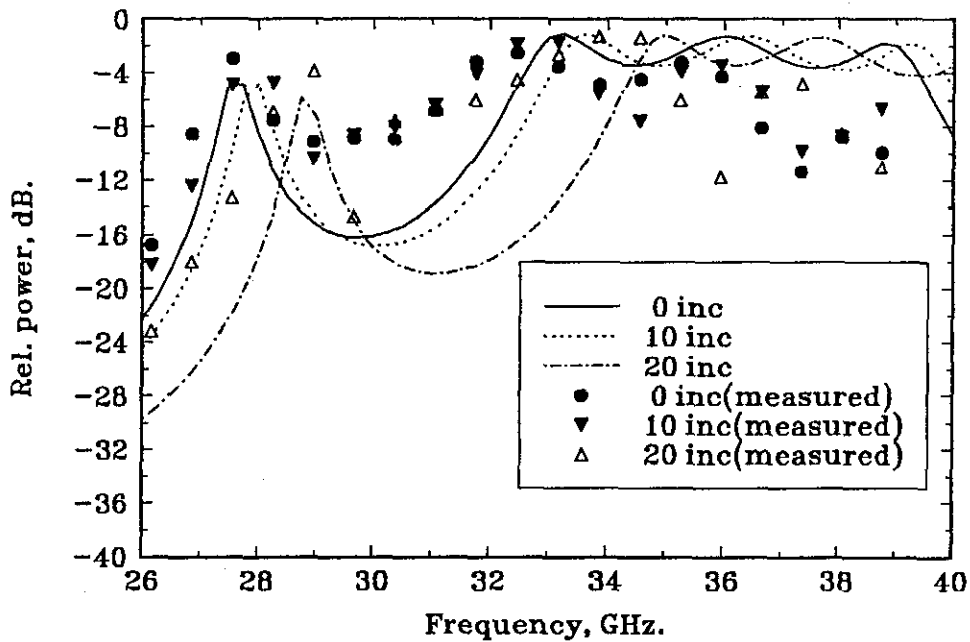


Figure 5.3.a

Frequency response of a 5-layer dielectric multilayer.  
at 30, 40 degree incidence (TE).

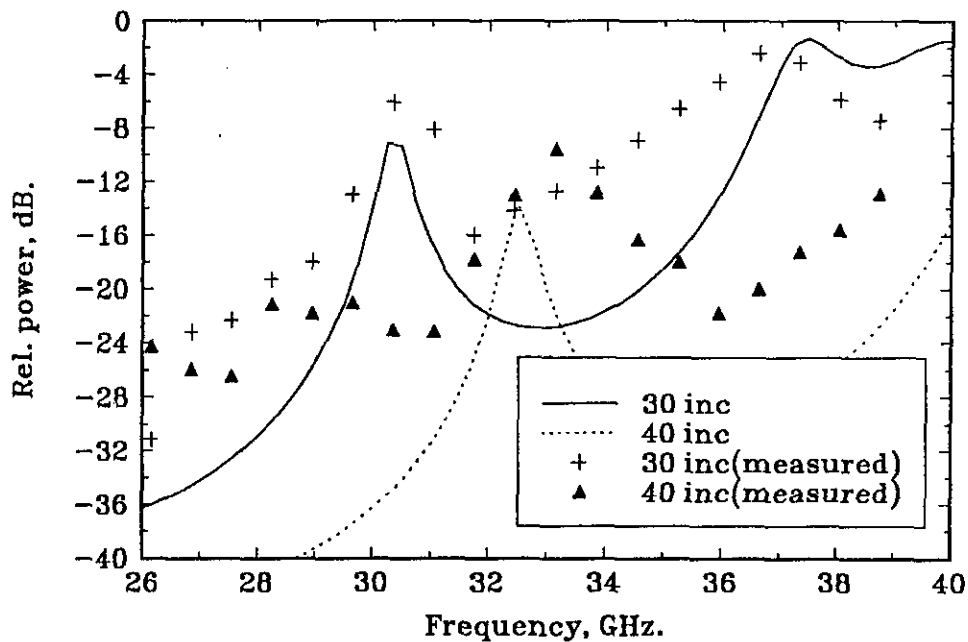


Figure 5.3.b

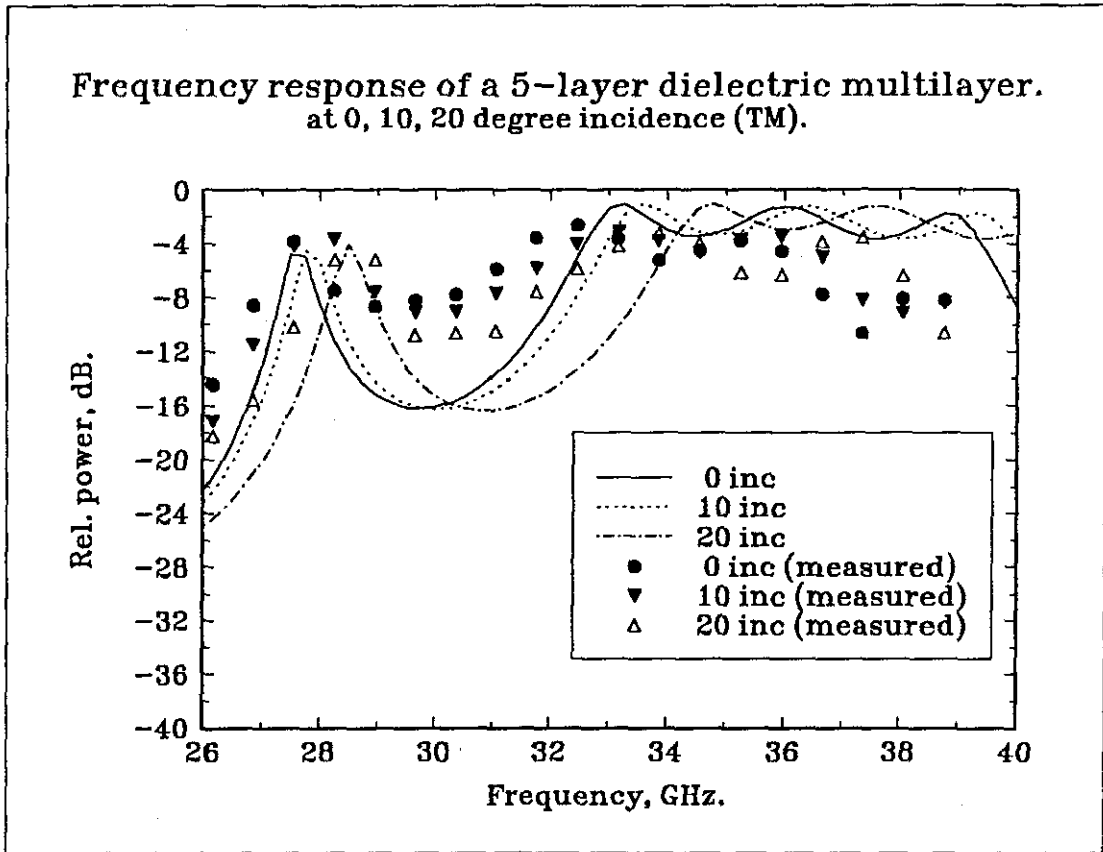


Figure 5.3.c

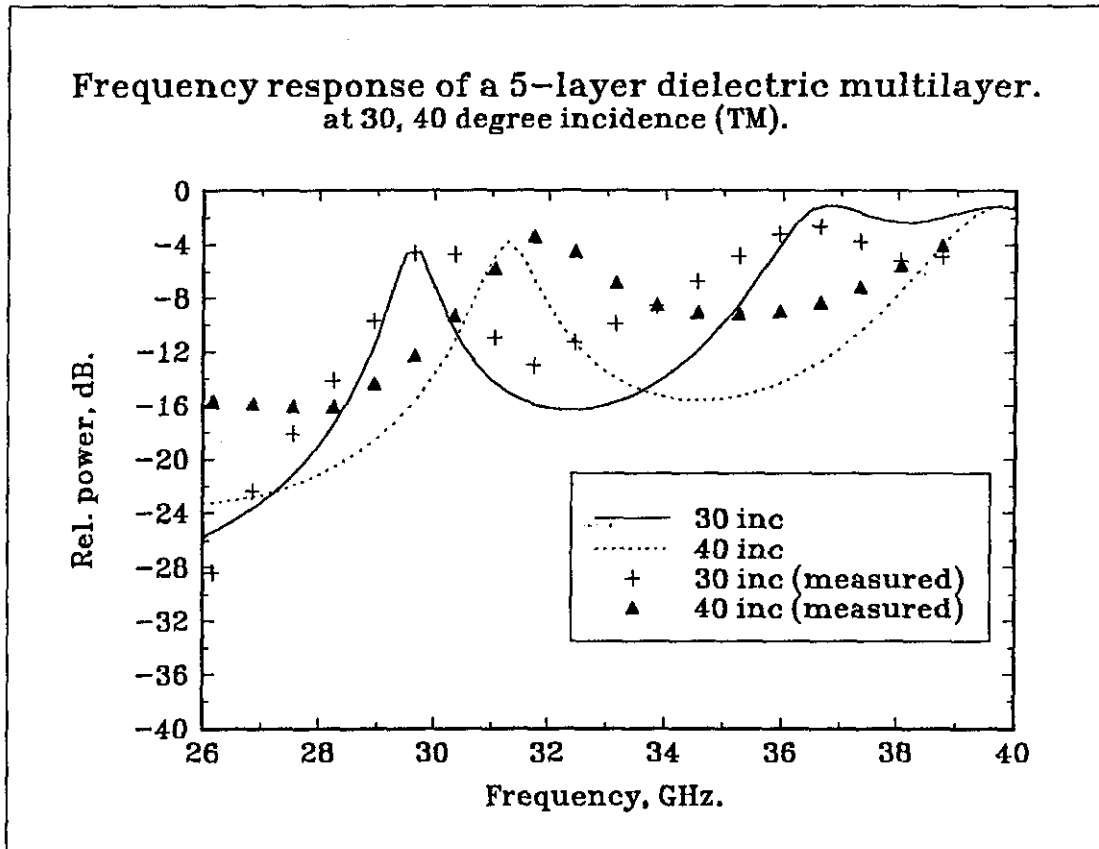


Figure 5.3.d

~2.8 GHz towards the high frequency regime, resulting in a reduction of amplitude of ~4.5 dB. The TM component behaves in a similar way, exhibiting a shift of 2 GHz to the high frequency region, although the amplitude remains unchanged. These results suggest that more sensitive control of the angular transmission properties of the filter can be accessed in the vicinity of the second order resonance rather than the fundamental or first orders.

Clearly the predicted resonant structure is observed experimentally. The discrepancy in some parts of the curves is mainly due to inaccuracies in the input parameters to the model, rather than the model itself. The dimensions and dielectric parameters are not exactly known, in particular it is unlikely that the electrical properties of the melamine laminate are the same as those at 1 MHz. Also the finite size of the DML which was used for the measurements could be a reason for this inaccuracy. Despite the relatively crude nature of the experimental and theoretical comparison the results nevertheless indicate that the multilayer does indeed behave as a spectral and angular filter in the manner predicted.

The applications of DML as a curved surface were studied with a view to converting the planar dome structure to a curved dome structure. Figures 5.4 show the frequency responses of the DML for curvatures H1 and H2 for both polarisations. For normal incidence, the transmitted power decreases as the curvature increases for the second order frequency 29.5 GHz. The peak at this frequency moves away to the high frequency region and is ~-17 dB at 45° incidence for H1 for TE polarisation. For H2, the second order peak in the TE frequency response remains almost the same for various incidences. The TM responses

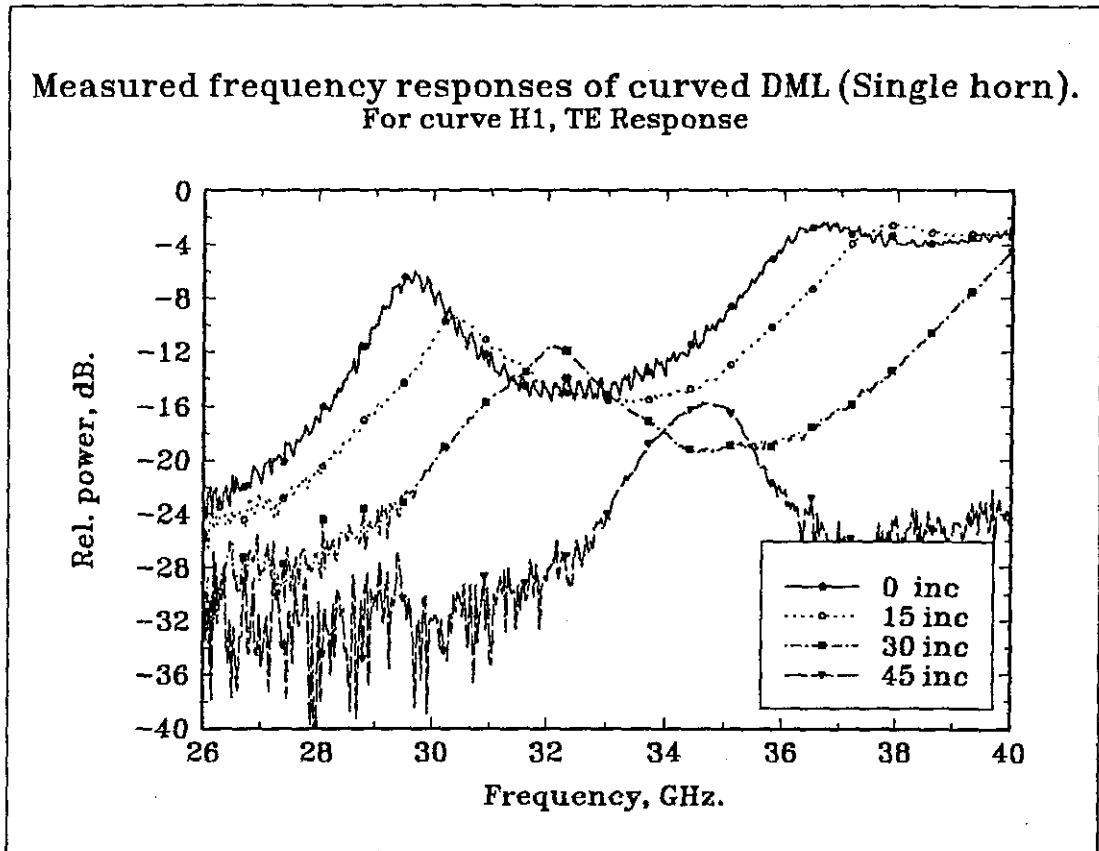


Figure 5.4.a

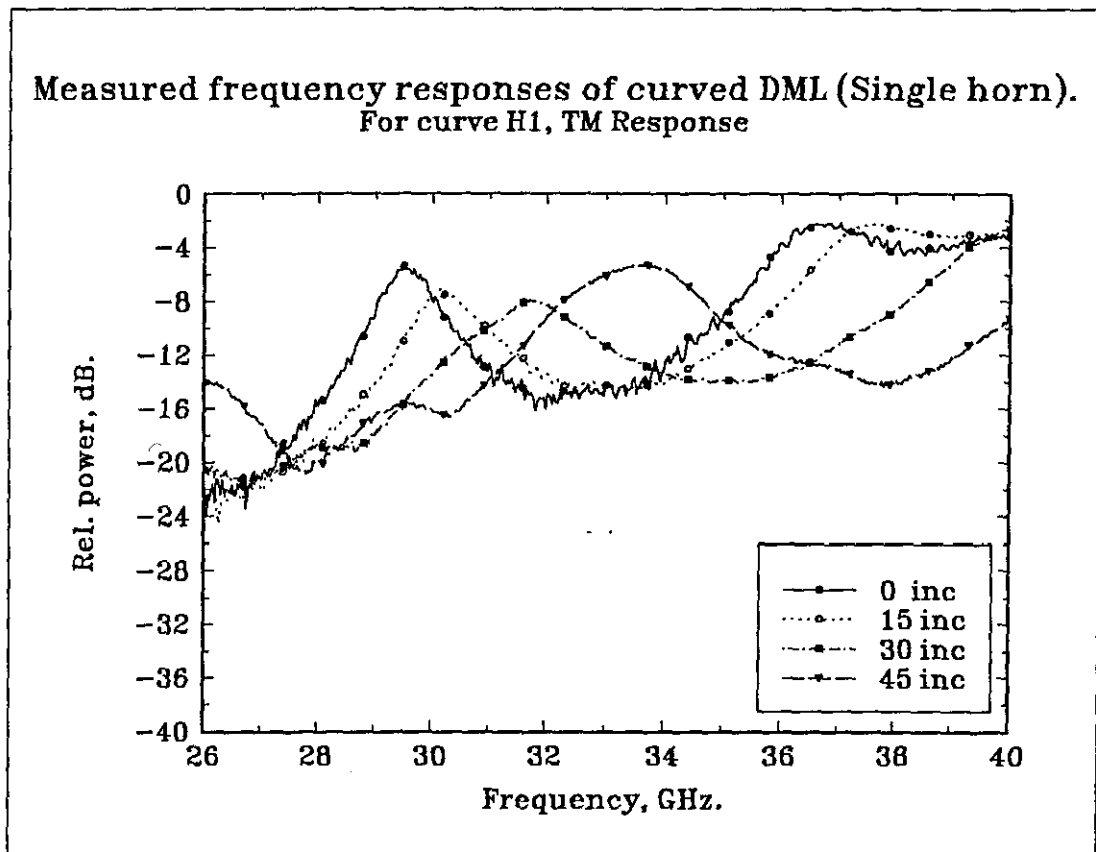


Figure 5.4.b

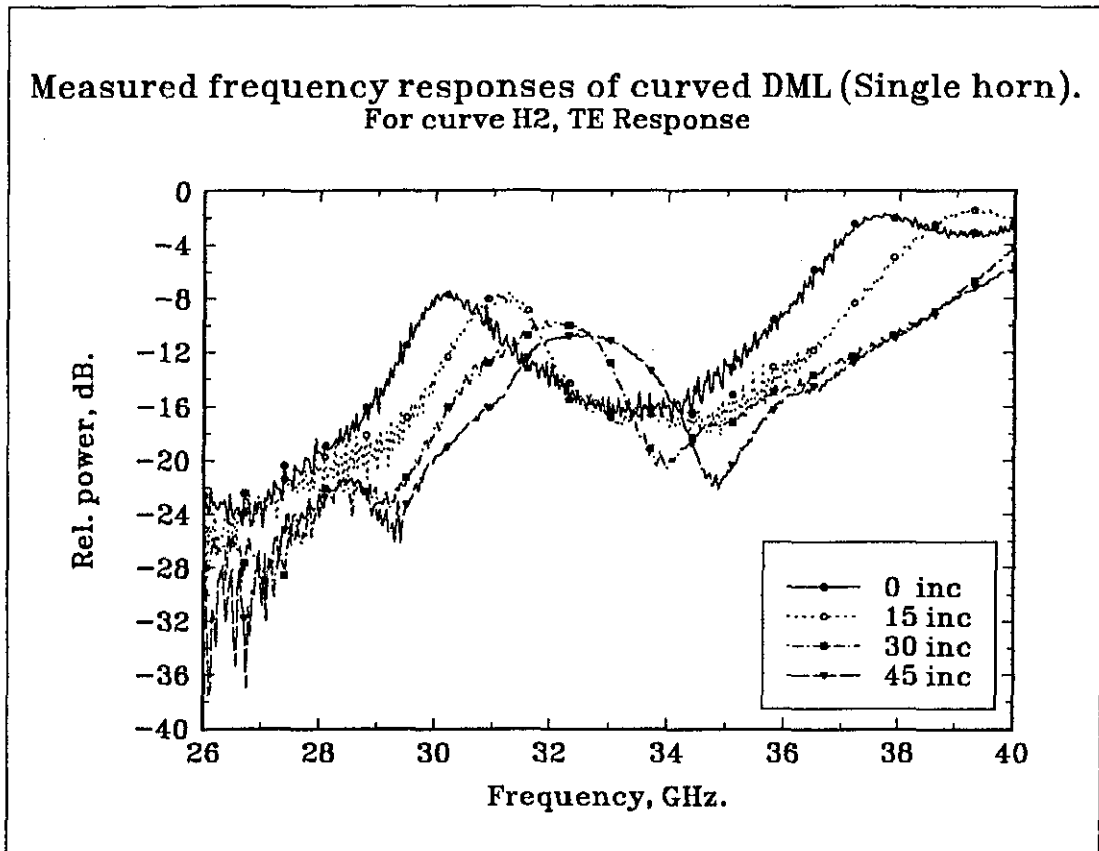


Figure 5.4.c

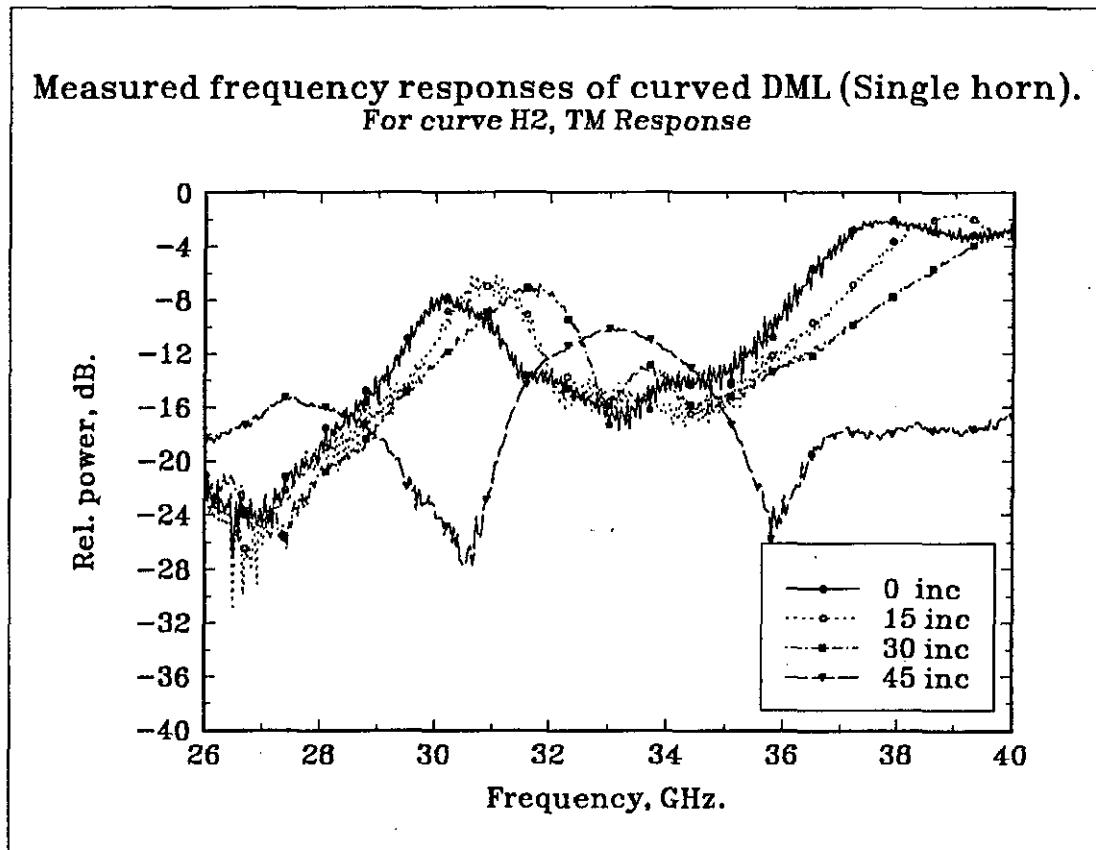


Figure 5.4.d

also show an increase in the signal absorbed in the DML, as the curvature is increased. The amplitude of the second order component remains almost the same for a range of incident angles, though more discrimination is offered by H1, as was true for TE polarisation.

### 5.7.1.2 Frequency Selective Surfaces

Measurements were conducted with tripole and crossed dipole slotted arrays.

For the tripole surface, two sets of measurements are possible for the same incidence. They are

(1) When one of the arms of the tripole slot is parallel to TE polarisation;

At this state the TE component is TE<sub>a</sub> and the TM component is TM<sub>b</sub>.

(2) When one of the arms of the tripole slot is parallel to TM polarisation;

Here the TE component is TE<sub>b</sub> and TM component is TM<sub>a</sub>.

The above definition of incidences is described geometrically in Figure 5.5. All the possible states of TE and TM polarisations were tested in the chamber and both the TE components (TE<sub>a</sub> and TE<sub>b</sub>) and TM components (TM<sub>a</sub> and TM<sub>b</sub>) gave nearly the same performance. Hence from here onwards only the TE<sub>a</sub> and TM<sub>b</sub> will be discussed in this thesis. Unlike tripoles, only one set of readings was taken for crossed dipole surface, due to the symmetry of the FSS element.

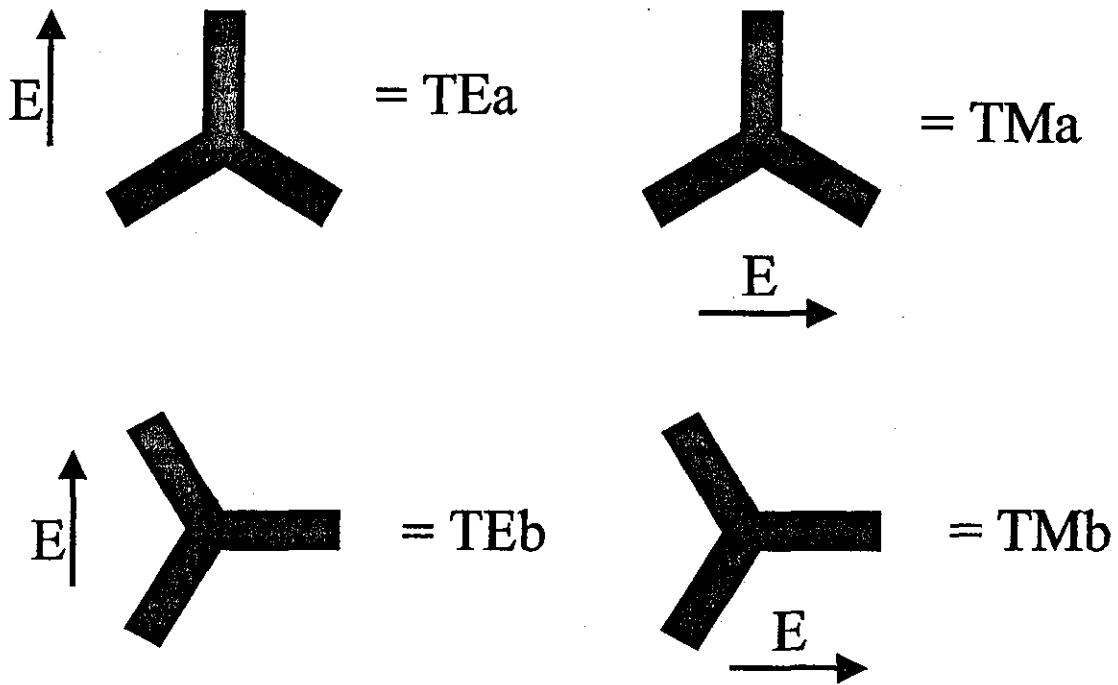


Figure 5.5 Various orientations of the tripole slots.

The simulated and measured frequency responses of planar(H0) crossed dipole and tripole slot FSS for both polarisations are shown in Figures 5.6 & 5.7. Measured values fit with the predicted values within a range of  $\pm 5$  dB.

For TM incidence for both FSS, the amplitude of the resonant frequency component drops drastically as the angle of incidence varies and increases at higher angles of incidence. For tripole slot FSS, at frequency  $\sim 29.5$  GHz, the signal amplitude reduces from 0 dB to  $\sim -15$  dB and at  $60^\circ$  it is  $\sim -7$  dB. The resonant peaks move to the low frequency region.

For TE incidence, the tripole surface shows a signal amplitude of  $\sim -3$  dB and unlike TM incidence, the amplitude reduces as the angle of incidence increases and it stays below  $-11$  dB at  $60^\circ$ . Similarly for the crossed dipole surface, the signal amplitude remains at  $\sim -2$  dB at  $10^\circ$  incidence and at  $60^\circ$  incidence it is well below  $-10$  dB. Like the TM, the resonant peaks for TE shift to a lower frequency.

These results suggest that for TM incidence these

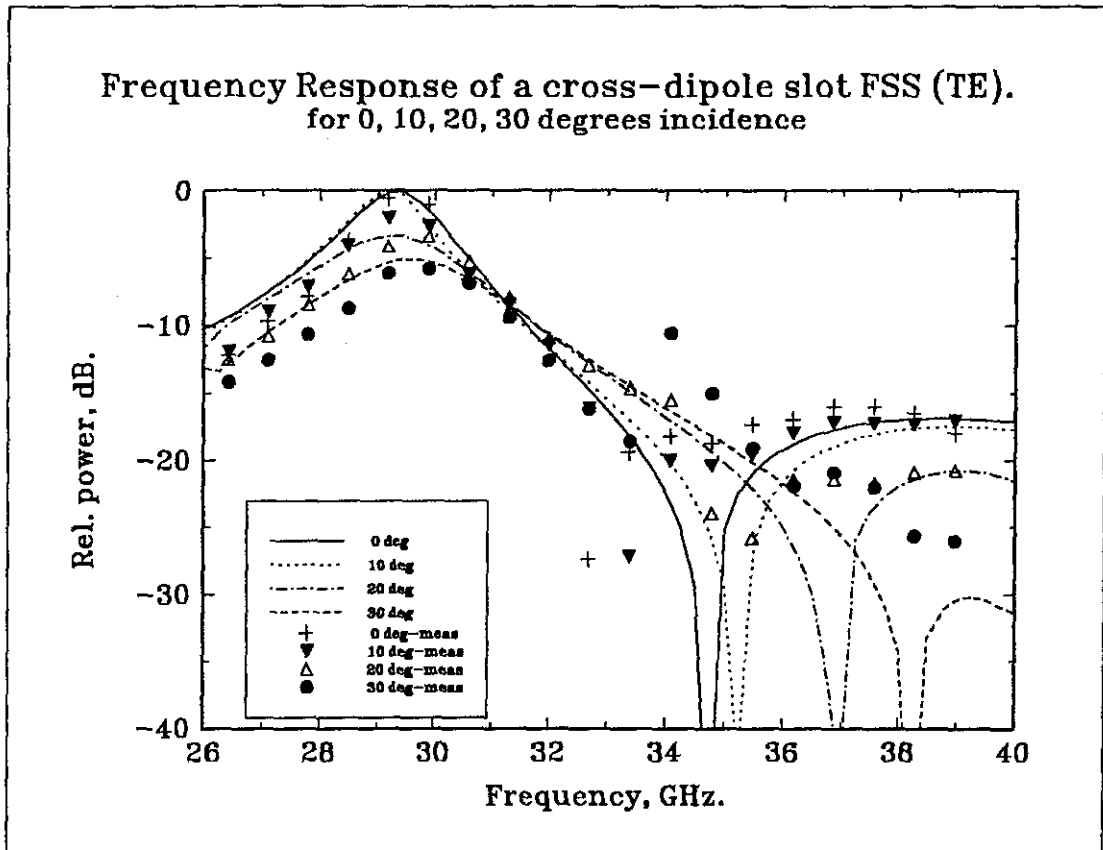


Figure 5.6.a

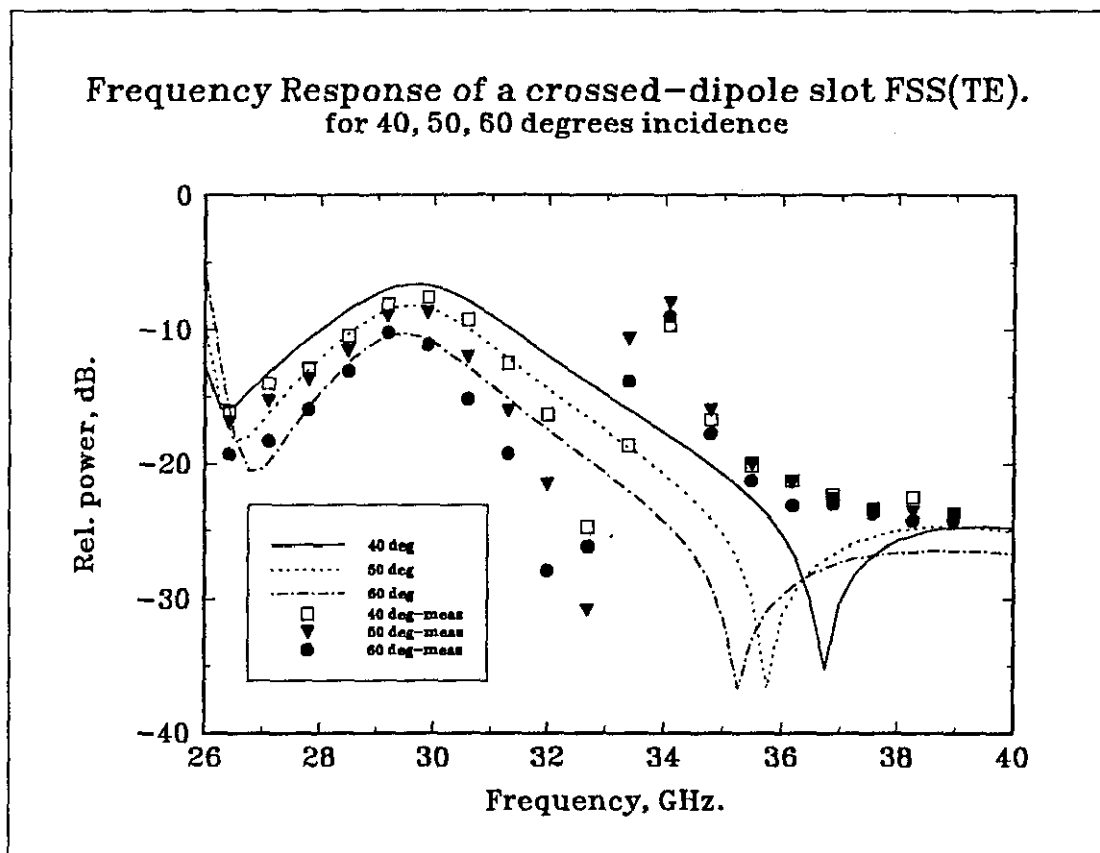


Figure 5.6.b

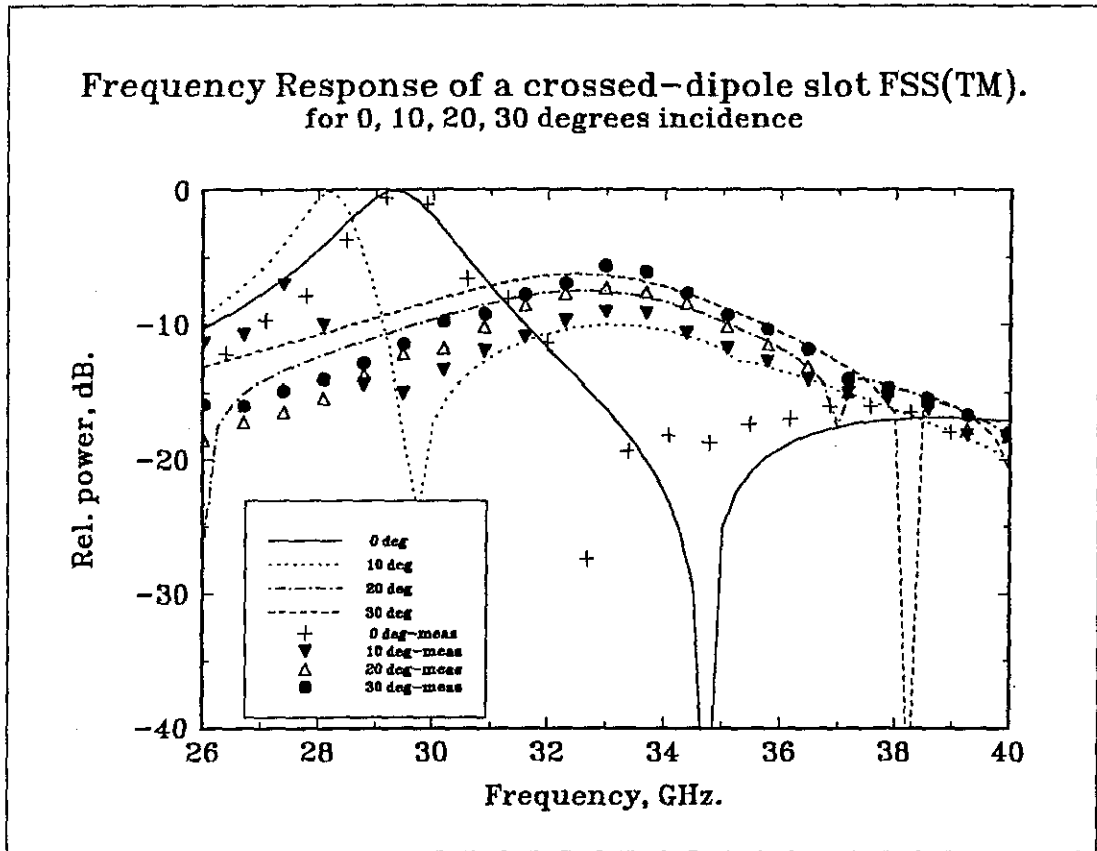


Figure 5.6.c

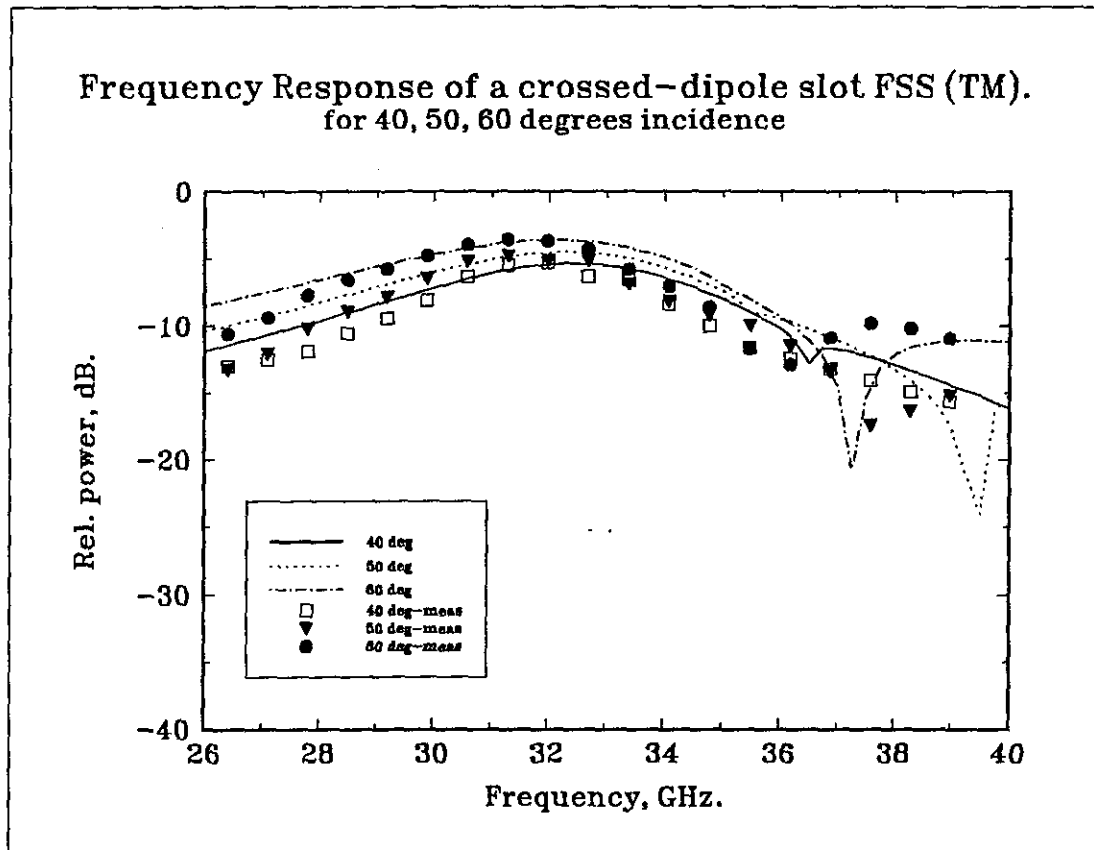


Figure 5.6.d

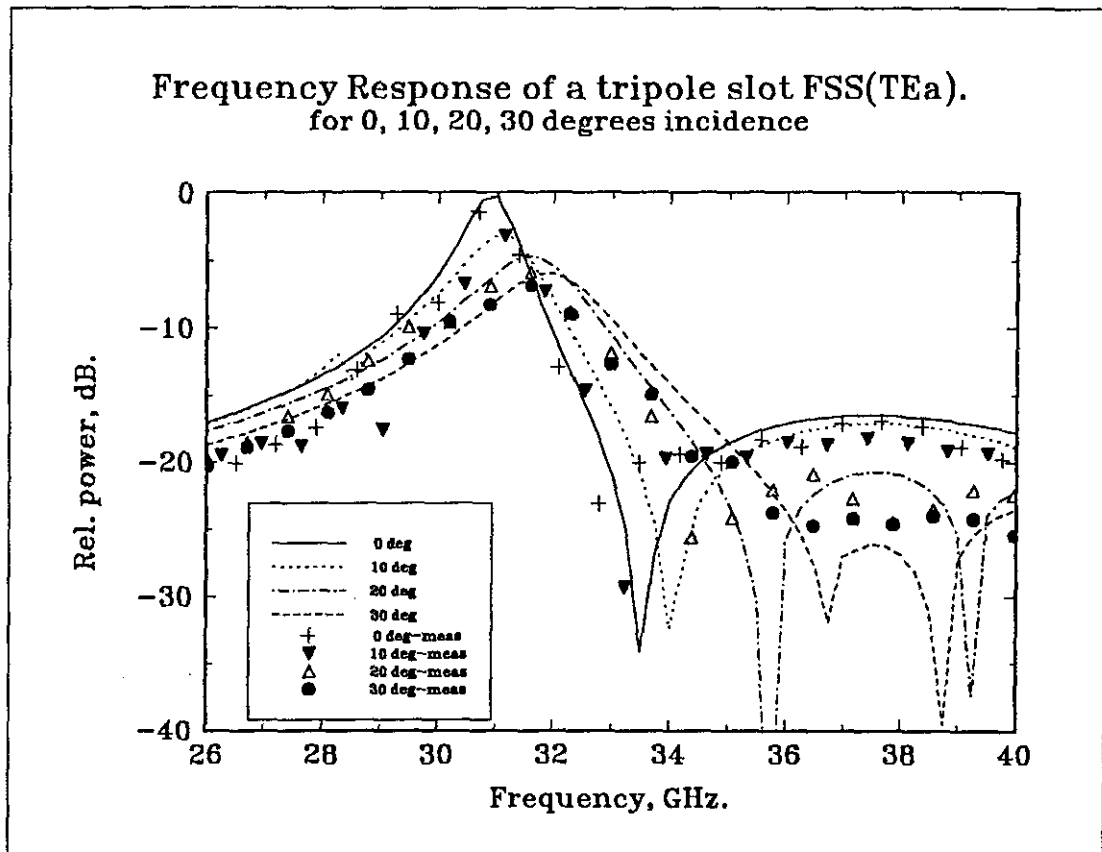


Figure 5.7.a

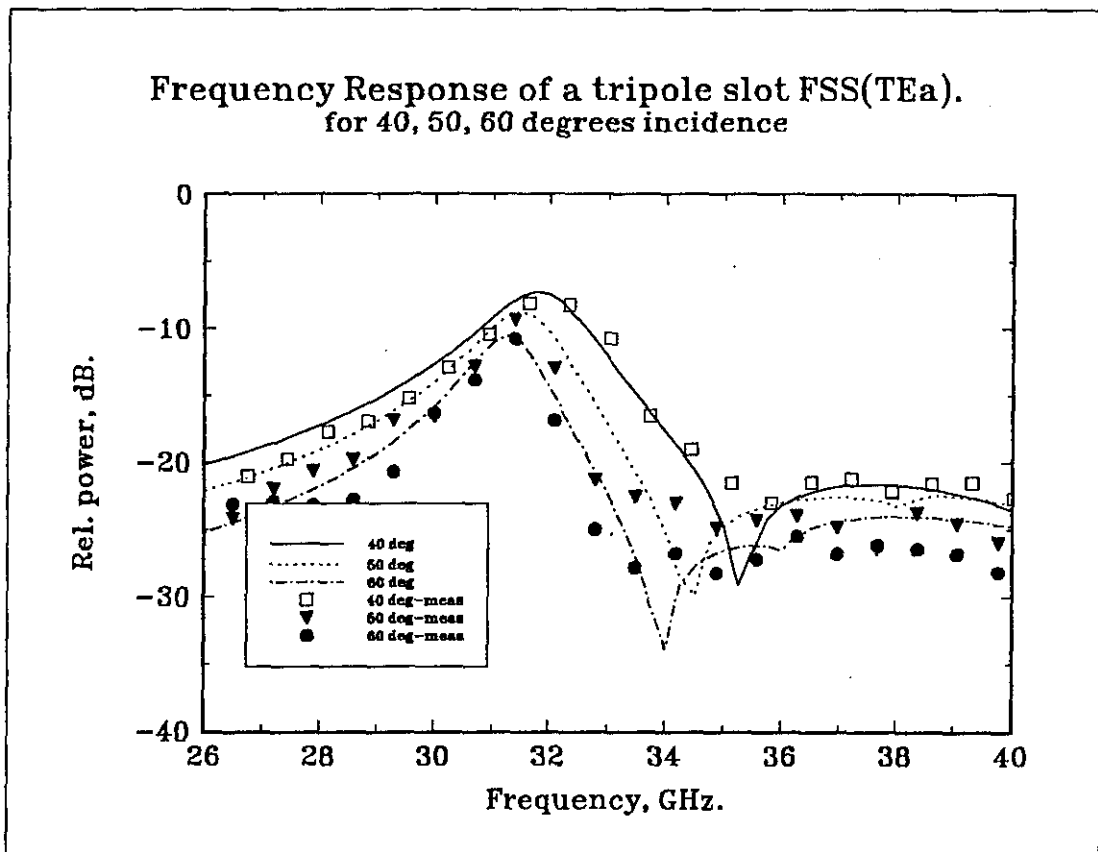


Figure 5.7.b

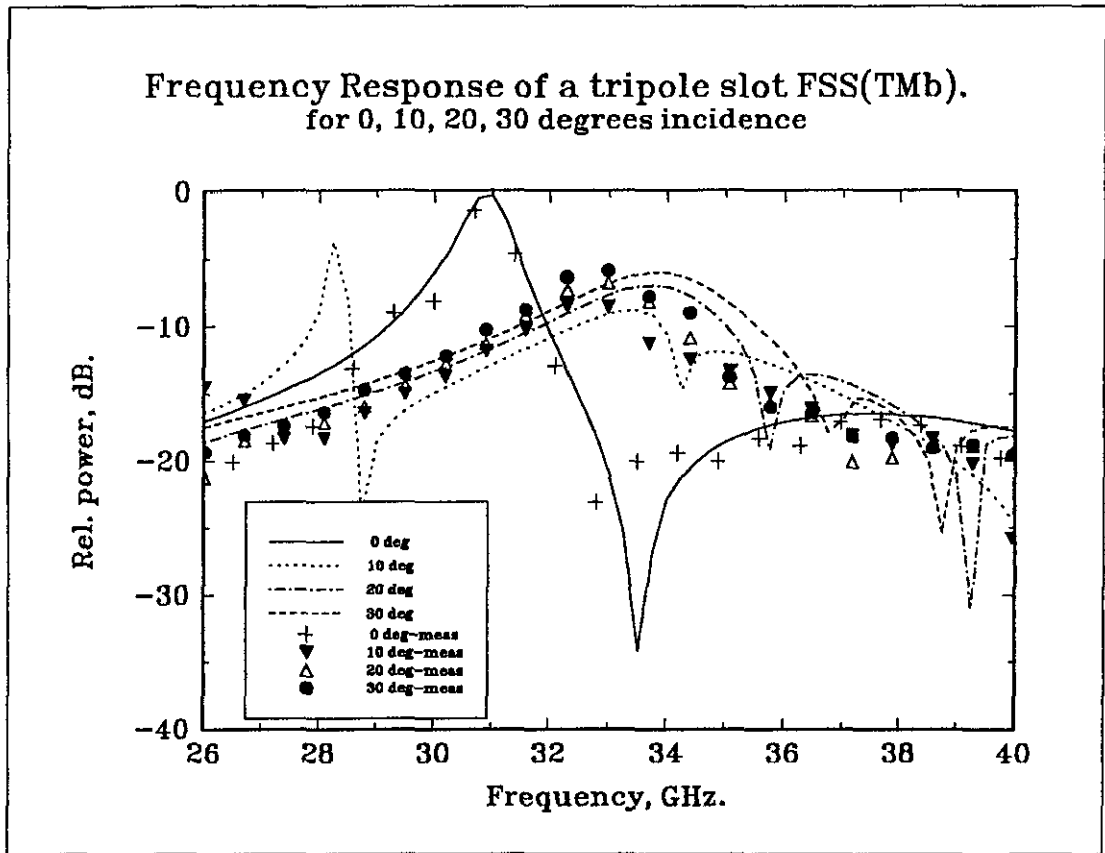


Figure 5.7.c

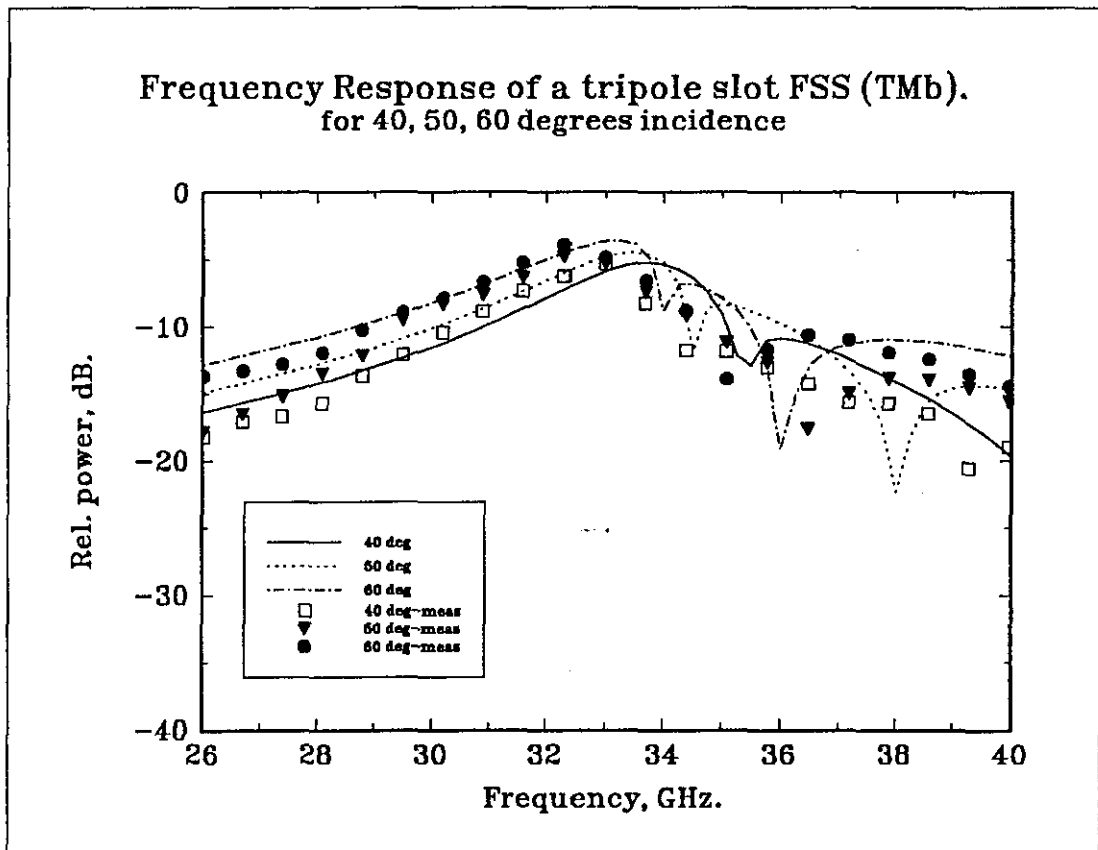


Figure 5.7.d

surfaces act as narrow bandpass filters and admit a narrowband of 0.75 GHz (-3 dB bandwidth) for tripole surface and 1.75 GHz (-3 dB bandwidth) for crossed dipole surface. For TE, a sharp filtering hasn't been observed, but a gradual decay of the transmitted signal, with angle of incidence is noted.

As the angle of TE incidence increases, the onset of grating lobes is noted in the frequency response of the crossed dipole surface (Figure 5.6.a and 5.6.b). Grating lobes appear when the periodicity between the slots approaches one wavelength. They have almost the same amplitude of the main resonance[19]. This effect has not been predicted by the theoretical model and suggests that as the periodicity increases the model becomes invalid, due to a finite number of slots on a finite surface. Nonetheless the TM gives almost the predicted values. The effect due to the finite size of the FSS is verified experimentally.

From planar surface(H0) measurements, it is concluded that the surface acts as an angular filter for TM incidence, which admits electromagnetic waves within a certain band and this provides the discrimination for frequencies in the proposed antenna design.

The performances of curved FSS(curve H1 and H2) are now studied in relation to that of the planar surface FSS(H0). As mentioned in section 5.6, no theoretical model is available for the evaluation of the curved FSS. The method of evaluation used is strictly based on the comparison of the available practical data from the planar surface.

With regard to the curved FSS (Figure 5.8), a degradation of signal strength is noted for both surfaces, for both curvatures and for both polarisations. For TM incidence, tripole FSS gives almost the same -3 dB bandwidth as the planar one. But the angular filtering effect seems to reduce as the curvature increases. For curve H1, at 15°

chapter  
3

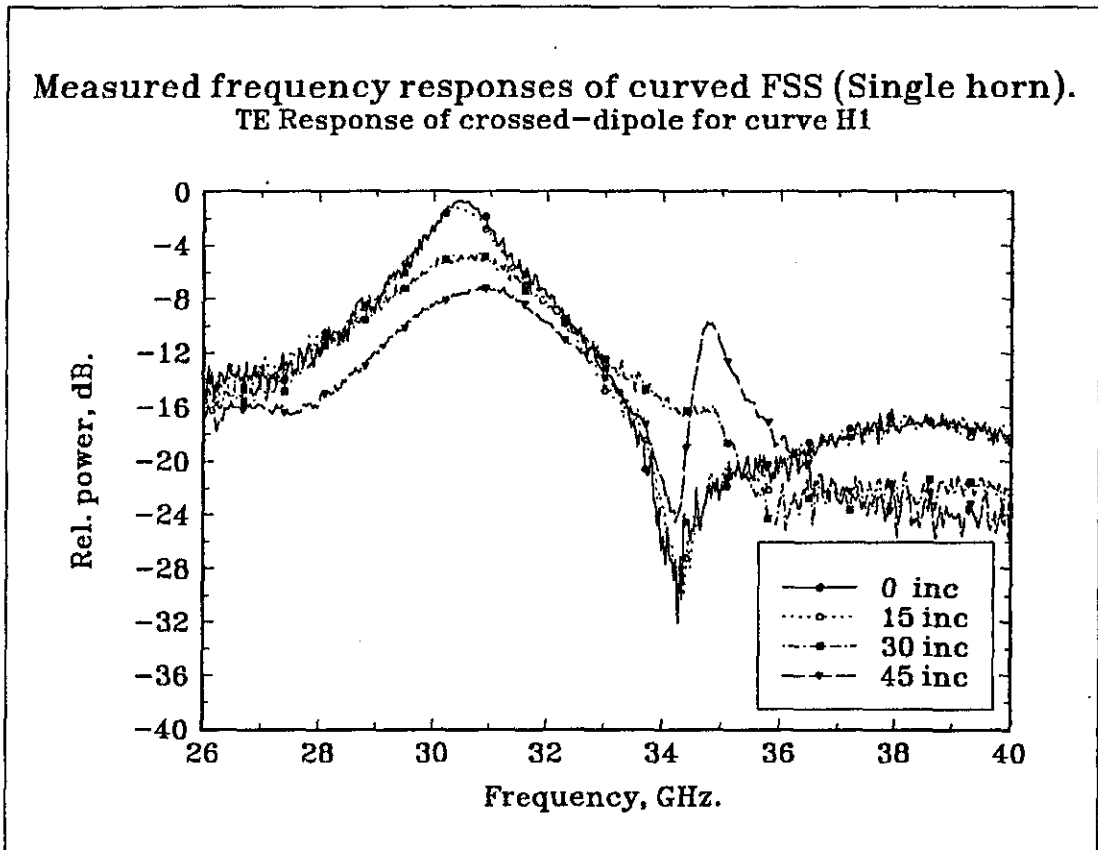


Figure 5.8.a

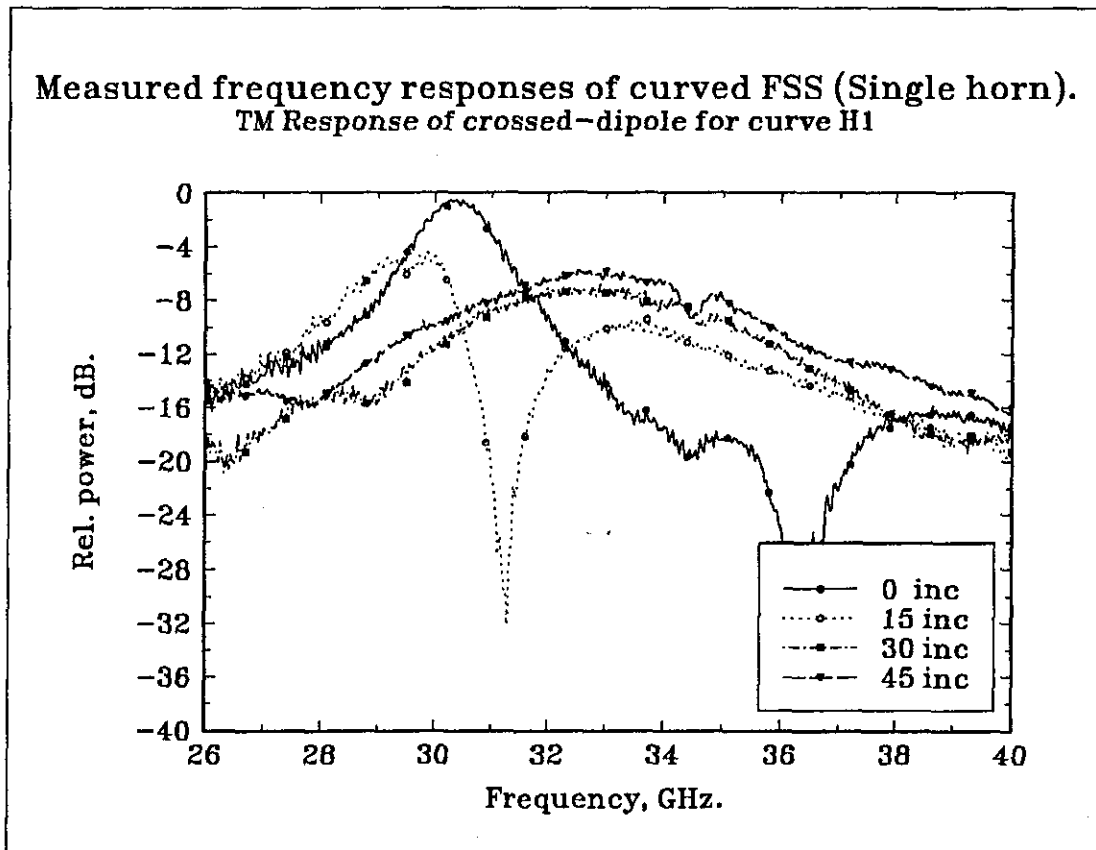


Figure 5.8.b

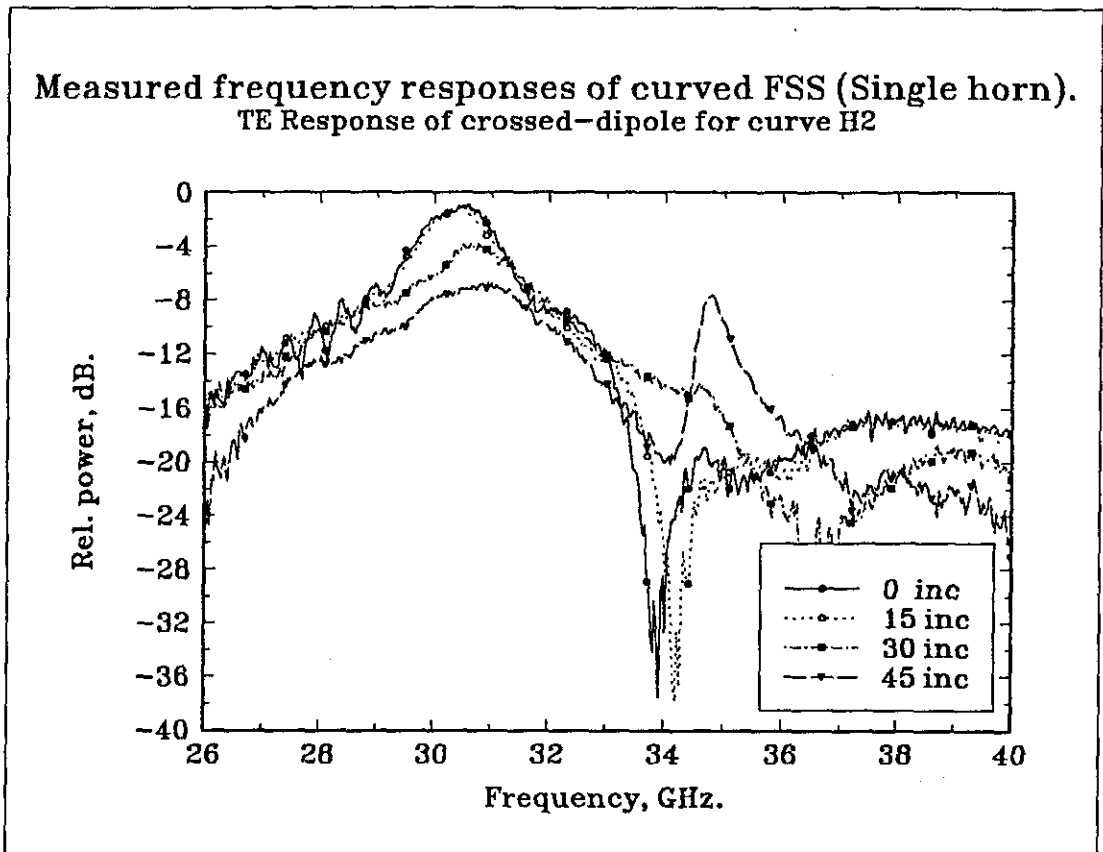


Figure 5.8.c

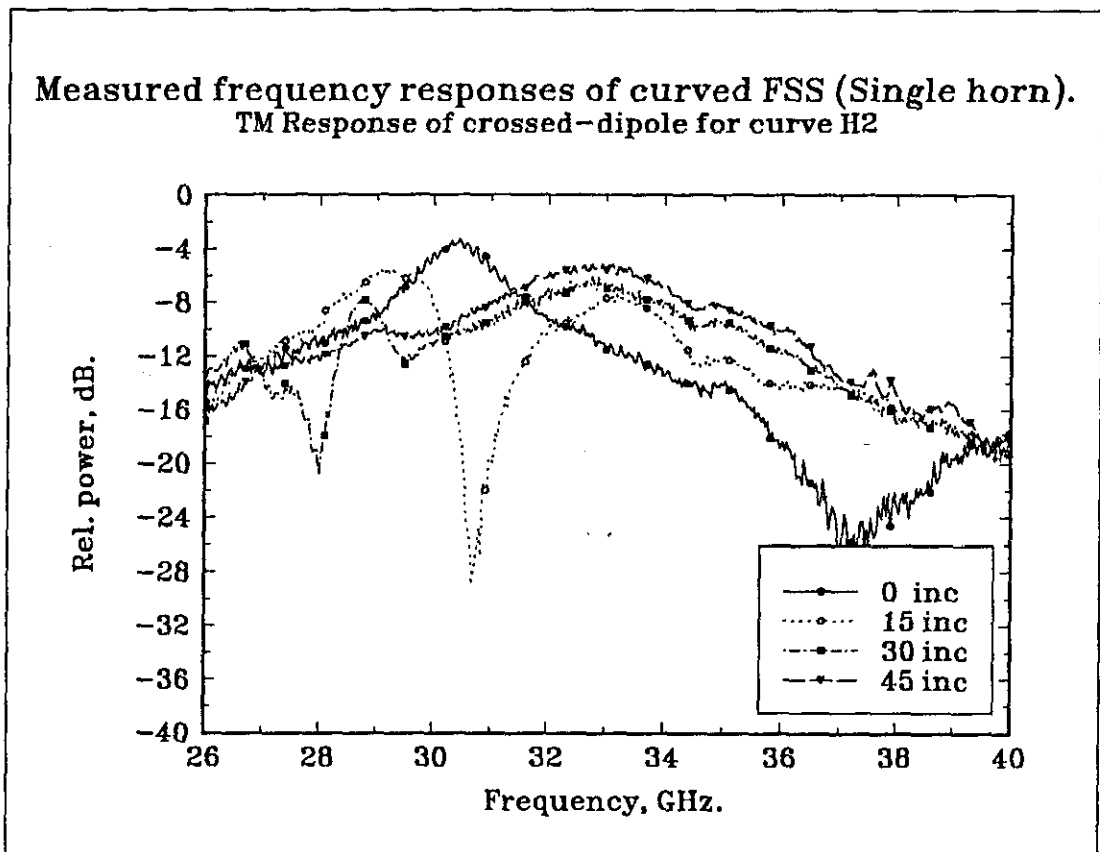


Figure 5.8.d

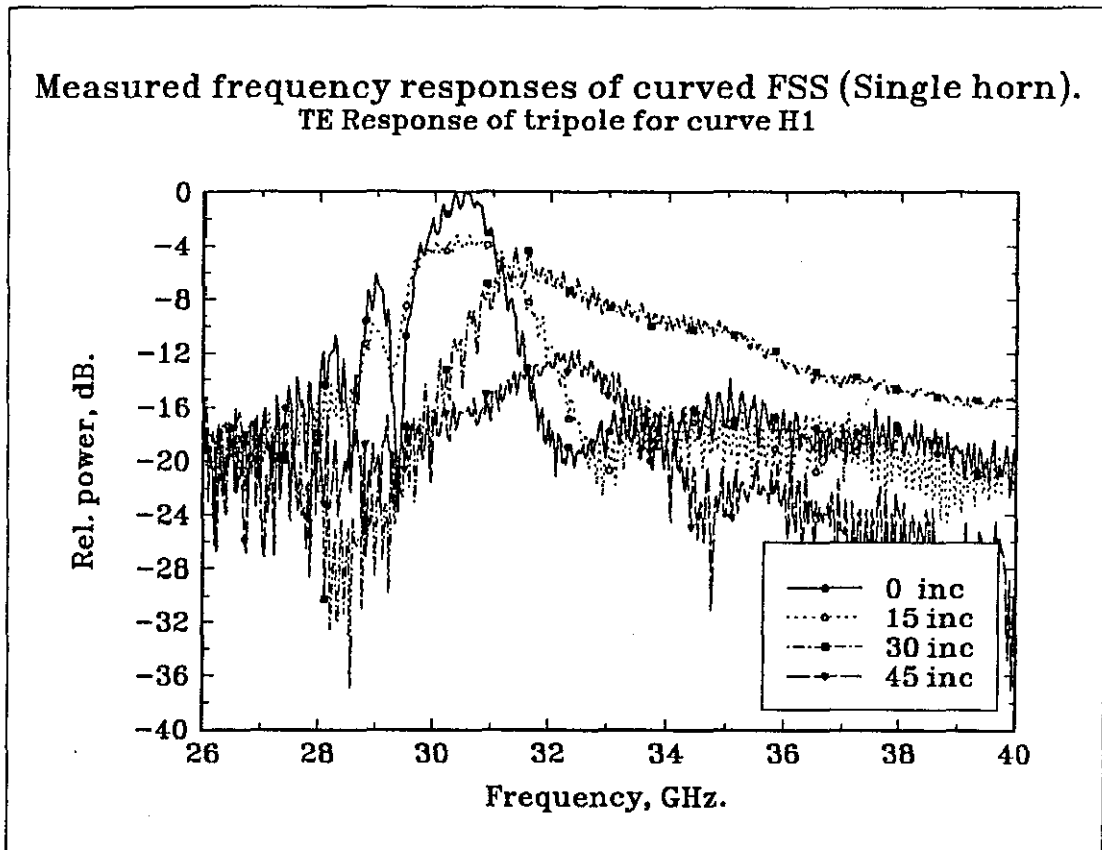


Figure 5.8.e

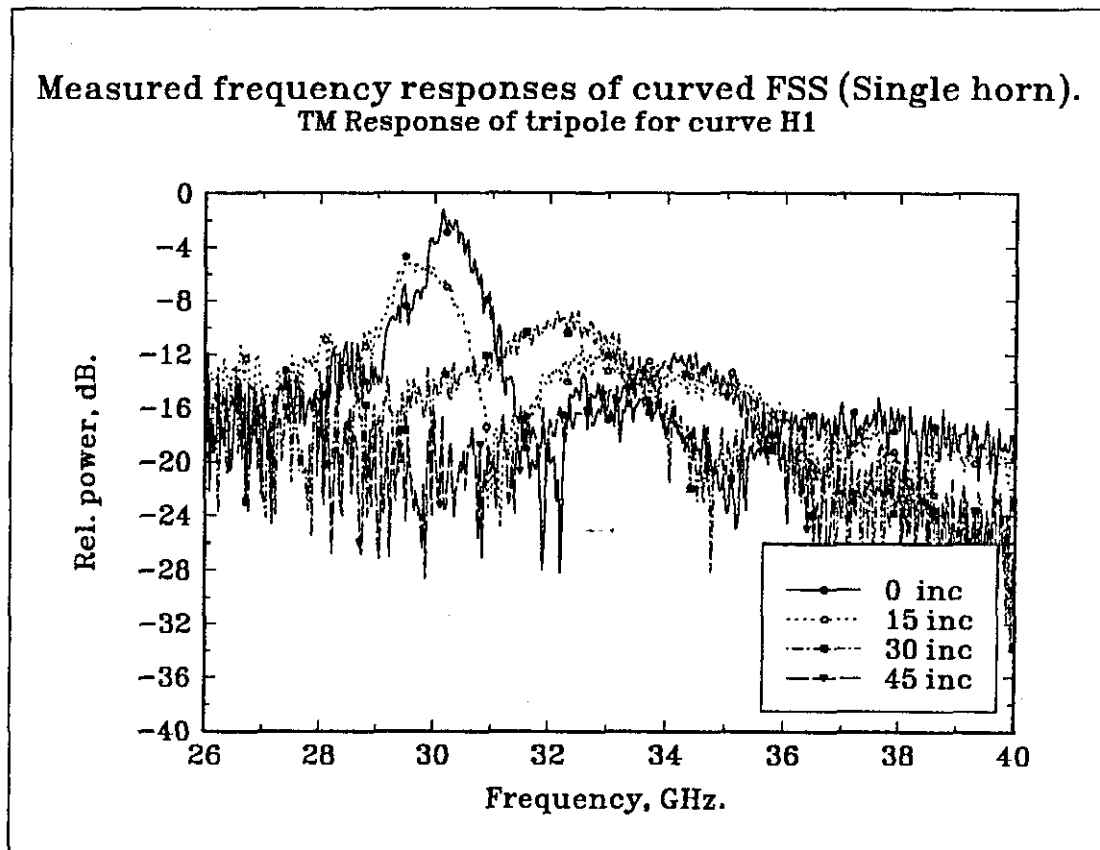


Figure 5.8.f

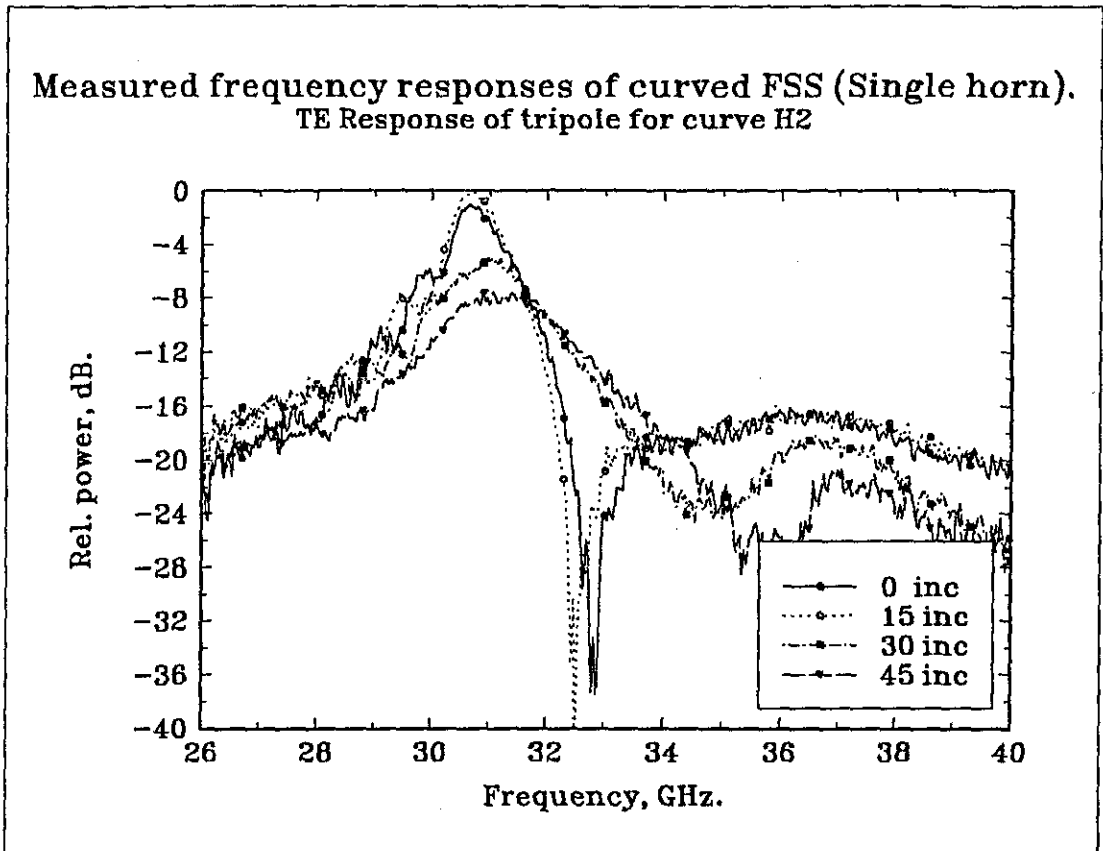


Figure 5.8.g

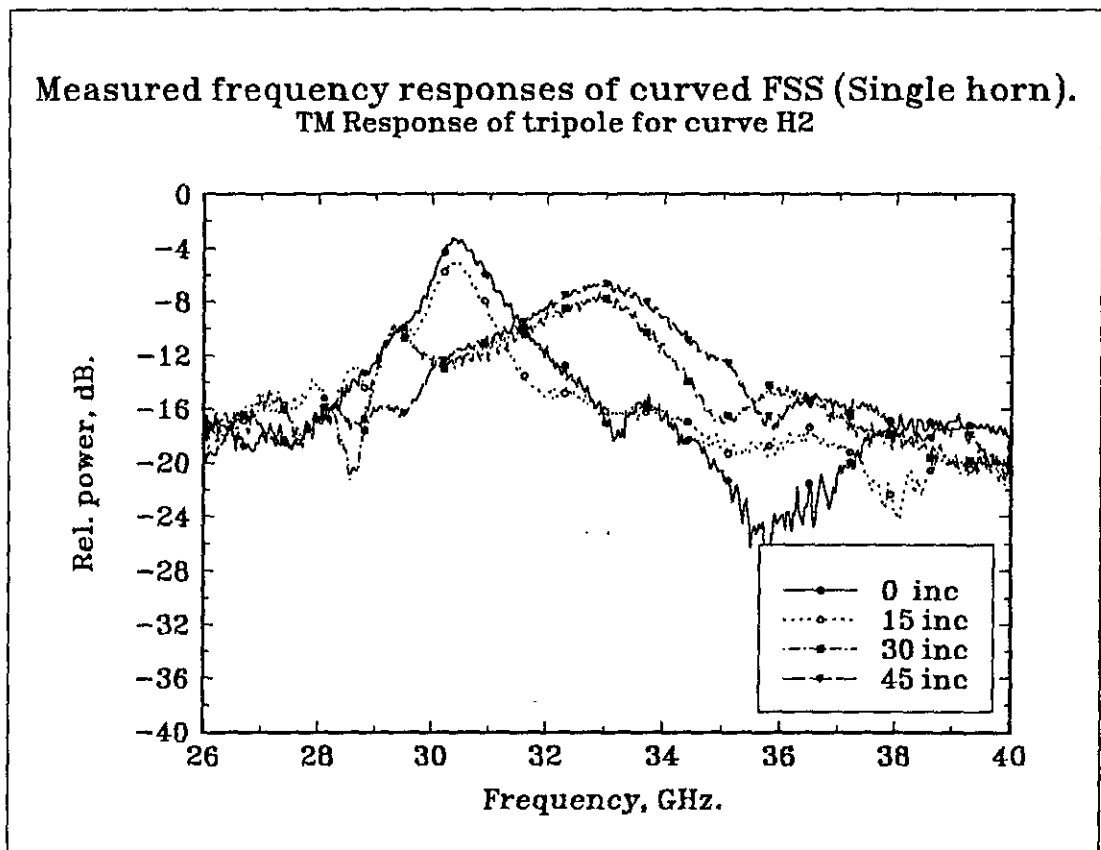


Figure 5.8.h

incidence and the resonant frequency of  $\sim 30$  GHz an amplitude of  $\sim -8$  dB is obtained and for curve H2, it is  $\sim -4$  dB. For TE incidence, the characteristics seem to repeat for various curvatures. For curve H1,  $\sim -4$  dB is observed for the signal at the resonant frequency, at  $15^\circ$  incidence and  $\sim -1$  dB for curve H2. Also a sharp null at  $\sim 33$  GHz is observed as the curvature increases.

A decrease of  $\sim -3$  dB in the transmitted power at the resonant frequency  $\sim 30$  GHz is obtained for the crossed dipole surface, for TM incidence as the curvature is increased. The null at  $\sim 30$  GHz seems to deepen with the curvature. For TE incidence the degradation of the transmitted power is nearly the same as the planar surface. Also the amplitude of the grating lobes increases with increase in curvature.

These results imply that these surfaces can be bent or curved to suit the requirement, but they give nearly the same angular filtering performances with a reduction in the maximum transmitted power and in bandwidth.

## 5.7.2 Plane Wave Measurements

### 5.7.2.1 Dielectric Multilayer

The simulated and measured angular responses of the structure are plotted for the second order resonant frequency ( $\sim 27.4$  GHz) in Figure 5.9. In broad terms, both polarisation states are well transmitted near normal incidence and as the angle of incidence increases to  $\sim 40^\circ$  the transmitted power decreases sharply. The TE component stays below  $-20$  dB at  $30^\circ$  and higher whilst the transmission of the TM component increases after  $\sim 40^\circ$ . These results indicate that the transmission response of the divergent beam would have an angular variation resulting in collimation. Even though the electrical parameters of the melamine layers are not known

accurately at the operating frequencies used here, the positions of the points are estimated fairly well within a range of 5 dB by the simple model.

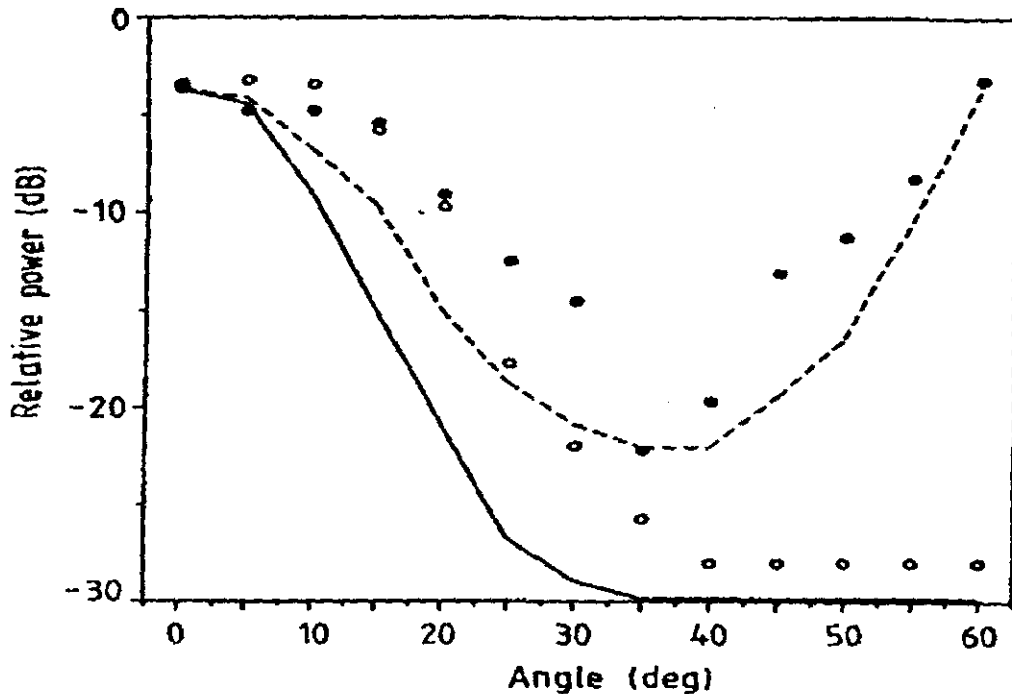


Figure 5.9. Theoretical and measured angular transmission responses of the DML. (open circles) - TE measured, (black circles) - TM measured, (solid line) - TE theory, (dotted line) - TM theory.

#### 5.7.2.2 Frequency selective surfaces

The plane wave transmission responses as a function of incidence angles, at ~30 GHz, are shown in Figure 5.10. For TM incidence, as the angle of incidence increases there is a sharp decrease in the transmission and at 25° incidence it is near -10 dB. There is an increase of up to -6 dB as the angle of incidence increases to 60°. The computed and measured values of both arrays were in good agreement. For TE incidence there is a slower attenuation which may originate from the fact that the incident electric field vector is always parallel to the surface

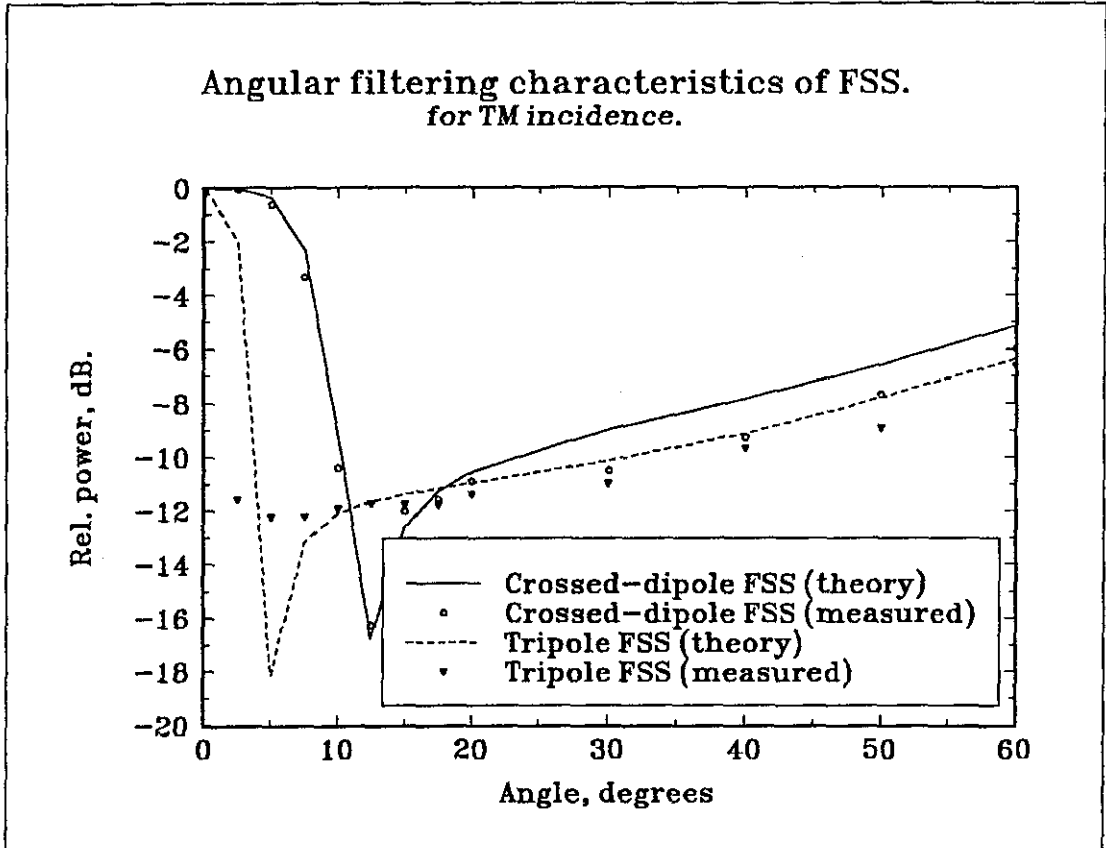


Figure 5.10.a

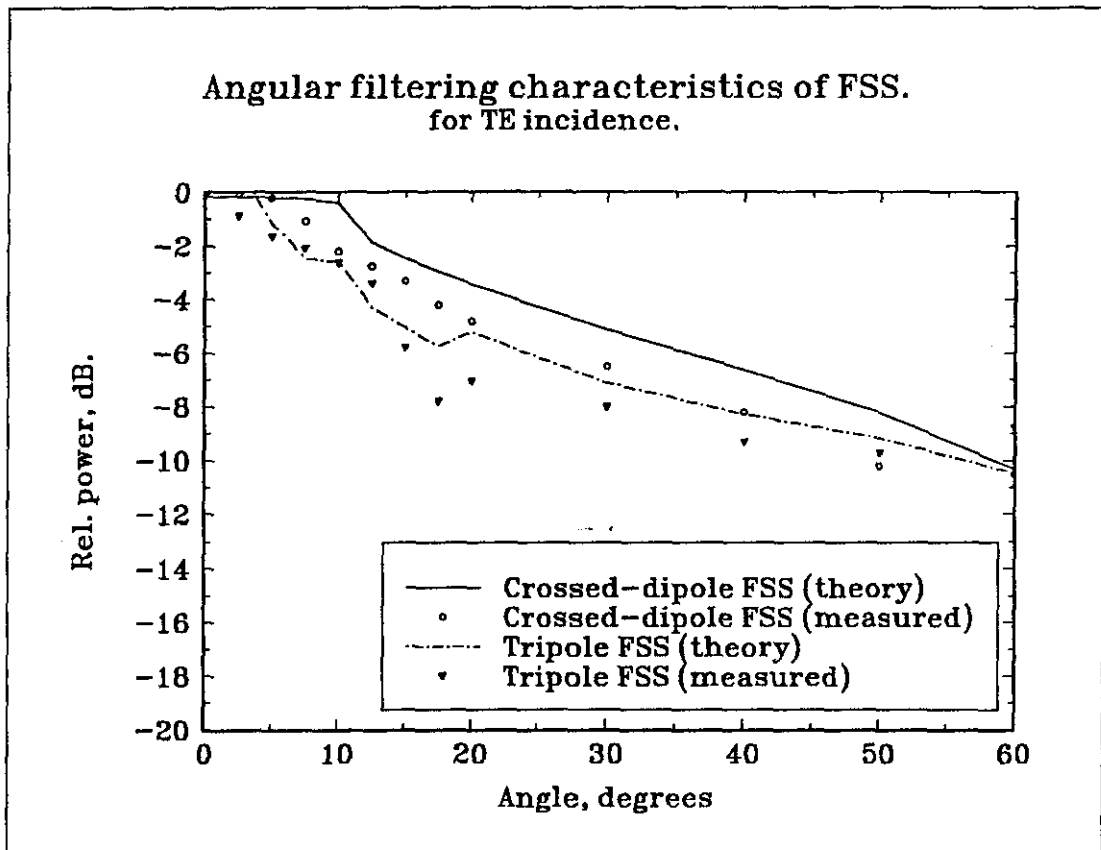


Figure 5.10.b

This paragraph to be inserted after page 1 (i.e. continuation of the paragraph at the bottom of page 1).

Indeed future multimission communication satellites will carry payloads operating at a number of frequency bands [1], e.g. 1.5, 4/6, 11/4, 20/30 GHz. In order to accommodate these <sup>Services</sup> surfaces, and satisfy weight and space constraints, antennas are required which will operate at three or more of these bands. Incorporating FSS into the antenna assembly will enable the system to operate at more than one frequency band simultaneously. They have often been considered for the reflector antenna applications. Typically, an FSS is employed as the main *subreflector* and the different frequency feeds are optimised independently and placed at the real and virtual foci of the subreflector. Hence, only a single main reflector is required for the multifrequency operation. For example, the *Voyager* FSS [2] was designed to diplex S and X bands. In that application, the S-band feed is placed at the prime focus of the main reflector, and the X-band feed is placed at the cassegrain focal point. Note that only one main reflector is required for this two band operation. Consequently, a considerable reduction in volume, weight, and most importantly, the cost of the antenna system is achieved with the FSS subreflector. Lee.c.k., et al [1], proposed a system where a single reflector antenna is used at multiple frequencies by employing these FSS surfaces to separate the individual bands. One such configuration operating at three frequency bands is shown in figure 2.3. Here the bands  $f_1$ ,  $f_2$  and  $f_3$  are separated by two subreflectors FSS1 and FSS2. In figure 2.3, FSS2 is required to separate two frequency bands. That is, reflect  $f_2$  and transmit  $f_3$ . FSS1, however, must transmit two frequency bands  $f_2$  and  $f_3$  while reflecting  $f_1$ . FSS1 must also be designed for a wide

4.17

-7.03

-16.46

-5.62

-1.82

-0.39

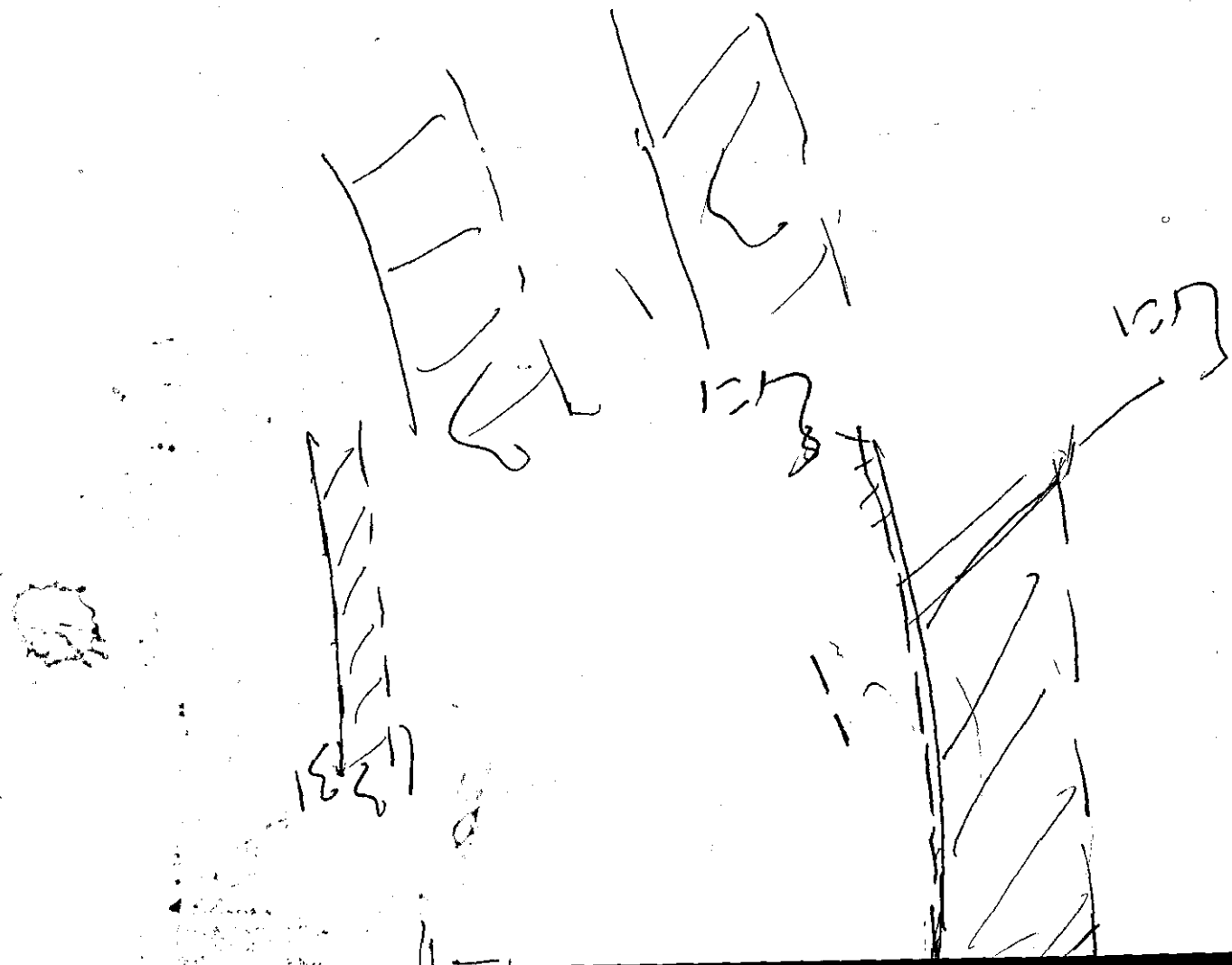
33,2508

31.00 .	*	-9.69447	
32.00 .	*	-7.70155	
33.00 .	*	-6.60377	
34.00 .	*	-5.55881	
35.00 .	*	-4.67440	
36.00 .	*	-3.93433	
37.00 .	*	-3.31624	
38.00 .	*	-2.80268	
39.00 .	*	-2.36531	
40.00 .	*	-1.98449	
7.00 .	*	-4.17787	
8.00 .	*	-7.03095	
9.00 .	*	-14.36323	
10.00 .	*	-16,46407.	
11.00 .	*	-5.62265.	
12.00 .	*	-1.82424	
13.00 .	*	-0.38594	
14.00 .	*	-0.02309	
15.00 .	*	-0.16475	
16.00 .	*	-0.56789	
17.00 .	*	-1.13232	
18.00 .	*	-1.81982	
19.00 .	*	-2.62018	
20.00 .	*	-3.53830	
21.00 .	*	-4.58955	
22.00 .	*	-5.79854	
23.00 .	*	-7.21037	
24.00 .	*	-8.88731	
25.00 .	*	-10.94110	
26.00 .	*	-13.58147	
27.00 .	*	-17.26320	
28.00 .	*	-23.72492	
	*	-49.13728	

TRG of. *mm*

1.94  
1.33  
0.4.

1.22  
1.86  
2.0  
2.1  
2.2  
2.3  
2.4  
2.5



29.00

30.00 .  
 31.00 .  
 32.00 .  
 33.00 .  
 34.00 .  
 35.00 .  
 36.00 .  
 37.00 .  
 38.00 .  
 39.00 .  
 40.00 .

\*  
 \*  
 \*  
 \*  
 \*  
 \*  
 \*  
 \*



17.15  
 -14.19186 -4  
 -12.01319 -10  
 -10.37826 -8  
 -9.07907 -7  
 -8.00672 -7  
 -7.09599 -1  
 -6.30348 -1  
 -5.59711 -1  
 -4.94743 -1

for the Decked softway  
 Dimensions are

h 2.5m, 6 CF, 17 fm

O

$r_1 = 3.8$ ,  $r_0 = 4.3$ , 8 CF (3.2), 35 fm  
 4.1 4.35



-8.81

-10.24

-13.87

-17.26

-23.72

-42.67

29 ←

-23.07

-17.38

-14.19

In addition,

range of reflection/transmission band ratios varying from

1:3 to 3:1.

15	8	7
16	7	13
17	10	22
14	4	21
16	12	11
17	4	6
17	4	
20	4	

u e z i m



irrespective of the angle of incidence. In addition, wider element spacing may be required to achieve sharper attenuation. But the wider the element spacing, the more power at boresight will tend to attenuate and this power will be shared by the grating lobes. The behaviour of TE incidence seems to suggest that a degradation of the spatial filtering performance might be expected.

### 5.7.3 Radiation Pattern Measurements

#### 5.7.3.1 Dielectric Multilayers

These measurements are required to substantiate the beam coverage required for the antenna system to pick up a weak signal in any given direction.

In Figures 5.11, the radiation patterns of the DML are shown, when used in conjunction with a Ku-band horn antenna. The patterns are compared with a reference pattern of the horn. There is a gradual reduction in the boresight received power as the curvature is increased. This loss could be attributed to the material absorption at the operating frequency range. The power reduction is  $\sim -1$  dB each as the geometry of the DML moves from H0 to H2 for TE and TM. The measured  $-5$  dB beamwidth of the horn antenna is  $\sim 36^\circ$  for TE and TM. For the DML the  $-5$  dB beamwidths are  $\sim 30^\circ$ ,  $\sim 24^\circ$  and  $8^\circ$  for H0, H1 and H2, respectively with reference to the horn antenna level. These values remain the same for the other polarisation state. The encouraging fact about the DML is that it gives almost the same radiation response for both TE and TM, unlike its FSS counterparts.

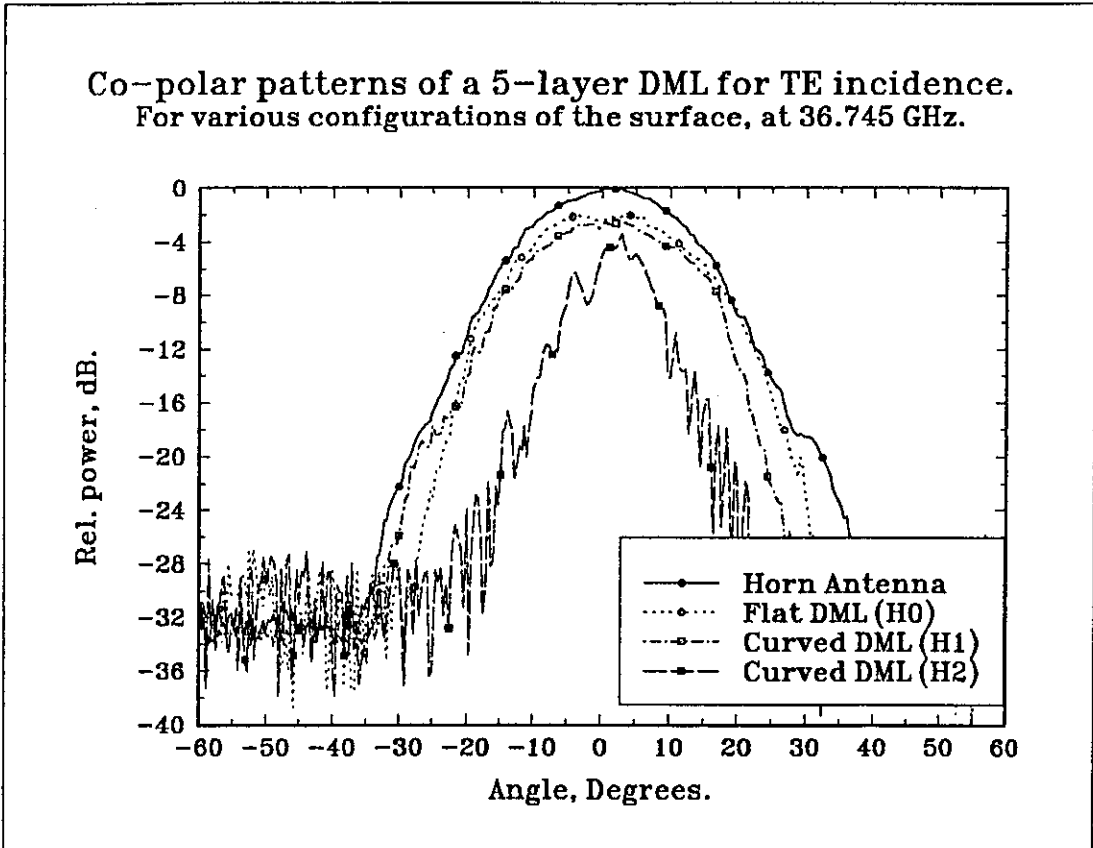


Figure 5.11.a

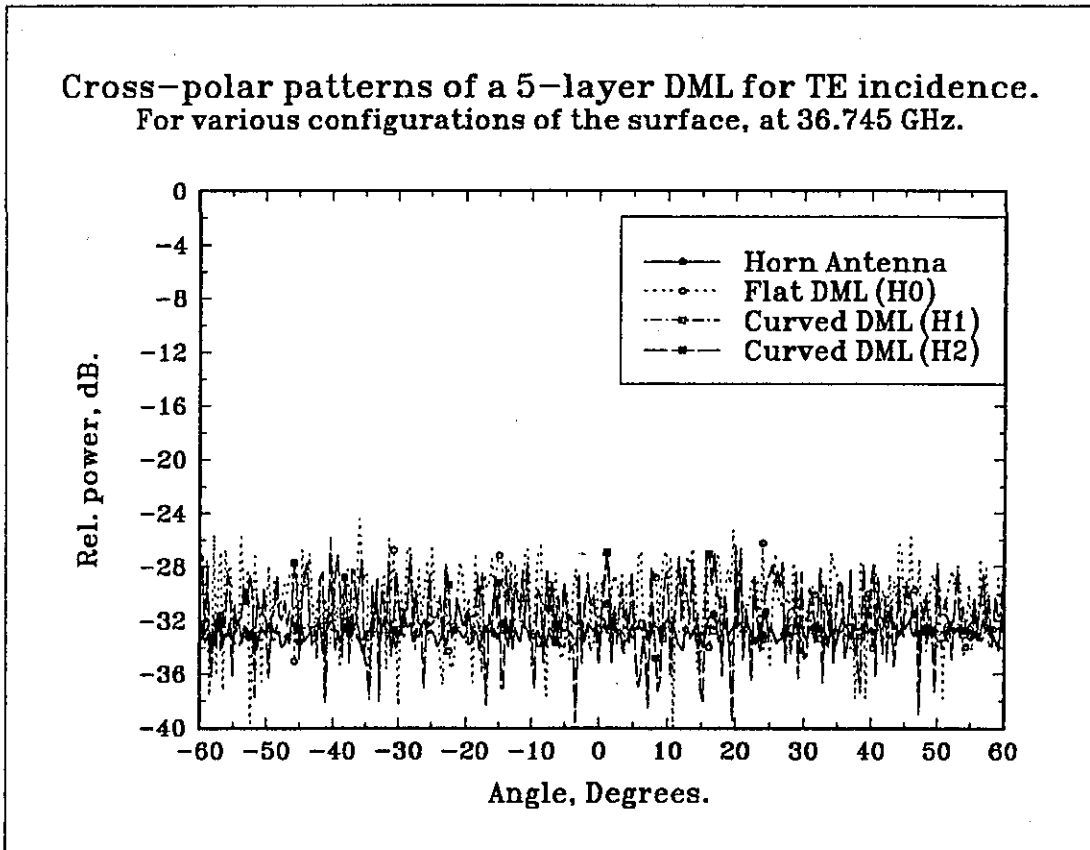


Figure 5.11.b

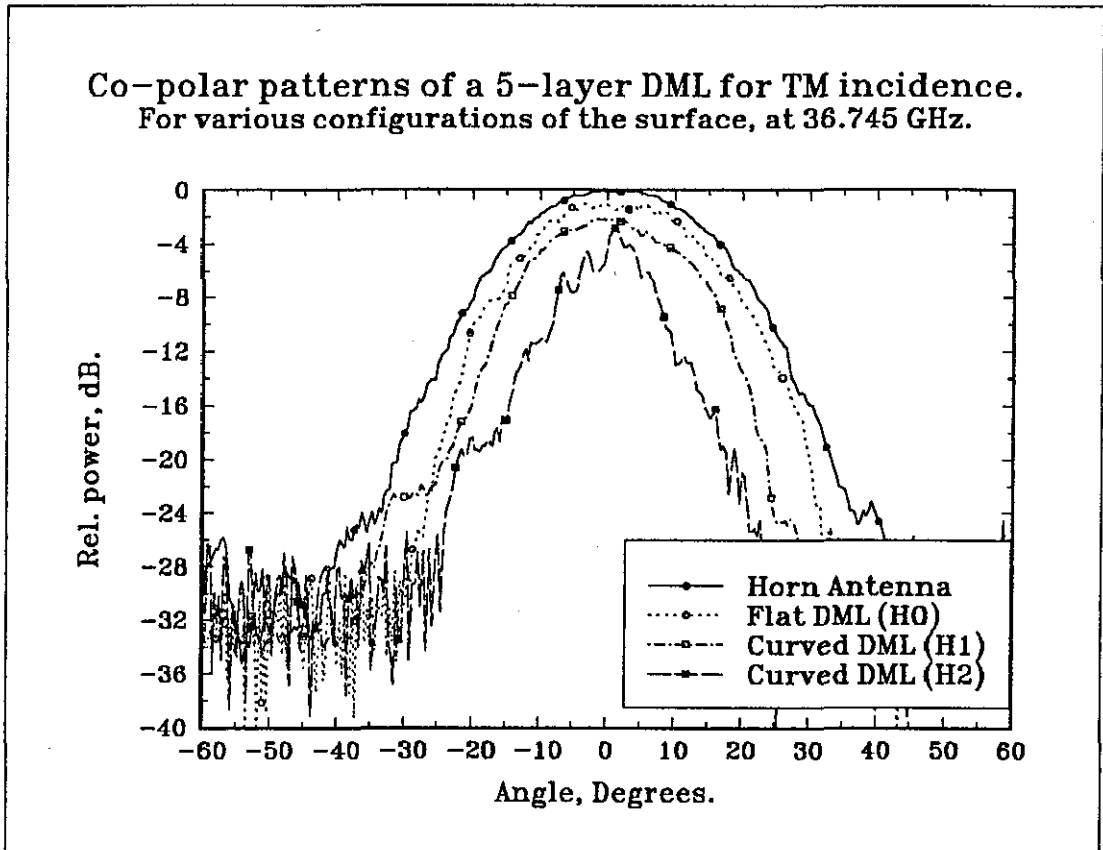


Figure 5.11.c

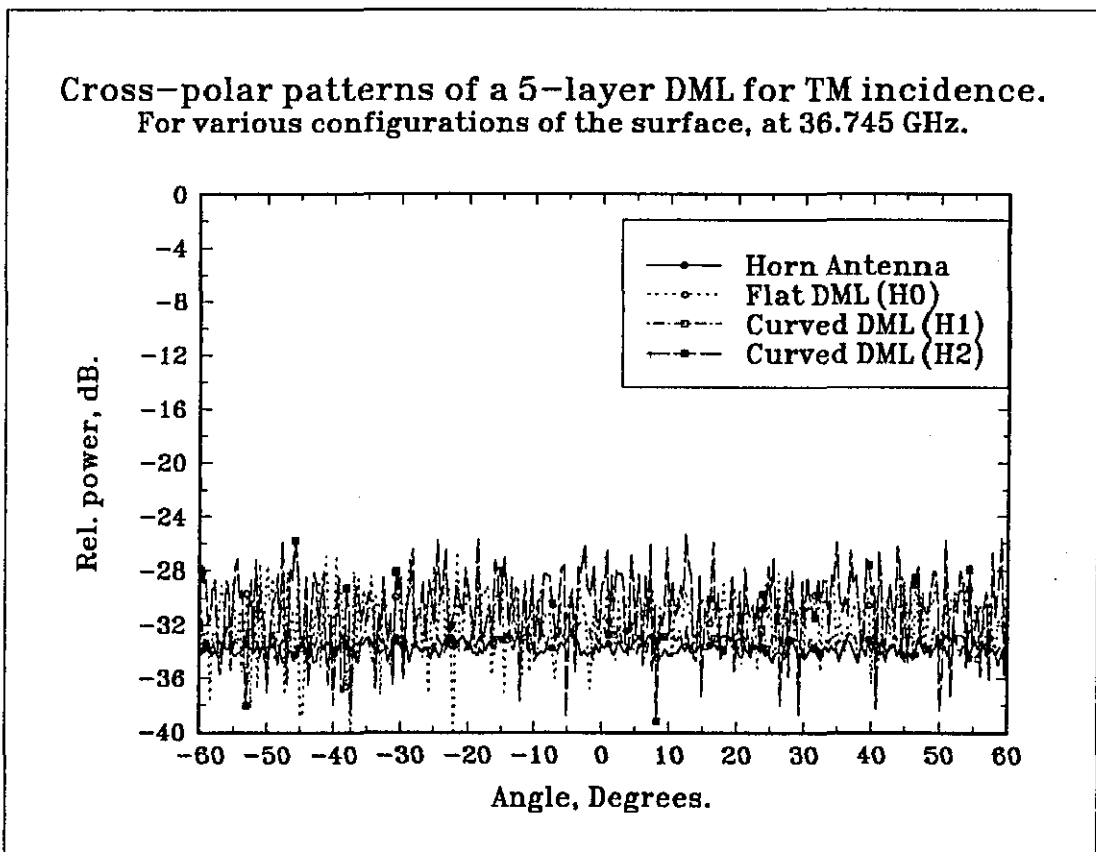


Figure 5.11.d

Another positive feature of the DML is its cross polar characteristics (Figure 5.11.b & 5.11.d). For all the curvatures and for both polarisations, they tend to stay around the noise level ( $< -32$  dB), which is the cross-polar level of the horn antenna.

### 5.7.3.2 Frequency Selective Surface

The measured patterns of the FSS filters for TE incidence are compared with a Ku-band horn patterns. Both surfaces were illuminated at normal incidence with the feed 30 cm away.

Radiation patterns for crossed dipoles and tripoles are shown in Figure 5.12.a and 5.12.c. Tripole FSS gives a narrow pattern for all the curvatures for TM incidence. It gives  $\sim 8^\circ$ ,  $\sim 9^\circ$  and  $\sim 5^\circ$  for H0, H1 and H2, respectively, compared with  $36^\circ$  for the horn. The power absorption at H0 is  $\sim 0$  dB and as the curvature is increased, this value increases by  $\sim 3.5$  dB (H1) and  $\sim 5.0$  dB (H2).

For crossed dipole FSS, the radiation pattern is broader than that of the tripole FSS for TM incidence. The lower degradation of the transmission coefficient against the angle of incidence produces a broader pattern for the crossed dipole FSS. Like the tripole surface the  $-5$  dB beamwidth (with respect to horn) as well as the power at boresight reduce for crossed dipole surface. Power attenuations are  $\sim 0$  dB,  $\sim -1$  dB and  $\sim -5$  dB for H0, H1 and H2, respectively. The beamwidth for H0, H1 and H2 are obtained as  $17^\circ$ ,  $11^\circ$  and  $7^\circ$  respectively.

For TE incidence, the radiation patterns of the tripole and crossed dipole surface coincide with that of the horn antenna. Moreover in both cases, the H-plane patterns are almost similar to that of the horn feed. No reduction in the beamwidth is observed.

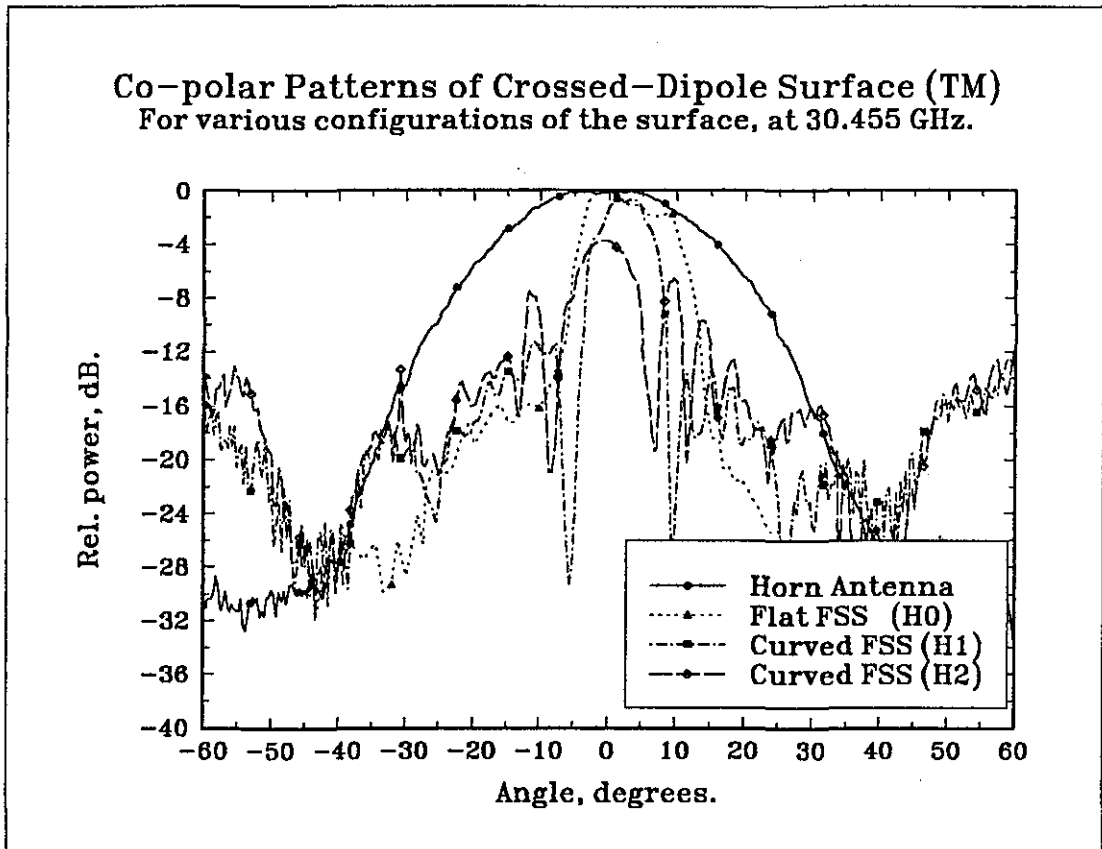


Figure 5.12.a

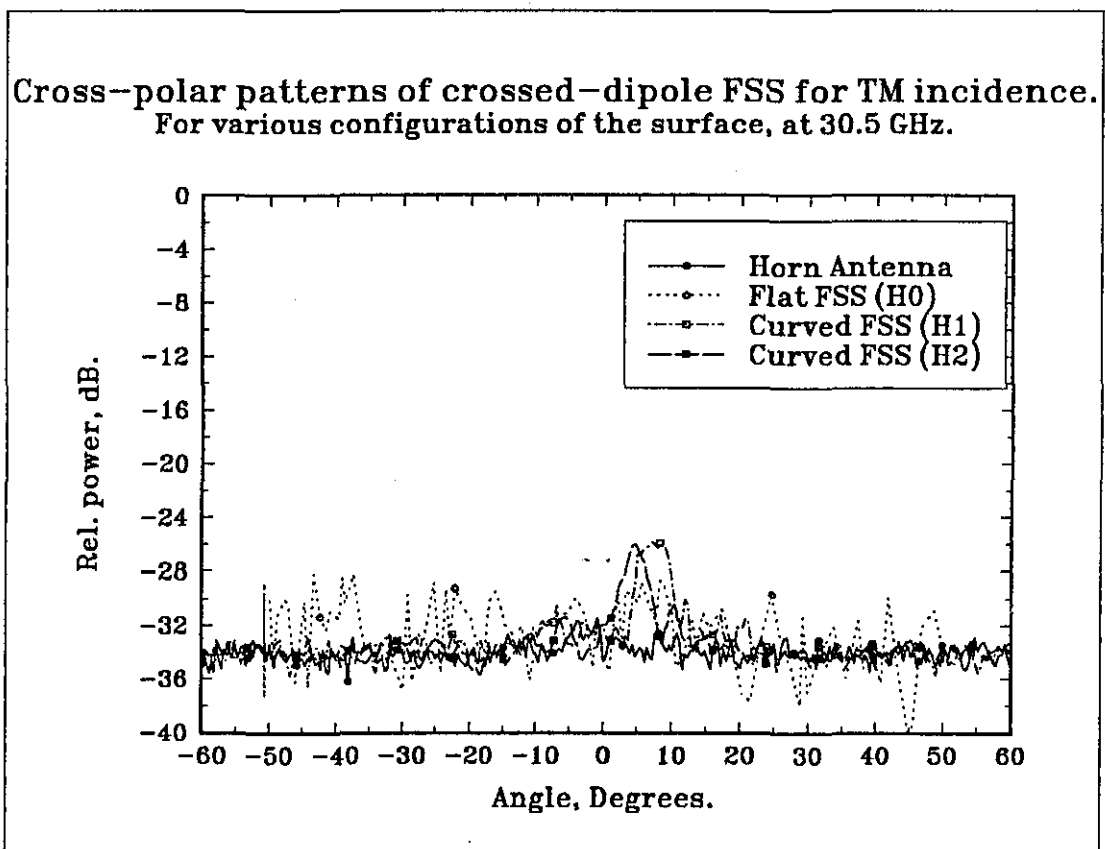


Figure 5.12.b

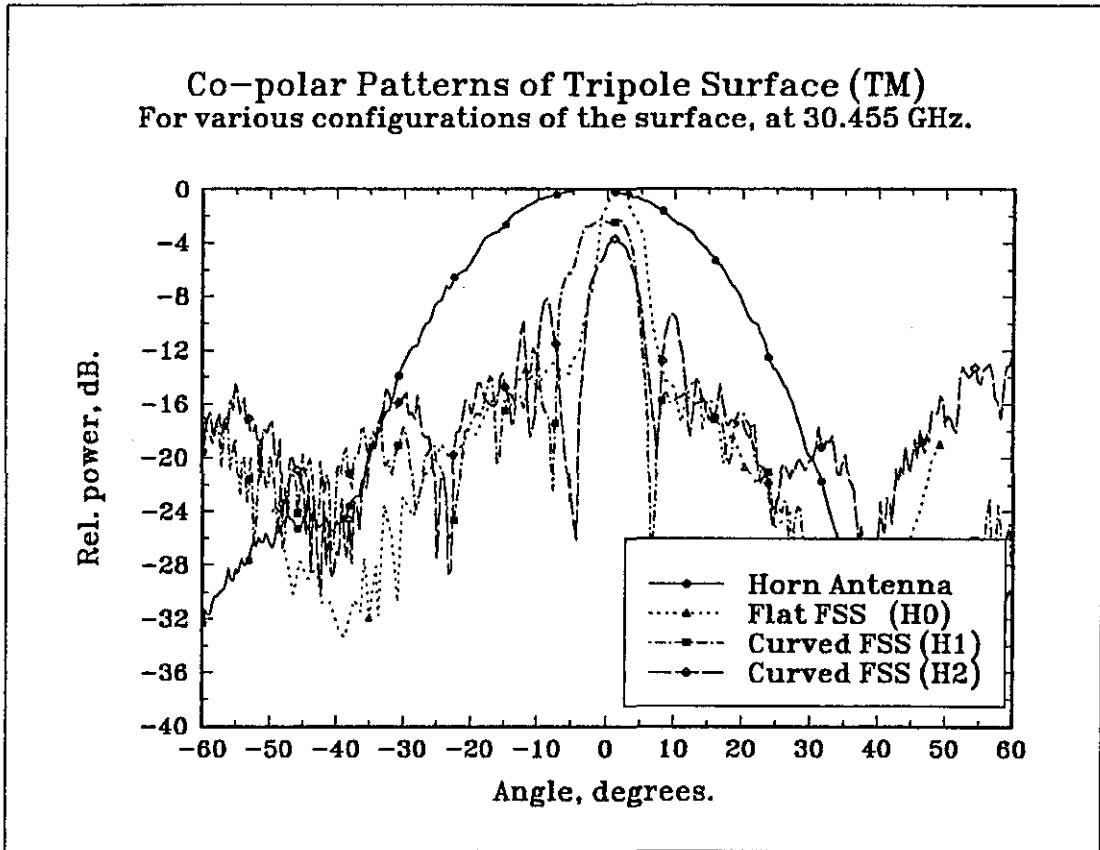


Figure 5.12.c

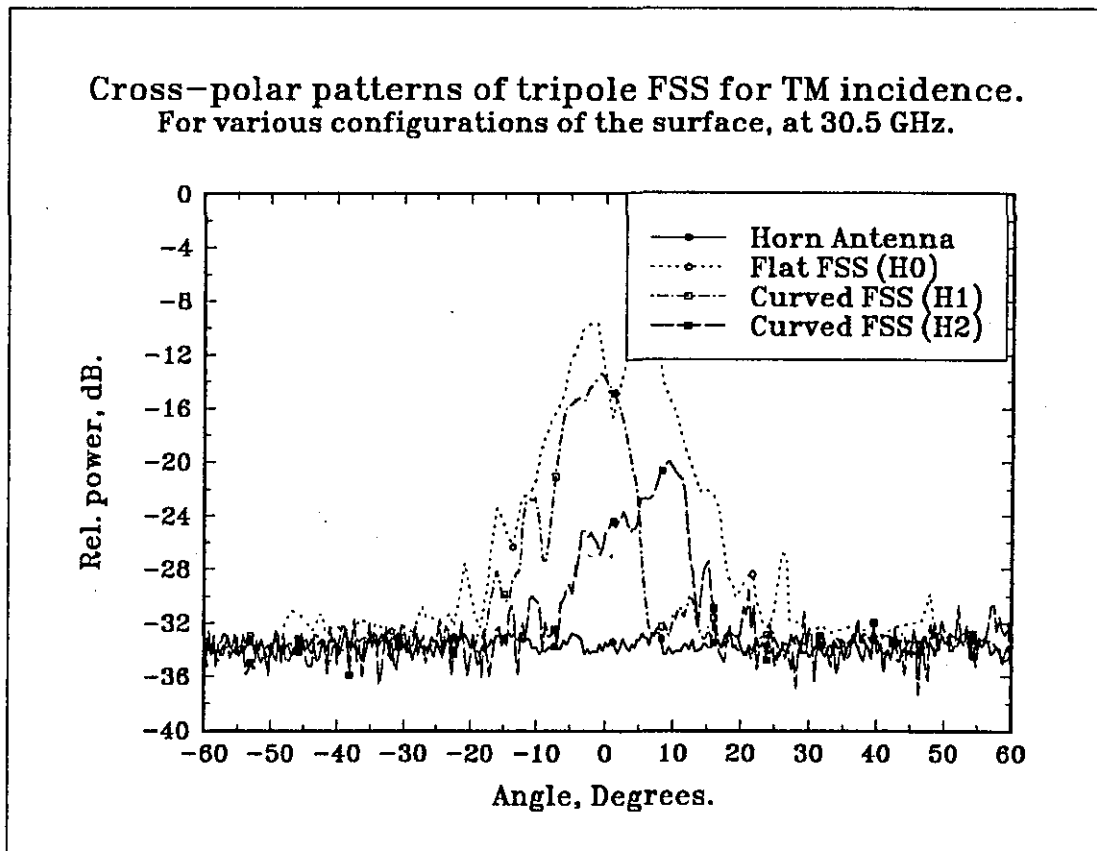


Figure 5.12.d

The cross polar patterns are illustrated in Figures 5.12.b & 5.12.d. For tripole FSS, a maximum of -10 dB is noted for H0 and as the curvature is increased, it reduces, whereas for the crossed dipole FSS, it remains reasonably low; for flat surface and gradually increases with the curvature. The maximum amplitude noted is ~-26 dB.

Both DML and FSS have their own merits as well as demerits. The DML gives broader patterns for both polarisations where as FSS gives a narrow pattern for TM incidence, especially for tripole. But when it comes to cross polarisation the DML leads the way by providing the polarisation level, almost similar to that of the horn antenna. The cross polarisation level seems to vary with curvature in the case of FSS, while for DML, it remains at the same as that for the planar surfaces, which is the noise level of the network analyser..

#### **5.7.4 Near field Measurements**

In the previous sections the effects of angular filtering and the corresponding radiation patterns were investigated. In this section the near field measurements are studied experimentally to determine the effects of curvature.

For a microwave antenna system, to predict the direction of arrival of a signal it is necessary to have a knowledge about where on the detector the signal strikes. Based on this information, with the help of necessary signal processing, the origin of the signal source can be determined.

The laboratory setup to measure the near field effects is shown in Figure 5.2.c. Three horn antennas were used to simulate a 'busy' electromagnetic environment in the chamber. The horns were turned on and off in sequence to

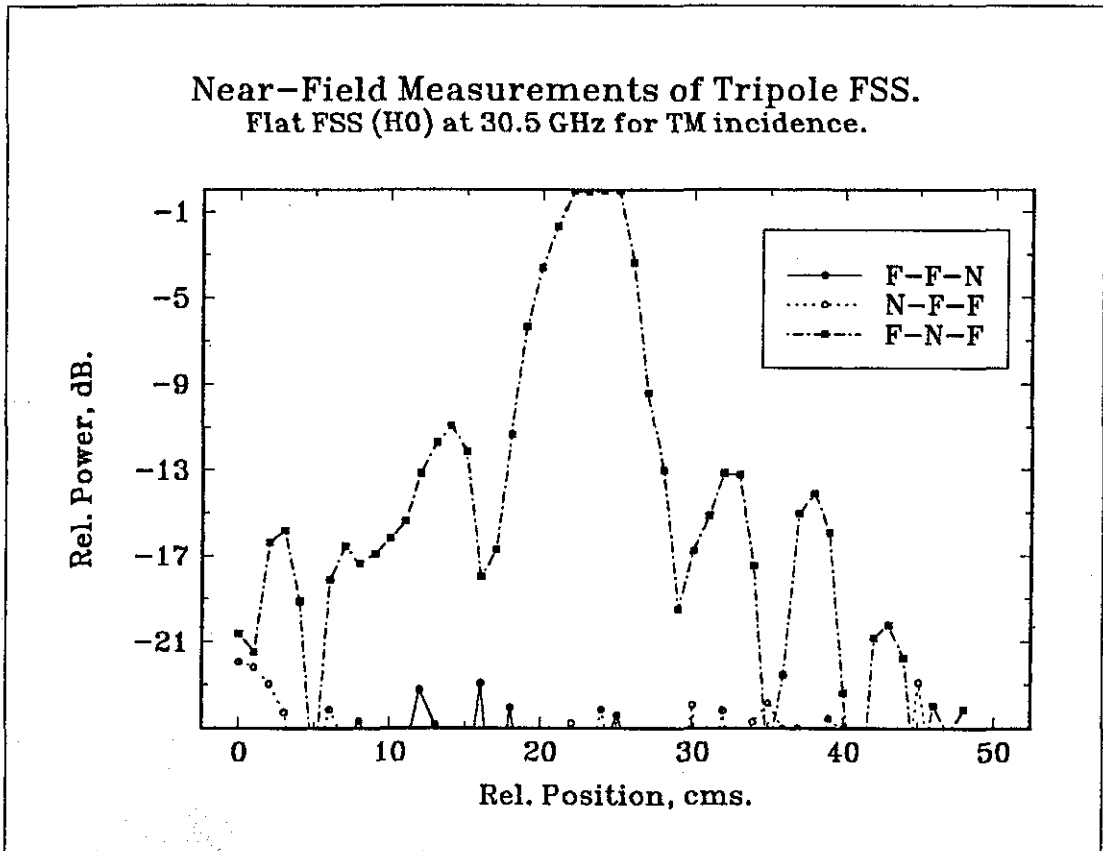


Figure 5.13.a

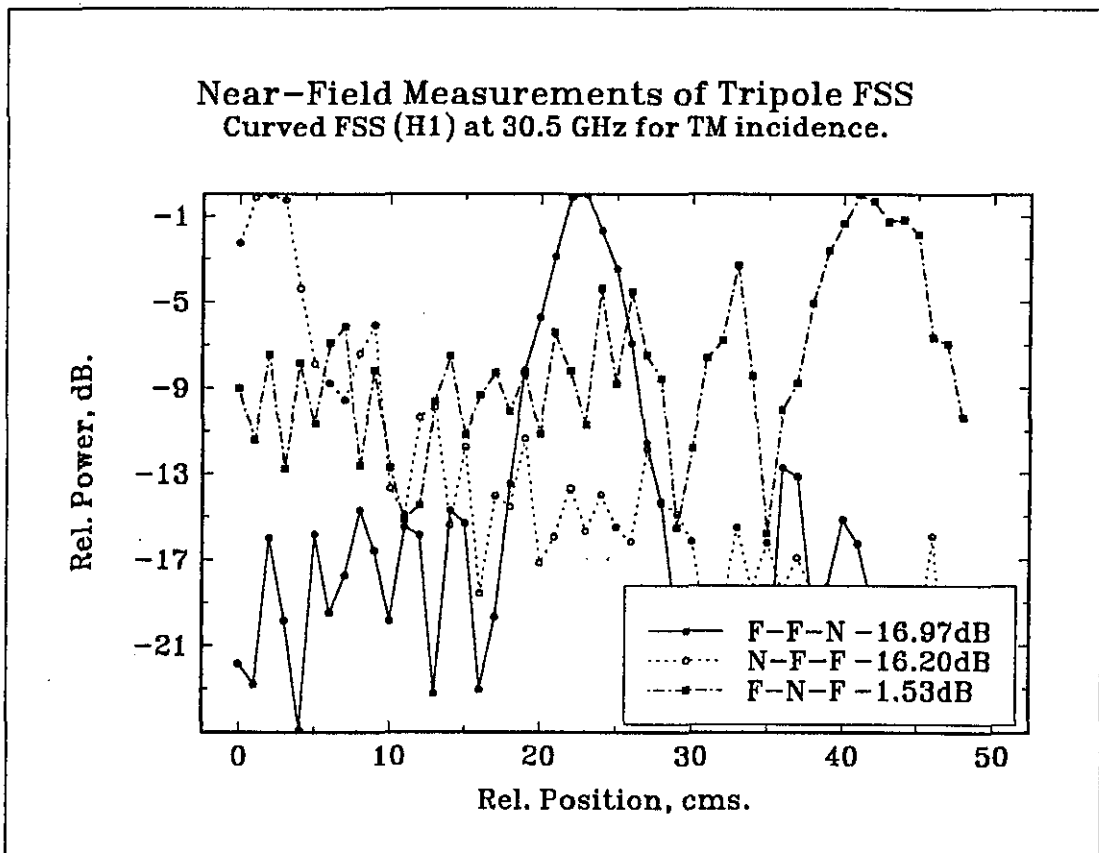


Figure 5.13.b

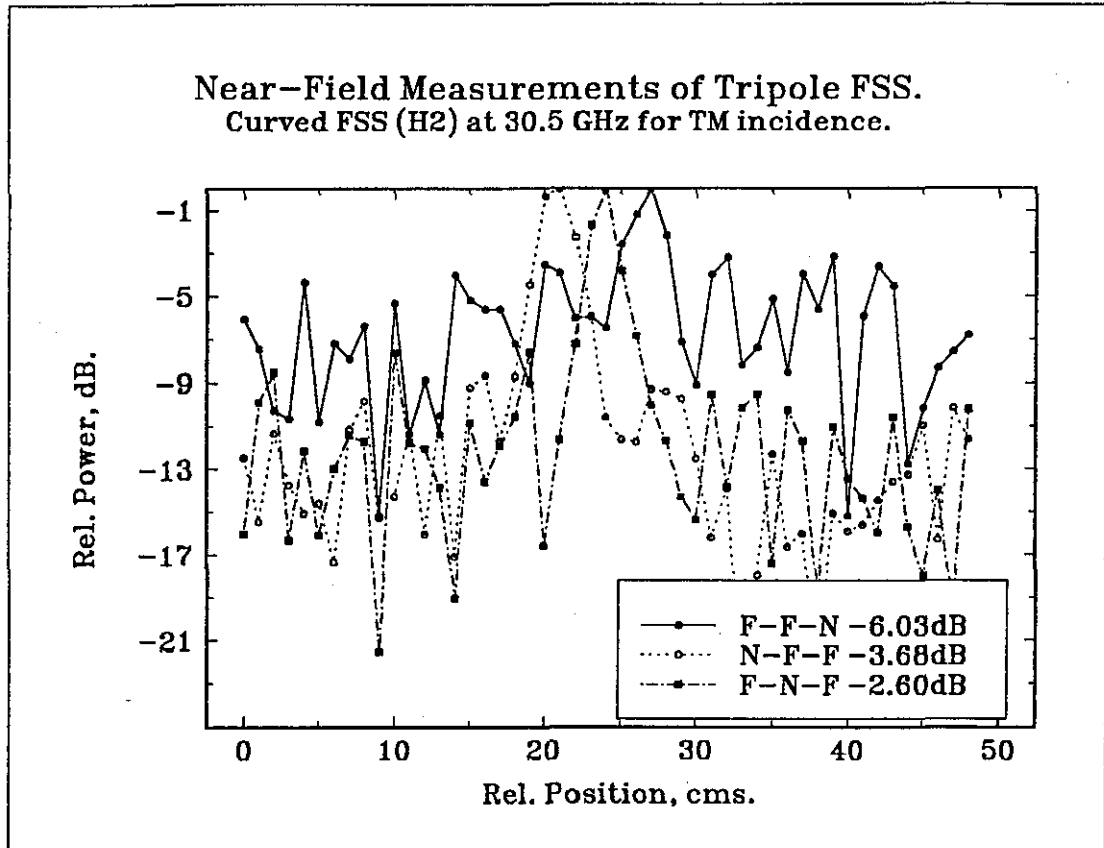


Figure 5.13.c

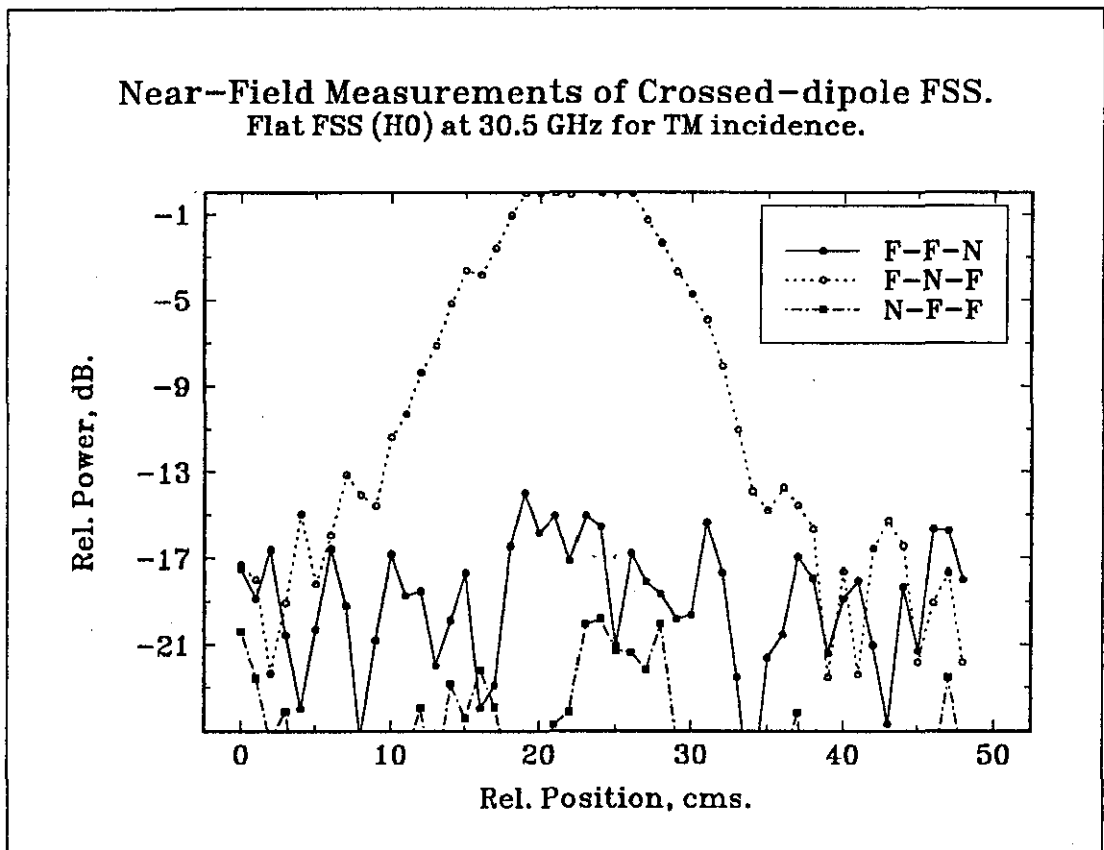


Figure 5.13.d

Near-Field Measurements of Crossed-dipole FSS.  
Curved FSS (H1) at 30.5 GHz for TM incidence.

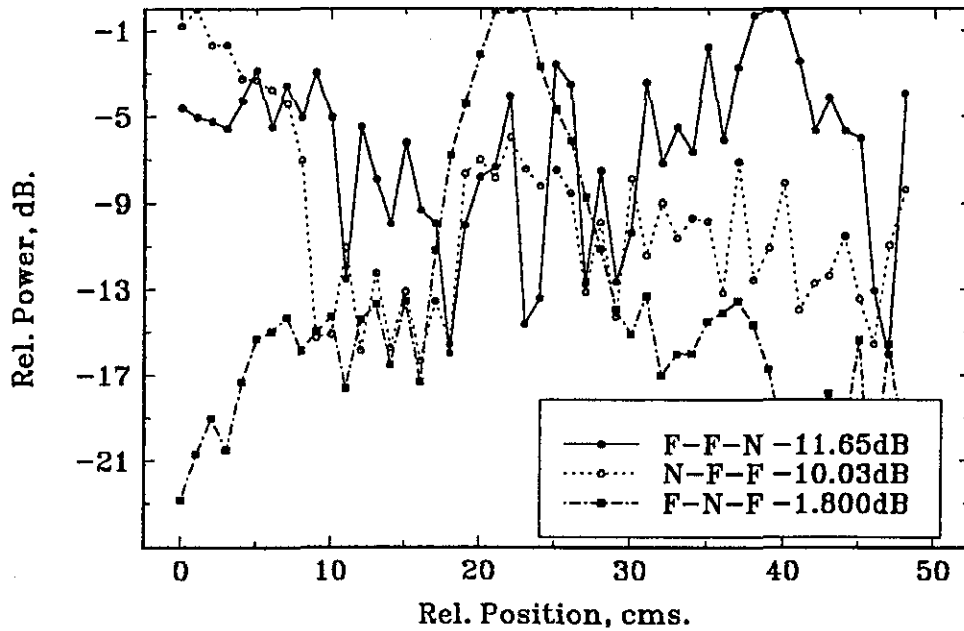


Figure 5.13.e

Near-Field Measurements of Crossed-dipole FSS.  
Curved FSS (H2) at 30.5 GHz for TM incidence.

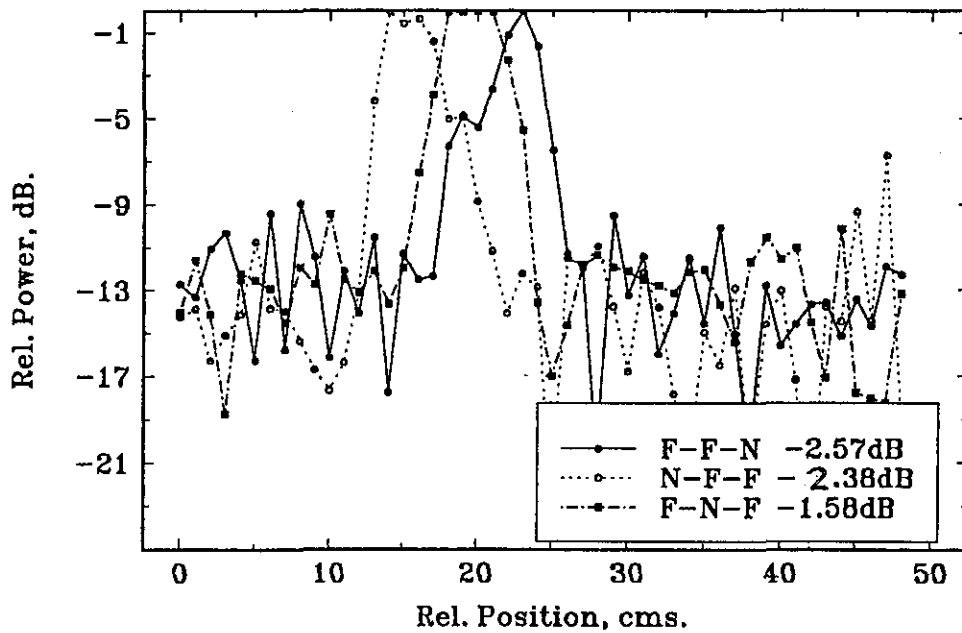


Figure 5.13.f

simulate the presence of a signal source. Measurements were carried out according to the procedure suggested in section 5.4.4. The detector horn is placed at a distance of 20 cms from the edge of the surface.

Initially the flat surfaces (H0) and then the curved surfaces (H1, H2) were tested. Figures 5.13 give the near field measurements of tripole and crossed dipole arrays for TM incidence. All the curves given were normalised. The terms F and N denote OFF and ON states of the signal power source. For flat surfaces (H0), the detector could not detect the signals coming from either side at an angle of  $30^\circ$  from the centre horn. Once a curvature is introduced, the signal sources slowly appear on the graph. For cross dipole and tripole surfaces, the curvature (H1) brings the signal sources onto the edge of the detector. The position of the signal sources are further moved towards the centre, when the curvature is increased. So it is evident from these graphs that the curvature determines the position on the detector, where the signal strikes. The more the curvature the smaller the region for the detector to be scanned.

For DML, the radiation patterns for the TE and TM are broader compared to the TM of the FSS. This means that although the detection of the sources are possible using DML, it cannot be observed as clearly as the FSS.

Once the curvature is optimised, such structures should be able to predict the direction of the signal source, depending upon the position on the detector, where a signal is incident.

### 5.8 Summary

In this chapter the behaviour of DML and FSS were assessed experimentally and compared with the theoretical data available. A DML consisting of five layers of

melamine sheets was used to study the microwave performance. Meanwhile, for FSS, tripole and crossed dipole slot designs were employed. The frequency responses, radiation pattern characteristics, plane wave measurements and near field measurements were carried out to assess the performance of the proposed passive antenna structure.

---

**References**

1. Hogg D.C., Guiraud F.O., Howard J., Newell A.C., Kremer D.P. and Repjar A.G., An antenna for dual wavelength radiometry at 21 and 32 GHz, 1979, IEEE Trans AP-27, pp.764-71.
2. Carniglia C.K., Comparison of several shortwave pass filter designs, 1989, Appl. Opt., Vol. 28, No. 14, pp.2820-3.
3. Yordanov O.I., Angelov I., Konotop V.V. and Yurkevich I.V., Prospects of fractal filters and reflectors, 1991, IEE Conf. Anten. & Propag, University of York, UK, pp.698-700.
4. Oksanen M.I., Hanninen J. and Tretyakov S.A., Vector circuit method for calculating reflection and transmission of electromagnetic waves in multilayer chiral structures, 1991, IEE Proc. H, Vol. 138, pp.513-520.
5. Rudge A.W., Milne K., Olver A.D. and Knight P (Eds), Handbook of antenna design, 1986, Peter Peregrinus, UK, Chapter 5.
6. Franchi P.R. and Mailloux R.J., Theoretical and experimental study of metal grid angular filters for sidelobe suppression, 1976, IEEE, Trans. AP-24, pp.174-181.
7. Hannan P.W. and Pedersen J.F., Axial conductance angular filter, 1984, IEEE AP-S Intl. Symp. Dig., Boston, Massachusetts, pp.917-920.
8. Rope E.L. and Tricoles G., An angular filter containing three periodically perforated metallic layers, 1979, IEEE AP-S Intl. Symp. Dig, Seattle, Washington,

pp.818-820.

9. Pedersen J.F. and Hannan P.W., A metal grid 5x5 foot angular filter, 1982, IEEE AP-S Intl. Symp. Dig, Albuquerque, New Mexico, pp.471-474.

10. Mittra R., Chan C. H. and Cwik T., Techniques for analyzing frequency selective surfaces-a review, 1988, Proc.IEEE, Vol.76, No. 12, pp.1593-1614.

11. Vardaxoglou J.C. and Hosseinzadeh A.H., Single and double layer FSS of tripole arrays, Sept 1989, Proc. 19th Microwave European Conference, pp.863-868.

12. Chen C.C., Transmission through a conducting screen perforated periodically with apertures, 1970, IEEE Trans. MTT-18, pp.627-632.

13. Scott.C., The spectral domain method in electromagnetics, 1990, Artech house inc, Boston, Chap 2.

14. Alexopoulos N.G., Uslenghi P.L.E. and Uzonoglu, Microstrip dipoles on cylindrical structures, Sept 1981, Proc. Allerton antenna appl. symp., Univ. of Illinois, pp.1-20.

15. Cwik. T. and Mittra. R., The effects of the truncation and curvature of periodic surfaces, 1988, IEEE Trans. AP-36, pp.612-622.

16. Chia Y.W., Simpkin R. and Vardaxoglou J.C., A study of a conical frequency selective surface, Journ. Internation. de nice sur les antenn, Nov 1992, pp.321-324.

17. Lagerholm R., Study of radiation patterns of antennas covered by curved dichroic radomes, Journ. Internation. de nice sur les antenn, Nov 1992, pp.317-320.

18. Chia Y.W., Vardaxoglou J.C. and Simpkin R.A., Scattering from conical frequency selective surfaces using a finite current model, 3rd Intl. conf. electromagn in aerospace applcns, Torino, Italy, Sept 1993, pp.119-122.

19. Kraus J.D., Antennas, 1988, McGraw-Hill, Inc, New York, Chap.11.

20. Debono P.P, Computer control of microwave equipment for antenna measurements, M.Sc dissertation, 1990, Loughborough University of Technology, UK.

## CHAPTER 6

**Beam Modulation Due to Varying Structure Parameters****6.1 Introduction**

In this chapter the variations of the antenna radiation characteristics due to variations in several structure parameters as well as signal parameters are discussed. This provides necessary information regarding the frequency response, beam formation and frequency scanning properties of the structures under discussion. Also the applications of passive antenna elements, such as DML and FSS, as focusers and beam directors are investigated.

An advantage of these passive filters compared to the existing form of lenses such as zoned lenses is the ability to reduce the physical size of the lens structure. FSS can be made to act as a diverger by appropriately selecting the element geometry. Certain structures help to change the direction of an incoming electromagnetic wave, to other directions by proper choice of element geometry. The design procedures are based on a simplified mathematical model and will therefore be used in parallel with experimental procedures. Mass reduction in the lens structure is obtained here by varying the element size of the FSS.

Beam steering is achieved using DML by varying the frequency of the incident wave. The steering is observed for the zero order beam at boresight. With FSS the beam steering for the first order component is studied. For the beam scanning applications one could consider the role of FSS as gratings.

Gratings have found plenty of applications in many areas of physics and engineering. Some important applications include: microwave lines and polarizers, twist reflector antennas, spectrum analysers, integrated optical devices, holography and acousto-optical devices. Because of their widespread applications, the diffraction properties of gratings have been studied extensively over the last few decades[1]. Periodic grating structures have recently been proposed to construct antennas with beam steering properties[2,3,4]. It is understood that the grating lobes are sensitive to variation in frequency and therefore can be steered. In this experiment, the first order grating lobe is studied. For this the FSS geometry is selected in such a way that the first order diffracted mode is propagating while the surface is illuminated by an electromagnetic wave. A surface with such a property is known as a blazed grating in the optical sense. It transfers the incident signal power to diffracted power.

A novel concept in beam steering is introduced here using FSS. The effect of this beam steering is studied by rotating the FSS which is mounted in front of a conventional antenna. For this system, one requires only a fixed frequency source which in turn reduces the cost of the system. Unlike steering the first higher order mode, in this application the fundamental mode is steered

Exploitation of the DML as an electromagnetic window is investigated in the Ku band. Comparisons are made with practical data obtained in the anechoic chamber. The same experiment is performed using a waveguide instead of an antenna to establish the beam forming features of the DML.

Due to the diverse properties of FSS one can consider them as candidates in a number of applications which require enhancements of existing antennas with regard to

beamforming or focusing tasks. In this chapter some procedures for attaining controlled modifications of the incident field that result in beam directing, filtered and focused radiation patterns are discussed. Planar single layer spatially varying array designs have been designed to produce the required combination of amplitude and phase changes. A number of prototypes have been manufactured and assessed experimentally in the 26-40 GHz frequency region.

## **6.2. Beamsteering**

A frequency scanning method was used to steer the beam using DML.

### **6.2.1 Dielectric Multilayers**

In sections 5.7.1.1 and 5.7.2.1 it was shown that the multilayer plane wave pass-bands are in effect shifted when the angle of incidence is varied. This suggests that one way to achieve steering is by varying the source frequency of a divergent beam incident on a multilayer filter placed in the near field. It is stressed that the direction of the beam is frequency dependent only in the sense that part of the signal incident on the multilayer will be reflected and hence the structure is behaving as a spatial filter.

The model used to calculate the responses presented in sections 5.7.1.1 and 5.7.2.1 is only exact for plane waves but nevertheless can be used to indicate the response characteristics of a multilayer filter when positioned in the near-field of the radiating source. Thus under the physical optics approximation, the radiation pattern of a wide angle source and multilayer filter, normalised with respect to the radiation pattern of the source, will be roughly equivalent to the plane wave angular transmission response. From Figure 5.4 it is

apparent that a satisfactory half power performance can be expected from the steered signal by varying the source frequency within a range of 0.6 GHz, centred around ~28 GHz. That is in the vicinity of the second order resonant frequency of the 9-layer structure.

A schematic diagram of the measurement setup is shown in Figure 6.1. The multilayer was placed in the near-field of a radiating microwave antenna such that radiation was illuminating the dielectric across a range of angles from  $0^\circ$  (in the centre of the multilayer) to  $\sim 25^\circ$  (near the edge of the multilayer). Because of the practical difficulties associated with supporting the structure in

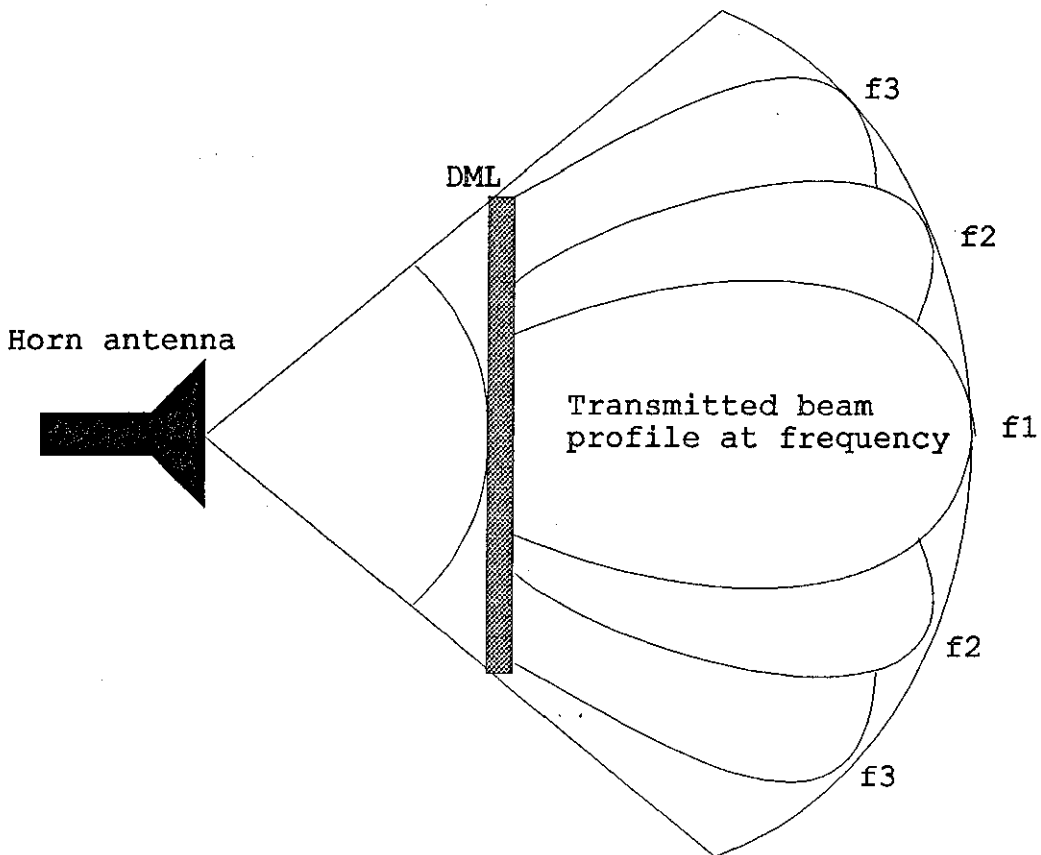


Figure 6.1 Schematic diagram for beam scanning using DML.

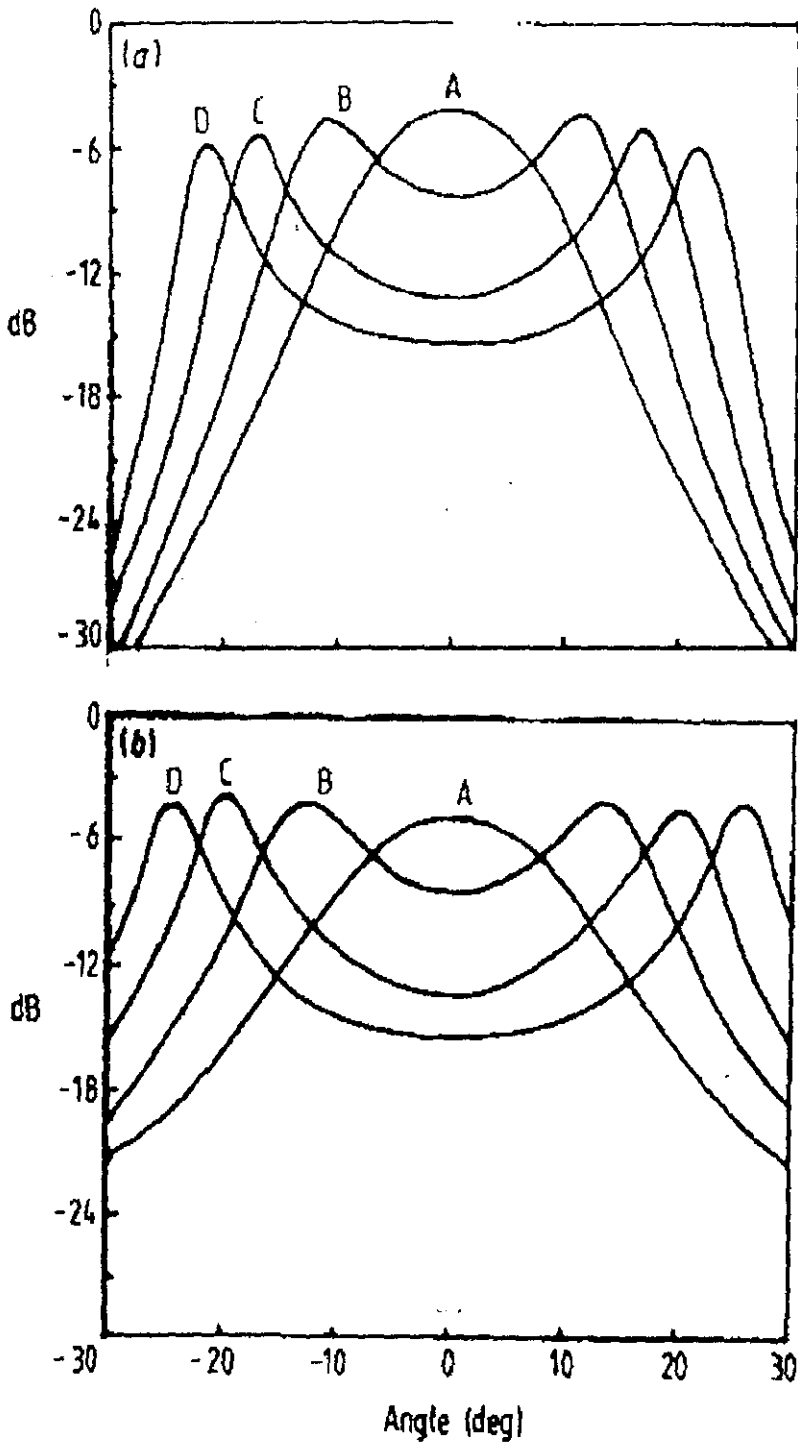


Figure 6.2.a. Simulated radiation patterns of the multilayer filter for (a) TE mode and (b) TM mode at source frequencies (A) 27.5 GHz; (B) 28 GHz; (C) 28.5 GHz; (D) 29 GHz.

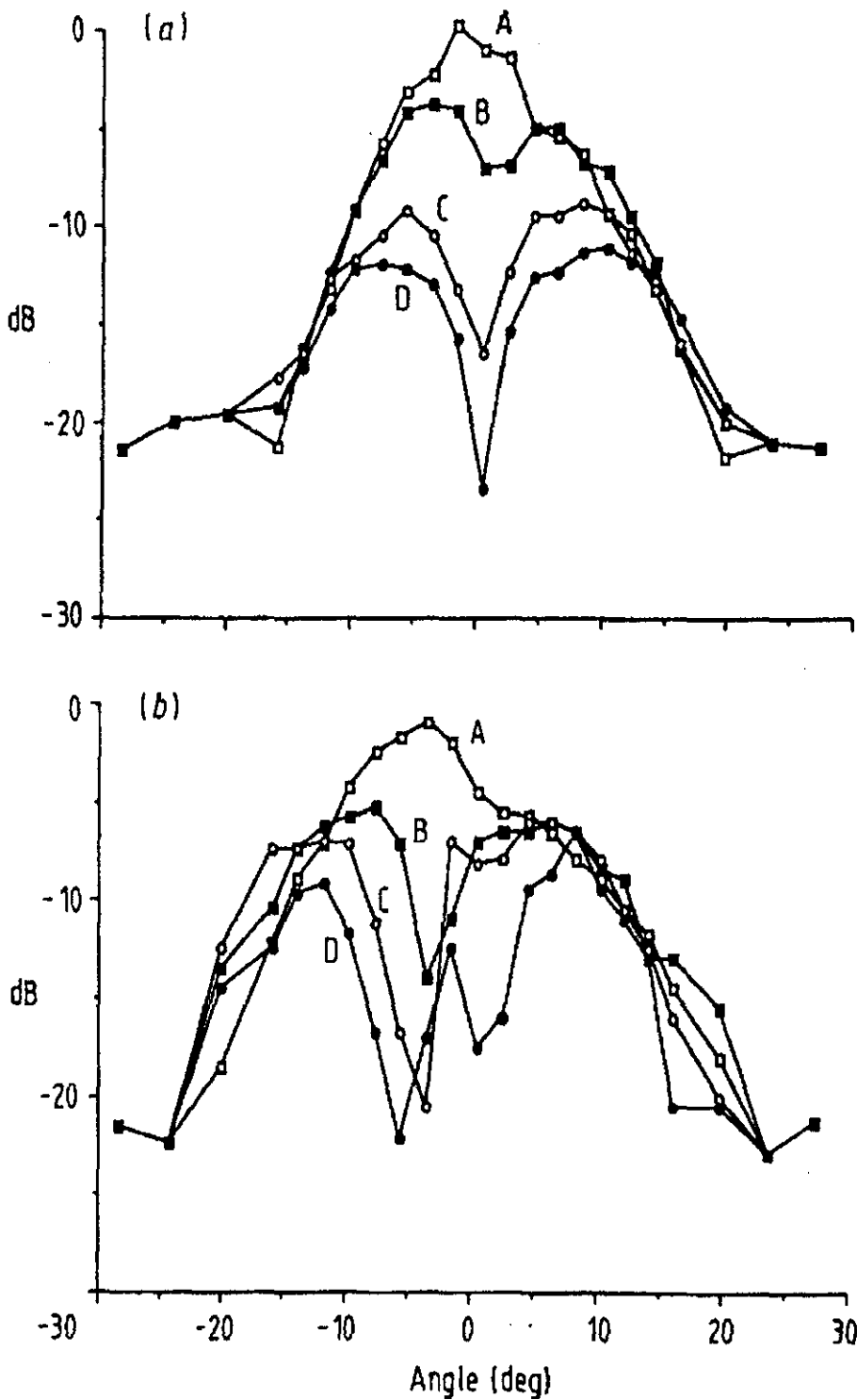


Figure 6.2.b. Measured radiation patterns of the multilayer filter for (a) TE mode and (b) TM mode at source frequencies (A) (open squares) 27.9 GHz; (B) (black squares) 28.5 GHz; (C) (open circles) 28.7 GHz; (D) (black circles) 29 GHz.

the measurement chamber and avoiding extraneous effects due to the edges of the multilayer, useful data were obtained in the range  $-20^\circ$  to  $20^\circ$ . The receiver probe was positioned as far away as possible from the multilayer (1.2 m) within the constraints of the chamber size.

The simulated radiation patterns in the region of the second order resonance ( $\sim 28$  GHz) for TE and TM polarisation states are shown in Figure 6.2.a. Since the theoretical angular transmission is highly directional, the beam is expected to be collimated by the structure as well as effectively steered. In Figure 6.2.b the radiation patterns, measured at  $\sim 1.2$  metres from the multilayer, are shown for a range of illumination frequencies. It will be noted that these data were chosen to be representative of the beam-steering process rather than to provide an exact comparison with the simulated data. It is apparent that the model used to predict the performance of the structure is qualitatively accurate but quantitatively inaccurate. This is not surprising as the source-multilayer interaction is clearly not fully described by a one dimensional model. In addition to this primary aspect it has been noted that the tolerances in the construction of the multilayer filter were relatively large ( $\sim 10\%$ ) and the precise dielectric parameters at the design frequencies are unknown. Nevertheless the structure performs the predicted filtering action, providing directional beam-steering under frequency control. The simulation also correctly predicts that the steering angle, for given frequency, is larger for TM modes than for TE and that the beamwidth at resonant frequency is larger for TM than TE.

In this experiment the main lobe is effectively steerable in the vicinity of the second order resonant frequency of the multilayer. In the optical regime, passive frequency controlled beam steering is usually achieved by employing a grating structure. However most of the transmitted

power lies in the unsteerable zero order mode and therefore would be unacceptably inefficient for analogous microwave antenna applications. The use of blazed grating would overcome this drawback but a further, more significant, problem exists with the use of conventional grating structures for beam steering at microwave frequencies, namely the small practical range of angular steering which is feasible. In this case it was found that the beam could in effect be steered by up to  $10^\circ$  under frequency control in the range 27.9 to 28.9 GHz although there is an associated reduction in the transmitted power as the beam is steered. This is due to the fact that the maximum amplitude of the signal impinging on the filter surface is at boresight and decreases away from boresight.

The main use of grating structures at microwave frequencies is for spectral filtering. More recent studies of doubly periodic gratings (FSS) are also mainly in the context of spectral filtering. Thus the attempt to demonstrate beam formation and steering as well as spectral selection, is novel. Optically analogous gratings are not used to beam steer at microwave frequencies as the available frequency band is not large enough to produce sufficient angular range. This can be seen in a crude approximation by the thin grating equation[5].

$$d \sin \theta = n\lambda \quad (6.1)$$

where  $n$  is the number of the order,  $\lambda$  is the wavelength,  $d$  is the periodicity of the gratings.  $\theta$  is the angle of incidence. After differentiation equation 6.1 gives

$$\Delta\theta = \tan\theta \cdot \Delta\lambda / \lambda \quad (6.2)$$

Thus for a thin grating the angular steering range is proportional to the size of  $\Delta\lambda/\lambda$ , where  $\Delta\lambda$  is the wavelength range over which a sweep is made and  $\Delta\theta$  is the shift in the beam. Whereas in many optical systems one can easily obtain  $\Delta\lambda/\lambda \sim 2$ , in a practical microwave communications system it is only reasonable to expect values of  $\Delta\lambda/\lambda \sim 0.1$  at the most, due to the limited allocation of frequency bands. Thus in practice, the angular steering would be at least an order of magnitude less than achievable at optical frequencies and therefore not as large as provided by the method proposed here.

### 6.2.2 Frequency Selective Surfaces

Two sets of procedures are discussed here for steering the beam using FSS. They are

1. Steering by Frequency Scanning
2. Steering by altering the position of FSS

#### 6.2.2.1 Steering By Frequency Scanning

An antenna has a main lobe pointing at the desired direction. In certain applications, it is necessary to steer the beam at various angles. Steering of the antenna beam from its boresight direction is accomplished by causing a progressive phase variation of the radiated fields across the antenna aperture. Several methods are available to achieve this in practice. For example in a phased array, the progressive phase shift can be provided by means of phase shifters at each array element; in a reflector antenna the same effect can be achieved by lateral displacement of the feed from the focus[6]. Though these techniques are relatively simpler, the cost and weight of the associated components is too expensive.

Linear, planar and conformal arrays can be designed with either fixed main lobe, or a scanned beam which is rapidly positioned in space by means of electromechanically or electronically actuated devices connected in the feedlines behind the array radiators. These devices change the phase or time-delay between radiators to produce the required phase progression along the array. Scans can be either one- or two-dimensional. Such systems are expensive to construct due to their complex nature of operation. To reduce the total operational cost of such systems, a method of steering the grating lobes using FSS is introduced, which is considered easy and cheap to produce due to the passive nature of the FSS[4].

Earlier works on frequency scanning have been based on the frequency dependent phase shift between the antenna elements created by delay in a transmission line, to which the elements were loosely coupled[7]. A printed circuit grid antenna at 2 GHz showed a slightly shifted frequency dependent beam[8]. Cascaded coupled microstrip resonators were used as frequency scanning antennas and resulted in scanning the beam upto  $\pm 30^\circ$ [9]. The method suggested here is the utilisation of passive filters to obtain the necessary scanning by varying the frequency of operation.

Several papers[2,3,4] have been published recently, to emphasis the applications of periodic structure, to construct antennas with frequency scanning properties, in the reflection mode. For these operations periodic arrays of elements were used. Here, the beam scanning properties are studied in the transmission mode. Periodic arrays of slots were used for this study. The basic principle is similar to that of the optical counterparts. The fundamental idea is to select a proper grating structure so that the first order diffracted wave is propagating

when an electromagnetic signal is incident on the surface. The propagation direction of the diffracted signal will be frequency sensitive and this signal is used to scan the range as the frequency is varied. In order to increase the signal power of this beam or aperture efficiency, it is necessary to channelise the incident power to the first order beam. Structures with this property are referred to as blazed gratings.

The blazed grating structure considered for the present study consists of a slotted array of crossed dipoles etched on dielectric sheet. The modal analysis method, explained in Chapter 4, was utilised for the design of the crossed dipole surface.

The performance of a frequency scanned grating is dependent on the blazed efficiency of the grating. It was found out in optimisation that the most sensitive parameters are the periodicity between the crossed dipole elements and the thickness of the dielectric layer.

The diffraction angles are calculated from an equation derived from the grating lobe equation, which is given in Chapter 4 (equation 4.14) as:

$$\text{i.e., } \sin\theta_{-1,0} = \pm \left( \frac{\lambda_0}{D1} - \sin\theta \right) \quad (6.3)$$

where  $\theta$  : the incident angle,  $\theta_{-1,0}$  : the first order diffracted angle,  $\lambda_0$  : the wavelength of the incident signal and  $D1$  : the element periodicity in the horizontal direction. The '+' and '-' signs refer to reflected and transmitted waves.

### 6.2.2.1.1 Numerical Results

Two crossed dipole surface geometries were used to study the frequency scanning performance of FSS. The FSS responses were calculated using the modal analysis method suggested in Chapter 4. It is evident from equation 6.3, that  $D_1$ , the horizontal periodicity plays a major role in determining the diffraction angle for the  $(-1,0)$  mode. The FSS geometries are given as follows. The slot lengths and the slot widths were selected as 4.2 mm and 0.2 mm respectively. The vertical periodicity is kept constant at 8.7 mm. The horizontal periodicities of the first and second surfaces were taken as 10 mm and 12 mm. Both the slot surfaces were backed by a 0.037 mm thick polystyrene layers.

These surfaces are assumed to be illuminated by a TM wave at an angle  $\theta=45^\circ$  and  $\phi=90^\circ$ . The primary intention of this exercise is to establish numerically the behaviour of the first order mode, in comparison with the zero order mode. The amplitude of the frequency responses are the normalised values for the zero order mode and non normalised values of the first order mode of the vertical component ( $E_y$  vector) of the field. The total incident field strength is assumed to be 1 volts/metre.

Figures 6.3.a and 6.4.a show the computed values of the zero order mode for the TM component for both the first and second surface. Figures 6.3.b and 6.4.b show the corresponding readings of the  $(-1,0)$  mode and the degrees of angular steering are given.

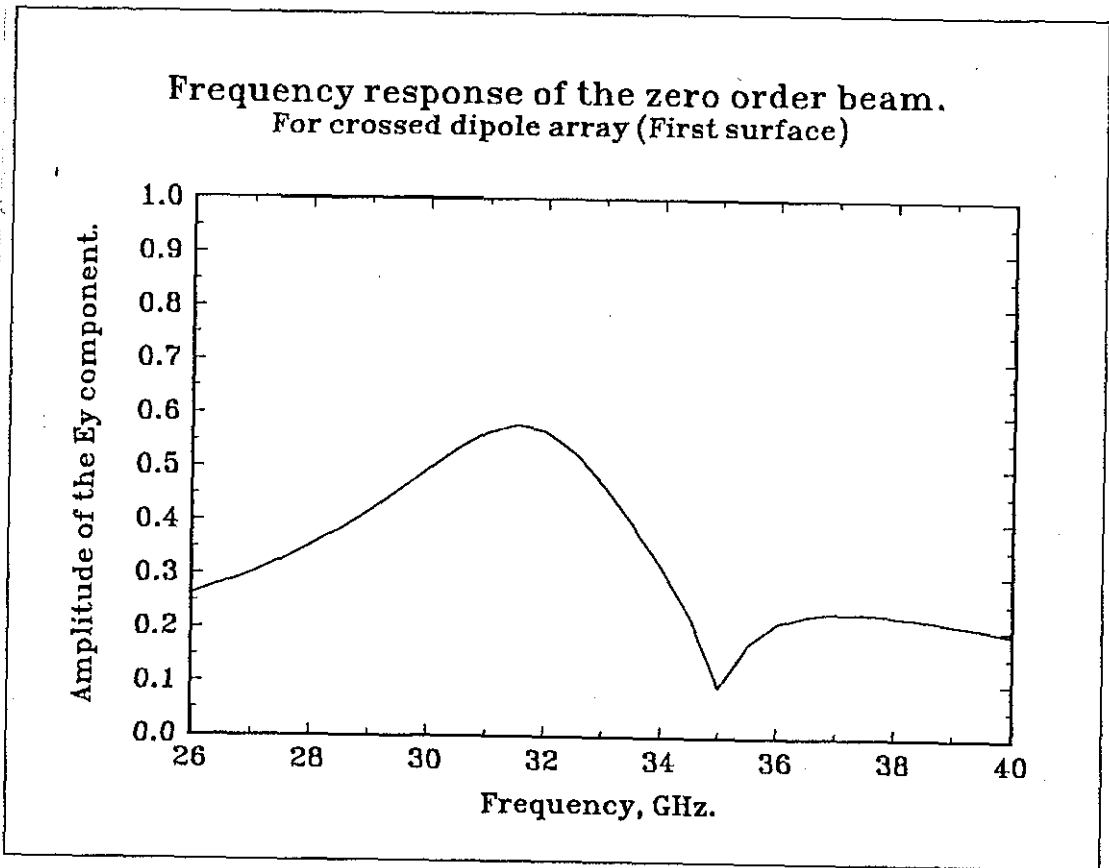


Figure 6.3.a

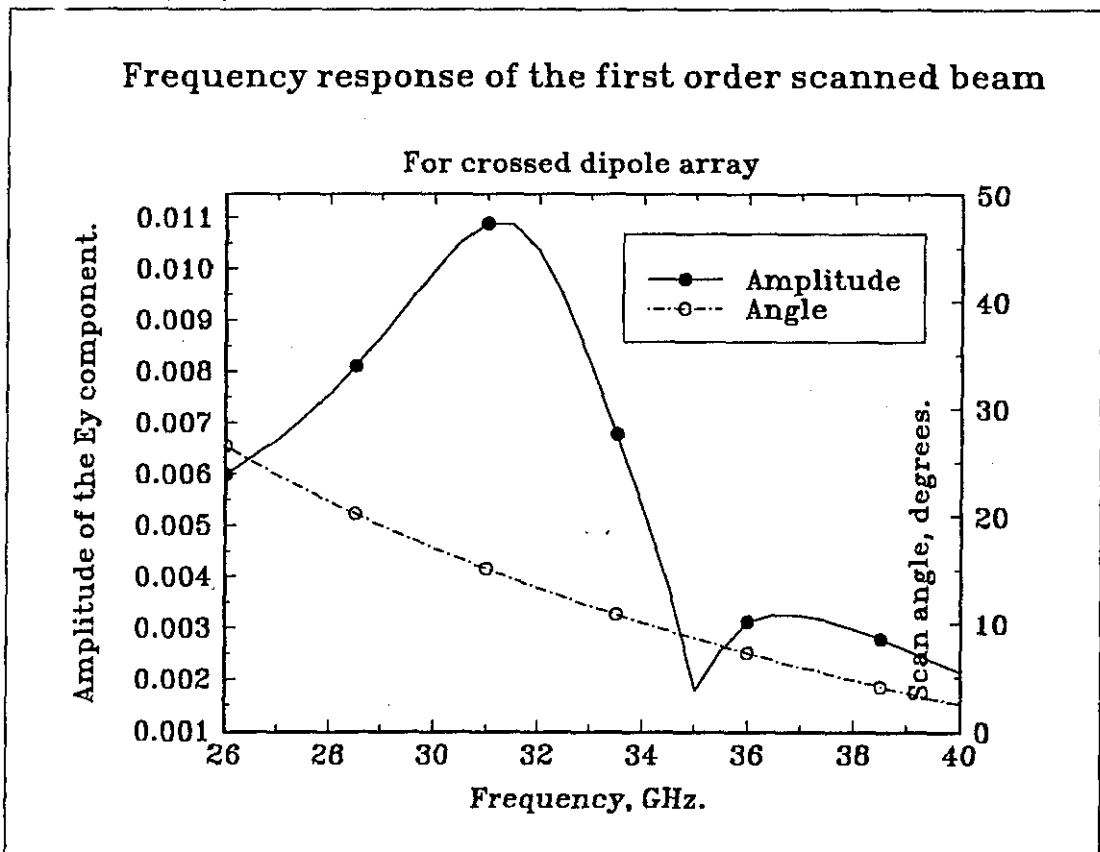


Figure 6.3.b

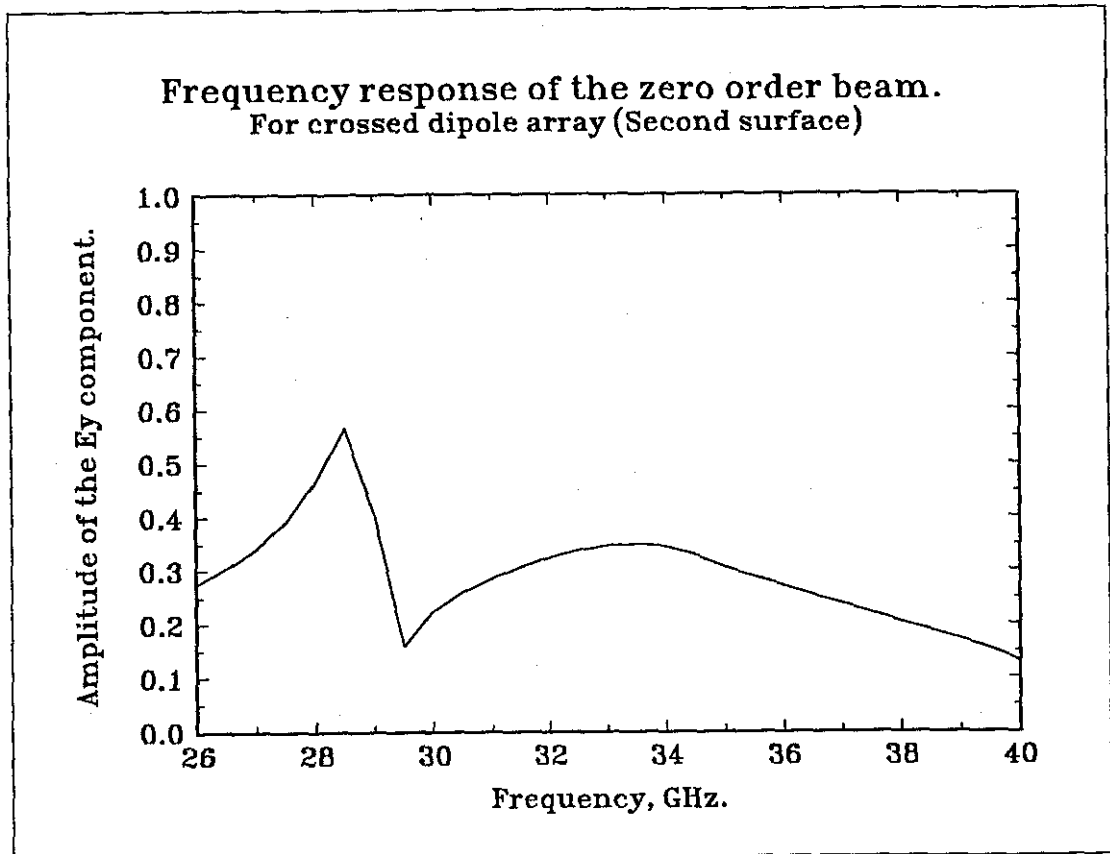


Figure 6.4.a

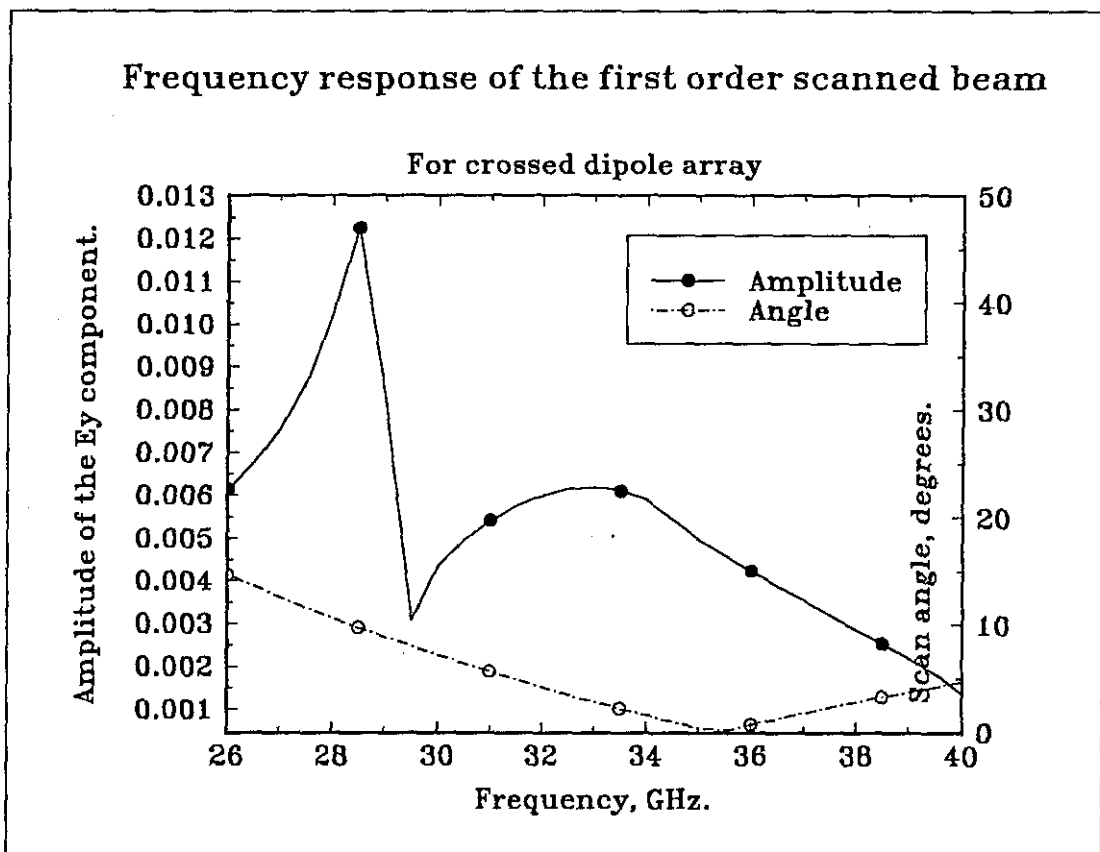


Figure 6.4.b

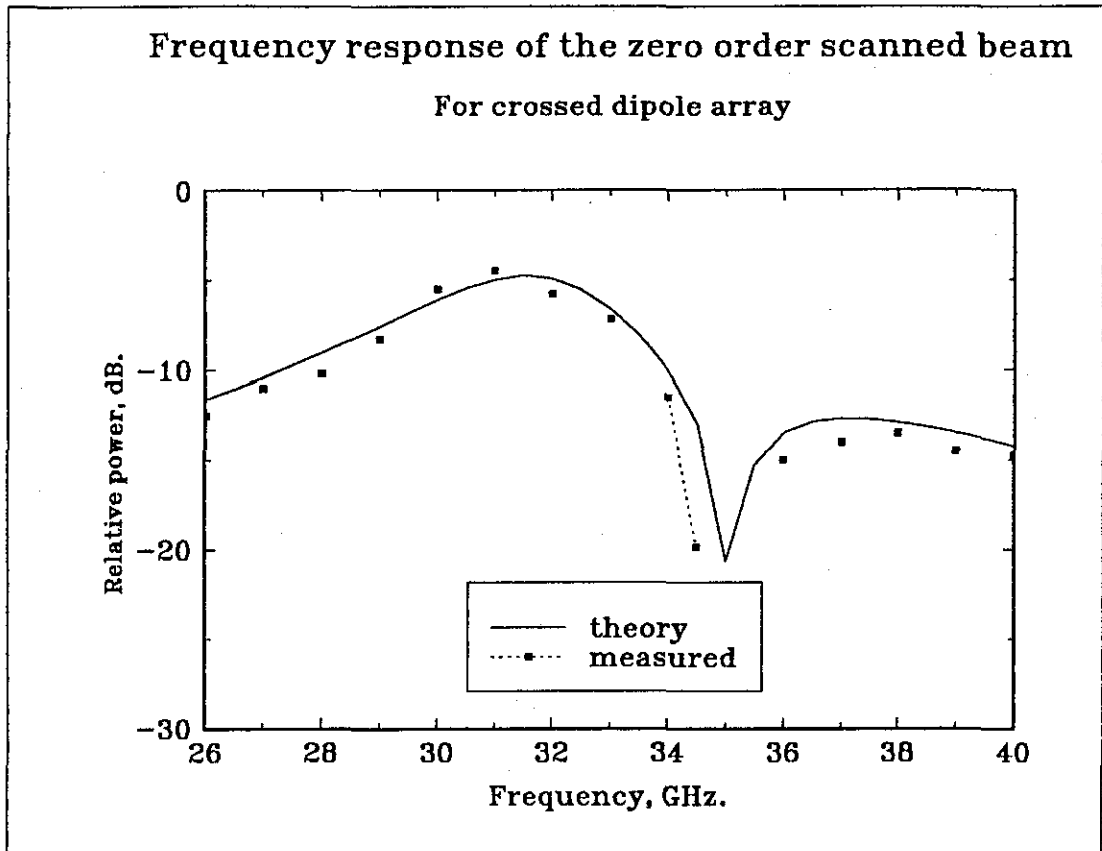


Figure 6.5.a

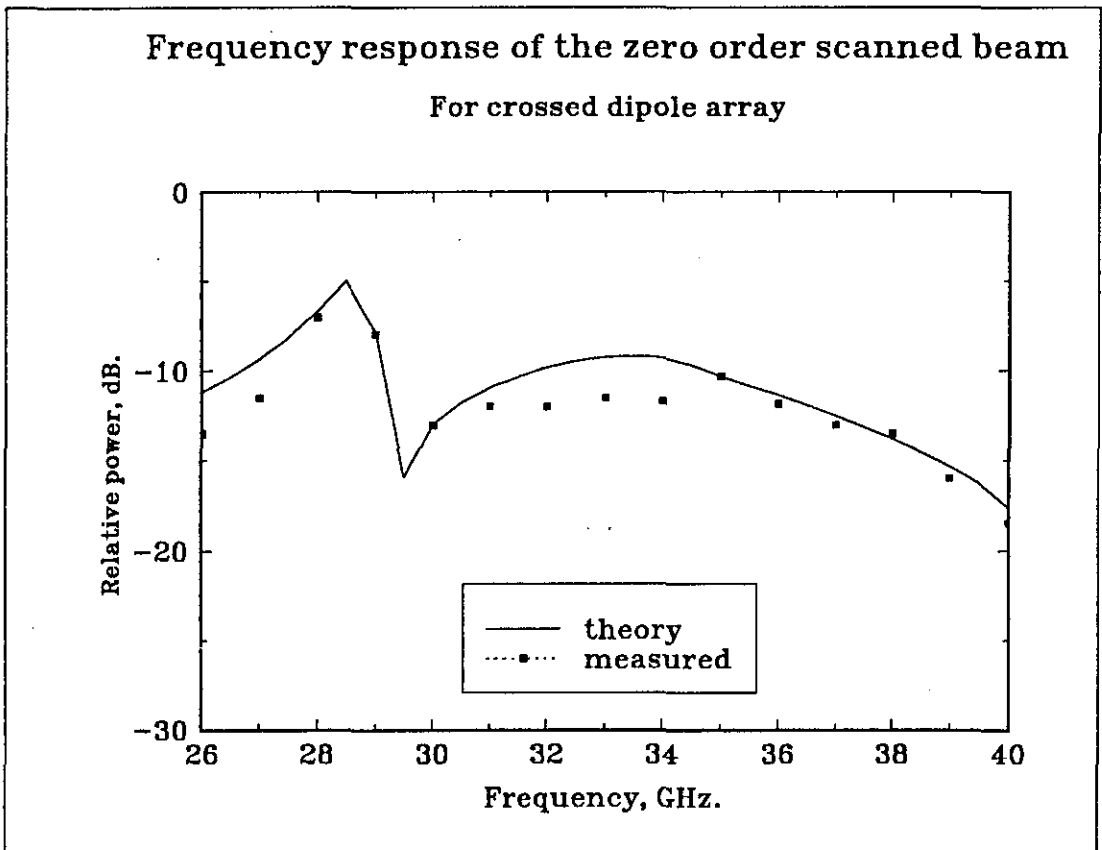


Figure 6.5.b

The  $E_y$  values of the first order mode of the first surface show an increase in amplitude between ~30 GHz and 32 GHz when compared to that of the zero order transmitted mode. This is equivalent to scanning of the first order beam from  $\sim 12^\circ$  to  $25^\circ$  as per Figure 6.3.b. Though the energy of the first order component is small compared to the zero order mode, this energy may be used for the first order beam scanning. Similarly for the second surface, the  $E_y$  values of the first order component is higher in the frequency region from 28 GHz to 29.1 GHz as shown in Figure 6.4.b. The  $E_y$  values of the first order mode vary from  $\sim 0.009$  to  $0.010$  which corresponds to a beam scanning coverage from  $9^\circ$  to  $12^\circ$ . It should be noted that the first order responses are not normalised with respect to any angle.

In Figures 6.5.a and 6.5.b the prediction of the zero order mode is compared with the measured data and they show a reasonably good agreement. The scan range for these surfaces averages to  $\sim 3^\circ/\text{GHz}$ . It has been noted from these computed values that the effective channelling of the power in the zero order mode to the first order transmitted mode is obtained over a narrow range of frequency. Also the reflected zero order mode and first order mode are effectively suppressed over this range.

#### 6.2.2.2 Steering by Rotating the FSS

Most of the existing steerable antenna systems use electronic, mechanical or frequency scanned antenna systems. For a mechanically scanned antenna, a rotatable

antenna is used to scan around the region. A electronic scanning implies the use of phased array antennas, to steer the beam by varying the phase of the signal. Here, a novel antenna concept is establish to keep the feed antenna at a fixed position and scan the region in front by means of a rotating FSS. The basic principle is to use a spatial movable filter in front of an antenna, so that by rotating the FSS in the horizontal or vertical axis, it can transmit and receive to or from a source. A schematic diagram of such a system can be envisaged as given in Figure 6.6.

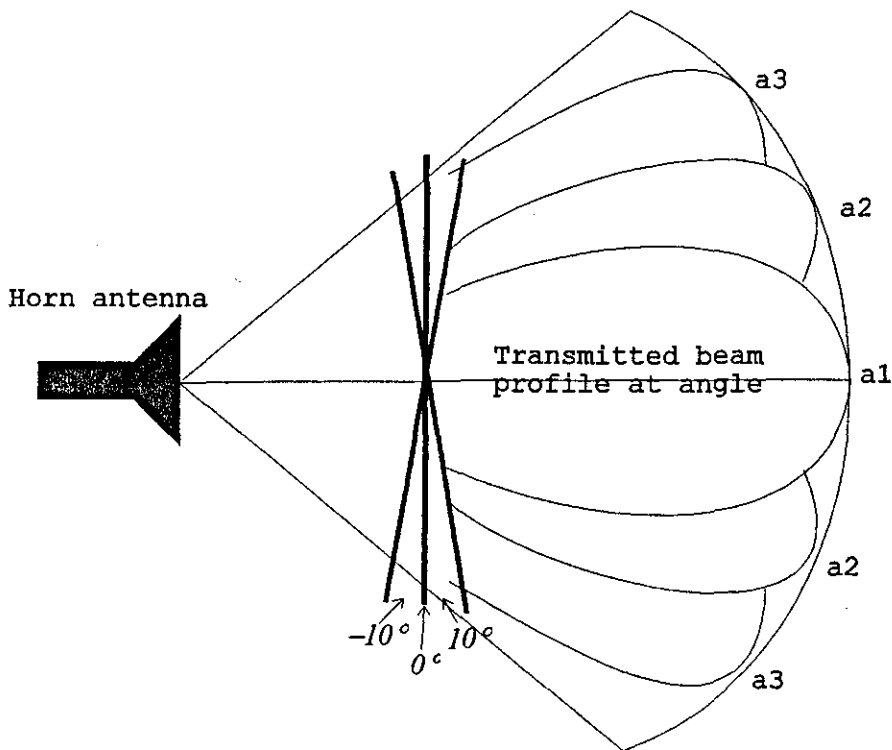


Figure 6.6 Schematic diagram for beam scanning by rotating the FSS

A tripole FSS was used to study the performance of such an antenna system. The dimensions of the FSS geometry are given in Figure 5.3. The size of the FSS was  $20 \text{ cm}^2$ . Such a geometry was chosen, so that the system can have a

narrow beamwidth performance. The FSS was placed in the far field of a horn antenna. As the filter is rotated, it changes the direction of the transmitted or received beam, which is dependent on the angular position of the filter.

The measured data are shown in Figure 6.7 for TM incidence. The filter was rotated in steps of  $2.5^\circ$ . A shift in the beam position is apparent with the shift in the filter position. A  $-3$  dB performance is observed in the region from  $-15^\circ$  to  $+15^\circ$ . After this range, the signal strength deteriorates sharply. This can be accounted for by the sharp angular filtering nature of

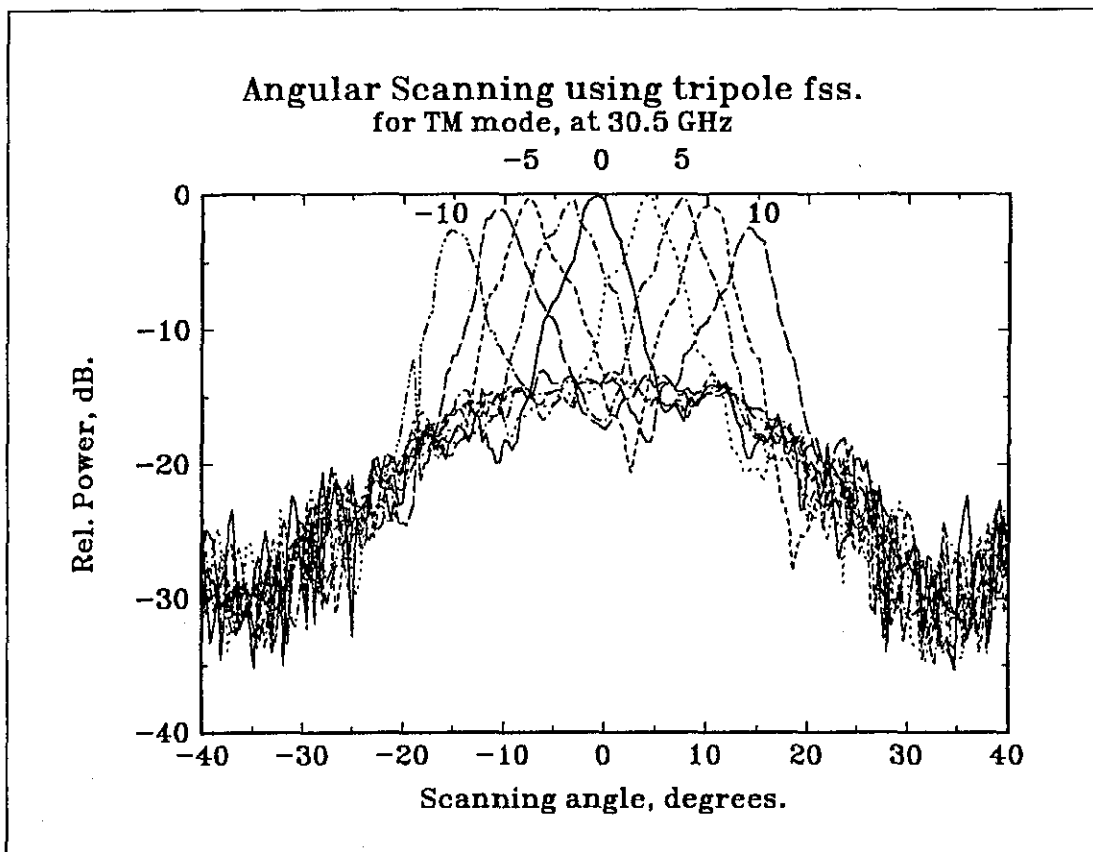


Figure 6.7.

the FSS, as given in Chapter 5. Though such a shift is also present for TE incidence, due to its broad beamwidth the resolution of the shift is poor.

### 6.3 Dielectric Multilayer As An Electromagnetic Window

For applications in communications, the dielectric multilayer filter should have low power absorption within a prescribed transmission band. It should provide high directivity by shaping the antenna beam. Such a window can also act as an apodiser by suppressing the sidelobes of the primary antenna. This property of a DML is investigated in this section of the chapter.

The type of dielectric filter studied here is given in Figure 3.1. The thicknesses of the layers are chosen according to the fundamental resonance frequency  $f_0$  given by[10]

$$t_h = \frac{c}{4f_0 \sqrt{[\epsilon_h(1 - j \tan \delta_h) - \sin^2 \theta_i]}} \quad (6.4)$$

$$t_l = \frac{c}{2f_0 \sqrt{[\epsilon_l(1 - j \tan \delta_l) - \sin^2 \theta_i]}} \quad (6.5)$$

where  $\tan \delta$  is the loss tangent,  $t$  is the thickness of the individual layer,  $\theta_i$  is the incident angle and  $c$  is the speed of light. Subscripts  $h$  and  $l$  represent the high and low permittivity regions.

These filters have higher order resonances depending on the number of layers used and their properties. Attention is focused here on the first order resonance which occurs at ~34 GHz for normal incidence, for which the

fundamental resonance is 36.2 GHz and exhibits a passband of 2 GHz. (Figure 5.4.)

### 6.3.1 Experimental Results

The antenna structure is tested by placing the dielectric multilayer in the far field of a pyramidal horn, which is used as a primary feed. The measured radiation patterns of the multilayer filter are compared with the feed patterns. The feed patterns are shown in Figure 6.8 for both TE and TM polarisations and in each graph both co- and cross-polarisations are shown. It can be seen that the cross-polarisation of the horn is below -25 dB. Figure 6.9 gives the radiation patterns of the co- and cross-polarisations of the TE and TM modes for the horn with multilayer filter. It can be seen that both the co-polar patterns of the TE and TM modes of the multilayer filter are more directive. The -3 dB beamwidth of the multilayer filter for co-polarisations is  $\sim 12^\circ$  compared with the beamwidth of  $\sim 24^\circ$  of the horn feed for both TE and TM. The sidelobe levels are also suppressed being well down in the noise region of the pattern.

The co-polar pattern of the novel antenna system shows an increase in the resolution and directivity. In particular, the resolution of the antenna is increased from  $\sim 32^\circ$  to  $\sim 20^\circ$  and the directivity from  $\sim 19$  dBi to  $\sim 24.5$  dBi. The filter achieves this reduction in the beamwidth without any increase in the cross-polarisation level and the gain of this system is approximately the same as that of the horn. Since this structure exhibits almost the same radiation patterns for co- and cross-polarisations for both TE and TM modes, it can be used for dual polarisation applications. The low cross-polarisation of the two modes is important for this type of operation. Thus by using this type of multilayer, the antenna performance can be extended into narrow band and dual polarisation applications.

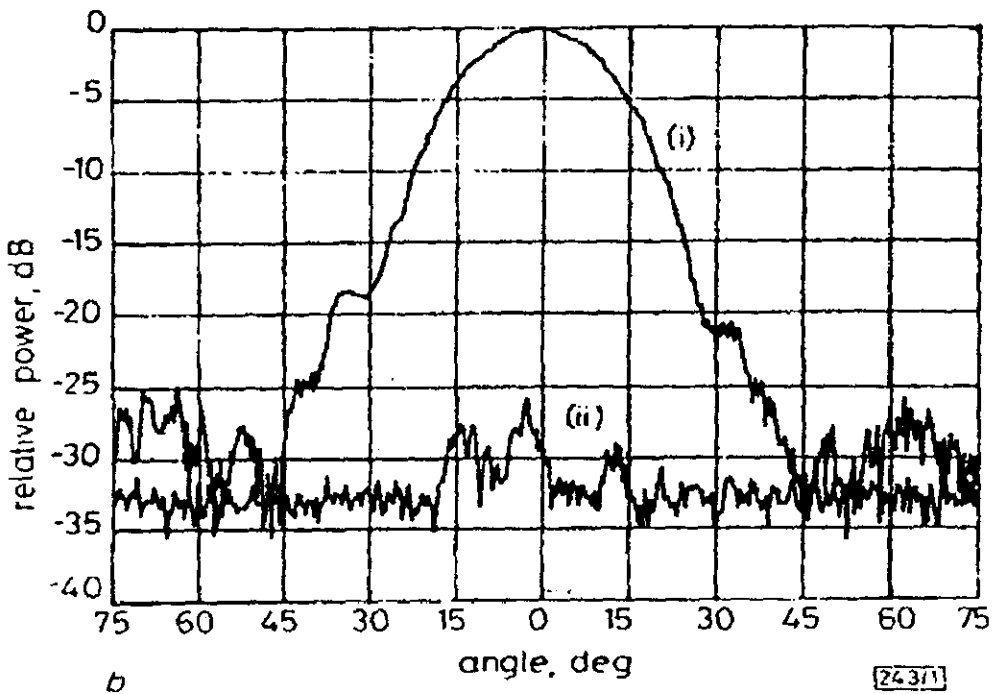
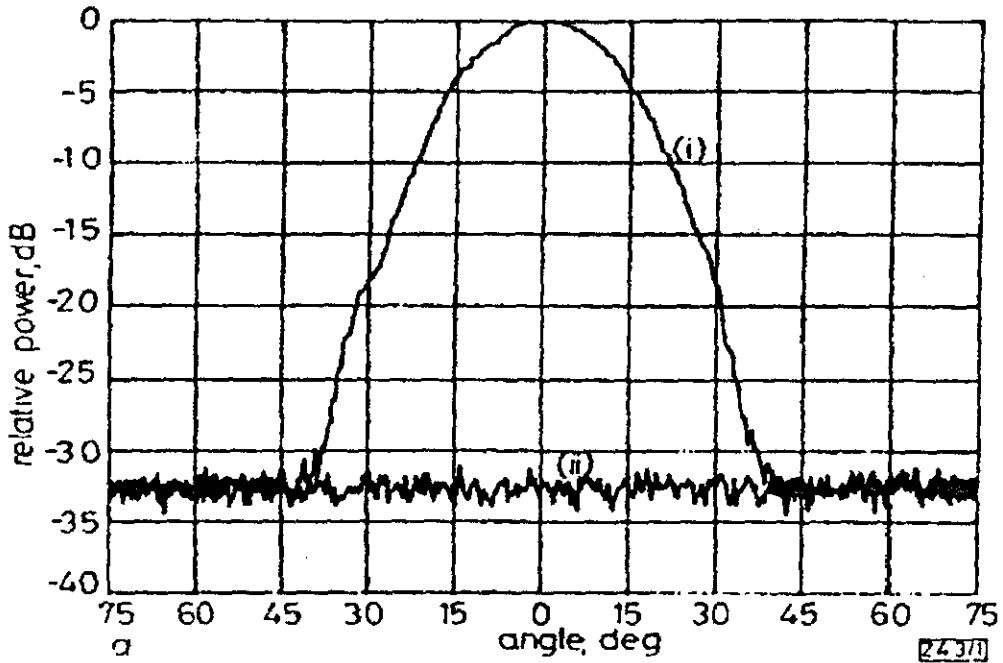


Figure 6.8. Measured radiation patterns for co- and cross polarisation of horn for TE mode and TM mode at resonance frequency. a. TE mode, b. TM mode

(i) co polarisation (ii) cross polarisation.

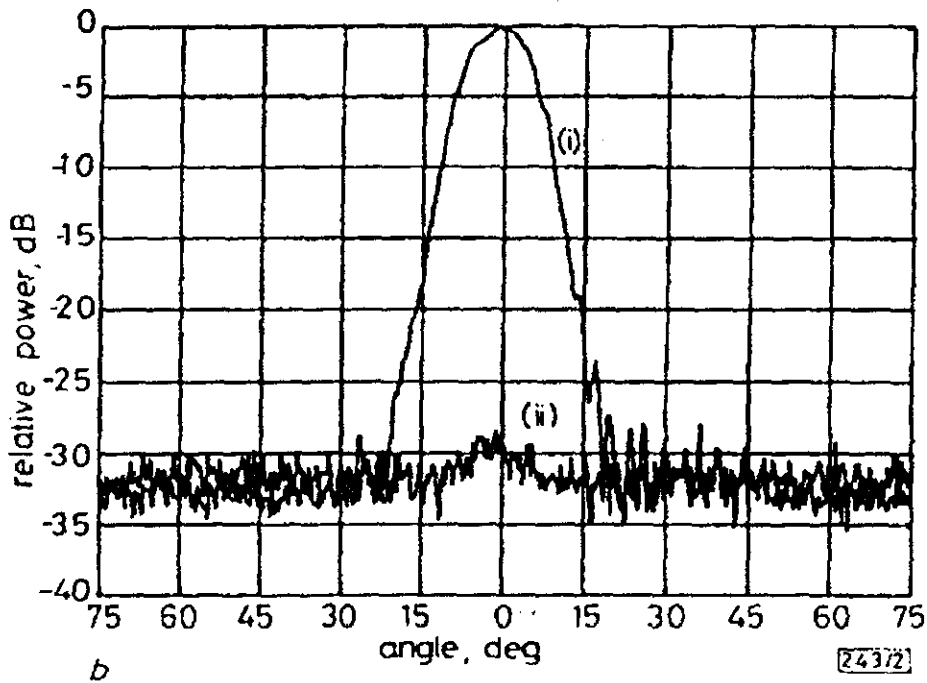
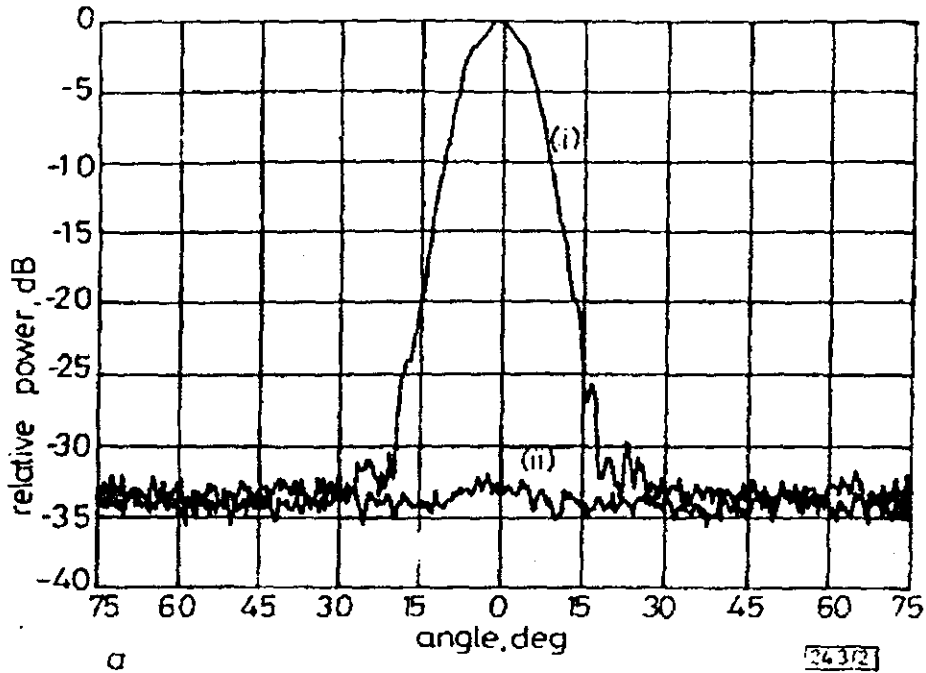


Figure 6.9. Measured radiation patterns for co- and cross polarisation of horn with multilayer filter for TE mode and TM mode at resonance frequency. a. TE mode, b. TM mode

(i) co polarisation (ii) cross polarisation.

In theory the passband and beamwidth of the antenna system can both be further reduced by increasing either the number of individual layers or the ratio  $\epsilon_h/\epsilon_l$ . It should be noted however that as the beam becomes narrower, the radiation efficiency of the system is reduced.

#### 6.4 Beamforming Using DML

The DML being investigated can also be used to produce a narrow beam with low side lobes and in this sense could be described as an apodizing aperture. This application is a simple alternative to the use of phased arrays in beam-forming [7]. The far field radiation pattern of the multilayer described above, placed in the near field of an open-ended waveguide, is shown in Figure 6.10 for the second order resonant frequency  $\sim 28$  GHz. It can be seen

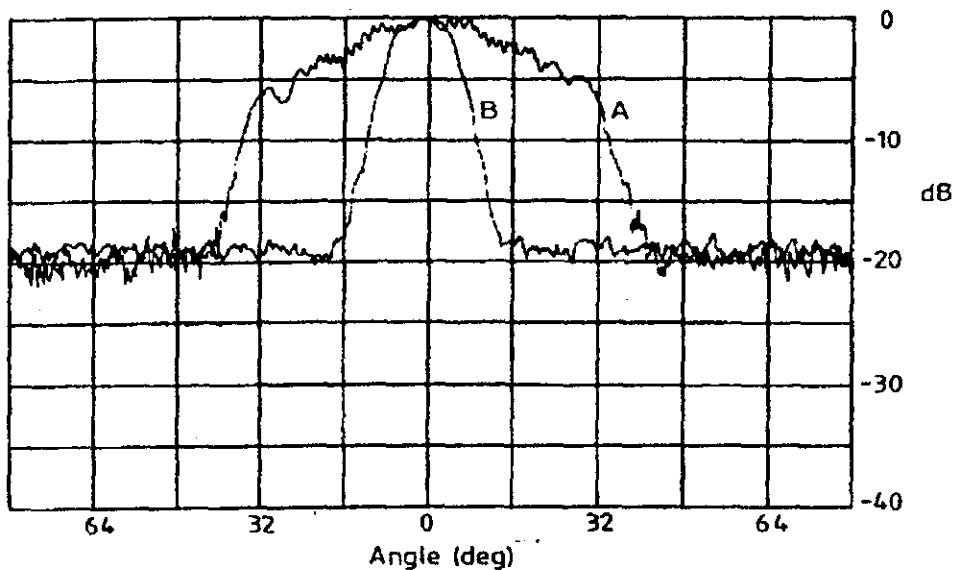


Figure 6.10. The collimating effect of the multilayer at the second order resonant frequency. Curves (A) and (B) correspond to open ended waveguide without and with multilayer filter respectively.

that the -3 dB beamwidth of the multilayer is close to  $10^\circ$ . Also note that the far field pattern displays no sidelobe level above the noise threshold ( $\sim -18$  dB).

## 6.5 Concepts Of Electromagnetic Lenses

Antenna systems using lenses play an important role among the different types of antennas which have been developed for use at various frequency bands[11,12]. Lenses have been used in conjunction with microwave horn antennas for a considerable period[13]. The general design approach is to place the lens at the aperture of the horn and to treat it as a phase correcting device which produces a plane wavefront from the rays emerging from the effective point source at the phase centre of the horn. By using the lens as a phase corrector, the flare angle of the horn can be made much larger than would be required, if its radiation pattern were to be limited by diffraction from the non-phase-corrected electric field distribution in the aperture. Thus a lens corrected horn can be made much more compact than a simple feed horn having equal directivity or gain.

Lenses are transmissive components, which operate by altering the phase of the electromagnetic wave as it passes through. The phase of the signal can be altered in several ways. The simplest being by altering shape of the component. For example, by curving both surfaces of a slab, inwards or outwards, a diverging or converging lens can be made. Also for focusing, the dielectric constant of the lens medium is varied such that the index of refraction is a maximum at the centre of the lens and minimum at the edge.

### 6.5.1 Focusing Action Of FSS

The focusing action using FSS is discussed in this section. The lengths of the slots are varied to obtain

the phase change to produce a focused beam. The lengths of the slots are changed, from the centre to the edge of the surfaces. This also means that the periodicities between the slots are changing. The lengths of the slots can be increased or decreased according to the requirements. To produce a converging lens, the length of the slots are decreased and for diverging lens, they are increased.

It has been shown that regular arrangements of periodic elements can be viewed as artificial dielectrics or phase shifting structures[14]. A plurality of elements or a FSS can be used to introduce a phase shift in the transmitted portion of the radiation incident on the array. The phase shift can be made stepped or progressive, by altering the geometry or dimensions of the array elements used. Therefore, using an array with phase shifting properties varying spatially across its surface, incident radiation can be influenced in such a way to beam form, beam direct, filter or converge the incident wave.

The basic principle involved in creating a newly formed wave front is to introduce symmetrical or anti symmetrical phase advances, increasing in relation to spatial distance from the axis (centre) or the perimeter of the array. The amount of beam shaping near the lossless region of the band depends on the variation of the transmission coefficient (amplitude and phase) to the local angles of incidence which are present on the structure.

An array with continually varying element dimensions (Fig 6.11.a) of the same periodicity is studied in this section. A progressive phase shift will therefore advance across the surface. Using the same postulate, arrays were

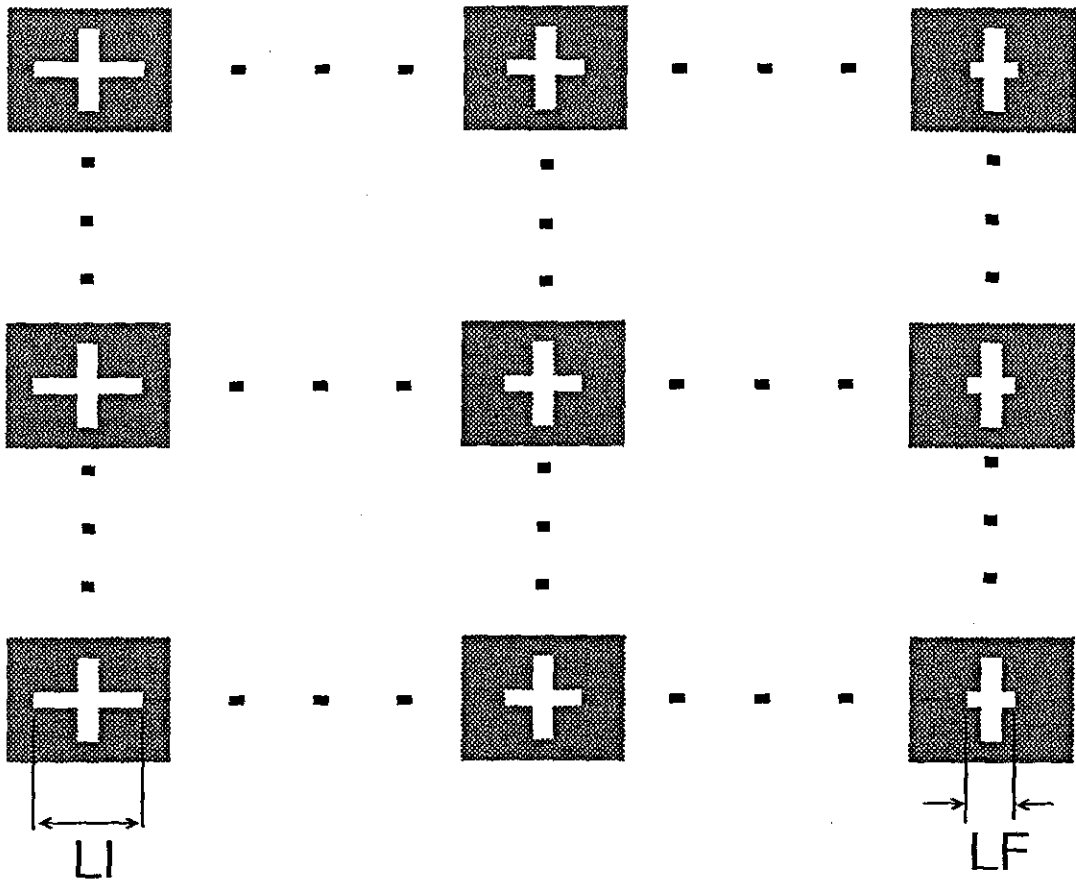


Figure 6.11.a Geometry of a tapered array.

assessed with symmetrical configurations of the above, as shown in Figures 6.13.a and 6.14.a. The elements were slotted crossed dipoles and were arranged on a regular grid.

### 6.6 Beam Directing Array

The design comprises a continual tapering of the elements' dimensions so that a net phasing effect may be introduced. Fig 6.11.a <sup>shows a</sup> slotted crossed dipole (20 cm square) single layer array. There was a total reduction of the horizontal arm length of about 50% from one side of the surface to the other. The vertical arm length and the lattice geometry (square of side 4.35 mm) remained unchanged. The element lengths were  $L1 = 4.15$  mm and  $LF = 2$  mm. With the incident field across the horizontal arm

(normal incidence) at 35 GHz (Position A), there was a relocation of the transmitted beam at about  $-9^\circ$ , in the H-plane which is shown in Figure 6.11.b. The results show evidence of a progressing phasing effect produced by a reduction of  $\lambda/2$  to  $\lambda/4$  element length and a slow wave near the edge of the array. Rotating the surface through  $180^\circ$  (Position B) in its own plane the beam appeared near  $+9^\circ$  which is symmetrically opposite to the previous case. For both orientations, there is less than 1 dB loss over a 5% bandwidth. In addition to the beam location, there is also a notable narrowing of the illuminating beam.

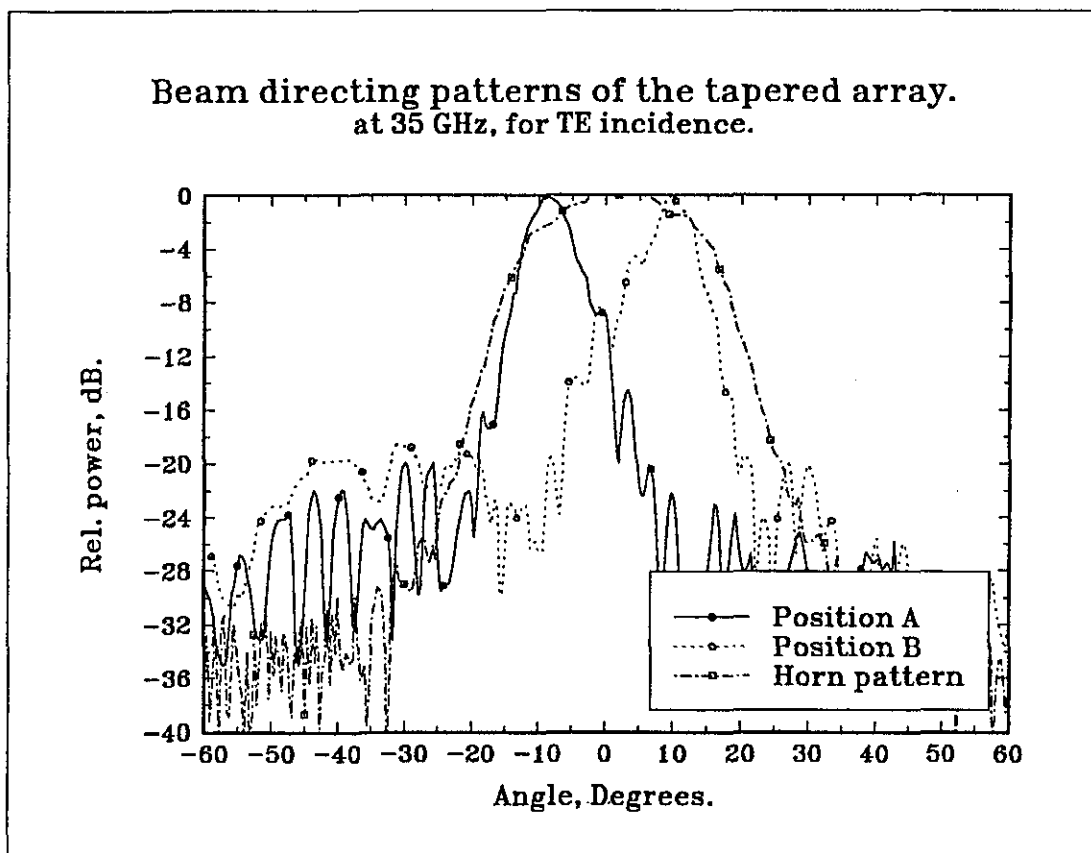


Figure 6.11.b.

### 6.6.1 A First Order Approximation Of Beam Directing

To explain the beam directing phenomenon, a first order approximation model of the continually tapered array is

presented. This model is entirely one-dimensional for the sake of simplicity.

According to this method the entire surface is divided into small arrays. i.e., a 20 cm long surface is divided into 400 arrays, each representing 0.5 mm of the surface length. The transmission coefficient of the region over which copper is coated is taken as zero. The transmission coefficients over the rest of the surface (slots) are calculated from the modal analysis method given in section 4.2. This analysis was run for the given slot lengths. This gives information regarding the transmission coefficients on the surface (i.e., the aperture distribution). Once the aperture distribution is known, the radiation pattern can be calculated using Fresnel-Kirchhoff Integral method[15,16,17].

Figure 6.12.(a, c, e, g) gives the aperture distribution of the crossed dipole surface at various frequencies. It should be noted that as the lengths of the slots are decreased, the periodicity between the slots increased and vice versa. As the frequency is varied, the resonant point of the surface also varies. The reason is that at a particular frequency only one slot on the surface resonates, depending upon the length of the slot. In Figure 6.12.a, at 33 GHz, the 18th slot from the centre of the surface to the left edge resonates. At this point, the phase also changes its polarity. As the frequency is increased the resonance moves towards the centre of the surface.

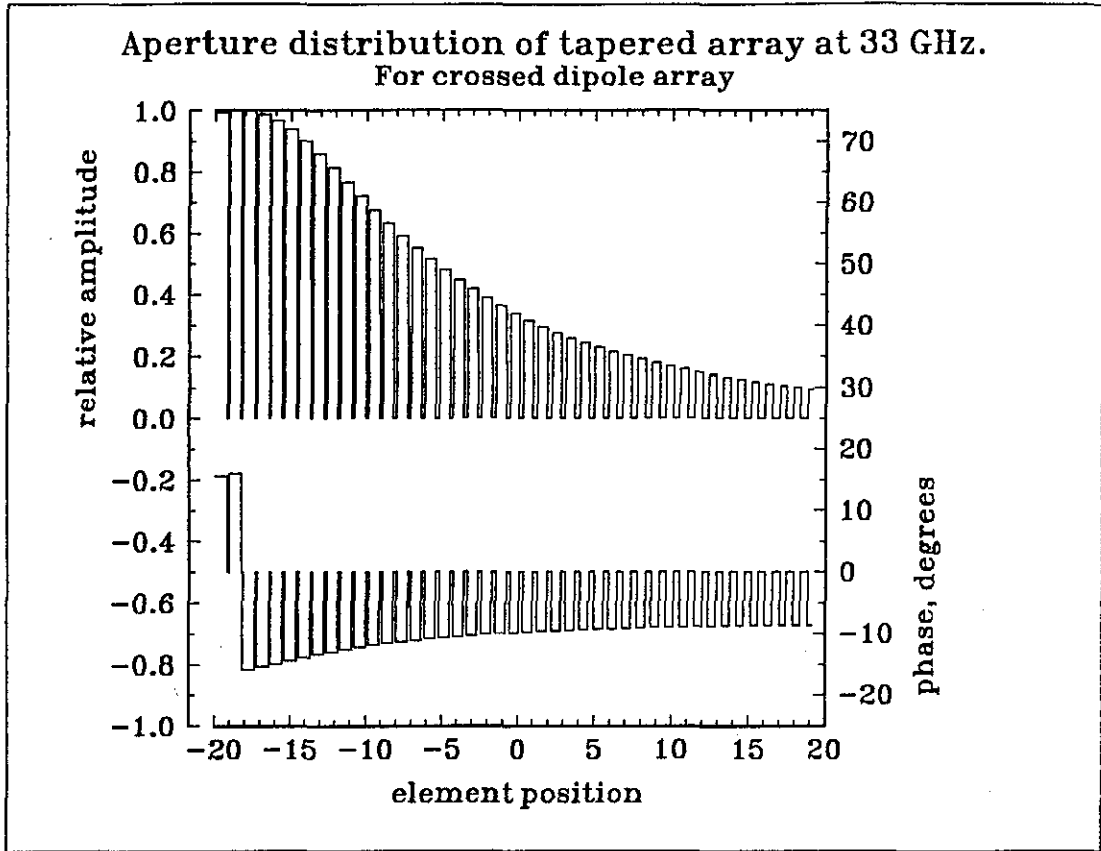


Figure 6.12.a

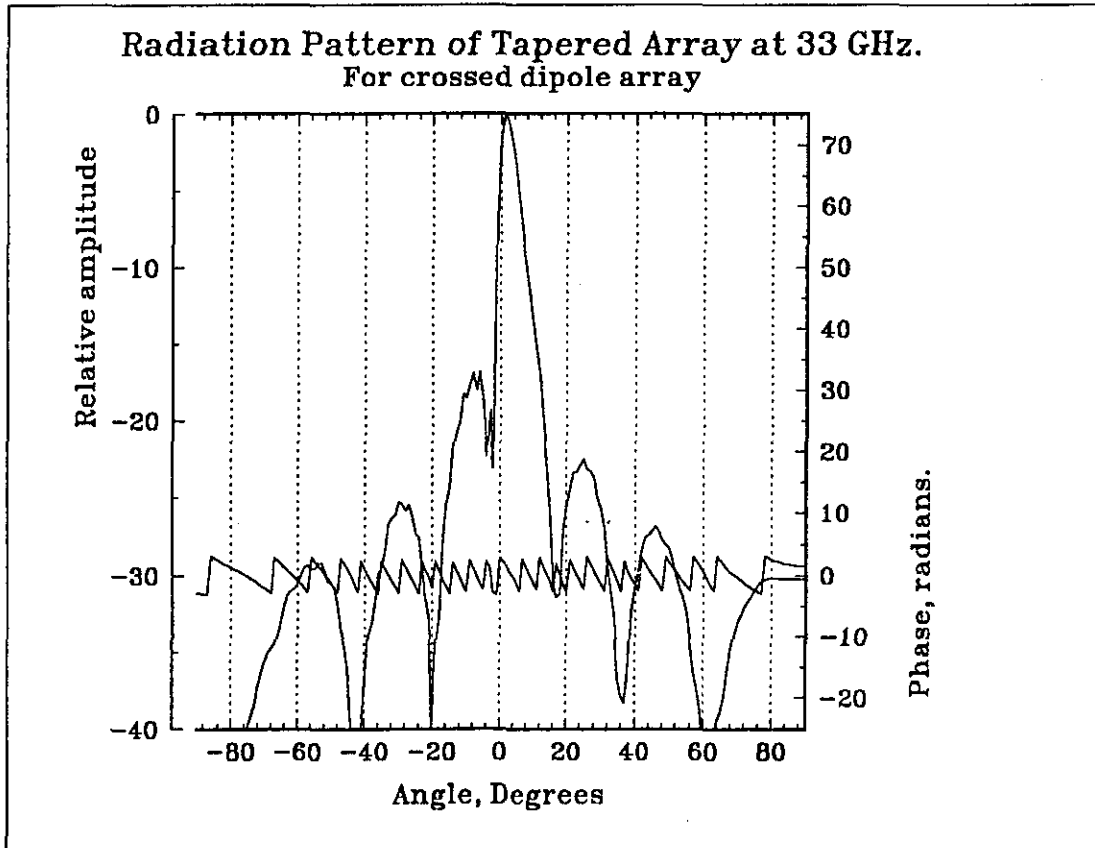


Figure 6.12.b

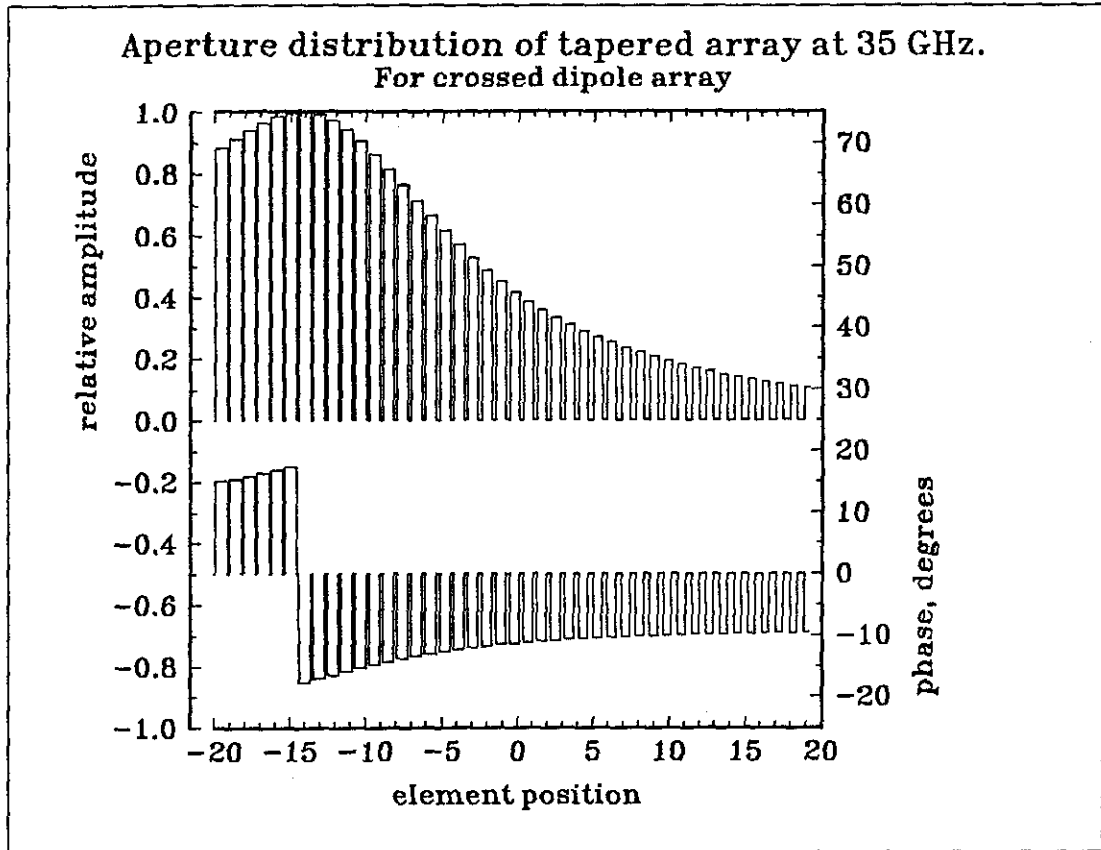


Figure 6.12.c

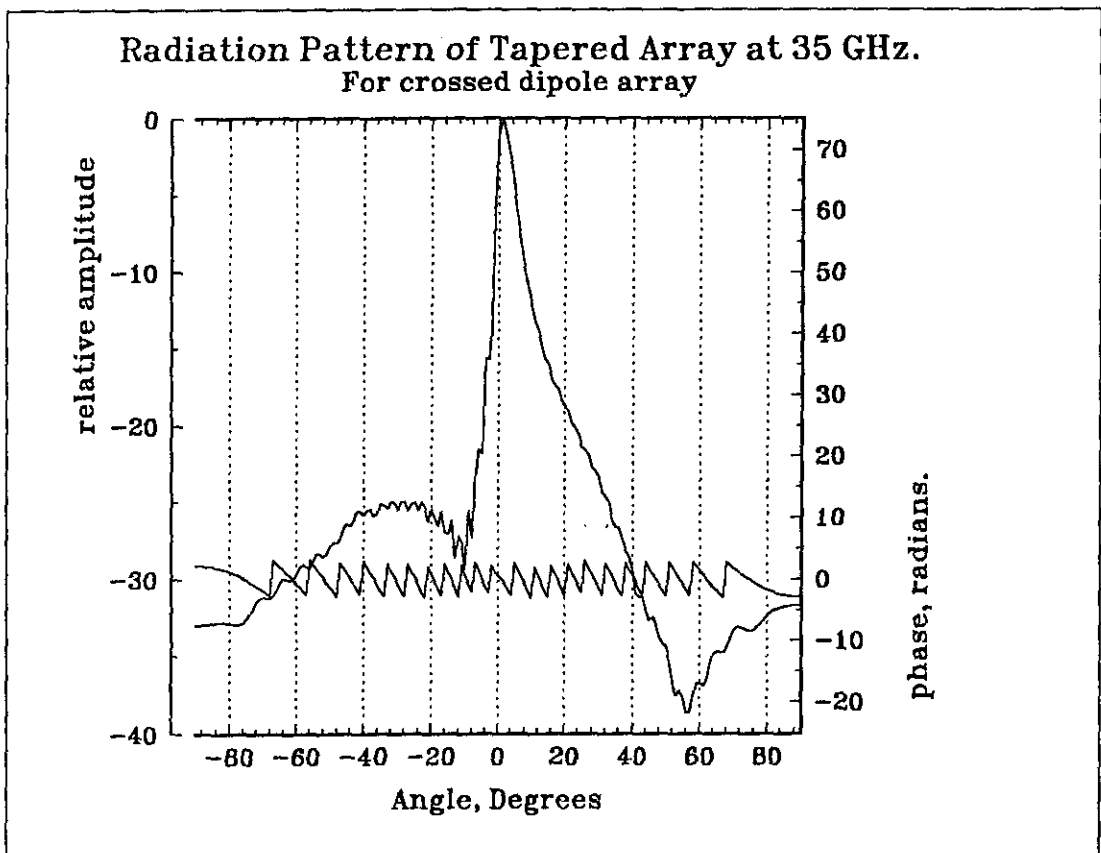


Figure 6.12.d

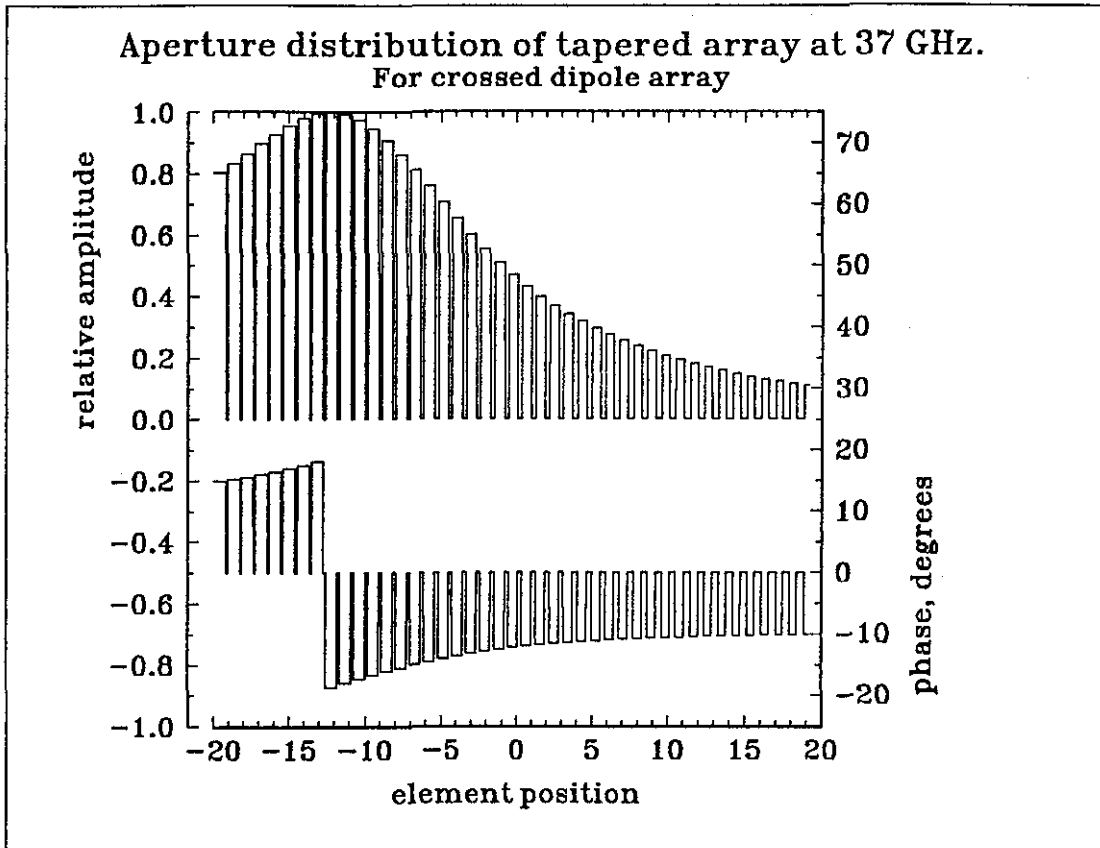


Figure 6.12.e

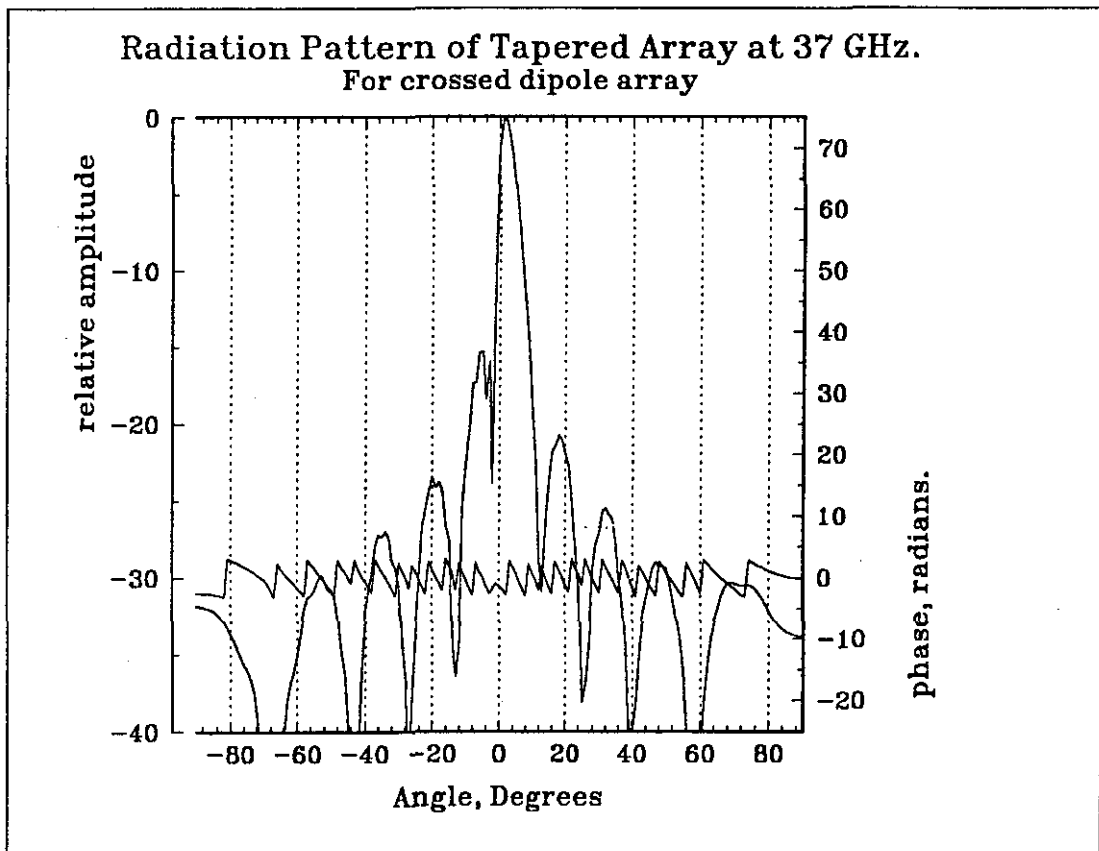


Figure 6.12.f

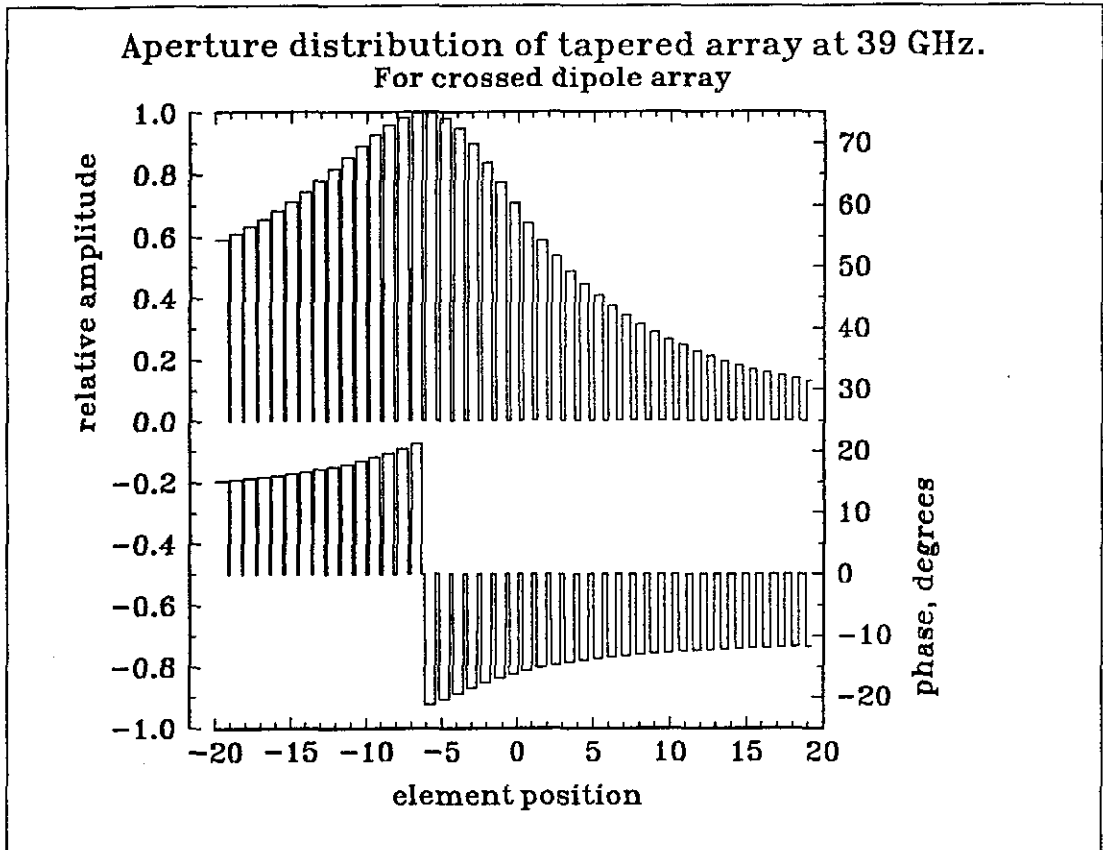


Figure 6.12.g

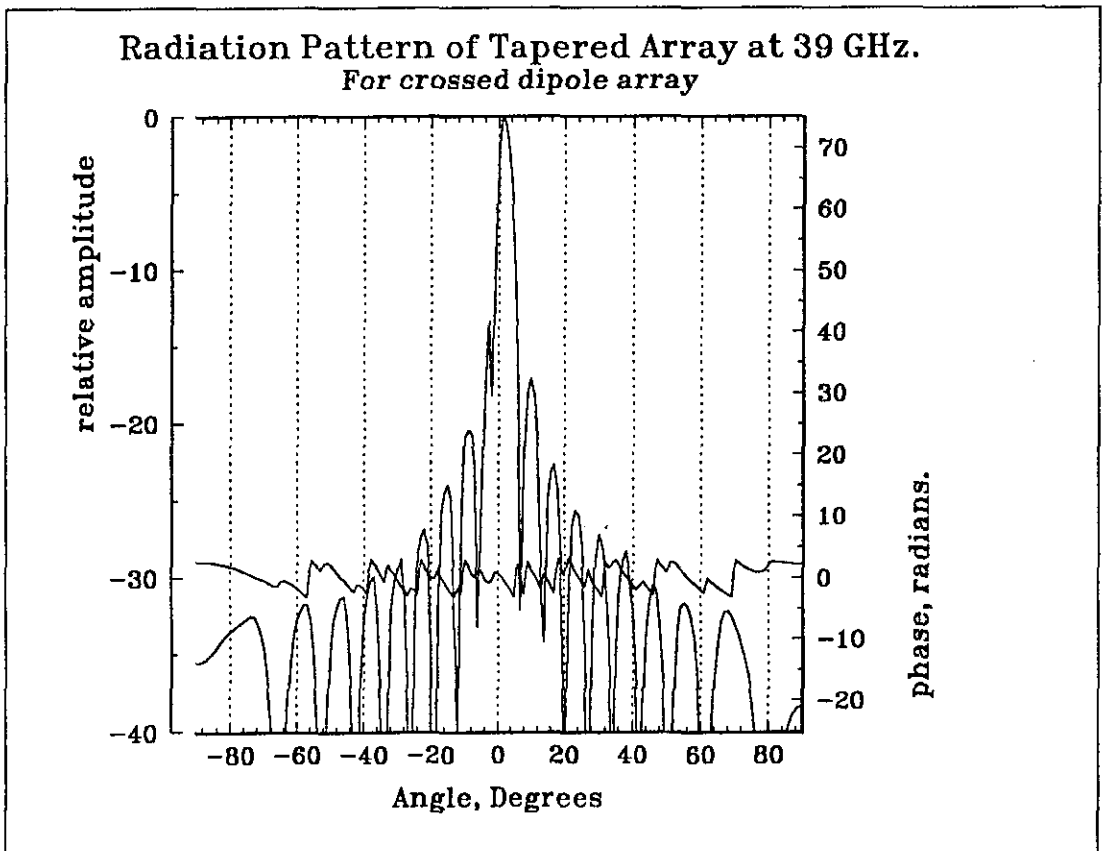


Figure 6.12.h

The corresponding effects on the radiation patterns are shown in Figures 6.12 (b, d, f, h). The peaks of the radiation patterns are at  $\sim 1^\circ$ . Once the frequency is increased, the sidelobes start to appear and at 39 GHz, distinct nulls are formed between the lobes. Also a reduction in the beamwidth is observed. Unlike other graphs

Figure 6.12.d shows a slightly broader pattern at the -20 dB level and below.

This approximation shows that the beam remains the same at the boresight as the frequency of the signal is varied. The effects due to the vertical arm of the crossed-dipole is ignored completely in this method. A more rigorous two dimensional approximation is required to show this effects and that is beyond the scope of this work.

#### 6.6.2 Symmetrically Tapered Array

Figure 6.13.a shows a symmetrical spatially varying slotted crossed dipole array. There is taper in both the vertical and horizontal arm lengths, from the left to right as well as from top to bottom of the surface. The dimensions were as follows:  $L_{HI} = L_{VI} = 4.15$  mm,  $L_{HR} = 3$  mm and  $L_{HF} = 2$  mm. There was a 33% reduction in the vertical arm. The radiation patterns in the E and H planes are shown in Figure 6.13.b, at 33 GHz, exhibiting similar features. A radiation intensity increase over 5 dB was measured when compared to the standard gain horn at the same frequency. Increases begin at about 30 GHz and occupy a bandwidth of 9%.

A different type of symmetrical arrangement of the array elements can be seen in Figure 6.14.a. This formation of elements is axi-symmetric where square loop zones increase in circumference from the centre of the surface. The element at the centre has equal length arm ( $L_I = 4.15$  mm) and the elements at the edge of the array reduced by

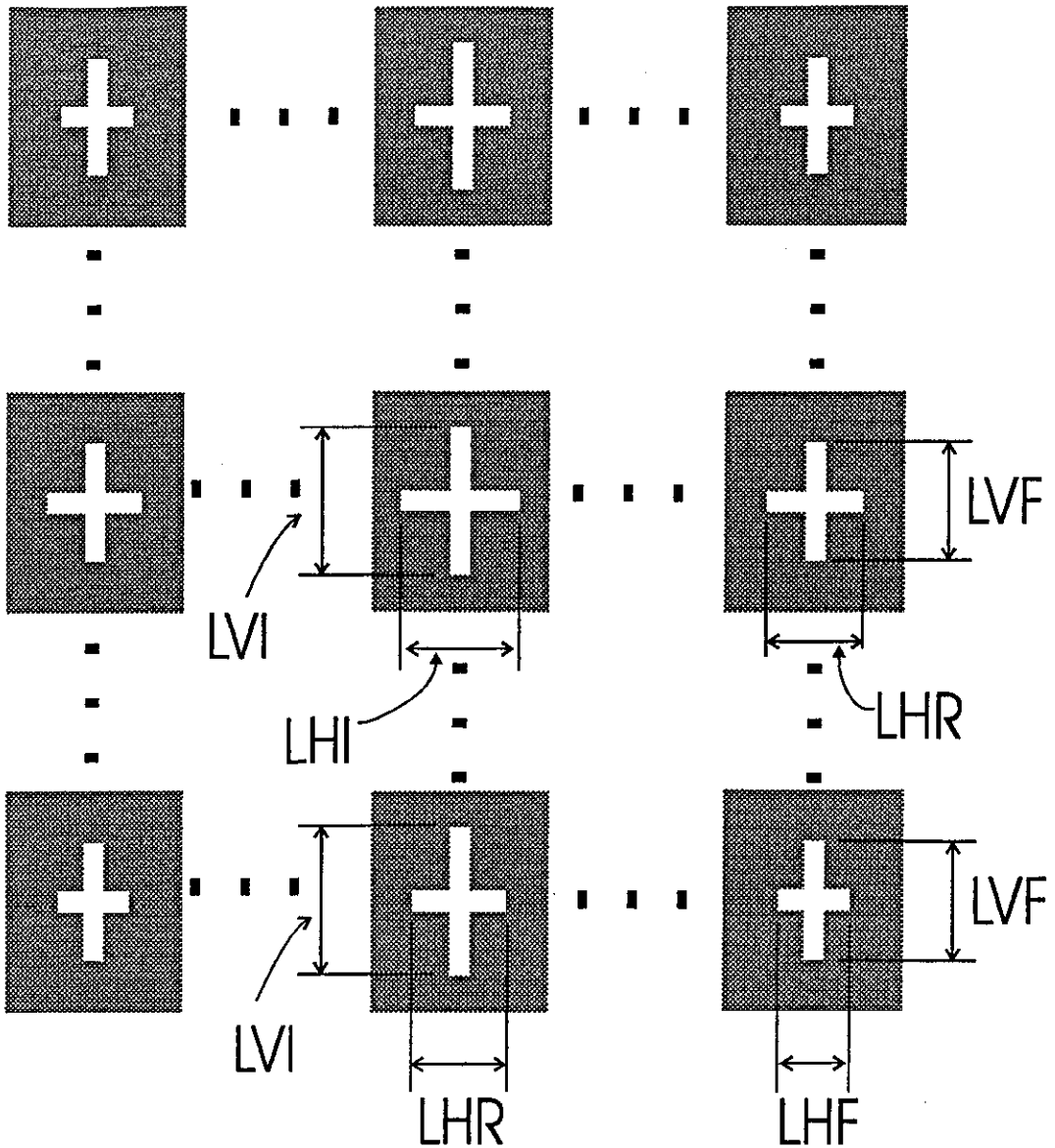


Figure 6.13.a. Geometry of the symmetrically tapered array 1.

28% ( $LF = 3$  mm). Similar comments could be made as with the previous array, with the exception of broader principle plane beams and suppressed sidelobe

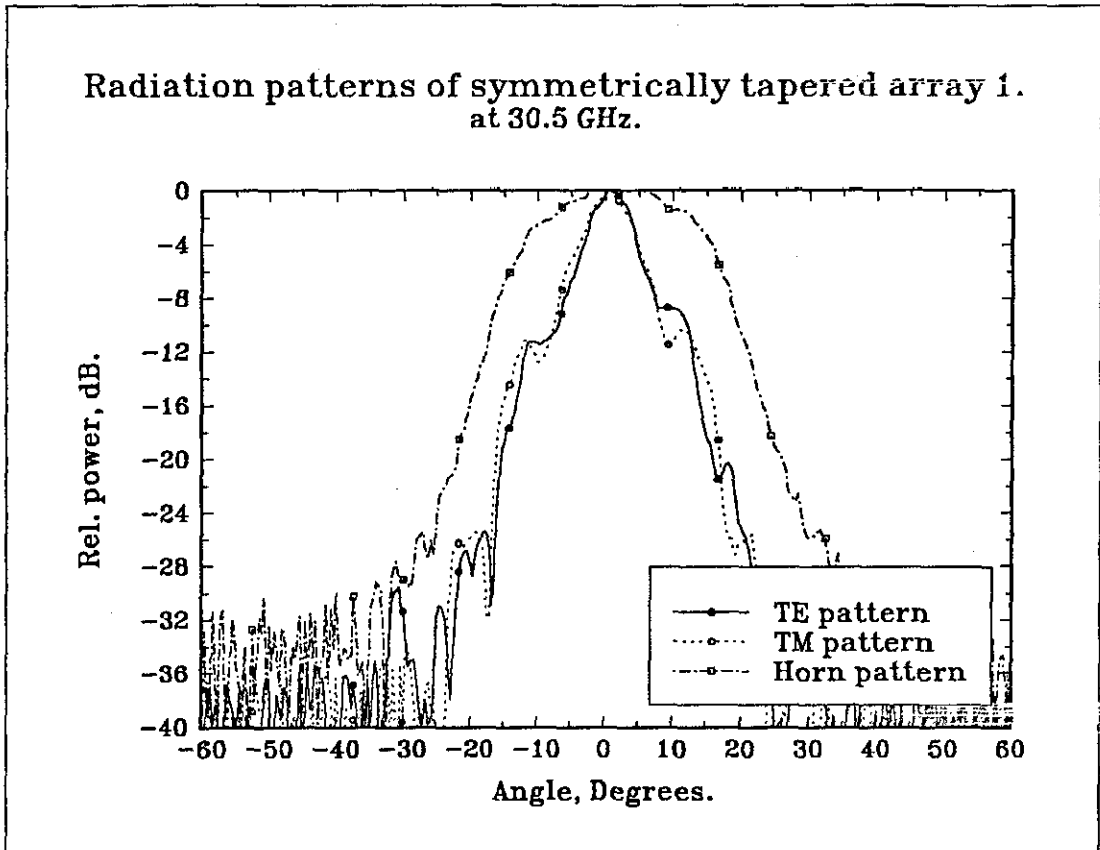


Figure 6.13.b.

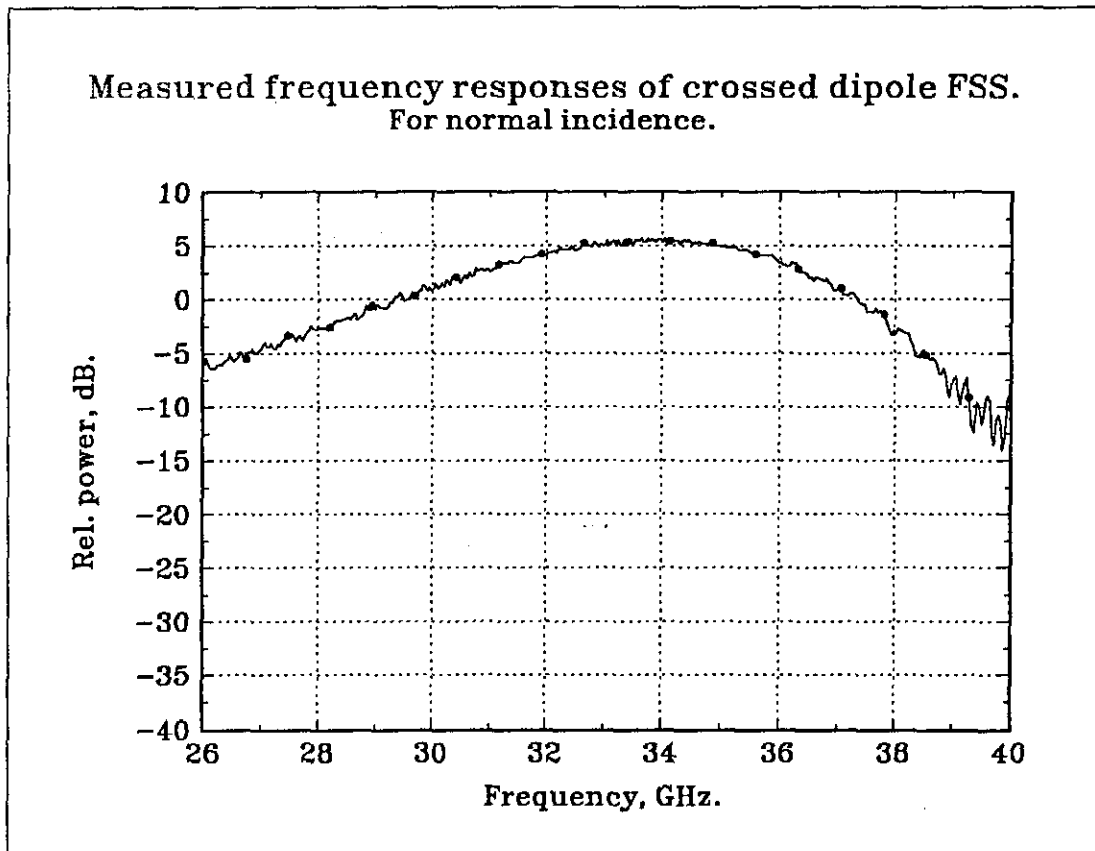


Figure 6.13.c.

performance, as shown in Figure 6.14.b. This is primarily due to the reduced tapering of the element lengths. A gain of  $\sim 4.35$  dB is observed at boresight with this surface.

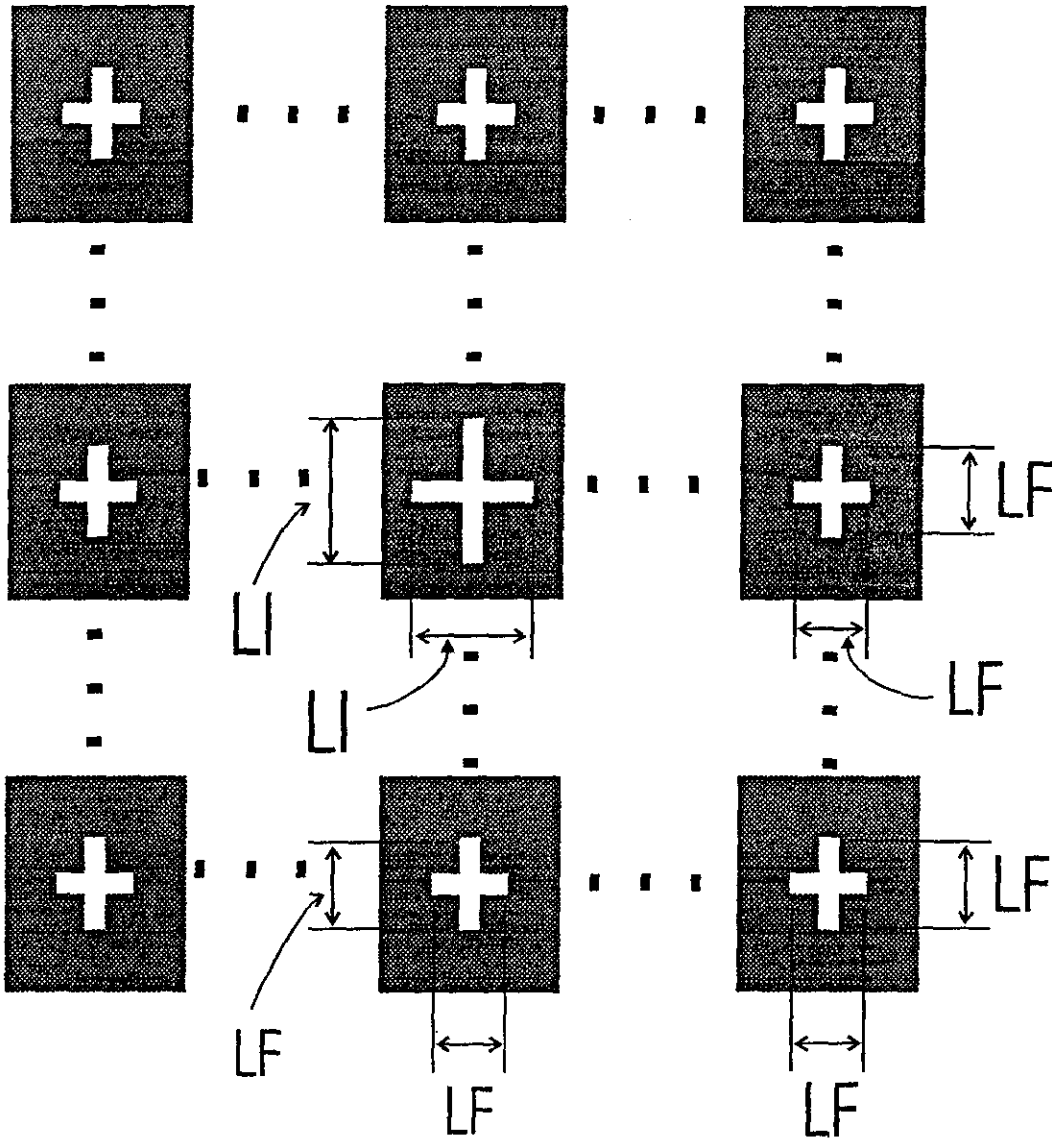


Figure 6.14.a. Geometry of the symmetrically tapered array 2.

The measured frequency responses at normal incidence for both the surfaces are given in Figures 6.13.c and 6.14.c. Both responses show indications of gain in a certain

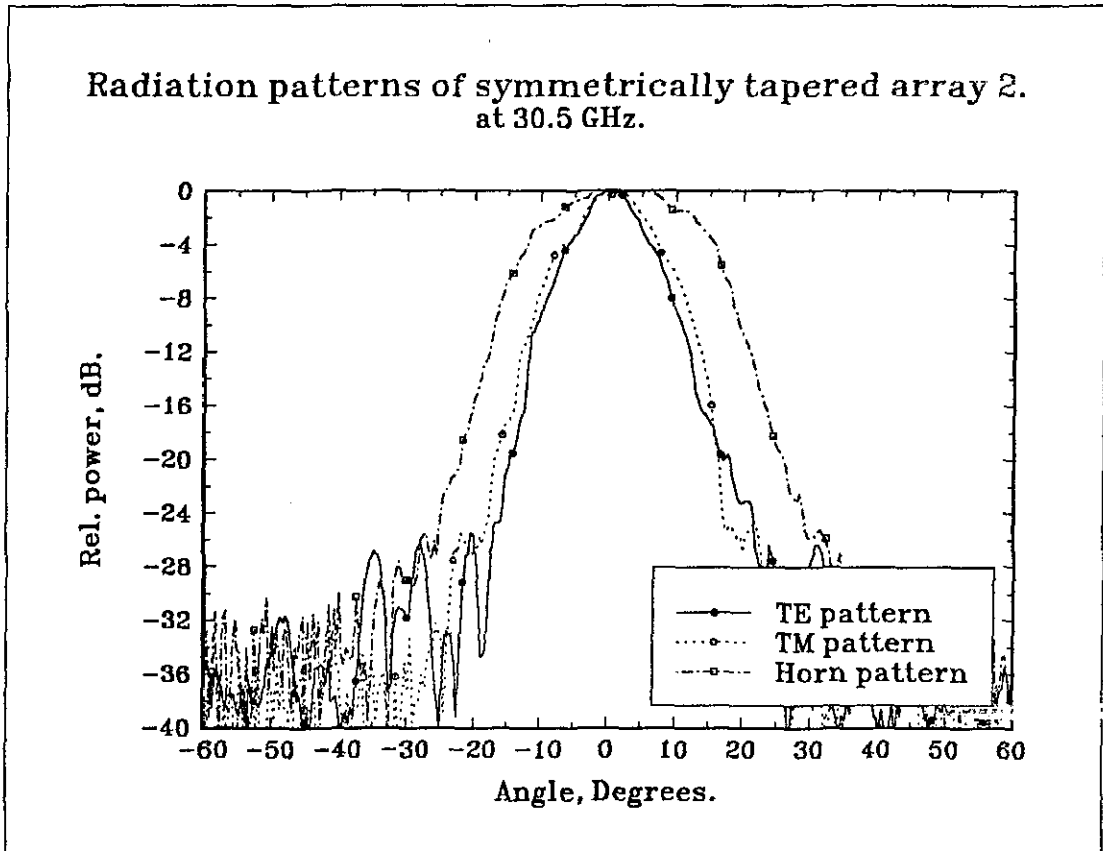


Figure 6.14.b.

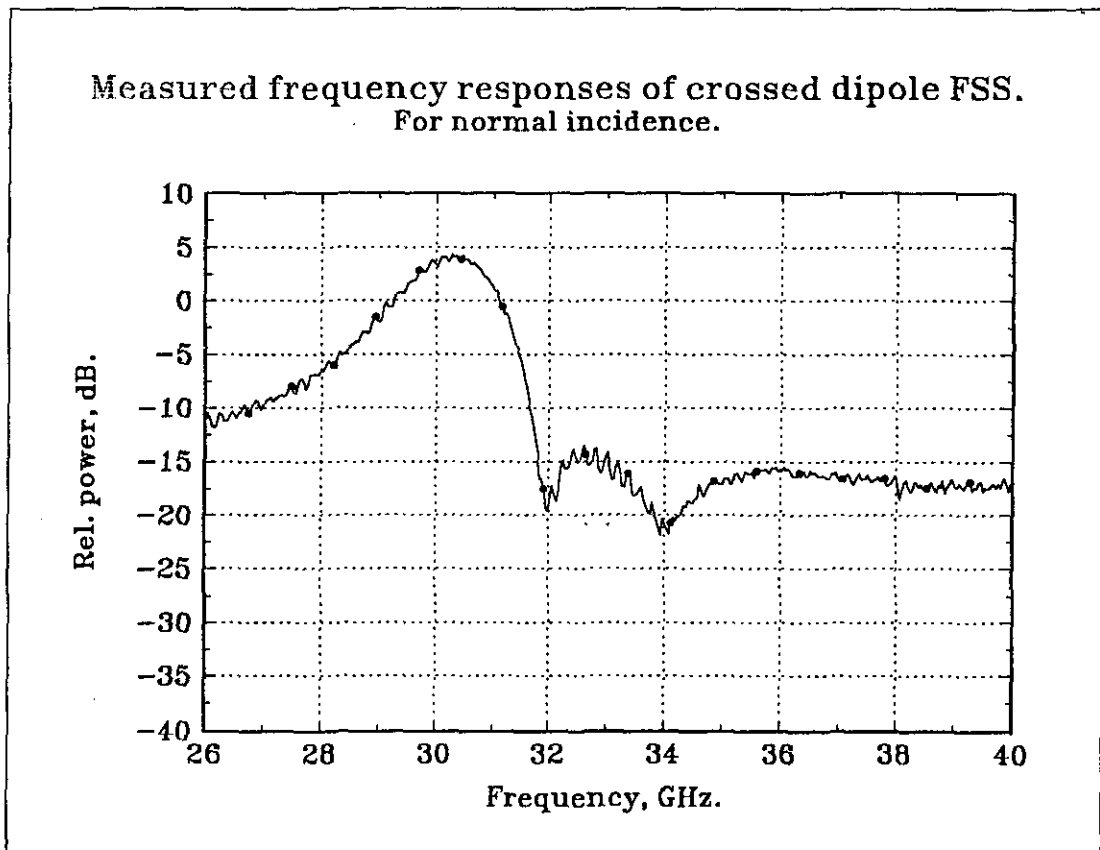


Figure 6.14.c.

frequency band. In Figure 6.13.c the maximum gain is ~5.5 dB. and the range at which the surface acts as a focussing object is from ~29.3 to ~37.3 GHz. Figure 6.14c shows a gain of ~4.3 dB from ~29.2 to ~31.1 GHz.

### 6.7 Summary

In this chapter the variation of the microwave beam due to variations in the slot geometries of the FSS as well as variations in the signal parameters has been investigated. Also the performance of DML as an electromagnetic window and beam steerer were studied. The same dielectric multilayer has also been demonstrated as an apodizing aperture. FSS have been used to steer the first order component by selecting a grating geometry such that the first higher order diffracted wave is propagating when the surface is illuminated by an electromagnetic wave.

Although the DML structure performs well as a beam-former, its passive beam-steering property (under frequency control) exhibits a significant reduction in efficiency as the angular scan increases.

It has been stressed that the model used to indicate the behaviour of the DML in this context was purely one-dimensional, and there may be significant contributions from two-dimensional effects (i.e. waves propagating parallel to the layers). In particular it would be expected that the source position and transverse dimension of the structure would be critical factors in the performance.

An investigation into the possibilities of alternative uses of planar periodic arrays was made. It had been shown that the continually varying single layer arrays can be used to modulate the direction of the beam as well as focusing of the beam. It is envisaged that the spatial

filtering, in conjunction with the converged beam, resulting from such planar structures could be used to improve side lobe performance and directivity in linearly polarised antenna systems.

---

**References**

1. Gaylord T.K. and Moharam M.G., Analysis and applications of optical diffraction by gratings, 1985, Proc. IEEE, Vol. 73, No. 5, pp.894-937.
2. Lagerholm R., Study of metallic strip gratings for frequency scanning, 1992, Microwave & Opt. Tech. Lett., Vol. 5, No. 14, pp.713-715.
3. Johansson F.S., Periodic arrays of metallic elements as frequency scanning surfaces, Mar 1987, Proc IEE Ant. & Prop. Conf, York, UK, pp.71-74.
4. Johansson F.S., Frequency scanned gratings consisting of photoetched arrays, 1989, IEEE Trans., AP-37, No. 8, pp.996-1002.
5. Hecht E. and Zajac A., Optics, 1979, Addison-Wesley Publishing Company, New York, Chapter 10.
6. Ruze J., Lateral feed displacement in a paraboloid, 1965, IEEE Trans., AP-13, pp.660-665.
7. Hansen R.C., Microwave scanning antennas, Vol. III, 1966, Academic, New York.
8. Tiuri M., Henriksen J. and Tallquist S., Printed circuit radio link antenna, Sept 1976, 6th European Microwave Conf., Rome, pp.280-283.
9. Danielsen M. and Jorgensen R., Frequency scanning microstrip antennas, 1979, IEEE Trans, AP-27, No. 2, pp.146-150.
10. Jackson D.R., A multiple layer radome for reducing the RCS of a microstrip patch, IEEE AP-S Intl. Symp. Dig, Dallas, Texas, 1990, pp.374-377.

11. James J.R. and Mompalao de piro A., Design data for aperture antennas using dielectric slab lenses, 1974, Tech. note: RT 76, Dept of Electrical and Electronic Engineering, RMCS, Swindon, UK.

12. Guo Y.J. and Barton S.K., A high efficiency quarter wave zone plate reflector, IEEE Trans., Microwave and Guid. Wave Lett, 1992, Vol. 2, No. 12, pp.470-471.

13. Dewey R.J., Design considerations for millimetre wave lens antennas, 1982, The Radio and Electronic Engineer, Vol.52, No. 11/12, pp.551-564.

14. Brown, J., Antenna Theory (Collin R.E. and Zucker F.J., Eds), 1969, McGraw-Hill, New York.

15. Hecht E., Optics, 1987, Addison-Wesley, New York.

16. Fowles, G., Introduction to Modern Optics, 1968, Holt, Rinehart and Winston, New York.

17. Guenther, B.D., Modern Optics, 1990, Wiley, New York.

## CHAPTER 7

## CONCLUSIONS

## 7.1 CONCLUSIONS

A novel antenna concept has been discussed in this thesis which enables signals to be classified according to the criteria: frequency band, propagation direction and amplitude. A critical component is the external filter and simulations of various designs have been presented based on a dielectric laminate and a frequency selective surface.

A nine layer DML was used to examine their viability as one of the spatial filter components. Periodic arrays of slots were also used as the external filters. Two types of array geometries were employed as FSS. They have been used to provide the necessary spectral and angular filtering effects.

The performance of the DML were tested and analysed. Both planar and curved measurements were conducted. For a planar surface the predicted frequency response was obtained in the chamber. The discrepancy in some part of the characteristics was attributed to the inaccuracies of the input parameters of the DML. In particular, the inaccuracies in the individual layer dimensions and the electrical parameters. It is unlikely that the electrical properties of the melamine layer are the same as those at 1 MHz. The physical shape, i.e., the finite size of the DML which was used for the measurements could be another reason for this error. Despite these drawbacks the predicted and practical comparison indicate that the DML

did indeed behave as a spectral and angular filter as expected. As an angular filter the practical values were estimated fairly well within a range of 5 dB by the simple model.

It is evident that as the number of layers is increased, the better the directivity of the filter. The TE and TM radiation characteristics showed almost the same patterns. The main advantage of the DML is the cross polarisation level. For both signal orientations they were kept down to the level of the horn antenna.

The curved multilayer behaves almost the same way as the planar multilayer. Theoretical models are not available at this stage, as it is beyond the scope of this thesis. For single horn measurements, as the curvature was increased, the signal power at the boresight was decreased. But a narrowing of beamwidth of the radiation patterns were observed for both TE and TM. For multiple horn measurements, discrimination of the TE and TM patterns were not possible due to their broad beamwidths.

The performance of the DML was also assessed with a view to steering the beam. It was found that the beam could be steered by up to  $10^\circ$  in a frequency range of  $\sim 27.9$  GHz to  $\sim 28.9$  GHz although there is an associated reduction in the transmitted power as the beam is steered. This is due to the fact that the maximum amplitude of the signal impinging on the filter surface is at boresight and decreases away from boresight. Since most of the transmitted power lies in the unsteerable zero order mode, the DML would be unacceptably inefficient for microwave antenna applications. The DML under scrutiny has been tested for its applications as a beam former. It provided a narrow beam pattern with low sidelobes, when used in conjunction with an open ended wave guide, thus emphasising its candidature as an apodising aperture.

For communication applications, the DML should have low absorption within a certain frequency range. It should have a high degree of directivity by shaping the antenna beam. Here the use of DML was established as an electromagnetic window. This DML would transmit signals at a certain frequency band without much reduction in the power and for some other bands the DML would reflect.

Also the low cross polarisation really stresses that the antenna performance could be extended into narrow band and dual polarisation applications.

Two different geometries of FSS were tested in the anechoic chamber. They were tripole slot FSS and crossed dipole FSS. During the investigations of the performance of FSS as spectral filters, it has been noted that the measured values agree with theoretical values within a range of  $\sim 3$  dB. This discrepancy could arguably be due to the finiteness of the surface. The important parameter in the design of a narrow band filter is the periodicity between the elements. The higher the periodicity the narrower the transmitted band and vice versa.

In the case of TM incidence for both FSS, the amplitude of the resonant frequency component drops drastically with angle of incidence and increases after  $\sim 15^\circ$ . For TE incidence, the amplitude of the signal decreases slowly and at  $60^\circ$ , it is at  $\sim -10$  dB level. For crossed dipole surface, as the TE incident angle increases the onset of grating lobes was noted. This effect has not predicted in the theoretical model and suggests that as the periodicity between the slots increases the model becomes invalid. This effect could be due to the finite number of slots existing on a finite surface.

Both the FSS were tested for their angular filtering properties. The computed and measured values of both the arrays were in good agreement. There was a sharp

attenuation for the TM incidence. For TE, a slower attenuation was observed.

The radiation patterns of both the FSS were studied. Among these, the tripole slot surface gave better directive performance than the crossed dipole slot surface. The TM pattern of the tripole slot FSS showed a much narrower beam width than the other surface. However, the TE patterns were rather broad for both surfaces. Thus the tripole slot FSS deserve a better degree of appreciation for its co-polarisation performance. Meanwhile the cross polarisation level of the tripole FSS is much higher than that of the crossed dipole FSS. For tripole FSS, a cross polar level of -10 dB was observed. The cross polar level for the crossed dipole FSS remained at noise level at  $\sim -33$  dB.

The properties of curved FSS were investigated with a view to making a redome structure. For TM incidence, the tripole FSS gave a narrow beam pattern for all the curvatures. For crossed dipole FSS, the TM beam pattern is broader than that of the tripole FSS. For TE incidence, the patterns remained the same as the flat FSS for both surfaces. Another interesting observation was in the cross polar levels of these curved FSS. For tripole FSS, the cross polar level seemed to decrease with increasing curvature, whereas for crossed dipole FSS, they seemed to increase with increasing curvature. This effect could be put down to the wave propagation behaviour through surfaces which have got slots with right angle joints as in crossed dipole FSS and  $120^\circ$  joints as in tripole slot FSS.

Multiple horn measurements were also carried out to observe whether the curved structure could distinguish signals coming from various directions. In comparison with DML, FSS gave a narrow beam pattern. Therefore stress were given to measurements using FSS. For a flat

surface, the receiver horn could only recognise the signal from boresight. As the curvature was increased, signals from the other directions came into the scan region. For the second curvature all the beams were visible towards the centre of the scan region. This suggests that further optimisation of the curvature is required to predict the direction of signal arrival. For TE, since the beam pattern was broad, such detection was not visible.

Numerical studies were carried out to analyse the capability of FSS as a frequency scanning surface in transmission. The principle used here was to suppress the zero order mode and convert that suppressed energy to the first order mode. This first order mode is sensitive to frequency variations. Such action could be accomplished by proper selection of a grating geometry. The numerical results showed an increase in power for the first order mode.

... data. A practical study was performed to look into the steering by rotating the FSS. The beam was shifted in a range of  $\pm 10^\circ$  with a maximum loss of  $\sim 3$  dB.

A practical study was carried out to investigate the possibilities of using FSS as a beam directing array and a focusing array. This was accomplished by tapering the slot geometry, in an appropriate fashion. Using the beam directing array a shift of  $\sim 9^\circ$  was observed. A numerical study was performed on a simple grating structure to establish the beam directing action. A gain of  $\sim 5.5$  dB and  $\sim 5$  dB were noted for the focusing array 1 and 2.

Further work is required to establish the optimum phase changes of these arrays. It is realised that the spatial filtering, in conjunction with a converged beam,

resulting from such planar structures could be used to improve sidelobe performance and directivity in linearly polarised antenna systems.

The properties of the passive spatial filters studied here are potentially applicable to the design of antennas, particularly in the contexts of mobile and satellite communications. These structures can in principle perform 'passive' frequency and angular selection when used in conjunction with a conventional antenna. It is likely that this would lead to an increase in the directivity of the antenna at minimal cost. Since the dynamic range of the frequency-controlled angular steering found is relatively low, the filters could find applications as a passive enhancement to an actively steerable antenna system. The enhancement is obtained by the fact that different frequencies can be transmitted into different directions, thus allowing for a distributed network of receivers.

Another useful application would be to increase the resolution of a remote sensing system in which the target locations are identified in terms of the frequency detected at the receiver. This may be especially relevant to improving the performance of surveillance and homing radars, for which it is important to minimise the footprint and hence maximise the possible resolution. The collimation described above will apply in the radial direction, thus a target plane perpendicular to the central propagation direction will be illuminated by an annular shaped footprint whose radius is controlled by the source frequency.

## 7.2 Suggestions for future work

The transmission characteristics of both DML and FSS were observed. Both of them, have their own advantages. The TE component of the multilayer attenuates rapidly, where as

for the slotted FSS array, it is the TM component. These facts have been proven theoretically and practically. But the combined effects of both multilayer and FSS are not well established and obviously, it is one of the suggestions for further investigations. Also the cross polarisation level introduced by tripole FSS is high, though its co-polarisation performance is good.

DML can also be used for beam directing and focusing objects. An alternative approach to tackle this situation is to use planar geometries, rather than curved ones. One possibility is varying the thicknesses of layers at a constant gradient.

Further improvement of the multilayer characteristics will be achieved by optimising their structure and composition. In particular it is expected that increased collimation of the scanned beam will be obtainable with additional layers and by the use of higher dielectric permittivity materials.

The effect of varying the element lengths to form a beam directing array and a focusing array have been analysed practically. But the theoretical model for such surfaces are not available anywhere at the preparation of this thesis. Also the modelling of curved surfaces using multihorn measurements are also not available. Theoretical analysis of such models prove to be another fruitful area of research.

## Appendix

The work carried out in this thesis has so far appeared in the form of following scientific and technical presentations.

### Published Papers

1. S. Chandran and P. R. Smith: Passive filter for increasing directivity in dual polarisation antenna systems: Electronics Letters, Vol. 28, No. 9, pp.827-8
2. S. Chandran and P. R. Smith: Modulation of a microwave beam by a dielectric multilayer filter: J.Phys.D, Vol. 25, No: 6, pp.1026-31.
3. S. Chandran and J. C. Vardaxoglou: Performance of two single layer frequency selective surfaces as spatial filters: Microwave and Optical Technology Letters, Vol.6, No. 6, pp.359-363.

### Conference Papers and Posters

1. S. Chandran, B. Little and J. C. Vardaxoglou: Phasing effects of cascaded and spatially varying planar arrays. ICAP 93, IEE Conf, UK. pp. 265-268.
2. S. Chandran, P. R. Smith and J. C. Vardaxoglou: Curved frequency selective surfaces in passive microwave antennas. 1993 JFIT Technical Conference Poster Session, UK.

# Modulation of a microwave beam by a dielectric multilayer filter

Gathish Chandran and Peter R Smith

Department of Electronic and Electrical Engineering,  
Loughborough University of Technology, Leicestershire LE11 3TU, UK

Received 21 May 1991, in final form 23 January 1992

**Abstract.** A theoretical and experimental study of passive, microwave beam modulation is presented using a planar dielectric multilayer structure in the frequency range 26–40 GHz. The structure is shown to exhibit both spectral and angular filtering properties with respect to plane waves. The same filter is also demonstrated to function as a collimating aperture and apodizer when combined with a conventional antenna. In addition the filter is used to steer a beam through a few degrees of arc by sweeping the source frequency from ~27 to ~29 GHz.

## 1. Introduction

The effectiveness of a microwave communication or radar transceiver system depends critically on its ability to distinguish between signals in terms of their amplitude, frequency and beam properties. The increasing use of the same spatial channel and spectral band for multiple signal propagation [1, 2] further complicates the electromagnetic environment and motivates the need for antenna systems which provide a steerable, narrow beam pattern within a narrow spectral band. Such antenna systems are also relevant to the imaging of buried objects [3], in the treatment of hyperthermia [4] and in radar imaging [5]. In all these applications, transmitter and receiver probes with low side lobes are required to avoid unwanted reflections and hence increase the resolution. Furthermore there is a requirement, particularly in mobile and satellite communications [6], for the beam to be steerable to allow flexible access between source and receiver locations.

Conventional methods for beam formation and steering are by employing active phasing of antenna arrays [7, 8]. Although beam steering by phased arrays provides faster and more flexible reconfigurations than mechanical systems, the hardware is relatively expensive and significant signal processing is required to interpret the array response [9]. Traditional antenna designs are aimed at providing wide band performance [10] but the increasing emphasis on frequency re-use within multibeam and multiband systems [11] suggests that some spectral filtering would be an advantage. Although spectral selection is normally performed within the receiver, in principle the antenna can be designed to provide passive discrimination, for example via the use of frequency selective surfaces (FSS) [12].

This paper addresses the passive role of an antenna in the contexts of beam formation and steering as well

as spectral selection. One approach to passive beam steering is via the variation of the carrier frequency of radiation passing through a structure with frequency dependent transmission properties. This has been achieved at microwave frequencies by using specially designed FSS [13] consisting of doubly periodic arrays of conducting elements on a dielectric substrate.

Another type of frequency selective structure is a dielectric multilayer, widely used in the construction of microwave components such as radomes [14, 15] and optical components such as mirrors and polarization filters [16, 17]. In the majority of applications the multilayers are employed as spectral filters and are usually designed to have a near uniform angular response in the pass band (e.g. for filters, dielectric mirrors and beamsplitters), or else they function at specific incidence angles (e.g. polarizing filters). In more specialist applications, more than one specific spectral pass band may be required [18, 19]. Recently, theoretical studies of fractal [20] and chiral [21] multilayer filters and reflectors have also been made.

In this paper we investigate the spectral, spatial and beam modulation properties of multilayers for Ku band microwaves. Special emphasis is placed on a theoretical and experimental analysis of the angular response which reveals a novel application of such structures. In particular, the possibility exists of extending the role of dielectric multilayers into that of frequency dependent spatial filters. It is found that the most efficient spatial filtering is not achieved at the fundamental or first-order spectral resonances, due to their relatively high bandwidths. We assess the performance of a multilayer composed of a glass fibre laminate and address the viability of its use as a passive beam steering and beam forming device.

In section 2 we investigate theoretically the plane wave response of the dielectric multilayer and the

Results from an experimental test are given in section 5. The filter's use as a passive beam steering device is addressed in section 4, and as a collimating aperture in section 5.

### Dielectric multilayer filters

The theoretical analysis of plane wave scattering from dielectric multilayer structures is well known [16]. Here the study is based on a structure familiar to spectral filter designers consisting of two materials arranged in an alternating sequence. For optimum effect the two materials must be composed of contrasting dielectric permittivity usually termed 'high' (H) and 'low' (L). In particular the combination HLHLHLHLH will be considered. This exhibits a fundamental resonance (pass band) with respect to normally incident plane waves when the thickness of the high (low) permittivity layer is  $\lambda/4$  ( $\lambda/2$ ), where  $\lambda$  is the wavelength in the material. In the context of microwave radiation our choice of material for the high permittivity layer is governed by the need to achieve narrow band performance at an appropriate frequency, to minimize the insertion loss and to limit manufacturing costs. For these reasons a high permittivity layer composed of the glass fibre laminate melamine (relative permittivity  $\sim 7.5$  and loss tangent 0.02 measured at 1 MHz), being tough, lightweight and durable, was selected. Melamine sheets with thickness  $\sim 0.76$  mm are considered as these are applied as standard and the resulting multilayer structures will possess transmission resonances near to the atmospheric attenuation window ( $\sim 25$ – $45$  GHz) between water and oxygen molecular absorption [22]. Expanded polystyrene is used for the low permittivity (L) layer. Having chosen these materials the fundamental resonance ( $\sim 36$  GHz) is fixed and, as a consequence, the design thickness of the polystyrene layer is  $\sim 4.2$  mm.

The simulated frequency responses of the melamine multilayer filter for  $0^\circ$  and  $30^\circ$  angles of incidence are plotted in figure 1. The response at normal incidence (figure 1(a)) is nearly symmetric about the fundamental resonant frequency ( $\sim 36$  GHz) and the departure from symmetry is due to material absorption within the melamine. Also clearly noticeable in figure 1(a) are higher order resonance features (labelled first and second) which arise because of the presence of more than one layer. When the angle of incidence changes to  $30^\circ$  the frequency response shifts by approximately 2 GHz as shown in figure 1(b). A notable change in the behaviour of the second-order response. The TE component shifts its position by  $\sim 2.8$  GHz towards the high-frequency regime, resulting in a reduction of amplitude of  $\sim 4.5$  dB. The TM component behaves in a similar way, exhibiting a shift of 2 GHz to the high-frequency region, although the amplitude remains unchanged. These results suggest that more sensitive control of the angular transmission properties of the

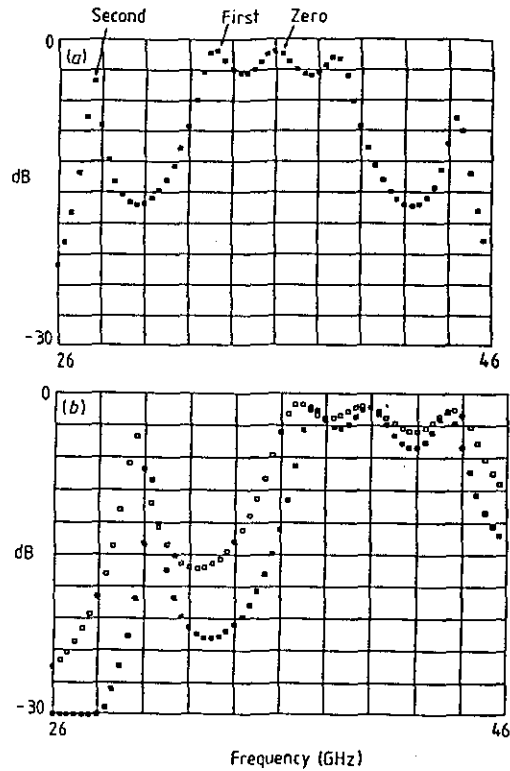


Figure 1. Simulated frequency responses of the multilayer filter at (a)  $0^\circ$  incidence and (b)  $30^\circ$  incidence. Black squares represent TE and open squares represent TM components.

filter can be accessed in the vicinity of the second-order resonance rather than the fundamental or first orders.

### 3. Plane wave measurements

The experiments were conducted in a laboratory with microwave absorber blocks situated in appropriate positions to obtain a near anechoic environment. The experimental set-up for plane wave measurements is shown schematically in figure 2(a). The aperture on the wooden frame onto which the multilayer is mounted can be rotated in a vertical plane. The centre of the aperture lines up with the transmitter and receiver horns, which are in the line of sight. The rest of the area, apart from the aperture in the wooden frame, is covered with microwave absorbers to avoid unnecessary reflections. For the angular response measurements, the aperture is rotated in steps of  $10^\circ$ , while the positions of transmitter and receiver horns are fixed. The pyramidal transmitter horn is excited by a microwave sweep generator (HP 8757B) in the range 26–40 GHz. An identical receiver horn is connected to a scalar network analyser (HP 8520B) from which data are directly downloaded to a plotter.

A five-layer melamine structure was made according to the design specified in section 2. The theoretical and measured frequency responses of this structure for normally incident plane waves are shown in figure 3. Clearly the predicted resonant structure is observed

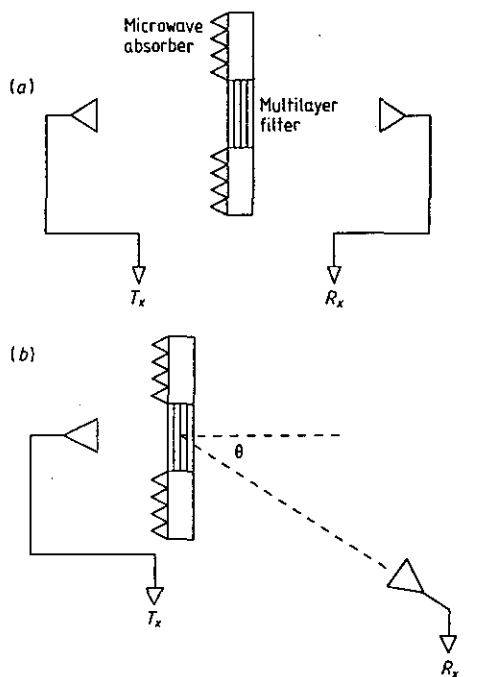


Figure 2. Schematic diagram of the experimental set-up for (a) plane wave measurements and (b) radiation (frequency scanning) pattern measurements.

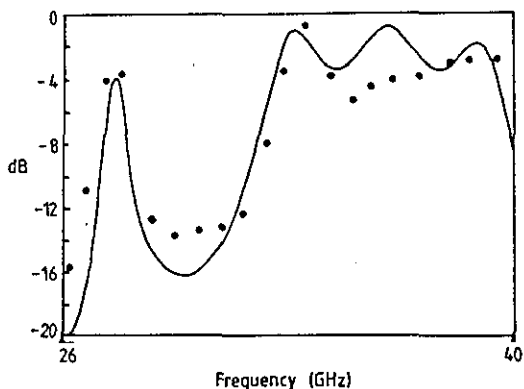


Figure 3. Transmission frequency response of the multilayer filter at normal incidence. The full curve shows the theoretical values; dots indicate the measured values.

experimentally. Even though the electrical parameters of melamine layers are not known accurately at the operating frequencies used here, the positions of the main resonances are estimated fairly accurately by the simple model.

The simulated and measured angular responses of the structure are plotted for the second-order resonant frequency in figure 4. In broad terms, both polarization states are well transmitted near normal incidence and as the angle of incidence increases to  $\sim 40^\circ$  the transmitted power decreases sharply. The TE component stays below  $-20$  dB at  $30^\circ$  and higher whilst the transmission of the TM component increases after  $\sim 40^\circ$ . These results indicate that the transmission response of a divergent beam would have an angular variation resulting in collimation.

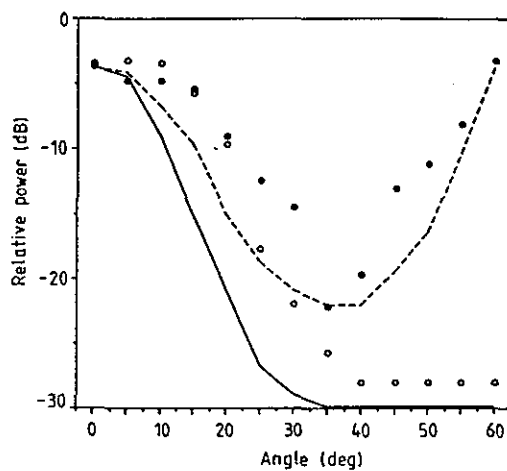


Figure 4. Theoretical and measured angular transmission responses of the multilayer filter.  $\circ$ , TE measured;  $\bullet$ , TM measured; —, TE theory; ---, TM theory.

#### 4. Beam steering

In sections 2 and 3 it was shown that the multilayer plane wave pass bands are in effect shifted when the angle of incidence is varied. This suggests that one way to achieve steering is by varying the source frequency of a divergent beam incident on a multilayer filter placed in the near field. It is stressed that the direction of the beam is frequency dependent only in the sense that part of the signal incident on the multilayer will be reflected and hence the structure is behaving as a spatial filter.

A conventional method for measuring the field pattern of an antenna consists in varying the angular position between the antenna being tested and a receiving probe located at a fixed distance. This is equivalent to moving the receiving probe over an arc of an imaginary spherical surface centred on the antenna and it is this method which is utilized for the radiation pattern measurements as illustrated in figure 2(b).

The model used to calculate the responses presented in sections 2 and 3 is exact for plane waves but, nevertheless, can be used to indicate the response characteristics of a multilayer filter when positioned in the near field of the radiating source. Thus, under the physical optics approximation, the radiation pattern of a wide angle source and multilayer filter, normalized with respect to the radiation pattern of the source, will be roughly equivalent to the plane wave angular transmission response. From figures 1 and 3 it is apparent that a satisfactory half power performance can be expected from the steered signal by varying the source frequency within a range of  $0.6$  GHz centred around  $\sim 28$  GHz—that is, in the vicinity of the second-order resonant frequency of the five-layer structure.

The multilayer structure was placed in the near field ( $\sim 25$  cm) of a radiating microwave antenna such that radiation was illuminating the dielectric across a range of angles from  $0^\circ$  (in the centre of the multilayer) to  $\sim 25^\circ$  (near the edge of the multilayer). Because of

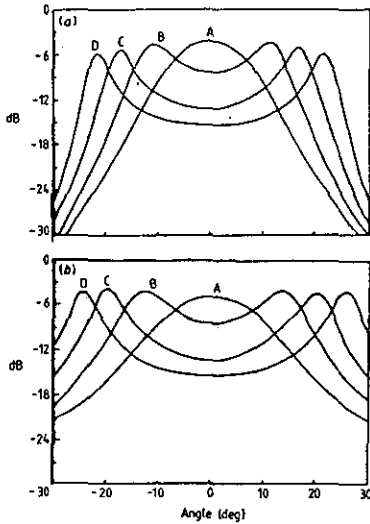


Figure 5. Simulated radiation patterns of the multilayer filter for (a) TE mode and (b) TM mode at source frequencies (A), 27.5 GHz; (B), 28 GHz; (C), 28.5 GHz; (D) 29 GHz.

The practical difficulties associated with supporting the structure in the measurement chamber, and avoiding extraneous effects due to the edges of the multilayer, useful data were obtained in the range  $-20^\circ$  to  $20^\circ$ . The receiver probe was positioned as far away as possible from the multilayer (1.2 m) within the constraints of the chamber size.

The simulated radiation patterns in the region of the second-order resonance ( $\sim 28$  GHz) for TE and TM polarization states are shown in figure 5. Since the theoretical angular transmission is highly directional, the beam is expected to be collimated by the structure as well as effectively steered. In figure 6 the radiation patterns measured at  $\sim 1.2$  m from the multilayer are shown for a range of illumination frequencies. We note that these data were chosen to be representative of the beam steering process rather than to provide an exact comparison with the simulated data. It is apparent that the model used to predict the performance of the structure is qualitatively accurate but quantitatively inaccurate. This is not surprising as the source-multilayer interaction is clearly not fully described by a one-dimensional model. In addition to this primary aspect we note that the tolerances in the construction of the multilayer filter were relatively large ( $\sim 10\%$ ) and the precise dielectric parameters at the design frequencies are unknown. Nevertheless the structure performs the predicted filtering action, providing directional beam steering under frequency control. The simulation also correctly predicts that the steering angle, for given frequency, is larger for TM modes than for TE and that the beamwidth at resonant frequency is larger for TM than TE.

**Beam forming**

The structure being investigated can also be used to produce a narrow beam with low side lobes and in this

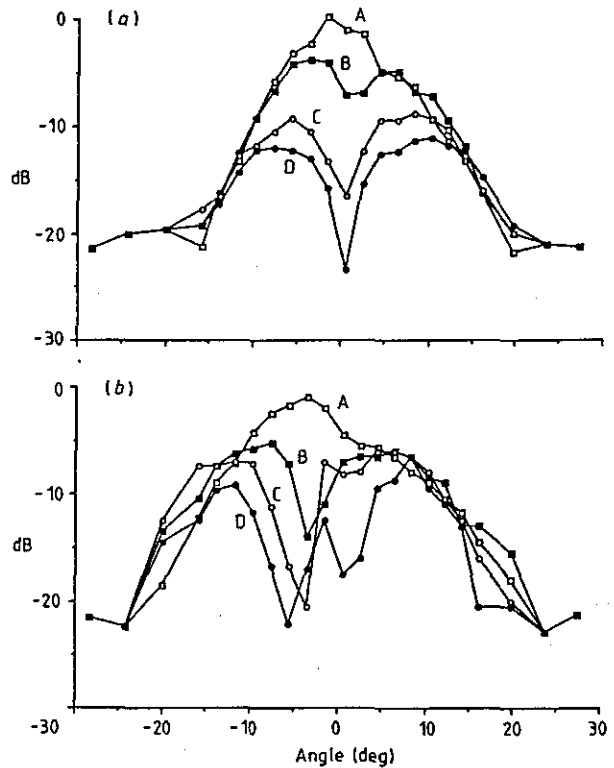


Figure 6. Measured radiation patterns of the multilayer filter for (a) TE mode and (b) TM mode at source frequencies (open squares) 27.9 GHz, (black squares) 28.5 GHz, (open circles) 28.7 GHz and (black circles) 28.9 GHz.

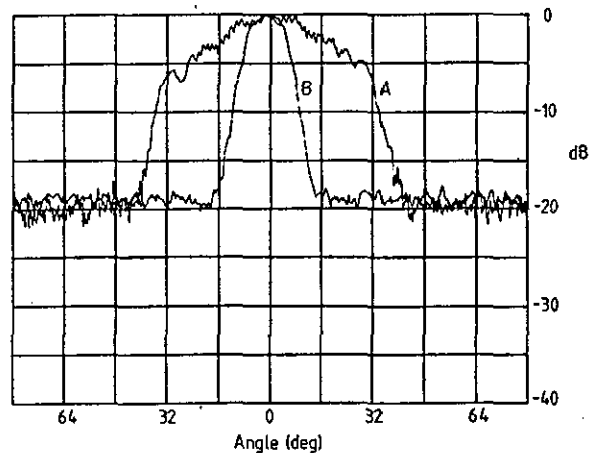


Figure 7. The collimating effect of the multilayer at the second-order resonant frequency. Curves (A) and (B) correspond to open ended waveguide without and with multilayer filter respectively.

sense could be described as an apodizing aperture. This application is a simple alternative to the use of phased arrays in beam forming [7]. The far-field radiation pattern of the multilayer described above, placed in the near field ( $\sim 30$  cm) of an open-ended waveguide, is shown in figure 7 for the second-order resonant frequency  $\sim 28$  GHz. It can be seen that the  $-3$  dB beamwidth of the multilayer is close to  $10^\circ$ . Also note that

the far-field pattern displays no side lobe level above the noise threshold ( $\sim 22$  dB).

## Discussion

We have investigated the microwave transmission properties of a dielectric multilayer consisting of five sheets of melamine. The plane wave transmission response was shown to be in good agreement with simple theory. A novel application was considered by positioning the multilayer in the near field of a radiating source. In this case it was found that the beam could in effect be steered by up to  $10^\circ$  under frequency control in the range 27.9 to 28.9 GHz although there is an associated reduction in the transmitted power as the beam is steered. This is due to the fact that the maximum amplitude of the signal impinging on the filter surface is at bore sight and decreases away from bore sight. The same dielectric multilayer has also been demonstrated as an apodizing aperture. In particular a diverging source with  $-3$  dB beamwidth of  $\sim 90^\circ$  was shown to be collimated by the multilayer down to  $\sim 10^\circ$  with no side lobes measurable as low as  $-22$  dB.

We stress that the model used to indicate the behaviour of the multilayer was purely one-dimensional, whereas we would expect significant contributions from two-dimensional effects (i.e. waves propagating parallel to the layers). Our results therefore suggest that a theoretical study of such structures would be fruitful and could lead to further optimization of the detailed design so that attenuation with steering angle would be reduced. In particular, we would expect the source position and transverse dimension of the structure to be critical factors in the performance.

In our experiment the main lobe is effectively steerable in the vicinity of the second-order resonant frequency of the multilayer. In the optical regime, passive frequency-controlled beam steering is usually achieved by employing a grating structure. However most of the transmitted power lies in the unsteerable zero-order mode and therefore would be unacceptably inefficient for analogous microwave antenna applications. The use of blazed gratings would overcome this drawback but further, more significant, problem exists with the use of conventional grating structures for beam steering at microwave frequencies, namely the small practical range of angular steerage which is feasible. For a thin grating the angular steering range is proportional to the size of  $\Delta\lambda/\lambda$ , where  $\Delta\lambda$  is the wavelength range over which a sweep is made. Whereas in many optical systems one can easily obtain  $\Delta\lambda/\lambda \sim 2$ , in a practical microwave communications system it is only reasonable to expect values of  $\Delta\lambda/\lambda \sim 0.1$  at the most, due to the limited allocation of frequency bands. Thus in practice, the angular steerage would be at least an order of magnitude less than achievable at optical frequencies and therefore not as large as provided by the method proposed here.

The properties of the filter studied here are potentially applicable to the design of antennas, particularly in the contexts of mobile and satellite communications. The multilayer can in principle perform 'passive' frequency and angular selection when used in conjunction with a conventional antenna. It is likely that this would lead to an increase in the directivity of the antenna at a minimal cost. Since the dynamic range of frequency-controlled angular steerage found is relatively low, the multilayer could find applications as a passive enhancement to an actively steerable antenna system. The enhancement is obtained by the fact that different frequencies can be transmitted into different directions, thus allowing for a distributed network of receivers. Another useful application would be to increase the resolution of a remote sensing system in which the target locations are identified in terms of the frequency detected at the receiver. This may be especially relevant to improving the performance of surveillance and homing radars.

Further improvement of the multilayer characteristics will be achieved by optimizing their structure and composition. In particular we expect that increased collimation of the scanned beam will be obtainable with additional layers and by the use of higher dielectric permittivity materials. Subsequent studies will also investigate the use of transversely non-uniform structures with a view to producing high gain as well as beam formation and steering.

## Acknowledgment

This work was carried out while one of us (SC) was a research associate supported by the Science and Engineering Research Council, UK.

## References

- [1] Milne K 1989 Radar and antennas: Part 1 *Electron. Commun. J.* **1** 271-80
- [2] Milne K 1989 Radar and antennas: Part 2 *Electron. Commun. J.* **2** 17-24
- [3] Olver A D and Cuthbert L G 1988 FMCW radar for hidden object detection *IEE Proc. F* **135** 354-61
- [4] Ling H and Lee S W 1984 Focusing of electromagnetic waves through dielectric interface *J. Opt. Soc. Am. A* **1** 965-73
- [5] Ulaby F T, Moore R K and Funk A K 1982 *Microwave Remote Sensing Active and Passive Vol II Radar Remote Sensing and Surface Scattering and Emission Theory* (Massachusetts: Addison Wesley)
- [6] Kitsuregawa T 1990 *Advance Technology in Satellite Communication Antennas: Electrical and Mechanical Design* (Boston: Artech House)
- [7] Hansen R C 1966 *Microwave Scanning Antennas Vol II* (New York: Academic)
- [8] Sole G C and Smith M S 1987 Multiple beam forming for planar antenna arrays using a three dimensional Rotman lens *IEE Proc. H* **134** 375-85
- [9] Hudson J E 1981 *Adaptive Array Principles* (London: Peter Peregrinus)
- [10] Balanis C A 1982 *Antenna Theory* (New York: Wiley)

- [11] Parson J D and Gardiner J G 1989 *Mobile Communication Systems* (London: Blackie)
- [12] Lee C K, Langley R J and Parker E A 1985 Single-layer multiband frequency selective surfaces *IEE Proc. H* **132** 395-9
- [13] Johansson F S, Josefsson L G and Lorentzon 1989 A novel frequency-scanned reflector antenna *IEEE Trans. Antennas Propag.* **37** 984-9
- [14] Skolnik M I 1980 *Introduction to Radar Systems* 2nd Edn (New York: McGraw-Hill) pp 264-70
- [15] Jackson D R 1990 A multiple-layer radome for reducing the RCS of a microstrip patch *IEEE Trans. Antennas Propag. Int. Symp. Dig. (Dallas, Texas)* pp 374-7
- [16] Lekner J 1987 *Theory of Reflection of Electromagnetic and Particle Waves* (Lancaster: Kluwer) pp 221-38
- [17] Chao S, Lin Y F, Lin J F and Lee C C 1990 Scattering loss of an optimum pair high reflectance dielectric mirror *Appl. Opt.* **29** 13 1960-3
- [18] Hogg D C, Guiraud F O, Howard J, Newell A C, Kremer D P and Repjar A G 1979 An antenna for dual wavelength radiometry at 21 and 32 GHz *IEEE Trans. Antennas Propag.* **27** 764-71
- [19] Carniglia C K 1989 Comparison of several shortwave pass filter designs *Appl. Opt.* **28** 14 2820-3
- [20] Yordanov O I, Angelov I, Konotop V V and Yurkevich I V 1991 *Prospects of Fractal Filters and Reflectors 7th Int. Conf. on Antennas and Propagation (University of York, UK)* (London: IEE) pp 698-700
- [21] Oksanen M I, Hanninen J and Tretyakov S A 1991 Vector circuit method for calculating reflection and transmission of electromagnetic waves in multilayer chiral structures *IEE Proc. H* **138** 513-20
- [22] Hall M P M and Barclay L W 1989 *Radio Wave Propagation* (London: Peter Peregrinus) ch 1, 10

difficulty in removing the photodetector response from the link response. Another was an additional electrical leakage that set in at 35 GHz. Although this leakage does not manifest itself in the form of dips in the electrical response, it tends to increase  $\alpha_0$  thereby lowering the device response. We attribute this to power leaking away from the dominant CPW mode without recoupling back into the same mode so as to cause dips in the electrical response [6]. From Fig. 2 it appears that further increasing the electrode thickness should improve the phase match. This required some modification in our fabrication process which concurrently changed the electrode wall angle, so the phase match was not improved. Our calculations do show that the phase match is critically dependent on the electrode wall angle, which implies that strict process control will be required to obtain a phase matched device.

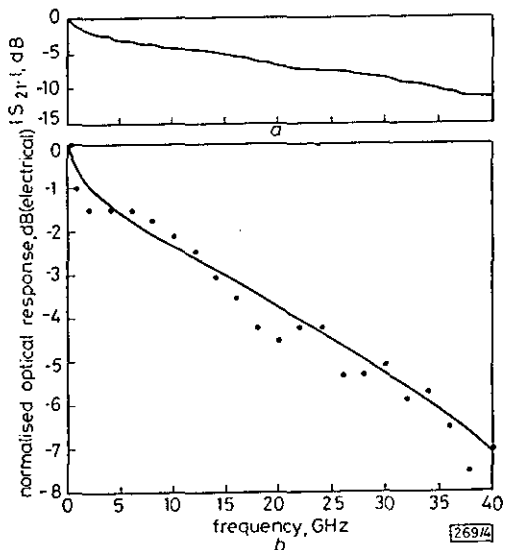


Fig. 4 Electrical and optical responses of device with 18  $\mu\text{m}$  thick CPW electrodes

- a Electrical response
- b Optical response
- experiment
- theory

We have achieved improved results in response and  $V_{\pi}$  for broadband LiNbO<sub>3</sub> modulators. These results are particularly important with respect to the approach of Reference 2 because our devices do not suffer from the nonlinear phase response of coded modulators [2]. Thus these devices can be used directly in the time domain for short pulse applications. As our devices are not yet truly phase matched, it is clear that further improvements will be made. As phase match is approached, longer devices may further reduce  $V_{\pi}$ , but details of this trade-off remain to be determined.

**Acknowledgment:** The authors appreciate the loan of the network analyser, the calibration and loan of detectors, and helpful assistance from R. D. Esman and K. J. Williams. This work was funded by the Office of Naval Technology Electro-optics block program.

3rd March 1992

G. K. Gopalakrishnan,† C. H. Bulmer, W. K. Burns, R. W. McElhanon† and A. S. Greenblatt (Naval Research Laboratory, Code 6571, Washington DC 20375-5000, USA)

† Also with Maryland Advanced Development Laboratory, Greenbelt MD 20770, USA

## References

- 1 KOROTKY, S. K., EISENSTEIN, G., TUCKER, R. S., VESELSKA, J. J., and RAYBON, G.: 'Optical intensity modulation to 40 GHz using a waveguide electro-optic switch', *Appl. Phys. Lett.*, 1987, **50**, pp. 1631-1633
- 2 DOLFI, D. W., NAZARATHY, M., and JUNGERMAN, R. L.: '40 GHz electro-optic modulation with 7.5 V drive voltage', *Electron. Lett.*, 1988, **24**, pp. 528-529

- 3 MIYAMOTO, H., OHTA, H., TABUSE, K., IWAOKA, H., and MIYAGAWA, Y.: 'A broad-band traveling-wave Ti:LiNbO<sub>3</sub> optical phase modulator', *Jpn. J. Appl. Phys.*, 1991, **30**, pp. 1383-1385
- 4 KAWANO, K., KITOH, T., JUMONJI, H., NOZAWA, T., and YANAGIBASHI, M.: 'New traveling-wave electrode Mach-Zehnder optical modulator with 20 GHz bandwidth and 4.7 V driving voltage at 1.52  $\mu\text{m}$  wavelength', *Electron. Lett.*, 1989, **25**, pp. 1382-1383
- 5 SEINO, M., MEKADA, N., YAMANE, T., KUBOTA, Y., and DOI, M.: '20 GHz 3 dB bandwidth Ti:LiNbO<sub>3</sub> Mach-Zehnder modulator'. ECOC, 1990, paper ThG1-5
- 6 GOPALAKRISHNAN, G. K., BURNS, W. K., and BULMER, C. H.: 'Electrical loss mechanisms in traveling wave LiNbO<sub>3</sub> optical modulators', *Electron. Lett.*, 1992, **28**, pp. 207-209

## PASSIVE FILTER FOR INCREASING DIRECTIVITY IN DUAL POLARISATION ANTENNA SYSTEMS

S. Chandran and P. R. Smith

*Indexing terms: Antenna radiation patterns, Microwave filters*

A novel design for a passive microwave filter is presented. The filter consists of a stacked array of low loss dielectric layers, whose permittivity profile alters in a near sinusoidal manner. The radiation property of the filter is investigated for both co- and crosspolarisation and it is shown that the filter acts as an apodiser and a beam shaper.

**Introduction:** The properties of dielectric multilayers as filters at optical frequencies have been examined by various authors [e.g. References 1 and 2]. Analogous microwave structures are not commonly used in microwave applications, although recently, a multilayer radome has been used to reduce the radar cross-section of a microstrip patch antenna [3]. Investigations have also been carried out by the authors on the properties of dielectric multilayers at microwave frequencies in the Ku band [4]. In that work, frequency response, the angular transmission properties, beam steering, frequency response and the beam-shaping action of the layers are discussed. In this Letter a new antenna system employing a dielectric multilayer as a narrowband spatial filter is explored. The co- and crosspolarisation performance is examined experimentally.

**Dielectric multilayer:** For applications in communications, the dielectric multilayer filter should have low power absorption within a prescribed transmission band. The widely used multilayer structures at optical frequencies are made by coating thin layers of materials of different chemical compositions on one or both sides of a substrate. At microwave frequencies the construction of analogous filters is less difficult due to the longer wavelength and low cost, light weight structures can be envisaged. Efficient performance can be obtained by using designs consisting of alternating sequences of high permittivity ( $\epsilon_h$ ) and low permittivity ( $\epsilon_l$ ) materials.

The particular filter studied here consists of five melamine layers ( $\epsilon_h = 7.5$ ,  $\tan \delta_h = 0.02$  at 1 MHz) and four polystyrene layers ( $\epsilon_l = 1$ ,  $\tan \delta_l \approx 0$  at 1 MHz) combined in an alternating sequence with the centre layer of melamine having twice the thickness of the other melamine layers. The thicknesses of the layers are selected according to the fundamental resonance frequency  $f_0$  given by

$$t_h = c/4f_0 \sqrt{[\epsilon_h(1 - j \tan \delta_h) - \sin^2 \theta_i]} \quad (1)$$

$$t_l = c/2f_0 \sqrt{[\epsilon_l(1 - j \tan \delta_l) - \sin^2 \theta_i]} \quad (2)$$

where  $\tan \delta$  is the loss tangent,  $t$  is the thickness of the individual layers,  $\theta_i$  is the incident angle and  $c$  is the speed of

These filters have higher order resonances depending on number of layers used and their properties. We focus attention on the first order resonance (see Fig. 3 of Reference 1) which occurs at  $\sim 34$  GHz for which the fundamental resonance is  $\sim 36.2$  GHz and exhibits a passband of  $\sim 2$  GHz.

**Experimental results:** The antenna structure is tested by placing the dielectric multilayer in the far field ( $\sim 26$  cm) of a pyramidal horn, which is used as a primary feed. The measured radiation patterns of the multilayer filter are compared with the feed patterns. The feed patterns are shown in Fig. 1 for both TE and TM polarisations and in each graph both co- and cross-polarisations are shown. It can be seen that the cross-polarisation of the horn is below  $-25$  dB. Fig. 2 gives the measured radiation patterns of the co- and cross-polarisations of the TE and TM modes for the horn with multilayer filter. It can be seen that both the copolar patterns of the TE and TM modes with the multilayer filter are more directive. The 3 dB beamwidth of the multilayer filter for copolarisations is  $\sim 12^\circ$  compared with the beamwidth of  $\sim 24^\circ$  of the horn feed for both TE and TM. The sidelobe levels are also suppressed being well down in the noise region of the pattern.

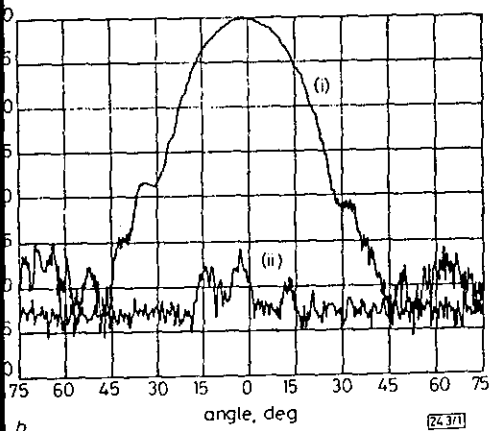
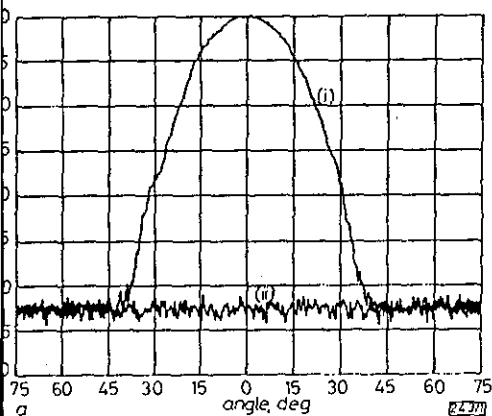


Fig. 1 Measured radiation patterns for co- and crosspolarisation of horn with multilayer filter for TE mode and TM mode at resonance frequency

- a TE mode
- b TM mode
- (i) copolarisation
- (ii) crosspolarisation

**Discussion:** The copolar pattern of the novel antenna system shows an increase in the resolution and directivity. In particular the resolution of the antenna is increased from  $\sim 32^\circ$  to  $\sim 12^\circ$  and the directivity from  $\sim 19$  dBi to  $\sim 24.5$  dBi. The antenna achieves this reduction in the beamwidth without any increase in the crosspolarisation level and the gain of this antenna is approximately the same as that of the horn. Because the multilayer structure exhibits almost the same radiation patterns for both TE and TM modes, it can be used for dual polarisation applications. The low cross-

polarisation of the two modes really stresses this type of operation. Thus by using this type of multilayer, the antenna performance can be extended into narrowband and dual polarisation applications.

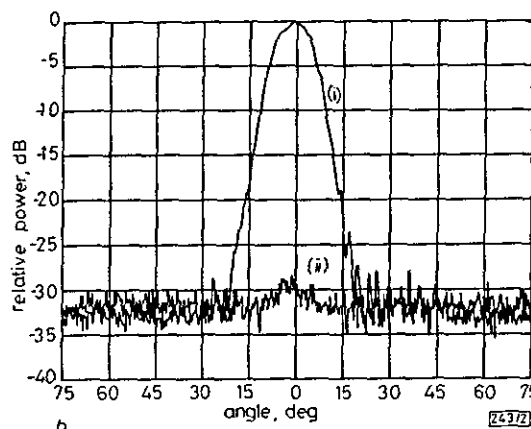
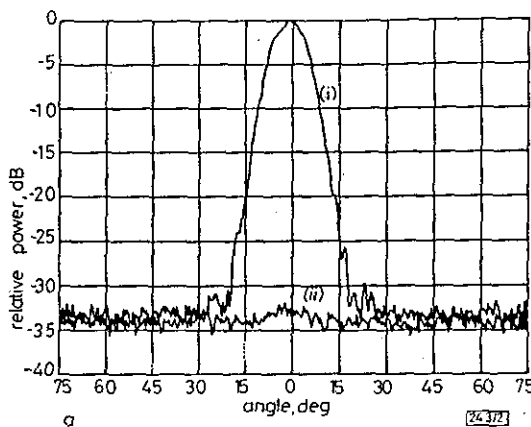


Fig. 2 Measured radiation patterns for co- and crosspolarisation of horn with multilayer filter for TE mode and TM mode at resonance frequency

- a TE mode
- b TM mode
- (i) copolarisation
- (ii) crosspolarisation

In theory the passband and beamwidth of the antenna system can both be further reduced by increasing either the number of individual layers or the ratio  $\epsilon_h/\epsilon_l$ . It should be noted however that as the beam becomes narrower, the radiation efficiency of the system is reduced. Investigations are in progress to increase the gain of this antenna system by optimising the filter geometry, moving away from planar structures.

**Acknowledgment:** This work was carried out while S. Chandran was a research assistant supported by the Science and Engineering Research Council, UK.

28th February 1992

S. Chandran and P. R. Smith (Department of Electronic and Electrical Engineering, Loughborough University of Technology, Leicestershire LE11 3TU, United Kingdom)

### References

- 1 MACLEOD, H. A.: 'Thin-film optical filters' (Adam Hilger, Bristol, 1989)
- 2 CARNIGLIA, C. K.: 'Comparison of several shortwave pass filter designs', *Appl. Opt.*, 1989, 28, (14), pp. 2820-2823
- 3 JACKSON, D. R.: 'A multiple-layer radome for reducing the RCS of a microstrip patch'. IEEE AP-S Intl. Symp. Dig., Dallas, Texas, 1990, pp. 374-377
- 4 CHANDRAN, S., and SMITH, P. R.: 'Modulation of a microwave beam by a dielectric multilayer filter', *J. Phys. D*, 1992 (in press)

IEEE Trans. Microwave Theory Tech., Nov. 1991, pp. 1847-1854.

N. Dib, W. Harokopos, P. Katehi, C. Ling, and G. Rebeiz, "Study of a Novel Planar Transmission Line," 1991 IEEE MTT-S International Microwave Symposium Digest, Boston, pp. 623-626.

L. Rexberg, N. Dib, and P. Katehi, "A Microshield Line Loop Antenna for Sub-mm Wavelength Applications," submitted to the 1992 IEEE Antennas and Propagation Symposium, Chicago.

G. Rebeiz, D. Kasilingam, Y. Guo, P. Stimson, and D. Rutledge, "Monolithic Millimeter-Wave Two-Dimensional Horn Imaging Arrays," IEEE Trans. Antennas Propag., Sept. 1990, pp. 1473-1482.

S. Gearhart, C. Ling, G. Rebeiz, H. Davee, and G. Chin, "Integrated 119  $\mu\text{m}$  Linear Corner-Cube Array," IEEE Microwave Guided Wave Lett., July 1991, pp. 155-157.

N. Dib, P. Katehi, G. Ponchak, and R. Simons, "Theoretical and Experimental Characterization of Coplanar Waveguide Discontinuities for Filter Applications," IEEE Trans. Microwave Theory Tech., May 1991, pp. 873-882.

W. Harokopos and P. Katehi, "Radiation Loss for Open Coplanar Waveguide Discontinuities," 1991 IEEE MTT-S International Microwave Symposium Digest, Boston, pp. 743-746.

W. Harokopos and P. Katehi, "Characterization of Microstrip Discontinuities on Multilayer Dielectric Substrates Including Radiation Losses," IEEE Trans. Microwave Theory Tech., Dec. 1989, pp. 2058-2065.

N. Dib and P. Katehi, "Modeling of Shielded CPW Discontinuities Using the Space Domain Integral Equation Method (SDIE)," J. Electromagn. Waves Appl., Vol. 5, No. 4/5, 1991, pp. 503-523.

D. Rowe and B. Lao, "Numerical Analysis of Shielded Coplanar Waveguides," IEEE Trans. Microwave Theory Tech., Nov. 1983, pp. 911-915.

D. Marcuse, "Electrostatic Field of Coplanar Lines Computed with the Point Matching Method," IEEE J. Quantum Electron., May 1989, pp. 939-947.

Received 3-20-92

Microwave and Optical Technology Letters, 6/6, 333-339  
 © 1993 John Wiley & Sons, Inc.  
 0895-2477/93

## PERFORMANCE OF TWO SINGLE-LAYER FREQUENCY-SELECTIVE SURFACES AS SPATIAL FILTERS

Mathish Chandran and John C. Vardaxoglou  
 Department of Electronic and Electrical Engineering  
 Loughborough University of Technology  
 Loughborough  
 Leicestershire, LE11 3TU  
 United Kingdom

### KEY TERMS

frequency-selective surfaces, spatial filtering arrays

### ABSTRACT

Two single-layer FSSs are presented as radiation filters in conjunction with a conventional horn antenna. The amplitude of the transmitted wave to the variation of the incidence angle is studied with a view to designing a spatial filter array. It is demonstrated that these single-layer arrays act as spatial filters, following a simple design of regular plurality of slotted elements. © 1993 John Wiley & Sons, Inc.

### INTRODUCTION

Frequency-selective surfaces (FSSs) are often used as passive frequency filters as, for example, duplexers in reflector systems [1] or radomes [2]. The separation of the transmission and reflection bands is primarily achieved by the choice of the element and lattice geometries under a particular state of illumination. In some cases the angle of incidence significantly alters the frequency response of the surface. This implies that there is a direct relationship between the frequency and angular characteristics. The effect of the angle of incidence to the waves transmitted through the surfaces has prompted the use of periodic arrays or FSSs as spatial filtering arrays (SFAs) [3-7]. However, most of the work reported in the literature deals with multilayer arrays and formations of metallic grids with dielectric substrates. In this Letter the performance of two single-layer SFAs which are comprised of arrays of crossed-dipole and tripole slotted elements is presented. The design procedure and the radiation pattern comparisons with a primary source are discussed. The spatial filtering proposed would be advantageous for side-lobe suppression and beam forming in antenna systems.

### DESIGN PROCEDURE

The elements under scrutiny are slotted crossed dipoles and slotted tripoles [8, 9]. A parametric study has been carried out using a modal analysis method, with regard to optimizing the performance of the transmitted response varying the periodicities (square lattice) as well as the lengths of the array elements. The dielectric substrate, lattice geometry, and the orientation of the element remained unaltered. The analysis was based on a vector Floquet mode expansion  $\Psi$  of the tangential fields [10]. A magnetic field integral equation was formulated for the unknown magnetic current  $\mathbf{M}$  [11, 12], in the presence of a dielectric slab of thickness  $d$ , as follows:

$$\sum_{m=1}^2 2\eta_{m00} b_m^{\text{inc}} \Psi_{m00} = - \sum_{mpq} (\xi_{mpq} \eta_{mpq} + \eta_{mpq}^d) \Psi_{mpq} \iint_{\text{unit cell aperture}} \mathbf{M} \cdot \Psi_{mpq}^* d\mathbf{r}, \quad (1)$$

where  $b^{\text{inc}}$  is the amplitude of the plane wave exciting the structure and

$$\xi_{mpq} = \frac{1 - \Lambda_{mpq}}{1 + \Lambda_{mpq}}, \quad (2)$$

$$\Lambda_{mpq} = e^{-2j\eta_{mpq}^d} \frac{\eta_{mpq}^d - \eta_{mpq}}{\eta_{mpq}^d + \eta_{mpq}}$$

$\gamma$  and  $\eta$  are the modal propagation constants and admittances, respectively, where in the dielectric region they are denoted by the superscript  $d$ ,  $(p, q)$  are the Floquet indices for TM ( $m = 1$ ) and TE ( $m = 2$ ) modes. A method-of-moments solution was employed to determine the magnetic current in each slot. Entire domain basis functions were used for this solution, of the form  $\cos(m'\pi u/L)$ ,  $\sin(n'\pi u/L)$ , where  $L$  is the length of the segment under consideration, which is along an arbitrary direction  $u$ .  $m', n'$  may take integer as well as half-integer values. In total, three magnetic current bases for the tripole array were used, each corresponding to index  $m' = \frac{1}{2}$ . Seven basis functions were used:  $m' = 1.3$  and  $n' = 2, 4, 6, 8, 10$ , in each horizontal and vertical arm of the

crossed dipole array. One hundred sixty-nine Floquet modes were found adequate to represent the tangential fields adjacent to the array. The transmission and reflection coefficients were calculated using the zero-order propagating mode.

A rapid variation of the transmission response with angle of incidence was the primary objective for the design of the filter. In the design process, the parameters were initially adjusted to obtain a passband near 30 GHz at normal incidence, beyond which the array is highly reflective with increasing incident angles. This was achieved by varying the array periodicity whilst keeping the element lengths fixed. The radiation pattern of the SFAs, under plane-wave illumination at normal incidence, will therefore be associated with the above variation. For practical purposes, such as the size of the array to the wavelength, it was found that an appropriate design for the tripole slots (SFA1) and crossed-dipole slots (SFA2) was a periodicity of 8.9 mm and 8.6 mm, respectively. Figure 1 shows the lattice and element geometries and the physical parameters of both designs. The arrays were backed by a 0.037-mm-thick dielectric substrate (polyester) with  $\epsilon_r = 3.0$ , and the copper thickness was about 10  $\mu\text{m}$ . The surfaces measured 60 cm square and were stretched over a rigid wooden frame.

The plane-wave transmission responses as a function of incidence angle, at 30.5 GHz, are shown in Figure 2. For TM incidence, as the angle of incidence increases there is a sharp decrease of the transmission and at 25° incidence it is near

-10 dB. There is an increase of up to -6 dB as the angle of incidence increases to 60°. The computed and measured values of both arrays were in good agreement. For TE incidence there is a slower roll off, which may originate from the fact that the incident electric field vector is always parallel to

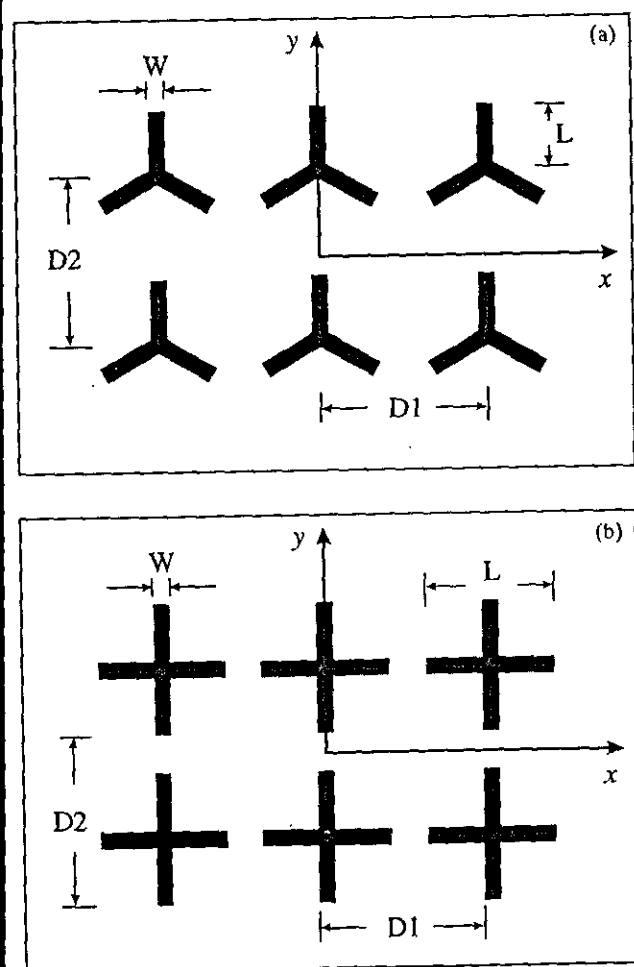


**Figure 1** Geometry of the two arrays with slotted elements (shaded portion) (a) SFA1:  $D1 = D2 = 8.9$  mm,  $L = 2.0$  mm,  $W = 0.2$  mm. (b) SFA2:  $D1 = D2 = 8.6$  mm,  $L = 4.2$  mm,  $W = 0.2$  mm

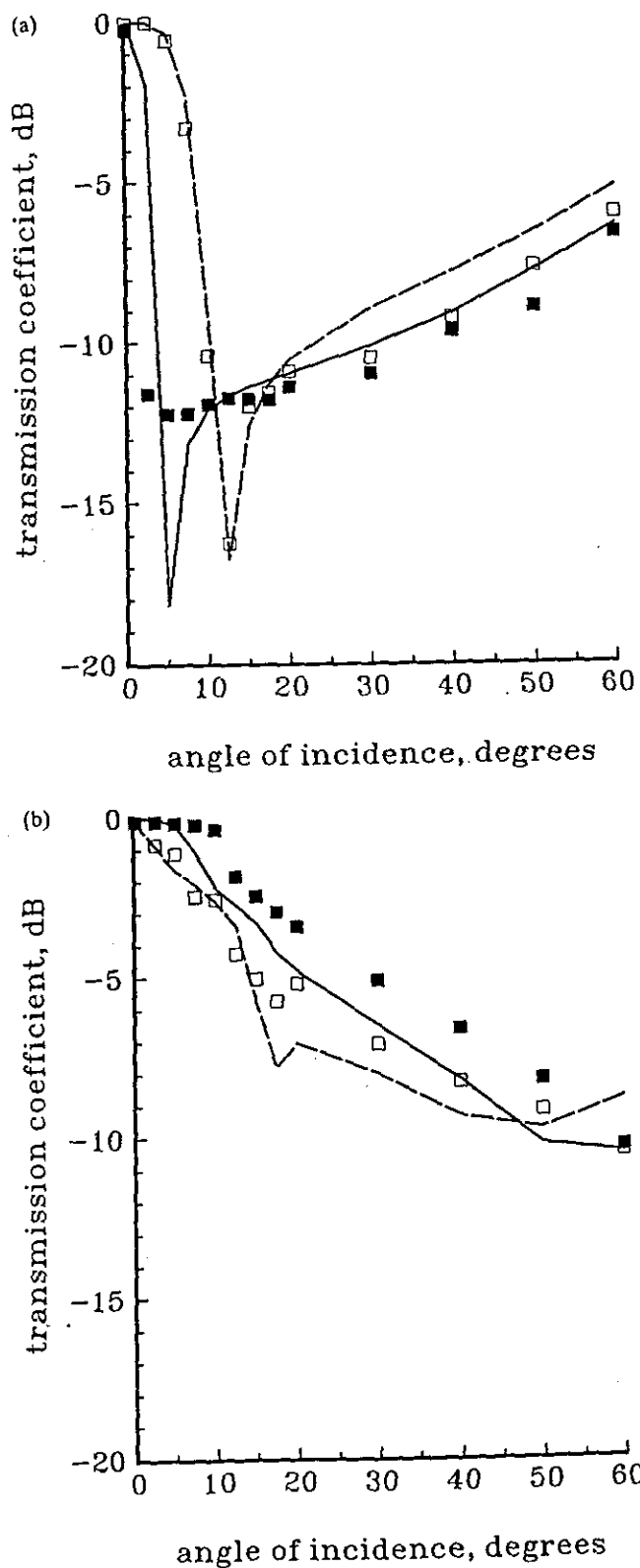


**Figure 2** Plane-wave transmission response as a function of incidence angle. (a) TM incidence, (b) TE incidence. SFA1: solid lines, theory; closed squares, measured values. SFA2: dashed lines, theory; open squares, measured values

the surface irrespective of the angle of incidence. In addition, smaller element spacing may be required to achieve sharper attenuation. The behavior of TE incidence seems to suggest that a degradation of the spatial filtering performance might be expected.

#### RADIATION PATTERN MEASUREMENTS

The measured radiation patterns of the FSS filters for E and H planes are compared with the feed (Ku-band standard py-

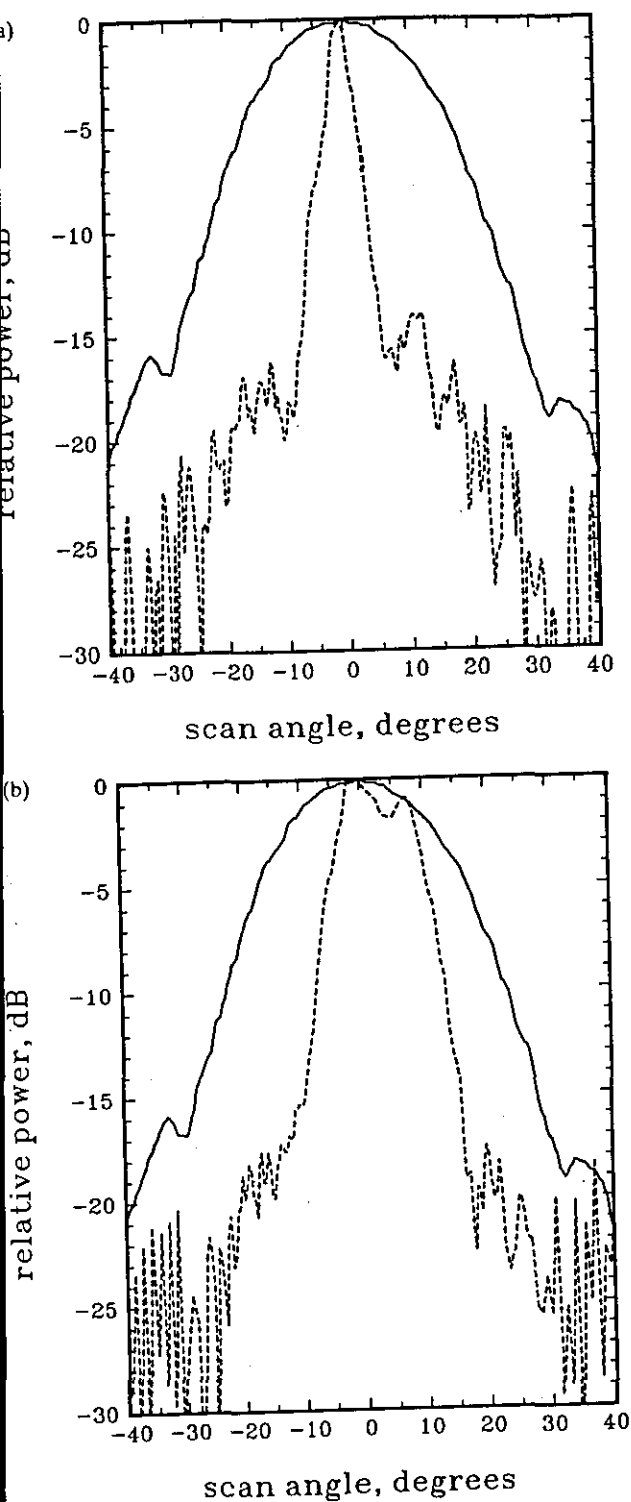


Figure 3 Copolar patterns in the E plane: (a) solid line, horn; dashed line, horn + SFA1. (b) solid line, horn; dashed lines, horn + SFA2

ramidal horn) patterns. Both surfaces were illuminated at normal incidence with the feed 30 cm away. Figure 3 shows the E-plane copolar component of the radiation pattern of the tripole array, SFA1, and crossed-dipole array, SFA2, at 30.5 GHz. The filtering effect is clearly illustrated, whereby a  $-3$ -dB beamwidth reduction of about 78% and 50% for SFA1 and SFA2, respectively, is obtained. Similar beamwidth reduction was also observed for the  $-10$ -dB level. It can be seen that there is a close relationship in the levels with Figure 2, up to  $10^\circ$  and  $15^\circ$  for SFA1 and SFA2, respectively. The slow transmission coefficient against the angle of incidence roll off of the SFA2 produces a broader pattern. Moreover, in both cases, the H-plane patterns are almost similar to that of the horn feed. The transmission bandwidth, defined between the  $-0.5$ -dB level, was about 1.2% and 2% for SFA1 and SFA2, respectively. A notable feature of this set of array designs is the depolarization of the incident field in transmission. Peak cross-polar levels for SFA1 of up to  $-10$  dB were recorded and can be attributed to the difference between the TE and TM plane-wave frequency responses.

#### CONCLUSION

Two single-layer array designs were fabricated and the radiation patterns were measured, indicating their spatial filtering properties. These SFAs were designed to exhibit an angular filtering effect near 30 GHz at normal incidence. The radiation pattern and theoretical values which were obtained by varying the angle of incidence using a plane-wave modal analysis correspond, which confirms the ease of the design procedure. As the beam becomes narrower, the cross-polarization levels increase. Despite that deterioration the spatial filtering of these surfaces is easily achieved and they can be incorporated in existing antenna systems. For enhanced performance, the effect of the lattice geometry and dielectric backing to the filtering properties needs to be addressed and forms the next phase in our studies.

#### ACKNOWLEDGMENT

This work was funded by a research grant from the Science and Engineering Research Council, UK.

#### REFERENCES

1. V. D. Agrawal and W. A. Imbriale, "Design of a Dichroic Cassegrain Subreflector," *IEEE Trans. Antennas Propagat.*, Vol. AP-27, 1979, pp. 174-181.
2. E. L. Pelton and A. B. Munk, "A Streamlined Metallic Radome," *IEEE Trans. Antennas Propagat.*, Vol. AP-22, 1974, pp. 174-181.
3. A. W. Rudge, K. Milne, A. D. Olver, and P. Knight (Eds.), *The Handbook of Antenna Design*, Peter Peregrinus Ltd., London, 1986, Vols. I and II, Chap. 5.
4. P. R. Franchi and R. J. Mailloux, "Theoretical and Experimental Study of Metal Grid Angular Filters for Sidelobe Suppression," *IEEE Trans. Antennas Propagat.*, Vol. AP-24, 1976, pp. 174-181.
5. P. W. Hannan and J. F. Pedersen, "Axial Conductance Angular Filter," *1984 IEEE AP-S Int. Symp. Digest*, Boston, MA, pp. 917-920.
6. E. L. Rope and G. Tricoles, "An Angular Filter Containing Three Periodically Perforated Metallic Layers," *1979 IEEE AP-S Int. Symp. Digest*, Seattle, WA, pp. 818-820.
7. J. F. Pedersen and P. W. Hannan, "A Metal Grid  $5 \times 5$  Foot Angular Filter," *1982 IEEE AP-S Symp. Digest*, Albuquerque, NM, pp. 471-474.

8. R. Mittra, C. H. Chan, and T. Cwik, "Techniques for Analysing Frequency Selective Surfaces—A Review," *Proc. IEEE*, Vol. 76, 1988, pp. 1593–1615.
9. J. C. Vardaxoglou and A. H. Hossainzadeh, "Single and Double Layer FSS of Tripole Arrays," *Proc. 19th Microwave European Conference*, 1989, pp. 863–868.
10. N. Amitay, V. Galindo, and C. P. Wu, *Theory and Analysis of Phased Array Antennas*, John Wiley & Sons, New York, 1972.
11. C. C. Chen, "Transmission through a Conducting Screen Perforated Periodically with Apertures," *IEEE Trans. Microwave Theory Tech.*, Vol. MTT-18, 1970, pp. 627–632.
12. C. Scott, *The Spectral Domain Method in Electromagnetics*, Artech House Inc., Boston, 1990, Chap. 2.

Received 9-15-92; revised 12-17-92

Microwave and Optical Technology Letters, 6/6, 339–342

© 1993 John Wiley & Sons, Inc.

CCC 0895-2477/93

## ATTENUATION PROPERTIES OF NORMAL MODES IN COATED CIRCULAR WAVEGUIDES WITH IMPERFECTLY CONDUCTING WALLS

Zhixun Huang

Beijing Broadcasting Institute  
Beijing 100024, China

Cheng Zeng

University of Science and Technology of China  
Anhui 230026, China

### KEY TERMS

Coated waveguide, characteristic equation, modal attenuation

### ABSTRACT

A new analytic characteristic equation is presented and applied to the analysis of attenuation properties of normal modes in coated circular waveguides including conductor loss. Approximate and numerical methods are employed to accomplish the solution to the new equation, resulting in some useful approximate formulas for calculations of modal attenuations. These formulas are applicable to the analysis and design of the coated circular waveguide including con-

ductor loss because of their good agreement with the numerical results obtained by the computer. © 1993 John Wiley & Sons, Inc.

### I. INTRODUCTION

The characteristic equation [1–3] for propagation constants  $k_z$  of normal modes in a coated circular waveguide is well known and has been widely adopted in many applications [4–8] to accomplish the approximate or accurate analysis of the attenuation properties of main low-order normal modes in the waveguide. For formulating the characteristic equation of normal modes in a multilayered coated waveguide, a matrix method [8] based on the mode-matching technique was presented which only involved the manipulation of  $4 \times 4$  matrices for any number of coating layers. In these studies, however, the metallic wall was usually assumed to be a perfect conductor in order to simplify the theoretical analysis. This relaxed treatment has certainly introduced some loss of accuracy in these results, especially for the cutoff waveguide, where high accuracy for calculations of modal attenuations is of utmost interest.

This Letter is devoted to the analysis of attenuation properties of normal modes in a coated waveguide under the condition of no restriction to the metallic wall. To this end, a new characteristic equation including conductor loss must be derived first. The method for formulating the characteristic equation in this Letter is still the matrix method, which involves the manipulation of  $2 \times 2$  matrices instead of  $4 \times 4$  ones as in [8]. In Section II, this novel method is presented first to formulate the characteristic equation for a multilayered coated waveguide, and subsequently a new analytic characteristic equation for a single-layer coated circular waveguide with an imperfect wall is obtained. In Section III, according to this new equation, attenuation properties of normal modes in the cutoff and the overmoded waveguides are discussed, respectively, using approximate methods. These approximate treatments result in some useful formulas for the analysis and design of the coated circular waveguide which agree well with the numerical results obtained from the computer by Müller's methods. These numerical results and their discussions are also presented in the same section.

### II. CHARACTERISTIC EQUATION OF NORMAL MODES

A generalized model is shown in Figure 1. Region 1 is the air layer. Region  $n + 1$  is the metallic conductor whose con-

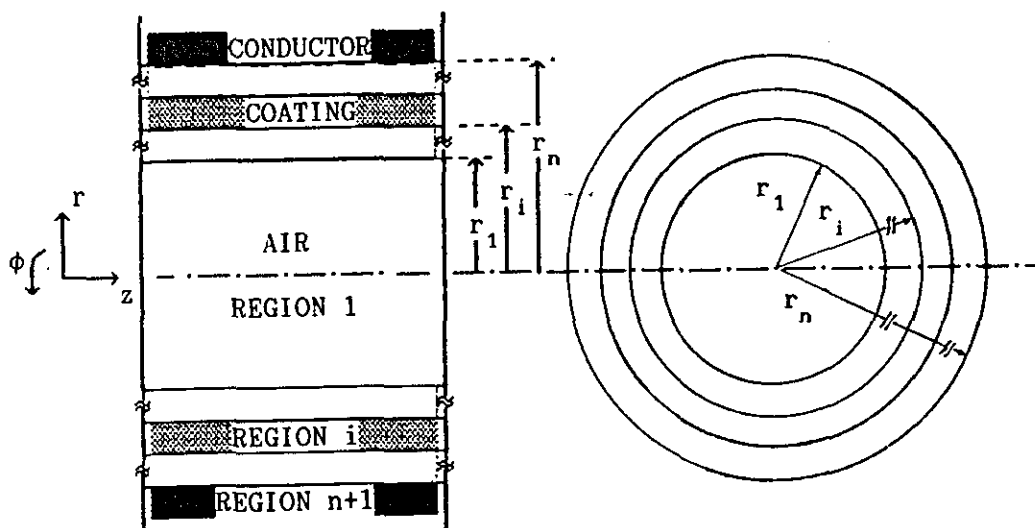


Figure 1 Geometry of a multilayered coated circular waveguide

**Eighth International Conference on**

# **Antennas and Propagation**

**30 March - 2 April 1993**

*Organised by*

the Electronics Division of the Institution of Electrical Engineers

*in association with*

**EUREL**

**International Union of Radio Science (URSI)**

**Institute of Electronics, Information and Communication Engineers of Japan**

**Institution of Electrical and Electronic Engineers (UKRI Section)**

**Institution of Electrical and Electronic Engineers Inc (Antennas and Propagation Society)**

## **Venue**

Heriot-Watt University, UK

# PHASING EFFECTS OF CASCADED AND SPATIALLY VARYING PLANAR ARRAYS

S C Chandran, B Little, J C Vardaxoglou

Loughborough University of Technology, UK

## INTRODUCTION

Passive arrays of elements such as Frequency Selective Surfaces can be used as frequency filters to separate different bands in a communications antenna system while maintaining the high radiation performance required. Cascaded surfaces can produce improved responses over single layers primarily due to the flexibility in the choice of the element and lattice geometries as well as their supporting dielectric structures and separation regions. Due to the diverse properties of these arrays one can consider them as candidates in a number of applications which require enhancements of existing antennas with regard to angular filtering (1), beamforming or focusing tasks.

This paper deals with some procedures for attaining controlled modifications of the incident field that result in beam direction, filtered and focused radiation patterns. Planar single and multilayer spatially varying array designs have been incited to produce the required combination of amplitude and phase changes. A number of prototypes (of up to four layers) have been manufactured and experimentally assessed in the 26-40 GHz frequency region. The bandwidth and polarisation performance will also be discussed.

## OUTLINE OF CONCEPTS

It has been shown that regular arrangements of periodic elements can be viewed as artificial dielectrics or phase shifting structures (2, 3). A plurality of elements or a Frequency Selective Surface can be used to introduce a phase shift in the transmitted portion of the radiation incident on the array. The phase shift can be stepped or progressive, by altering the geometry or dimensions of the array elements used. Therefore, using an array with phase shifting properties varying spatially across its surface, incident radiation can be influenced in such a way as to *beamform, beamdirect, filter or converge the incident wave.*

The basic principle involved in creating a newly formed wave front is to introduce symmetrical or asymmetrical phase advances, increasing in relation to the spatial distance from the axis (centre) or the perimeter of the array. The amount of beam shaping near the lossless region of the band depends on the variation of the transmission coefficient (amplitude and phase) to the local angles of incidence which are present on the structure.

The first exercise deals with a multilayer structure of strip zone arrays. In order to achieve the required phase variations each surface was divided into zones within which the geometry of the array remained the same, as shown in Fig. 1a. A parametric study has been performed using a modal analysis and equivalent circuit methods (4, 5) with regard to optimising the performance of the transmitted beam by varying the lattice geometries as well as the distance separating the arrays. The aim was to minimise the reflected wave component, whilst obtaining the required phase shifts. The analysis is based on a coupled integral equation formulation in which an iterative method solution was employed to determine the element currents. Propagating and evanescent mode coupling have been taken into account by expanding the tangential fields in the separation region as sets of Floquet modes. The elements that have been considered in this study were conducting square loops.

An asymmetric array (single layer structure) with continually varying element dimensions (Fig. 2a) of the same periodicity formed the second part in the study. A progressive phase shift will therefore advance across the surface. Using the same postulate, arrays were assessed with symmetrical configurations of the above, Figs. 3a and 4a. The elements were slotted crossed dipoles and were arranged on a regular grid.

## STRIP ZONE ARRAY DESIGN

Discrete zones of the array are defined, as shown in Fig. 2a, within which the geometry of the elements remains the same, hence giving a constant phase shift across the zone. The complete structure comprises of 4 layers (of the order outer, inner, inner, outer) over the 5 central zones, doubled up to eight layers for the outer strip where a greater phase shift is required. The phase shifts were  $-97^\circ$ ,  $-54^\circ$ ,  $+76^\circ$  and  $+147^\circ$  for zones 0 to 3 respectively. In this array strip zones were designed, creating a phasing effect in one plane only. The array was designed for a normally incident plane wave, and an electrical separation of  $72^\circ$  between the layers at 30 GHz. The separation was introduced by considering the thickness of the dielectric substrate on which the array elements were printed and by adding a thin layer of expanded polystyrene sheet. The array was comprised of seven zones each 5.43 cm across, making the array dimensions 38cm by 28cm.

the experimental set-up used in the testing of the multilayer structure, the transmitting and receiving horns were 2.1 m apart, with the element to be tested situated at a distance of 0.89 m from the transmitting horn. Both frequency and angular scans were performed in the measurement of the planar arrays.

Although the arrays were designed for normal incidence at around 30 GHz, investigations of the properties of each array were made for a variety of different orientations. Both TE and TM incidence were simulated, at angles of incidence up to  $45^\circ$ . Fig. 2b shows the radiation pattern of the structure for TM:30° incidence at 27.5 GHz. When compared with the primary source (standard pyramidal horn) notable filtering occurs associated with a radiation intensity increase. The increase peaked about 5 dB above the boresight level of the horn and had a nominal value of about 2 dB from 26 - 29 GHz. It can be attributed to the phase advances and minor diffraction arising from the edges of the structure. These increases were lower for TE incidence with lower sidelobes in the filtered radiation pattern. The crosspolar performance was moderate with peaks of about 25 dB below the boresight level.

## CONTINUALLY VARYING ARRAY DESIGN

### Beam directing array

This design comprises of a continual tapering of the elements dimensions so that a net phasing effect may be produced. Fig. 2a shows the four corners of a slotted crossed dipole (20cm square) single layer array. There was a total reduction of the horizontal arm length of about 50% from one side of the surface to the other. The vertical arm length and lattice geometry (square of side 4.35 mm) remained unchanged. The element lengths were  $LI=4.15$  mm and  $LF=2$  mm. With the incident electric field across the horizontal arm (normal incidence) at 35 GHz, there was a deflection of the transmitted beam at about  $-9^\circ$ , in the H-plane which is shown in Fig. 2b. This result shows evidence of a progressive phasing effect produced by a deflection of  $\lambda/2$  to  $\lambda/4$  element length and a slow wave along the edge of the array. Rotating the surface through  $90^\circ$  in its own plane the beam appeared near  $+9^\circ$  which is symmetrically opposite to the previous case. For both orientations there is less than 1 dB loss over a 5% bandwidth. In addition to the beam location, there is also a notable narrowing of the illuminating beam.

### Asymmetrical tapering

Fig. 3a shows the bottom left hand quarter of an asymmetrically spatially varying slotted crossed dipole array. There is taper in both the vertical and horizontal arm lengths, from the left to right as well as from top to bottom of the surface. The dimensions were as follows:  $LHI=LVI=4.15$  mm,  $LHR=3$  mm and  $LHF=2$  mm. There was a 33% deflection in the vertical arm. The radiation patterns in the E

and H planes are shown in Fig. 3b, at 33 GHz, exhibiting similar features. A radiation intensity increase over 5 dB was measured when compared to the standard gain horn at the same frequency. Increases begin at about 30 GHz and occupy a bandwidth of 9%.

A different type of symmetrical arrangement of the array elements can be seen in Fig. 4a, where the elements of the bottom right quadrant are drawn only. This formation of elements is axisymmetric where square loop zones increase in circumference from the centre of the surface. The element at the centre has equal length arm ( $LI=4.15$  mm) and the elements on the edge of the array reduced by 28% ( $LF=3$  mm). Similar comments could be made with the previous array with the exception of broader principal plane beams and better sidelobe performance, as shown in Fig. 4b. This is primarily due to the reduced tapering of the element lengths.

## CONCLUSION

We have made a preliminary investigation into the possibilities of alternative uses of planar periodic arrays which are entirely passive. It was shown that continually varying single layer arrays performed better than the strip zoned designs. The disadvantage of the latter is that it is bulky and difficult to construct accurately. However it produced a wideband angular filtering that may otherwise be difficult to achieve, (1). Further work however is needed with regard to the predictions using finite array theory nomenclatures, (6) to establish the correct phase changes including the mutual coupling effects. It is envisaged that the spatial filtering, in conjunction with the converged beam, resulting from such planar structures could be used to improve sidelobe performance and directivity in linearly polarised antenna systems.

## ACKNOWLEDGEMENTS

The work is supported by a research grant from the Science and Engineering Research Council, UK.

## REFERENCES

1. Vardaxoglou, J.C. and Chandran, S. C., 1993, *Microwave and Optical Tech. Letters*, in press
2. Brown, J., 1969, 'Antenna Theory', (Colin, R.E. and Zucker, F.J., Eds), McGraw-Hill, USA
3. Griffiths, H.D., Vernon, A.M. and Milne, K., 1989, *Int. Conf. Antennas and Propagat., UK*, 45-49
4. Stylianou, A.S., Debono, P. and Vardaxoglou, J.C., 1992, *IEE Proc.-H*, 139, 6, 535-541
5. Evans, F., 1988, 'A study of the analysis and synthesis of FSS using equivalent circuits', MSc in IT thesis, LUT
6. Stylianou, A.S. and Vardaxoglou, J.C., 1992, *Electron. Lett.*, 28, 506-508

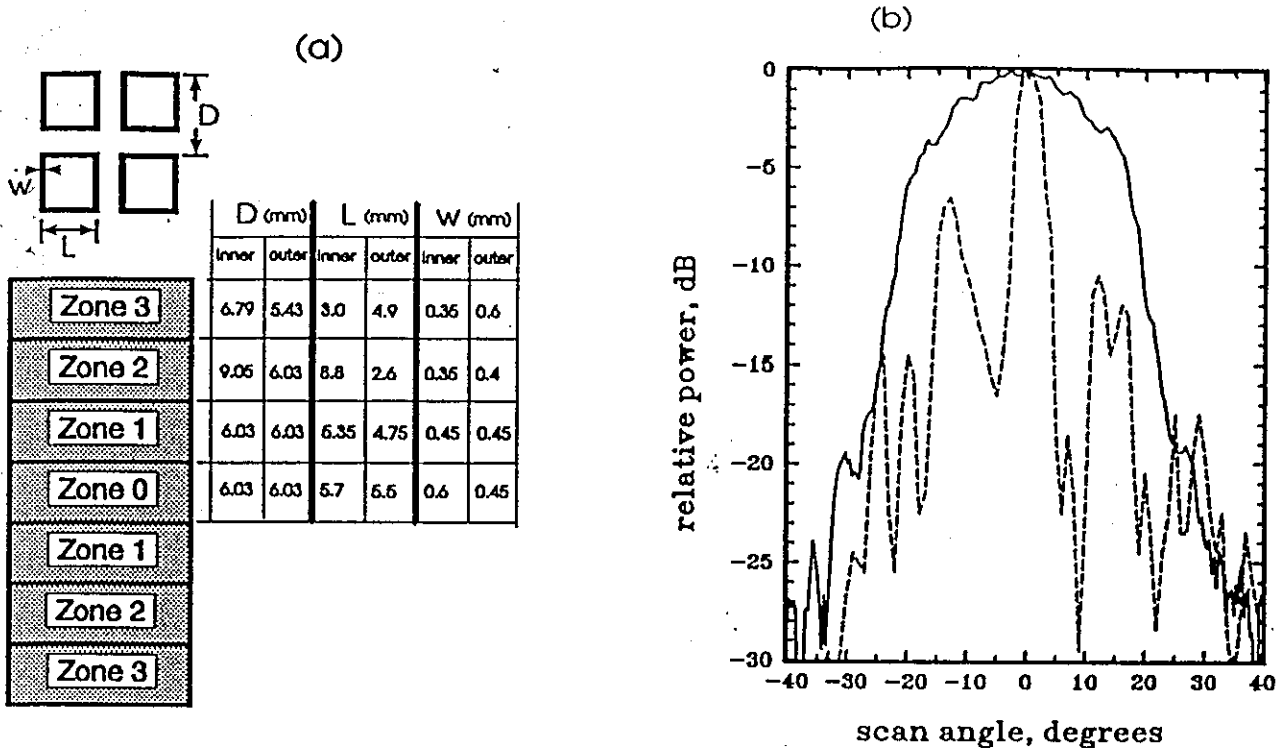


Fig. 1. (a) Square loop array geometry and zone layout.

(b) Radiation patterns in the E-plane. ——— Horn, - - - Horn + Surface.

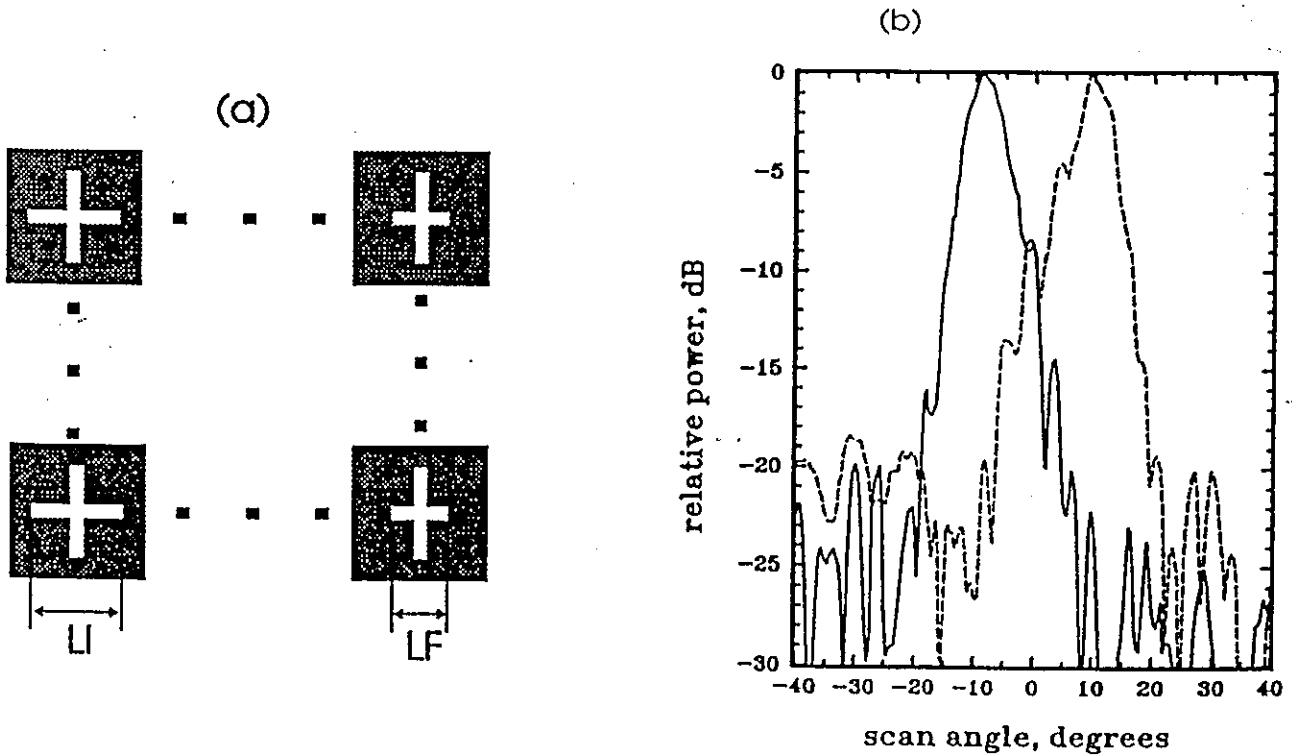


Fig. 2. (a) Array geometry. (b) ——— H-plane radiation pattern at 35 GHz, - - - Surface rotation through  $180^\circ$ .

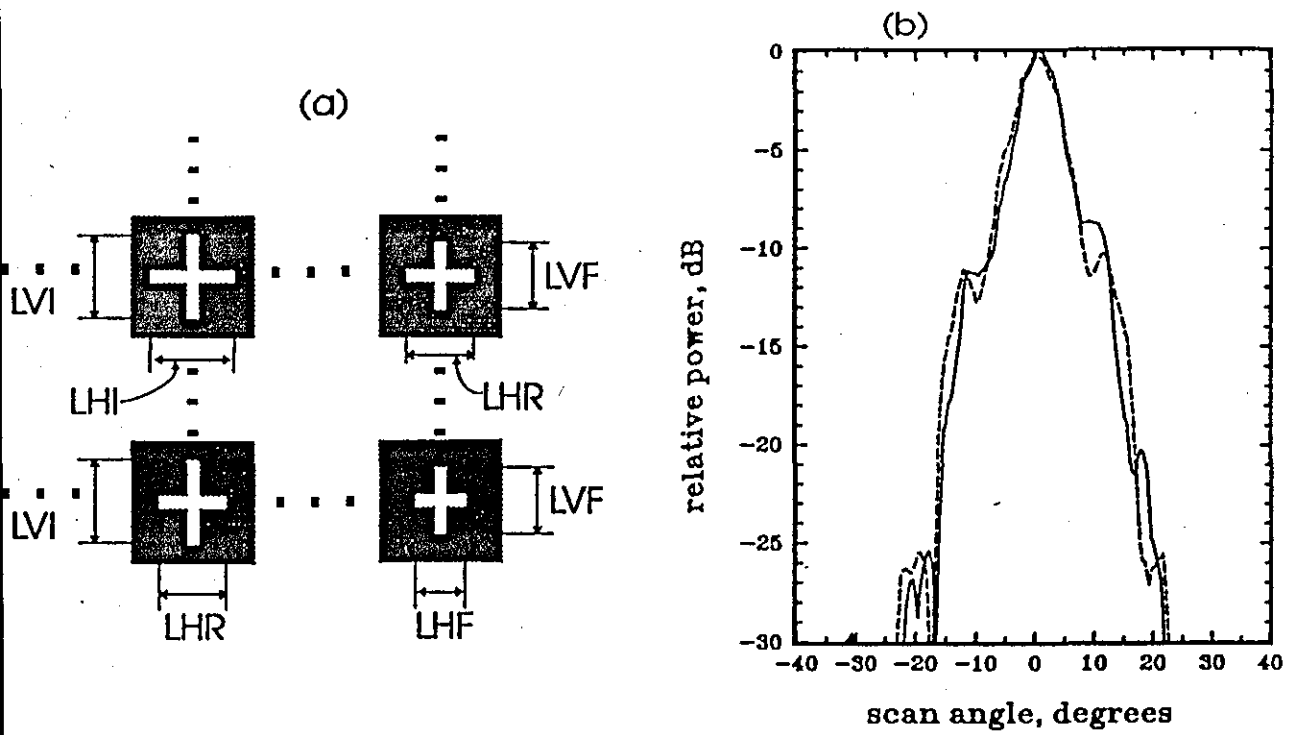


Fig. 3. (a) Array geometry. (b) Radiation patterns at 33 GHz, — H-plane, - - - E-plane.

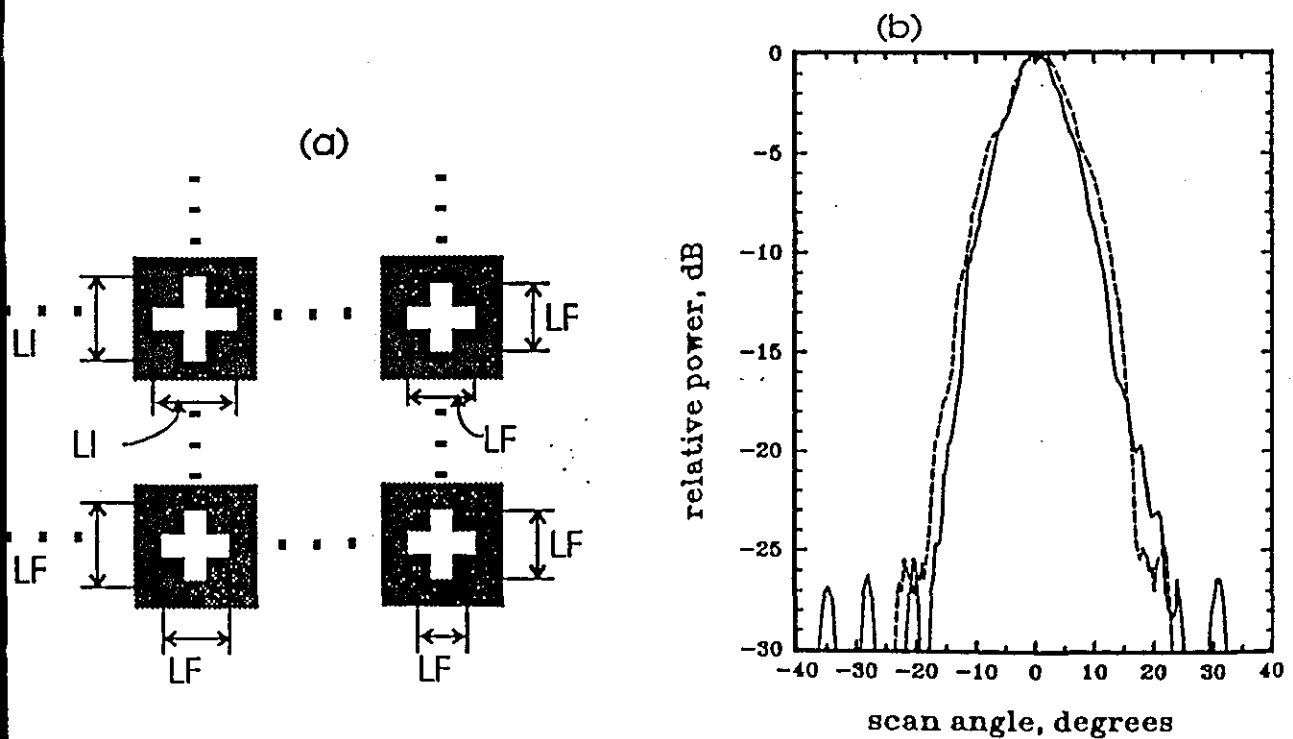


Fig. 4. (a) Array geometry. (b) Radiation patterns at 33 GHz, — H-plane, - - - E-plane.

